MISSOURI COOPERATIVE HIGHWAY RESEARCH PROGRAM
FINAL REPORT

90-5

DETERMINATION OF AASHTO LAYER COEFFICIENTS
Volume I
BITUMINOUS MATERIALS

MISSOURI HIGHWAY AND TRANSPORTATION DEPARTMENT
FEDERAL HIGHWAY ADMINISTRATION

DETERMINATION OF AASHTO LAYER COEFFICIENTS

Volume I:

BITUMINOUS MATERIALS

Study 90-5

Prepared for

MISSOURI HIGHWAY AND TRANSPORTATION DEPARTMENT

by

DAVID N. RICHARDSON

JEFFREY K. LAMBERT

PAUL A. KREMER

DEPARTMENT OF CIVIL ENGINEERING

UNIVERSITY OF MISSOURI - ROLLA

ROLLA, MISSOURI

in cooperation with

U.S. DEPARTMENT OF TRANSPORTATION

FEDERAL HIGHWAY ADMINISTRATION

December 1994

EXECUTIVE SUMMARY

The purpose of this investigation was to determine layer coefficients for several MHTD specified pavement materials. The coefficients are necessary as input to the AASHTO pavement design method. Volume I of this study involves asphaltic materials, and is reported herein. Volume II deals with unbound aggregate base and soil-cement base materials, and is reported elsewhere.

Besides determining layer coefficients, the study also entailed the determination of the effect on layer coefficient by changes in asphalt cement grade, aggregate gradation, testing temperature, aggregate source, and asphalt content within the limits of MHTD specifications. This resulted in 48 mix designs.

All materials were sampled and delivered to UMR by MHTD personal. Choice of material sources was made by MHTD. The types of pavement materials were Type C, Type I-C, and bituminous base. The specific materials making up these types were two grades of asphalt cement, two sources each of surface mix coarse aggregate and base mix coarse aggregate, and one source each of natural sand, manufactured sand, mineral filler, and hydrated lime.

Routine index and specification tests were performed. For the asphalt cement, the tests were: penetration at 38° and 77°F, kinematic viscosity, absolute viscosity, specific gravity, and softening point. The aggregates were tested for gradation, specific gravity, and particle shape/texture. Equipment was fabricated for the particle shape/texture tests.

The optimum asphalt content of each of the 12 gradation/aggregate source

combinations was determined by use of the Marshall mix design method (75 blow, manual flat-faced hammer). Use of AC10 and AC20 grades resulted in 24 mixes. And, 24 additional mixes were made which had 0.5% asphalt added above optimum, for a total of 48 mixtures.

Maximum theoretical specific gravities were determined in two ways: 1) Rice method, and 2) calculation from material proportions and specific gravities. Ninety-six specimens were tested. A voids analysis was conducted to determine the effect of estimation of maximum theoretical specific gravity. The estimation method involves the assumption that the effective specific gravities of low absorption aggregates is midway between the bulk and the apparent specific gravities. The voids analysis indicated that the estimation method correlated very well with results from Rice method testing. However, for absorptive aggregates (eg., the bituminous base materials in this study), the estimation method underpredicted air voids by about 1%.

Ten methods of characterizing gradation curve shape and position were used. Two of these were original to this study. The first involved the area between the gradation curve and the maximum density line as plotted on FHWA 0.45 power paper. The second method involved determination of the slopes of three portions of each gradation curve. The method of determining the area between the 0.45 power maximum density line (MDL) and the gradation line had only a fair (R^2 = 0.79) correlation with resilient modulus (M_R). This was because the magnitude of the area was not sensitive to relatively small differences in position of the gradation curve relative to the MDL. The second unique method involved calculation of the slope of

three different parts of the gradation curve. This method was shown to be of assistance in creating a more accurate M_R regression model. However, it was not quite as helpful as Hudson's $\bar{A}$, which is much easier to calculate. But, Hudson's $\bar{A}$ was not quite as helpful as merely including certain critical sieve sizes directly into the regression equation.

Each mix was tested for indirect tensile strength. A regression model was fit to the data, which included 96 test results. The regression model was relatively strong (adj-R^2 = 0.840) and was a function of asphalt viscosity, effective asphalt content, percent accumulative retained on the #4 sieve, and coarse aggregate particle shape.

Each mix was tested for total resilient modulus (indirect tension) . Necessary software and equipment were developed to perform the tests and to acquire, store, and analyze the data. A total of 192 specimens were tested at three temperatures for a total of 576 tests. The resilient modulus test is sensitive to testing conditions of temperature, specimen rocking, specimen surface irregularities, choice of point of LVDT fixation, LVDT tip design, and resolution of both vertical and horizontal LVDT's. Constant diligence is required by the operator to assure that the very small deformations being measured are representative of actual deformations. A relatively strong (adjusted R^2 = 0.946) regression model was fit to the UMR M_R data.

The results of the M_R testing were analyzed statistically to determine the variables that were significant to changes in M_R. The analysis of the data indicated that temperature was by far the most important variable that affects M_R, followed by

asphalt viscosity and whether the gradation was very fine or very coarse. Overasphalting by 0.5% tended to lower M_R, but was not statistically significant. Increases in (-) #200 material and decreases in (+) #4 material tended to increase M_R. Particle shape of coarse or fine aggregate did not seem to affect M_R in a consistent manner. It should be noted that both coarse aggregates were crushed limestones, and that all mixes contained varying amounts of manufactured sand, so large ranges in particle shape were not present. And, all other things held constant, decreasing air voids tended to increase M_R.

Resilient modulus data from other studies found in the literature were merged with the UMR data. A general regression model was fit to the overall data base. The model was not as strong as the UMR model, but was deemed superior because it represented a much wider range in magnitudes of variables. The equation is a function of pavement temperature, air voids content, asphalt viscosity, percent passing the #200 sieve, percent accumulative retained on the 3/4 in sieve, and effective asphalt content.

$$\log M_R = 6.871 - 0.017T - 0.024P_{air} + 0.043\eta_{70} + 0.018P_{200} - 0.004AR_{3/4} - 0.011P_{effv}$$

In order to compare pavement temperatures in Missouri and at the Road Test, air temperature data from 104 weather stations in Missouri were analyzed to produce an air temperature contour map of Missouri. Pavement thickness data for MHTD and Road Test flexible pavements were analyzed for mean pavement thickness. This information was necessary to calculate pavement temperatures. Mean vehicle speed data was supplied by MHTD. This was converted to load dwell times and loading

frequency for MHTD pavements. The same was done for AASHO Road Test pavements.

UMR, AASHO Road Test, and MHTD 1990 mix design data were used to estimate resilient modulus, mixture stiffness (Shell method), and dynamic modulus at both laboratory conditions and field conditions of pavement temperature and loading rate. This was done in order to see which type of modulus would be most useful for layer coefficient determination. The Odemark equation was used to rate the three methods of obtaining mixture modulus or stiffness. The ranking, in descending order of ability to predict resilient modulus, was: M_R estimated from the above general regression equation, Shell mixture stiffness, and dynamic modulus.

Five different methods of calculating mixture stiffness (S_m) were compared; each varied in the manner of handling asphalt aging or source. Of the five different methods, the method of Bonnaure, which uses the Ullidtz asphalt aging approximations, was found to be the most accurate for the purposes of this study.

Two options to obtain layer coefficients were presented for possible use. The first involves the determination of M_R by test (or by estimation of resilient modulus by the general regression equation) for a pavement temperature of 68°F, then entering the proper AASHTO nomograph to obtain the corresponding layer coefficient. The second option is to again determine the M_R by test or to estimate the resilient modulus, but the moduli must be converted to the pavement temperature conditions in the locale of interest. Then, the layer coefficient is computed via the Odemark equation which relates the MHTD M_R to the AASHO Road Test M_R.

Option One resulted in a fixed layer coefficient per material. For 1990 mixes,

frequency for MHTD pavements. The same was done for AASHO Road Test pavements.

UMR, AASHO Road Test, and MHTD 1990 mix design data were used to estimate resilient modulus, mixture stiffness (Shell method), and dynamic modulus at both laboratory conditions and field conditions of pavement temperature and loading rate. This was done in order to see which type of modulus would be most useful for layer coefficient determination. The Odemark equation was used to rate the three methods of obtaining mixture modulus or stiffness. The ranking, in descending order of ability to predict resilient modulus, was: M_R estimated from the above general regression equation, Shell mixture stiffness, and dynamic modulus.

Five different methods of calculating mixture stiffness (S_m) were compared; each varied in the manner of handling asphalt aging or source. Of the five different methods, the method of Bonnaure, which uses the Ullidtz asphalt aging approximations, was found to be the most accurate for the purposes of this study.

Two options to obtain layer coefficients were presented for possible use. The first involves the determination of M_R by test (or by estimation of resilient modulus by the general regression equation) for a pavement temperature of 68°F, then entering the proper AASHTO nomograph to obtain the corresponding layer coefficient. The second option is to again determine the M_R by test or to estimate the resilient modulus, but the moduli must be converted to the pavement temperature conditions in the locale of interest. Then, the layer coefficient is computed via the Odemark equation which relates the MHTD M_R to the AASHO Road Test M_R.

Option One resulted in a fixed layer coefficient per material. For 1990 mixes,

Also, it must be kept in mind that the M_R predictive equations are based on data that represents well-graded gradations. They should not be applied to mixes with significantly different characteristics or materials, such as stone mastic mixtures.

It is highly recommended that the MHTD pursue M_R testing of various mixtures in present use in order to update or replace the above equation by use of a more representative data set of the materials. A greater degree of accuracy will also probably be achieved. Then, both Options One and Two will render more representative layer coefficient values for MHTD designers.

It should be remembered that this study is in the mold of the traditional method of determination of layer coefficients, that is, by a comparison of some sort of strength or stiffness of MHTD materials to Road Test materials. Tendencies for asphaltic material problems with thermal cracking and rutting, for instance, are not directly addressed. To address a wider range of material issues, creep testing and gyratory shear testing may be in order, however, these kinds of tests were beyond the scope of this project. Also, this project was conceived in 1989 and the bulk of the testing was performed in 1991, before the SHRP project results became generally known. In the future, it may be that some of the recommendations coming out of the SHRP program can be used to update the quest for layer coefficient determination.

LIST OF FIGURES

LIST OF TABLES

where:

SN = structural number

a_1,a_2,a_3 = layer coefficients for the surface, base, and subbase layers, respectively

m_2,m_3 = drainage coefficients of the base and subbase, respectively

D_1,D_2,D_3 = thickness of surface, base, and subbase layers, respectively.

Drainage coefficients are essentially modifiers of the layer coefficients, and take into account the relative effects of the internal drainage of the pavement structure on performance of the pavement. Determination of drainage coefficients is addressed in a second report submitted by UMR to the MHTD concurrent with this study (2).

A preliminary review of the literature indicates that reported values for layer coefficients vary widely, as reported in Table 1.

Table 1. Reported Layer Coefficients.

Layer Coefficient	Material/Layer	Value	Ref
a_1	asphalt surface	0.30 - 0.57	3 - 8
a_2	asphalt treated base	0.10 - 0.62	4,5,7,8
	cement-treated base	0.12 - 0.50	4 - 7
	lime-treated base	0.12 - 0.26	3,6
	unbound granular base	0.03 - 0.23	4 - 10
a_3	unbound granular subbase	0.02 - 0.15	4,5,9

The range of layer coefficients determined at the AASHO Road Test are shown in Table 2 (5,11).

Table 2. Range of Layer Coefficients at the AASHO Road Test.

Coefficient	Minimum	Maximum	Reported
a_1	0.33[1]	0.78[1]	0.44[1]
a_2	0.12[2]	0.23[2]	0.14[2], 0.34[3]
a_3	0.07[4]	0.12[4]	0.11[4]

Note: [1]asphaltic concrete surface layer
[2]unbound crushed stone base
[3]asphalt-bound base
[4]unbound sandy gravel subbase

Examination of Eq. 1 indicates that the thickness of any particular layer is, to a significant extent, dependent upon the layer coefficients. Hence, an accurate determination of layer coefficients can have a significant economic impact in regard to the design of the pavement structure.

It has been postulated that the magnitude of any layer coefficient is a function of several factors. For example, the asphalt surface layer coefficient a_1 is dependent upon mix characteristics, pavement temperature, vehicle speed, layer thickness, and compacted mix stiffness. For an unbound granular base, the layer coefficients a_2 and a_3 have been shown to be dependent on the state of stress in the layer, degree of saturation, compactive effort, aggregate properties, and base layer thickness.

As originally used in the AASHO Road Test results, layer coefficients were actually regression coefficients which were the result of relating layer thicknesses to road performance under the conditions of the Road Test. The problem is to

translate the Road Test findings to other geographic areas where the construction materials and climate are different. Layer coefficients must be determined in order to use Eq. 1 for design purposes. In a pure sense, layer coefficients are abstract mathematical entities but in a practical sense they must be related to something tangible. Most commonly, layer coefficients are determined on the basis of relative layer material strength or stiffness considerations. Over the years since the AASHO Road Test, many methods have been used to determine values for layer coefficients.

OBJECTIVES AND SCOPE

This report is based on methods which optimize the combination of economy, accuracy, and length of study. In brief, the study entails determination of stiffness values for several commonly used MHTD types of pavement materials. The stiffness values were determined by both direct laboratory modulus testing and by approximation techniques. These stiffness values were related to layer coefficients and then verified for reasonableness by comparing the resulting coefficients for MHTD materials to AASHTO materials. The report includes a method suitable for use in routine design which will enable the pavement designer to solve Eq. 1 and hence obtain the desired layer thicknesses.

The approach taken for determination of layer coefficients was the traditional one (5,12), which is to take some measure of strength, stability, or stiffness of a particular mix and compare it to the same parameter (such as resilient modulus) for the counterpart AASHO Road Test material. The

comparisons are usually done by use of the AASHTO Design Guide chart or some ratio of the two parameters. Thus, the influence of rutting is not directly addressed.

The materials for which layer coefficients were determined were limited to two types asphalt surface mixes (Types C and I-C), one type of bituminous base mix, two types of cement treated base mixes, and one type of unbound granular base/subbase. The report is separated into two volumes: Volume I covers bituminous materials; Volume II deals with unbound granular and cement-treated materials (13).

DETERMINATION OF LAYER COEFFICIENTS: METHODOLOGY

Layer coefficients were determined by use of two methods and the results were compared: 1) AASHTO nomographs, and 2) Equivalent stiffness.

AASHTO NOMOGRAPHS

The moduli determined in the laboratory phase were used directly with the layer coefficient nomographs in the 1986 AASHTO Guide, which reflect generic moduli-layer coefficient relationships. There are charts for dense graded asphalt surface course (a_1), unbound granular base (a_2), unbound granular subbase (a_3), cement treated base (a_2), and bituminous treated base (a_2). The relationships between layer coefficients and moduli were developed by Van Til et al. (5). Thus, by determining resilient modulus of asphalt mixtures and unbound base materials, and static modulus of cement-treated bases, the corresponding layer coefficients can be determined.

The nomographs were used in a second manner. Data from all approved MHTD mix designs for 1990 were used in a regression equation developed in this study which estimates resilient modulus. The resulting estimated moduli were applied to the nomographs to determine layer coefficients.

EQUIVALENT STIFFNESS

A second method of layer coefficient determination involved the solution of the following equation which relates MHTD material properties to AASHO Road Test properties as reported in the literature:

$$a_{n,MHTD} = a_{n,AASHO}\left[\frac{modulus,\ MHTD}{modulus,\ AASHO}\right]^{1/3} \quad . \ . \ . \ . \ . \ . \quad (2)$$

where: a_n = a_1 for Type C or I-C surface course mixtures

= a_2 for bituminous stabilized base course mixtures .

The moduli may be one of several types such as resilient modulus (M_R), dynamic modulus ($|E^*|$), or mixture stiffness (S_m). The above equation, originated by Odemark (14), was discussed by Corree and White (12) and is based on structural engineering concepts of equivalent stiffness for a composite layered material. Hereafter, Eq. 2 will be referred to as the Odemark equation.

MATERIAL TYPES AND SOURCES

All materials in the study were approved MHTD materials and were used in the specific mixtures as normally intended by MHTD. The material sources were selected and sampled by MHTD personnel.

ASPHALTIC CEMENT CONCRETE

Two types of asphaltic cement concrete were studied. These were MHTD wearing course mixtures: Type C and Type I-C. Included in the study were two grades of asphalt cement, two sources of coarse aggregate; one source of natural sand, two sources of manufactured sand, one source of mineral filler, and one source of hydrated lime. The materials, sources, and identification codes are shown in Table 3. All sources are located in Missouri except as noted. The two coarse aggregates were chosen by MHTD personnel to give a range of particle shape and texture.

PLANT MIX BITUMINOUS BASE

The plant mix bituminous base mixtures contained the same asphalt cements and natural sand as did the Types C and I-C mixtures. Two sources of coarse aggregate were used, and are shown in Table 3. The coarse aggregates were chosen by MHTD personnel to give a range of particle shape and surface texture.

Table 3. Material Types and Sources.

Nomenclature	Material	Sources	Location
DR-1	AC-20 grade asphalt cement	Sinclair Oil	Tulsa, OK
DR-2	AC-10 grade asphalt cement	Sinclair Oil	Tulsa, OK
DR-4	crushed St. Louis limestone	Weber Quarry North	Vigus
DR-5	crushed Burlington limestone	Conco Quarry	Willard
DR-6	crushed Gasconade dolomite	Lake Quarry #14	Osage Beach
DR-7	crushed Burlington limestone	Conco Quarry	Willard
DR-8	natural Missouri River sand	St. Charles Sand Co. #1	Bridgeton
DR-9A	manufactured Burlington limestone sand	Conco Quarry	Willard

DR-9B	manufactured St. Louis limestone sand	Weber Quarry	Vigus
DR-10	mineral filler	Columbia Quarry	Valmeyer,IL
DR-11	hydrated lime	Ash Grove Cement	Springfield

ESTIMATION OF ASPHALT MIXTURE STIFFNESS

GENERAL

Pavement engineers are interested in longevity of the pavement. Longevity is a function of material durability and structural response to load. Usually the pavement is designed structurally to give a favorable response to load, and durability is taken care of through specification of good materials. The elastic response to load of any material is a function of its stiffness, as defined by some sort of modulus. Thus, direct measurement or estimation of modulus becomes desirable. This reasoning has given impetus to the effort by the pavement industry to produce a type of modulus test that is suitable for practical use.

In order to determine layer coefficients via the Odemark equation, the mixture stiffness, dynamic modulus, or resilent modulus must be determined for each mix. This section deals with determination of mixture stiffness. Subsequent sections will deal with dynamic modulus and resilient modulus.

ASPHALT CEMENT STIFFNESS (S_b)

The stiffness of an asphalt mixture (S_m) has been defined as S_m = stress/strain (15). S_m has been shown by Van der Poel to be a function of asphalt binder stiffness (S_b), binder volume, and aggregate volume. While working with creep and dynamic testing of dense-graded asphalt mixtures, he developed a method with which to estimate binder stiffness (S_b). The use of his method involves a nomograph (Fig. 1). The required input data include penetration index

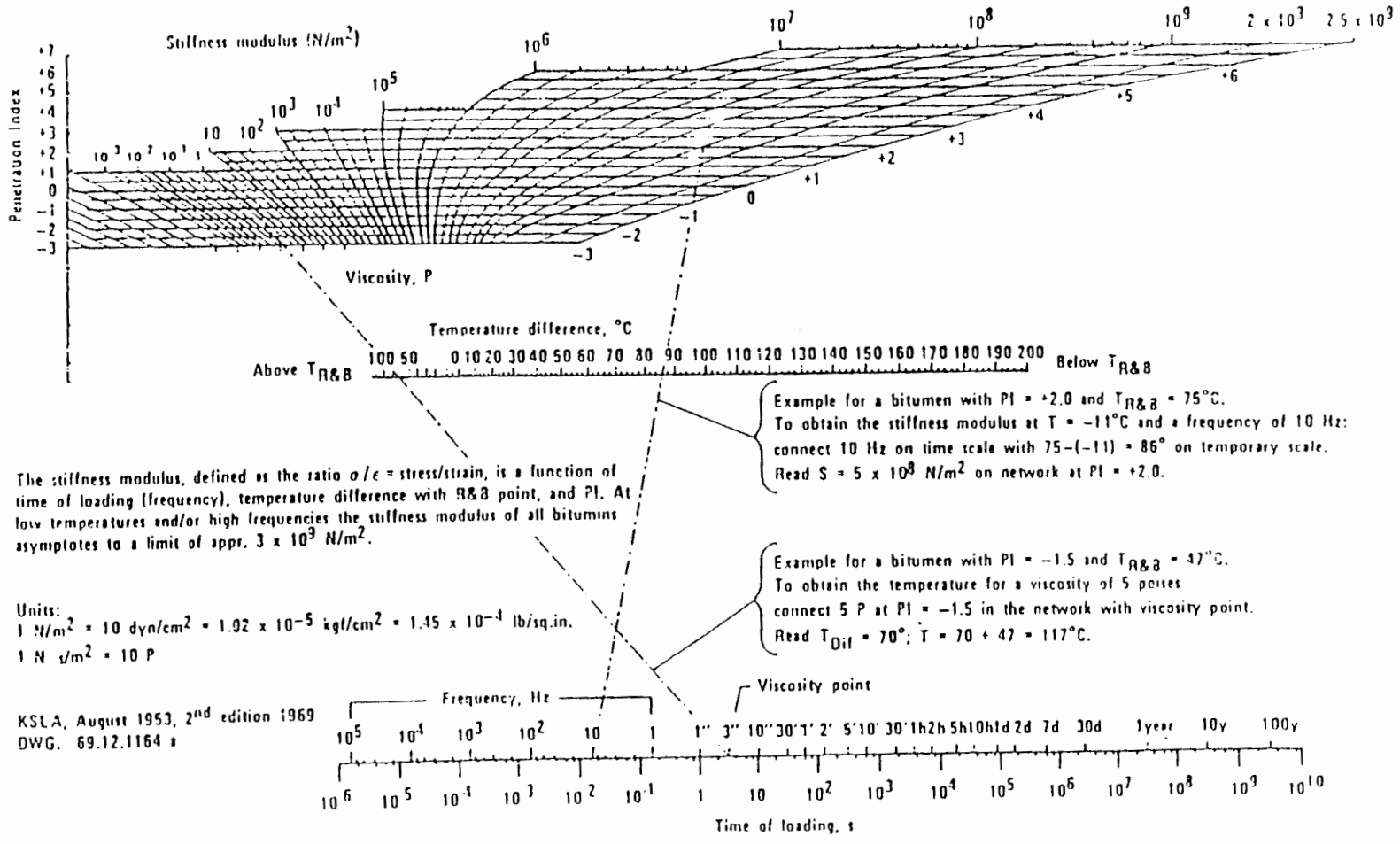

Fig. 1. Van der Poel Nomograph.

(PI), ring and ball softening temperature, binder temperature of interest, and duration of loading (or frequency of loading, if sinusoidal loading is employed).

S_b is very much dependent upon temperature: higher temperatures lead to lower asphalt stiffness. The amount of change in stiffness brought about by a change in temperature is termed the "temperature sensitivity" or "temperature susceptibility". Various researchers have developed indices to define temperature sensitivity. Probably the most common is the penetration index (PI).

Pfeiffer and Doormaal (16) developed the PI to characterize the temperature sensitivity of an asphalt cement. The penetration index of an asphalt cement is calculated from the results of penetration tests performed at two or more temperatures (T_1 and T_2), typically 77°F(25°C) or 39.4°F(4°C). The following formulae are used for calculating PI:

$$PI_{pen/pen} = \frac{20 - 500A}{1 + 50A} \quad \text{(3)}$$

$$\text{where: } A = \frac{\log pen \text{ at } T_1 - \log pen \text{ at } T_2}{T_1 - T_2} \quad \text{(4)}$$

The parameter "A" is the slope of the penetration - temperature curve, a measure of temperature susceptibility. The units of temperature should be in °C. In the original method, in lieu of performing the penetration test at the higher temperature, a penetration of 800 was substituted. This value corresponds to approximately the softening point for most asphalts. Thus, if T_1 is 25°C, then T_2 will be the ring and ball softening temperature. The calculation of A becomes:

$$A = \frac{\log 800 - \log pen\ @\ 25^{\circ}C}{RB\ softening\ point - 25^{\circ}C} \quad . \quad . \quad . \quad . \quad . \quad . \quad (5)$$

Use of the Pfeiffer and Doormaal method is shown in Fig. 2.

The calculation of PI from the results of two or more actual penetration tests has been shown by Heukelom (17) to give more accurate results (Eq. 4). Heukelom recommended use of a "Bitumen Test Data Chart" (BTDC) which allows plotting of both penetration and viscosity versus temperature on the same graph, thus extending the range of temperature. This is shown in Fig. 3.

Some asphalts exhibit different slopes for different parts of the penetration/viscosity temperature curve. Thus, Heukelom recommended that the portion of the curve representing the temperature range of interest should be used, if possible, in computing the PI. Heukelom recommended that in the low temperature (penetration) range, the curve should be established with several penetration tests, and that the PI should be calculated from this, rather than the curve derived from Pfeiffer and Doormaal's original method. Secondly, Heukelom recommended that the line should be extrapolated downward to intersect the penetration = 800 line, and the temperature at this point ($T_{pen\ 800}$) should be used in the Van der Poel nomograph instead of the $T_{R\&B}$. This is shown in Fig. 3. In practice, the ring and ball temperature specification is no longer commonly specified. And, performing penetration at a second temperature is easier than running the ring and ball test. Thus, in this study, PI was calculated based on performing the penetration test at two temperatures.

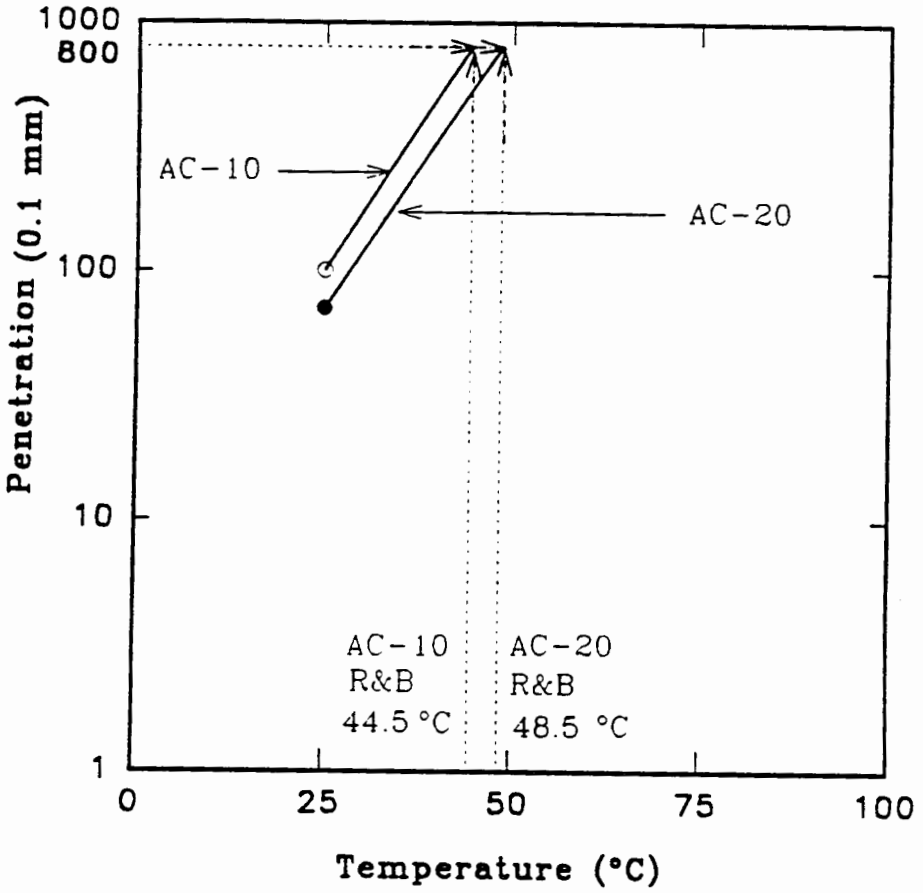

Fig. 2: Determination of $PI_{R\&B}$.

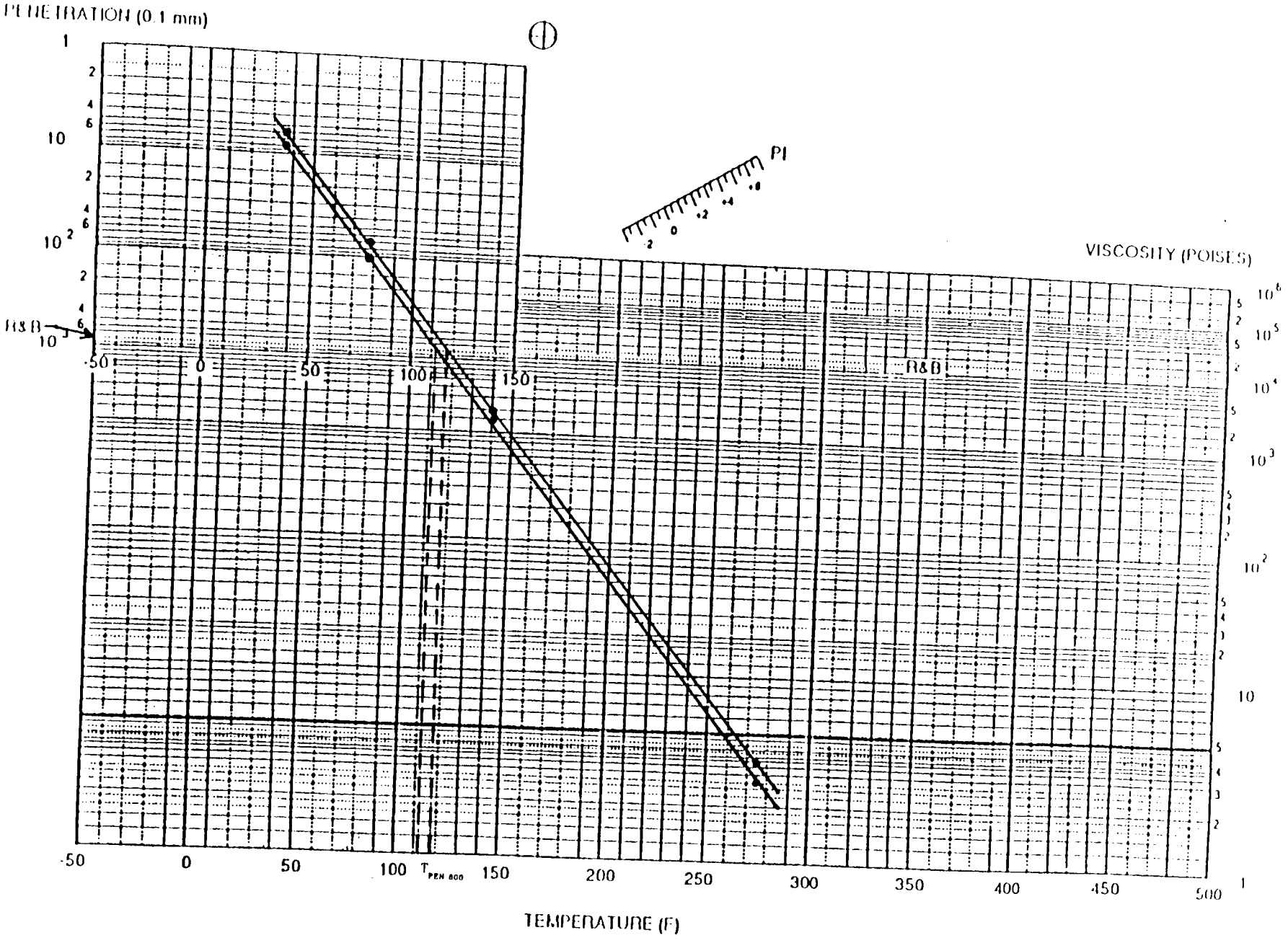

Fig. 3. Determination of $T_{PEN\ 800}$.

BONNAURE MIXTURE STIFFNESS (S_m)

In conjunction with Van der Poel's method of estimating binder stiffness, several investigators (15,18-20) have provided methods to approximate the stiffness of the asphalt mixture (S_m). Most methods involved a narrow range of asphalt mixture types. However, Bonnaure et al. (21) developed an equation to arrive at S_m which is based on dynamic testing of a wide range of mixture types. Bonnaure et al. utilized the Van der Poel binder stiffness value (S_b), but on plant-aged asphalts, to better represent asphalt stiffness in the field. This procedure has been adopted in the Shell pavement design method (22). A nomograph depicting its use is shown in Fig. 4. The Bonnaure et al. equation is as follows:

for $5 \times 10^6 < S_b < 10^9$ N/m^2:

$$\log S_m = \left[\frac{S_w + S_x}{2}\right](\log(S_b) - 8) + \left[\frac{S_w - S_x}{2}\right]|\log(S_b) - 8| + S_y \quad (6)$$

for $10^9 < S_b < 3 \times 10^9$ N/m^2:

$$\log S_m = S_y + S_w + 2.096\,(S_z + S_y + S_w)\,(\log S_b - 9) \quad (7)$$

where:

S_m = mixture stiffness, N/m^2

$$S_x = 0.6 \log\left[\frac{1.37\ V_b^2 - 1}{1.33\ V_b - 1}\right] \quad (8)$$

$$S_y = 8.0 + 5.68 \times 10^{-3}\ V_a + 2.135 \times 10^{-4}\ V_a^2 \quad (9)$$

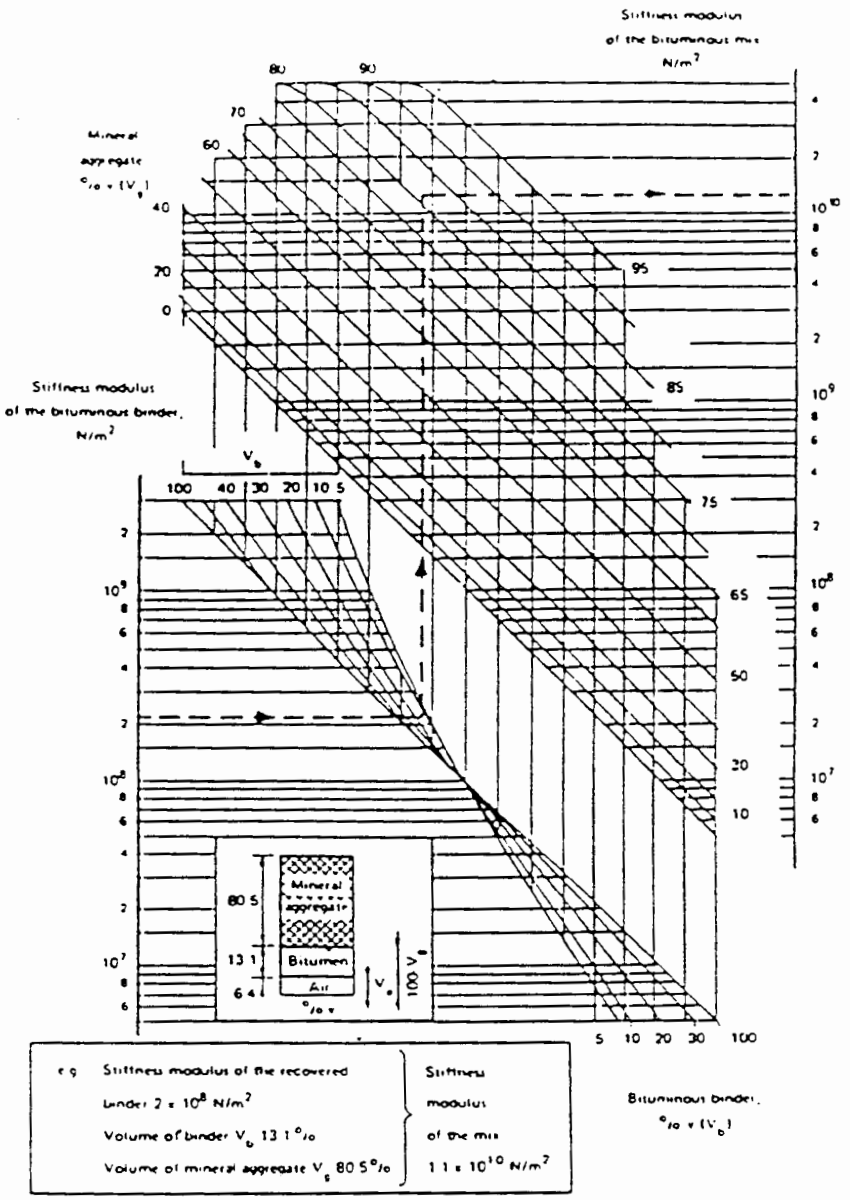

Fig. 4. Determination of Mixture Stiffness (S_m).

$$S_z = 10.82 - 1.342 \left[\frac{100 - V_b}{V_a + V_b}\right] \quad (10)$$

$$S_w = 0.76\ (S_z - S_y) \quad (11)$$

V_a = %volume of aggregate

V_b = %volume of binder.

Plant-aged asphalt penetration and ring and ball values can be obtained from recovered asphalt from field cores or simulated from recovered laboratory-aged asphalt residue. In lieu of laboratory aging of asphalt, Coree and White (12) drew upon the work of Ullidtz (23) to approximate aged asphalt penetration (pen_r) and PI (PI_r) values to arrive at S_b:

$$Pen_r = 0.65\ Pen_i \quad (12)$$

$$PI_r = \left[\frac{27 \log pen_r - 31.2}{76.35 \log pen_r - 219.27}\right] \quad (13)$$

where: Pen_i = original penetration at 77°F.

Thus, knowing characteristics of the asphalt and conditions of temperature and loading, S_b(N/m^2) can be calculated instead of using Fig. 1:

$$S_b = \left[(1.157 \times 10^{-7}\ t^{-0.368}) (e^{-PI_r}) (T_{R\&B.r} - T_p)^5 \right] \times 10^6 \quad (14)$$

where: t = time of loading, sec

PI_r = PI of recovered asphalt

$T_{R\&B.r}$ = $T_{R\&B}$ or T_{pen800} on recovered asphalt

= 99.13 - 26.35 log pen_r, °C (15)

T_p = asphalt temperature, °C.

Coree and White (12) drew on work by Witczak (24) to estimate the prevailing pavement temperature (T_p), which is a function of air temperature and asphalt pavement layer thickness. Witczak's equation predicts pavement temperature (T_p) at any depth:

$$\bar{T}_p = 6.0 - \frac{34}{(z + 4)} + \bar{T}_A \left[1 + \frac{1}{(z + 4)}\right] \quad \text{(16)}$$

where: $\bar{T}_A$ = mean air temperature

z = depth in the asphalt layer, in, usually taken at one-third depth.

Alternatively, the mean-value theorem (25) can be employed to find the expected mean layer temperature $\bar{T}_p$ in a layer of z-thickness:

$$\bar{T}_p = 6.0 - \frac{34 \ln\left[\frac{4}{z+4}\right]}{Z} + \bar{T}_A\left[1.0 - \left(\ln\left[\frac{4}{z+4}\right]\right)/2\right] \quad \text{(17)}$$

where: $\bar{T}_A$ = average yearly air temperature, °F

z = thickness of asphalt layer, in.

The Ullidtz "S_b" equation is based on the Van der Poel nomograph. It is considered applicable for the ranges of:

$$0.01 < t < 0.1 \text{ sec}$$

$$-1.0 < PI_r < +1.0$$

$$-10°C < T_{R\&B,r} - T_p < 70°C$$

McLEOD MIXTURE STIFFNESS (S_{mPVN})

McLeod (20) developed an alternate approach to determining S_b, which was orginally proposed by Lefebvre (26). McLeod felt that the PI did not handle waxy asphalts well because these asphalts tend to exhibit a false softening point. He advanced a different measure of temperature sensitivity called the "penetration-viscosity number" (PVN), which is calculated as follows:

$$\log V = 4.25800 - 0.79670 \log P \quad (18)$$

$$\log V = 3.46289 - 0.61094 \log P \quad (19)$$

$$PVN = [(\log L - \log X)/(\log L - \log M)] (-1.5) \quad (20)$$

where: V = viscosity in Cs at 275°F (135°C) for an asphalt with a PVN = 0.0 (Eq. 18) or PVN = -1.5 (Eq. 19)

P = penetration at 77°F (25°C)

L = antilog of log V (Eq. 18)

M = antilog of log V (Eq. 19)

X = viscosity in Cs at 275°F (135°C) for the asphalt at any PVN (the asphalt of interest).

McLeod modified the Van der Poel nomograph to allow substitution of PVN for PI. He also substituted a "base temperature" for the $T_{R\&B}$. To use his S_b nomograph, one first needs to determine the difference between base temperature and the penetration test temperature. This is done by use of Fig. 5. Then one enters McLeod's S_b nomograph (Fig. 6) with load duration, difference between base

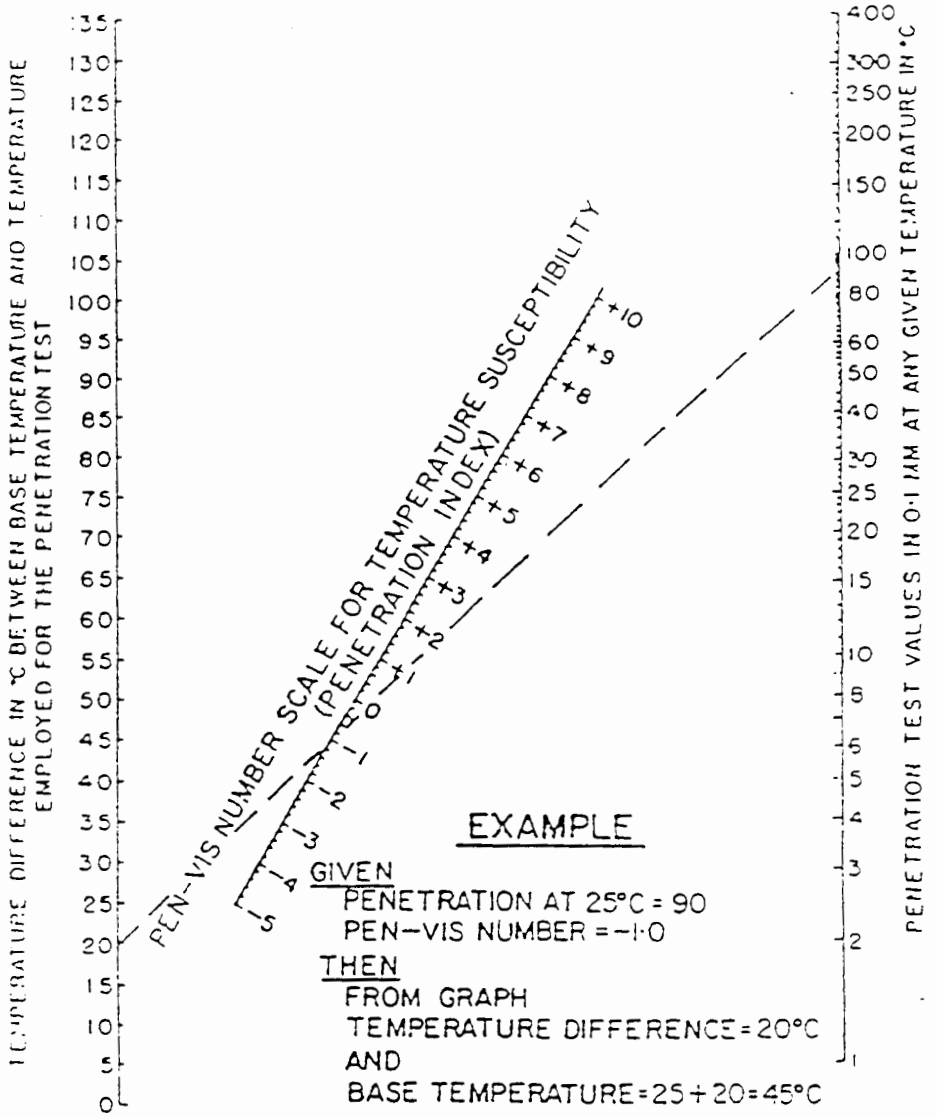

Fig. 5. McLeod's Temperature Difference Nomograph.

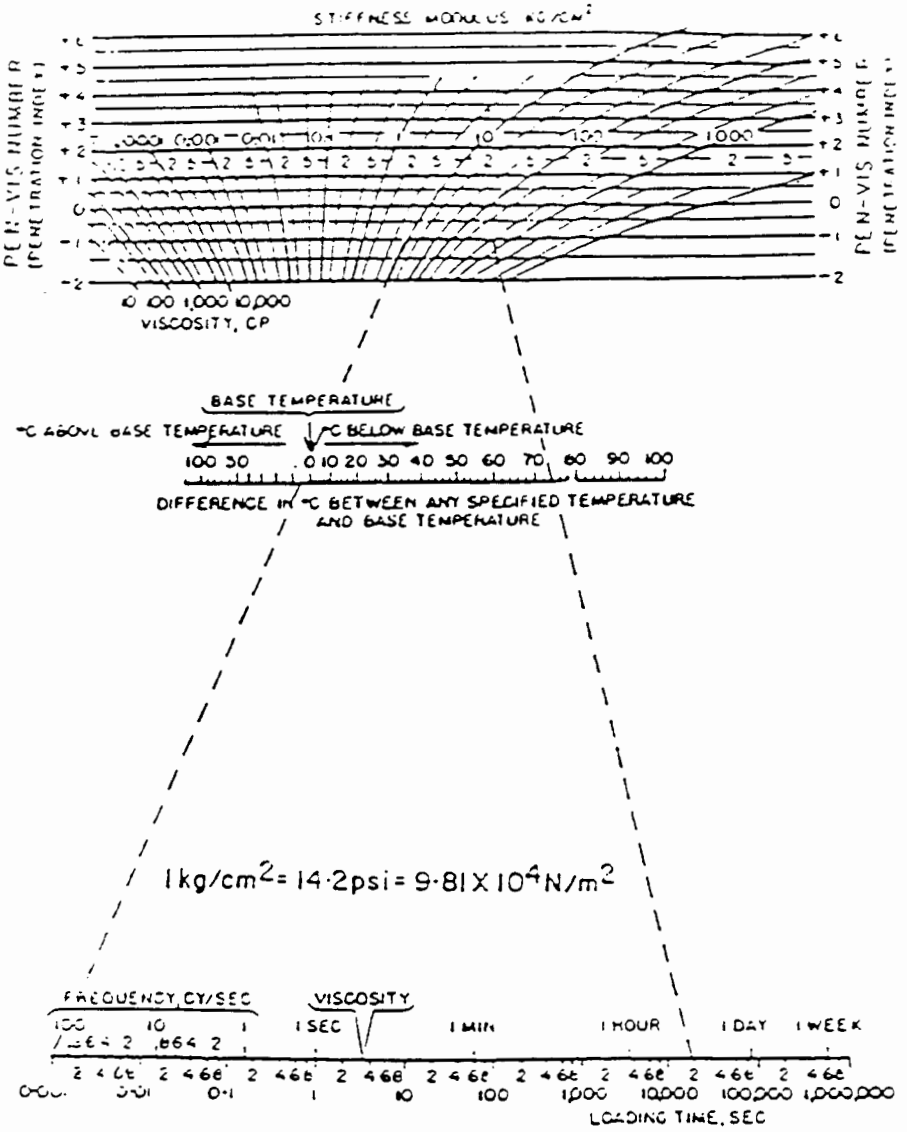

Fig. 6. McLeod's Modified Van der Poel Nomograph.

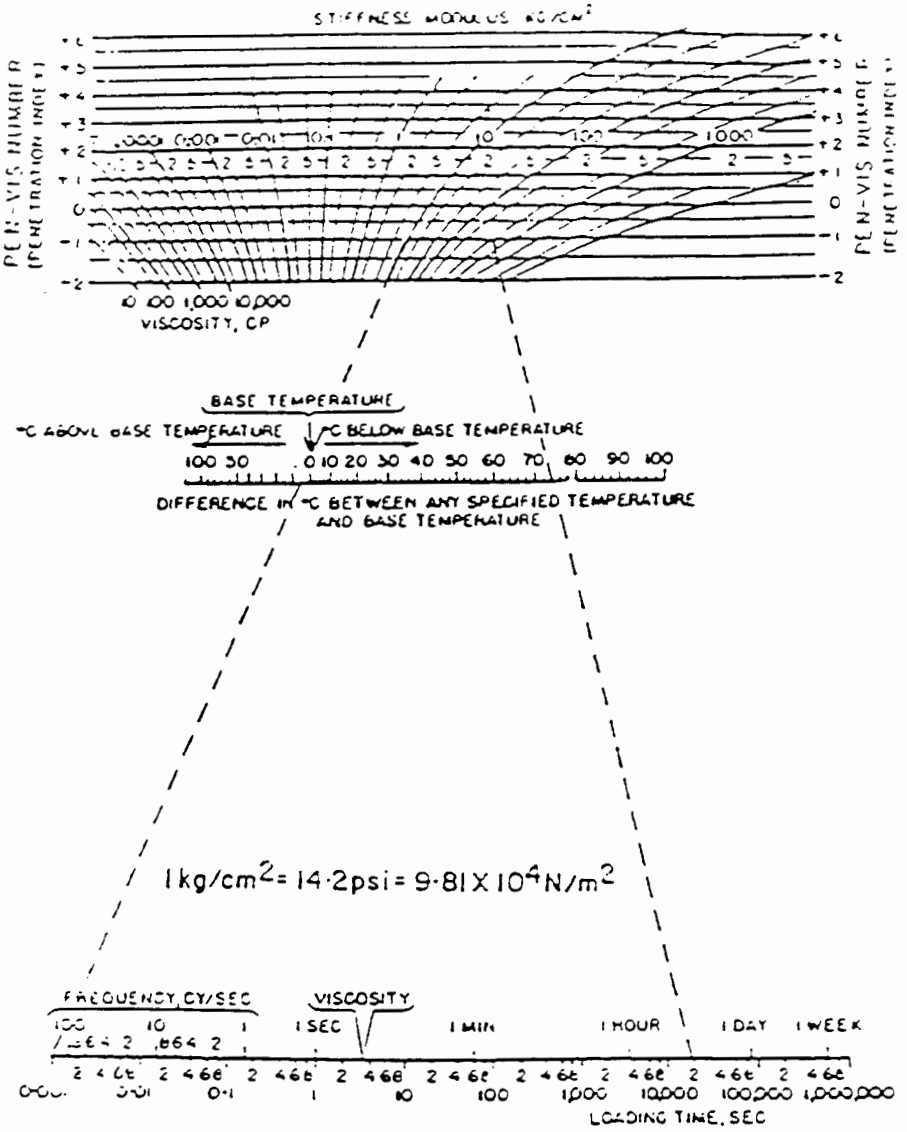

Fig. 6. McLeod's Modified Van der Poel Nomograph.

3. Alternate equations for conversion of penetration values at 4° and 25°C were developed in this study from a review of the literature (27-30):

$$\log Pen_{4aged} = 0.942 \log Pen_{4orig} - 0.124 \quad (21)$$

$$\log Pen_{25aged} = 0.559 Pen_{25orig} + 6.033 \quad (22)$$

Unaged penetration data developed in the present study were then substituted into these equations to estimate aged penetration values. This information was substituted into Eqs. 3 and 4 to calculate aged PI values. Aged $T_{R\&B}$ values were estimated by substituting the values for Pen_{25} calculated via Eq. 22 into Eq. 15.

4. In a similar manner to method 3 above, an alternate equation for conversion of PI values directly to aged PI was developed:

$$PI_{aged} = 0.530 PI_{orig} - 0.639 \quad (23)$$

Aged $T_{R\&B}$ was calculated by the following methods:

1. Conversion of pen_{orig} values to pen_r values via Eq. 12 and then substitution into Eq. 15.
2. An alternate aged $T_{R\&B}$ equation was developed from the literature:

$$T_{R\&B,aged} = 0.843 T_{R\&Borig} + 12.501 \quad (24)$$

Then S_b was calculated by use of two methods:

1. Calculation of S_b via Eq. 14 by use of the various values of PI_r.

2. Calculation of S_b via Fig. 6 by use of PVN from Fig.5.

S_m values were then calculated via Eq. 6 by use of $S_b$values determined from each of the above two ways. This resulted in five different ways to calculate mixture stiffness as summarized in Table 4. Mixture stiffnesses from all methods were then correlated to laboratory-derived values of resilient modulus to determine which S_b method was superior.

Table 4. Alternate Methods of Mixture Stiffness Determination.

Mixture Stiffness Parameter	Methods of Parameter Determination				
	Pen_r	PI	$T_{R\&B}$	S_b	S_m
S_m	Eq. 12 (Ullidtz)	Eq. 13 (Ullidtz)	Eq. 15 (Ullidtz)	Eq. 14 (Ullidtz)	Eq. 6 (Bonnaure)
S_{mm}	Eq. 12 (Ullidtz)	Eq. 3 and 4 (Pfeiffer and Doormaal)	Eq. 15 (Ullidtz)	Eq. 14 (Ullidtz)	Eq. 6 (Bonnaure)
$S_{mrm,aged}$	Eq. 21 and 22 (Richardson)	Eq. 3 and 4	Eq. 24 (Richardson)	Eq. 14 (Ullidtz)	Eq. 6 (Bonnaure)
$S_{m,aged}$	N/A	Eq. 23 (Richardson)	Eq. 24 (Richardson)	Eq. 14 (Ullidtz)	Eq. 6 (Bonnaure)
S_{mPVN}	N/A	Eq. 20 (McLeod) for PVN	Fig. 5 (McLeod)	Fig. 6 (McLeod)	Eq. 6 (Bonnaure)

SUMMARY

The mixture stiffness (S_m, S_{mm}, $S_{m,aged}$, $S_{mrm,aged}$, S_{mPVN}) of the mixtures examined in this study were estimated by six methods; five using an aged form of S_b and one using S_{bPVN}. The results were correlated with actual test results of

resilient modulus to judge which estimation method was best. Then the results were used in the Odemark equation to determine layer coefficients:

$$a_n = a_{n,\ AASHO}\left[\frac{S_m,\ UMR\ or\ MHTD}{S_m,\ AASHO}\right]^{1/3}$$

ESTIMATION OF DYNAMIC MODULUS

GENERAL

Shook and Kallas (31) developed a regression equation to estimate the dynamic modulus of various bituminous mixtures from mixture properties. Numerous modifications have appeared in the literature (32-34), culminating in two alternate equations. The choice of equation depends on the character of input data available to the user. Both equations were used in this study to assist in determining layer coefficients. The two equations are presented by Akhter and Witczak (34), and are as follows:

$$\begin{aligned}\log |E^*| = {} & 1.45716 - 0.0256272 * P_{air} + 0.0127921 * P_{3/4} + 0.0627099 * \eta \\ & - 0.00837349 * T + 0.147306 * \log f + 0.0000193164 * \log f * T^2 \\ & - 0.0000254103 (P_{effv} - P_{opteffv} + 8.0)^{0.5} * T^2 \\ & - 0.000149152 * P_{effv} * P_4 + 0.00591768 * P_{200} * P_{absw}\end{aligned} \quad (25)$$

$$\begin{aligned}\log |E^*| = {} & 1.42841 - 0.0233473 * P_{air} + 0.013004 * P_{3/4} + 0.0627099 * \eta \\ & - 0.008145 * T + 0.146970 * \log f + 0.0000193776 * \log * T^2 \\ & - 0.000073466415 * T^2 - 0.000138513 * P_{effv} * P_4 \\ & + 0.00583715 * P_{200} * P_{absw}\end{aligned} \quad (26)$$

where $|E^*|$ = dynamic modulus, psi

P_{air} = percent air voids

$P_{3/4}$ = accumulative percent retained on the 3/4 in sieve, by weight of aggregate (called $AR_{3/4}$ in the rest of this report)

P_4 = accumulative percent retained on the #4 sieve, by weight of aggregate (called AR_4 in the rest of this report)

P_{200} = percent passing #200 sieve, by weight of aggregate

f = frequency of load application

η = absolute viscosity @ 70°F, poises x 10^6

P_{effv} = percent effective asphalt content, by volume

T = temperature, °F

$P_{opt\ effv}$ = percent effective optimum asphalt content, by volume

P_{absw} = percent absorbed asphalt, by weight of mix.

The dynamic modulus ($|E^*|$) is defined as the elastic portion of the complex modulus, which also takes into account the viscous nature of asphalt cement. The complex modulus is expressed as follows:

$$E^* = E' + iE''$$

where: $E' = |E^*| \cos \delta$

$E'' = |E^*| \sin \delta$

i = imaginary number

δ = phase angle, represents lag of strain peak behind stress peak.

If the phase angle is assumed to be zero, which approximates what would occur for short, relatively light load applications, then the complex modulus is

reduced to one term, which is commonly called the dynamic modulus:

$$|E^*| = \frac{\sigma_{max}}{\epsilon_{max}} \quad . \quad . \quad . \quad . \quad . \quad . \quad . \quad . \quad . \quad . \quad . \quad (27)$$

where: σ_{max} = maximum applied sinusoidal stress

ϵ_{max} = maximum recoverable strain.

The dynamic modulus can be determined by applying axial compressive cyclic pulses in the form of a compressive sine wave to 4 in (10.2 cm) diameter 8 in (20.3 cm) long cylinders. The test has fallen into disuse because of its cumbersome testing technique and because it has been criticized for not being appropriate for pavement design/analysis methods which use elastic layer assumptions. It has been largely supplanted by the repeated load indirect diametral tensile test, which is discussed later in this report. However, the Akhter and Witczak equations are still well-known. Their usefulness was examined in this study.

SUMMARY

The dynamic modulus concept is useful for this study as follows. The required input for Eq. 26 (referred to hereafter as the Akhter-Witczak equation) is available from Road Test data, UMR-study data, and MHTD mix design data. Thus, use of Road Test, UMR-study, and MHTD dynamic moduli in the form of estimated values can be used in the Odemark equation in the determination of layer coefficients:

$$a_{n,\ UMR\ or\ MHTD} = a_{n,AASHO}\left[\frac{|E^*|_{UMR\ or\ MHTD}}{|E^*|_{AASHO}}\right]^{1/3}$$

RESILIENT MODULUS

The resilient modulus is a repeated load test that is similar to the dynamic modulus but with several important differences. The applied stress wave form is usually in the form of a stress pulse followed by a rest period, rather than the sinusoidal wave form (with no rest period) as used in the dynamic modulus test. The test equipment is less complex. There are two different ways in which the test can be performed. One method, AASHTO T-274 (35), utilizes compression testing of 4 in (10.2 cm) diameter 8 in (20.4 cm) high specimens in a triaxial chamber. The second method (which is now the predominant method), ASTM D4123 (36), involves the inducement of indirect tensile stress diametrally to Marshall-type specimens. The latter test is more convenient to perform, and is the method used in this study. It is the recommended test in both AAMAS (Asphalt-Aggregate Mixture Analysis System)(37) and in the latest SHRP (Strategic Highway Research Program)(38) protocol.

Several regression equations were developed in this study to enable practitioners to estimate the resilient modulus of asphalt mixtures by the simple substitution of mix characteristics and other readily accessible data into the equation. One equation is solely based on experimental data generated in this study. A more generally applicable equation was developed by use of resilient modulus data gleaned from the literature combined with data from this study.

Layer coefficients were determined by applying the resilient modulus data developed in this study along with estimations of resilient modulus to the AASHTO nomographs. Also, layer coefficients were determined by use of the equivalent stiffness method (Odemark equation). The input included estimated resilient modulus data and estimated resilient modulus from AASHO Road Test mixtures:

$$a_{n,\ UMR\ or\ MHTD} = a_{n,\ AASHO} = \left[\frac{M_{R,\ UMR\ or\ MHTD}}{M_{R,AASHO}}\right]^{1/3}$$

LABORATORY INVESTIGATION

MIX DESIGNS

Mix designs were developed for Type C, I-C, and plant mix bituminous base. The main thrust of this portion of the study was to determine layer coefficients for the three types of mixtures based on repeated load indirect tensile diametral tests. This is the test recommended in the 1986 AASHTO pavement design method (1). A secondary goal was to develop regression equations to enable the subsequent prediction of resilient modulus without having to actually perform the test in cases where M_R test data is unavailable.

As mentioned previously, the factors that affect asphalt mixture stiffness most significantly are temperature, effective asphalt content, voids, asphalt viscosity, loading frequency or duration, and gradation.

The study was limited to observing the effects on resilient modulus by varying aggregate gradation, coarse aggregate type, temperature, asphalt cement grade, asphalt content, and indirectly, void content. The latest SHRP protocol (38)

has omitted test load frequency as a variable, therefore frequency was not varied in this study.

The proposal for this study did not include the performance of mix designs for two reasons: 1) limited available funds and limited contract duration, and 2) the thrust of the research was to study the effects of varying the aggregate gradation across an acceptance band, with the interaction of asphalt content and grade. However, to assist in determining optimum asphalt content during this part of the study, Marshall mix designs were performed for all mixtures containing AC-20 grade asphalts. Some mixtures had AC-10 asphalt substituted for the AC-20 with no change in mix design because mixing and compaction temperatures were controlled to give the same viscosities independent of asphalt grade.

Two gradations each were chosen for the Type C, I-C, and bituminous base mix materials, resulting in six gradations. These were picked by a process which involved determining the coarsest and finest job mix formula (JMF) gradations that were approved by the MHTD during the 1990 and partial 1991 seasons. Then, to get an even wider separation of gradation, the coarsest JMF gradation was pushed to a coarser gradation by use of the maximum allowable tolerance on each sieve. Likewise, the finest JMF was pushed to a finer gradation via the maximum allowable tolerances. Some adjustment was necessary to keep the gradations within the master specifications on some sieves, and at the - #200 sieve in order to prevent cross-over of the experimental gradation lines at that point. It was realized that some of these mixes may not have been approved in routine work,

but they do approximate where some gradations may end up in the field after adjustment.

Two coarse aggregate sources each were used for the Type C, I-C, and bituminous base materials. These were chosen by MHTD personnel to exhibit a wide variation in particle shape and texture.

Two asphalt cement grades were chosen (AC-10 and AC-20) to represent the most commonly used grades for MHTD mixes.

Using the above 12 gradation/coarse aggregate combinations, Marshall mix analyses were made to determine optimum asphalt contents. Once these were determined, an additional asphalt content was determined by arbitrarily adding 0.5% asphalt to the previously determined optimum asphalt contents. Thus, 48 mixtures in all were evaluated in the resilient modulus testing: 16 mixtures each for the Type C, I-C, and bituminous base mixtures. These are shown in Table 5.

Table 5. Asphalt Mixture Mix Design Parameters.

	Coarse Aggregate 1				Coarse Aggregate 2			
	AC-10		AC-20		AC-10		AC-20	
Asphalt Content	Opt.	+0.5 %	Opt.	+0.5 %	Opt.	+0.5 %	Opt.	+0.5 %
Fine Gradation	X	X	X	X	X	X	X	X
Coarse Gradation	X	X	X	X	X	X	X	X

Note: 1. This chart applicable to Type C, I-C, and bituminous base mixes. Thus 48 mixtures were used.
2. "X" denotes that this combination of parameters was represented by a mix.

The choice of using the Marshall mix design method for determining

optimum asphalt contents was based on several factors. First, it is the most commonly used method by state and federal agencies, private practice, the Asphalt Institute, and the National Center for Asphalt Technology. Second, the MHTD utilizes this method to a certain extent in its mix design evaluation. Third, personnel communication with MHTD personnel indicates that the Marshall method will be the preferred method if a contractor QC/QA program is initiated, and fourth, the UMR Bituminous Laboratory is equipped with Marshall equipment and has experience with using this method.

The optimum asphalt contents were chosen based on percent air voids as a major criteria, but also were optimized in an attempt to satisfy MHTD requirements for stability, voids filled, dust/asphalt, VMA, percent natural sand, inclusion of hydrated lime, percent asphalt, and makeup of fines where applicable. Although flow is not specified by the MHTD, this parameter was also used as a guidance criteria.

It was decided that in order to make comparisons from mix to mix within a given type (C, I-C, or bituminous base) of mixture, the percent of aggregate constituent (coarse, natural sand, manufactured sand, mineral filler, and hydrated lime) per sieve would be kept constant. For example, for the Type C mixes, at the #16 sieve, all 16 mixtures would retain 0% coarse aggregate, 79% natural sand, 21% manufactured sand, and 0% mineral filler.

The decision about the kind of materials going into each mix type was made by examining the 1990(-91) MHTD-approved job mixtures. It was found that, on

average, the Type C mixtures contained 48.0% coarse aggregate, 24.1% natural sand, 22.9% manufactured sand, and 5.0% mineral filler. The percent retained of each type of aggregate on a particular sieve had to be changed from sieve to sieve in some cases in order to make the total contribution of each material type reasonable. The gradations are given in Table 12 in the "Results" section of this report.

The following are brief descriptions of the test methods employed in this study. Where applicable, AASHTO (39) standards were used.

ASPHALT CEMENT

Penetration

Both grades of asphalt were tested for penetration as per AASHTO T49-89. Test temperatures were 77°F (25°C) and 37.8°F (3.2°C). The penetration at 77°F (25°C) information was necessary for calculating $PI_{R\&B}$, $PI_{pen/pen}$, PVN, and for use in the Ullidtz aged penetration equation. Penetration at 37.8°F (3.2°C) was necessary for calculating $PI_{pen/pen}$. Both were used for estimating T_{pen800}.

Kinematic Viscosity

The asphalt cements were tested at 275°F (135°C) in accordance with AASHTO T201-90. This information was required for calculation of PVN, for determination of mixture mixing and compaction temperatures, and for estimation of viscosity at 70°F (21.1°C).

Absolute Viscosity

Test temperature of this AASHTO T202-90 procedure was 140°F (60°C).

These data were necessary for determination of mixture mixing and compaction temperatures and for estimation of viscosity at 70°F (21.1°C).

Specific Gravity

The AASHTO T228-90 procedure was performed on the asphalts at 77°F (25°C). These data were used for volume calculations in the mix design process and for estimation of absolute viscosity at 70°F (21.1°C).

Ring and Ball Softening Point

This AASHTO T53-89 procedure was performed in order to calculate $PI_{R\&B}$ and for use with the Van der Poel nomograph. Fig. 7 depicts the ring and ball softening point device.

AGGREGATE

Initial Gradation

Gradations of the aggregates, mineral filler, and hydrated lime supplied by MHTD personnel were determined in accordance with AASHTO T 27-88, T 37-87, and T 19-87, respectively. Weighing was performed on an electronic balance capable of reading to the nearest 0.1 g. This information was useful for determining the necessity of additional material to build the test gradations.

Final Gradation

Each of the 12 gradations were built on a sieve by sieve basis as mentioned previously. Final gradations were necessary for determination of aggregate specific gravity and for making asphalt mixture specimens. Fig. 8 depicts the steel storage bins used for each fraction of each type of aggregate.

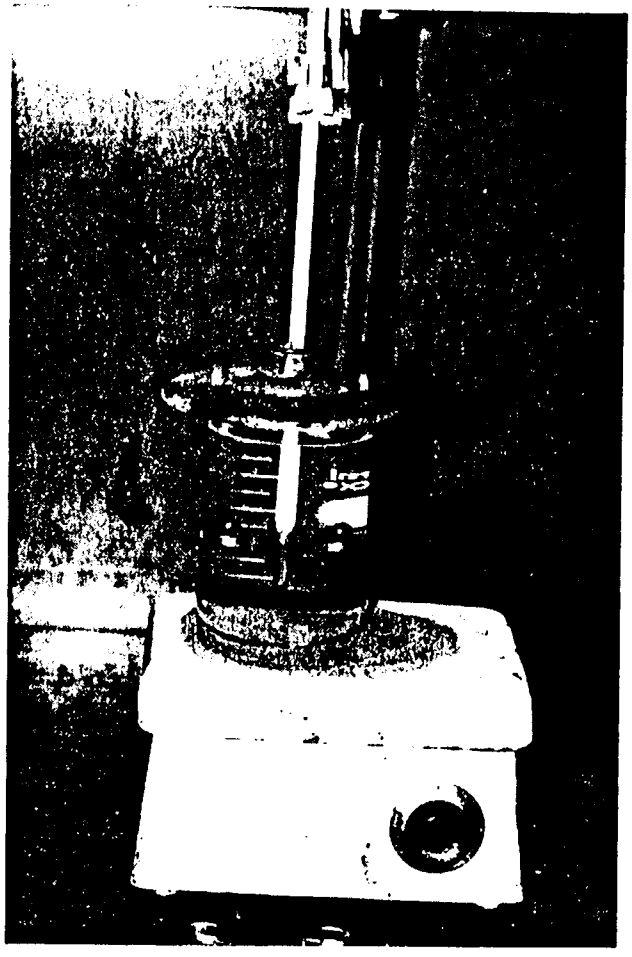

Fig. 7. Ring and Ball Softening Point Device.

Fig. 8. Asphalt Mixture Aggregate Fraction Storage Bins.

Particle Shape and Surface Texture

Numerous studies have shown that aggregate particle shape and texture have a significant effect on various properties of dense-graded asphalt cement concrete mixtures. It is difficult to separate the effects of shape and texture. The general consensus seems to be that as angularity and surface roughness increase, the following also increase: stability, resistance to rutting, VMA, and optimum asphalt content. Opinions are somewhat mixed as to the effect of shape and texture on static indirect tensile strength (IDT). In regard to IDT, Kalcheff and Tunnicliff (40) found little difference between various particle shape/textures. The explanation was that, in compression, particles attempt to slide past each other, therefore shape/texture is important. But, in tension, the effect is much less pronounced. However, Hadley, et al. (41,42) found that more angular/rough particles do tend to result in higher IDT values. Also, the literature indicates that the characteristics of the fine aggregate are much more important than those of the coarser fraction.

Numerous test methods have been devised to quantify particle shape and/or texture. These can be divided into direct methods (those that result in measurements or aspects of individual particle shape or texture) and indirect methods (those that measure some sort of bulk aggregate property, such as void content, which is related to particle shape/texture). Recent evaluations of these methods were reported by Meier and Elnicky (43), Mogawer and Stuart (44), and Kandhal et al. (45) at NCAT (National Center for Asphalt Technology). It appears

that efforts are being concentrated in the area of fine aggregate evaluation, and that there are several methods available which can be used in lieu of the standard test, ASTM D 3398 (46) which is somewhat cumbersome to perform. Kandhal et al. recommended the National Aggregate Association's (NAA) proposed method (A or B) for fine aggregate (47). Both of these are indirect methods of particle shape determination.

In this study, the (-) #8 to(+) #100 sieve size material of each asphalt mixture blend were tested using the NAA Method A. The method is given in Appendix A of this report. For the (+) #4 size, the blends were tested in accordance with ASTM D 3398. This method is given in Appendix B. The results of both methods were used in developing the indirect tensile strength and resilient modulus regression equations discussed later in the "Results" section of this report. Photographs of the NAA test device and the D3398 equipment are shown in Figs. 9 and 10.

Specific Gravity

Aggregate fractions of each of the 12 gradations were separated at the #4 and #100 sieve sizes and tested in accordance with AASHTO T85-88 and T84-88 for the (+)#4 and (-)#4 to (+)#100 material, respectively. For the (-)#100 material, specific gravity was determined in accordance with MHTD T37-4-84. These data were used for voids analyses calculations. Weighing was performed on a scale readable to the nearest 0.1 g.

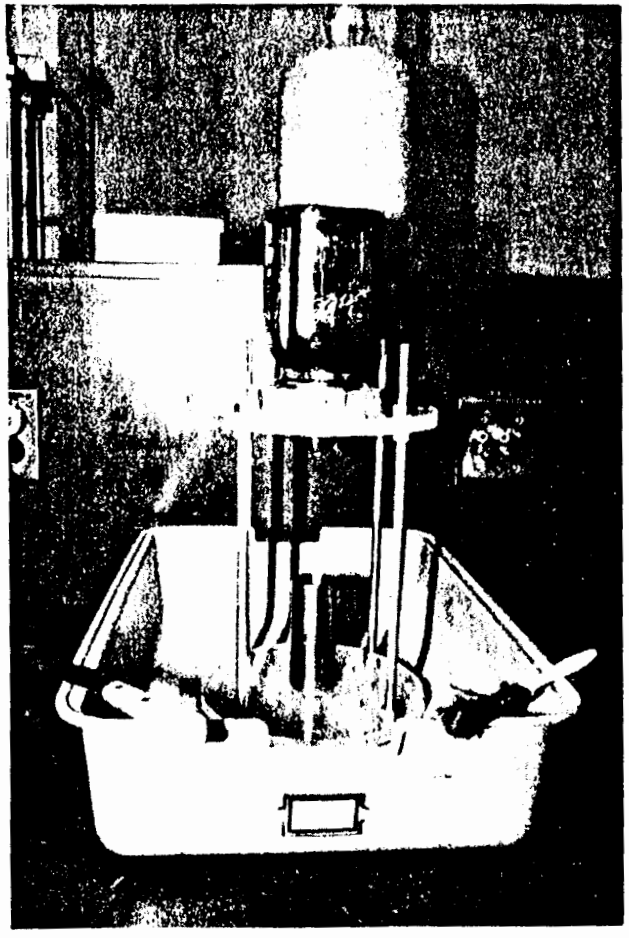

Fig. 9. NAA Method Particle Shape Device.

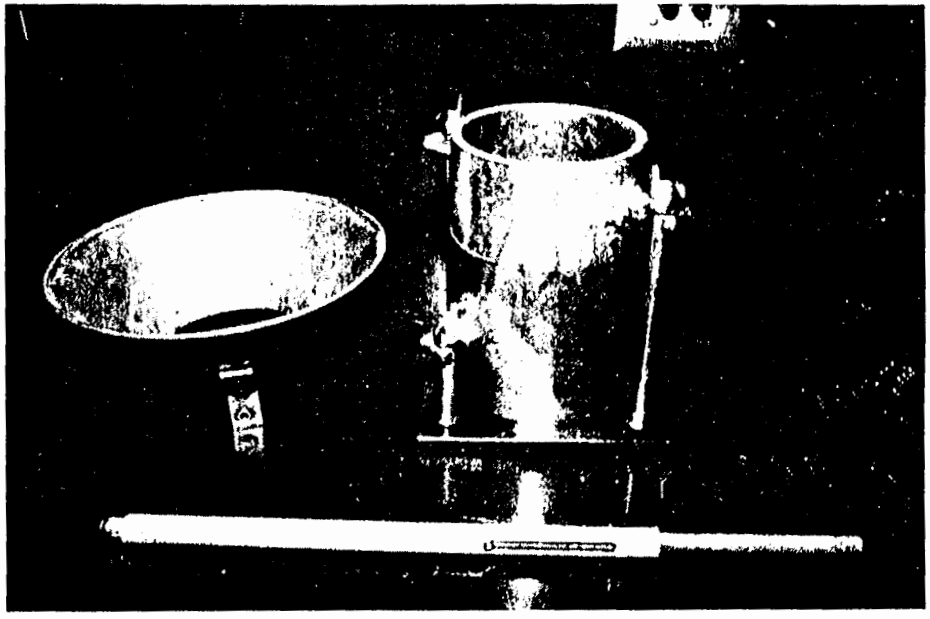

Fig. 10. D3398 Particle Shape Equipment.

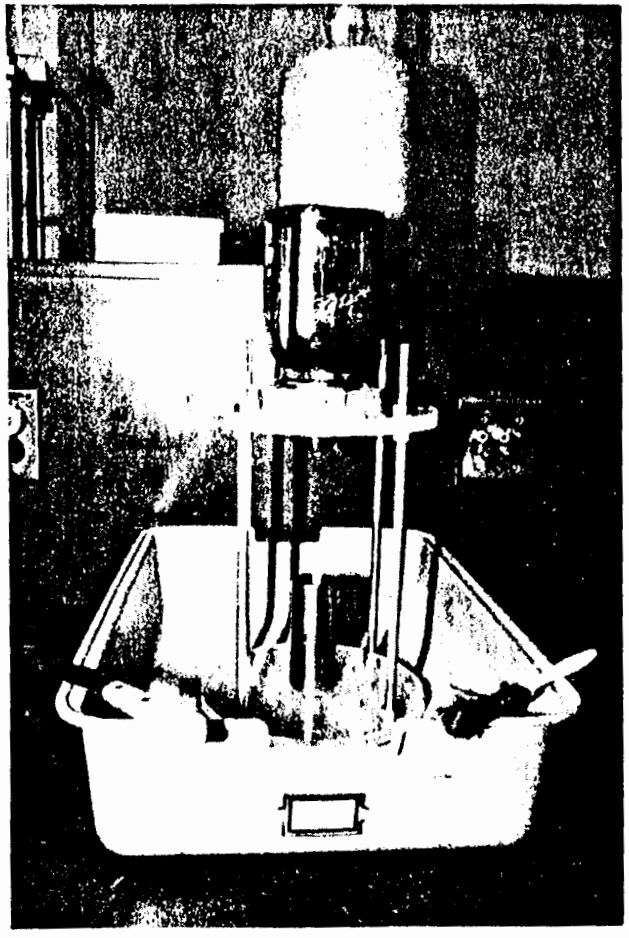

Fig. 9. NAA Method Particle Shape Device.

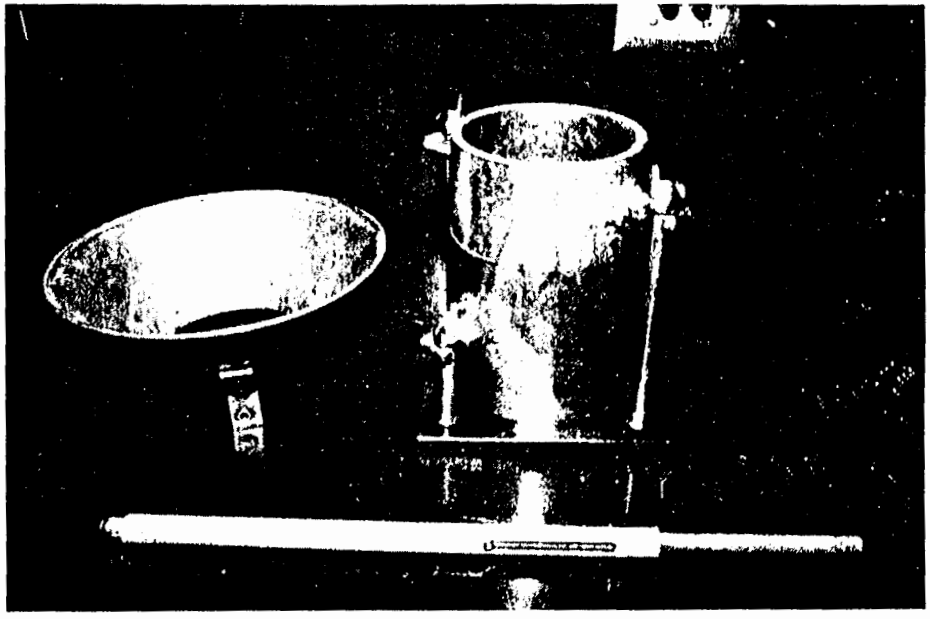

Fig. 10. D3398 Particle Shape Equipment.

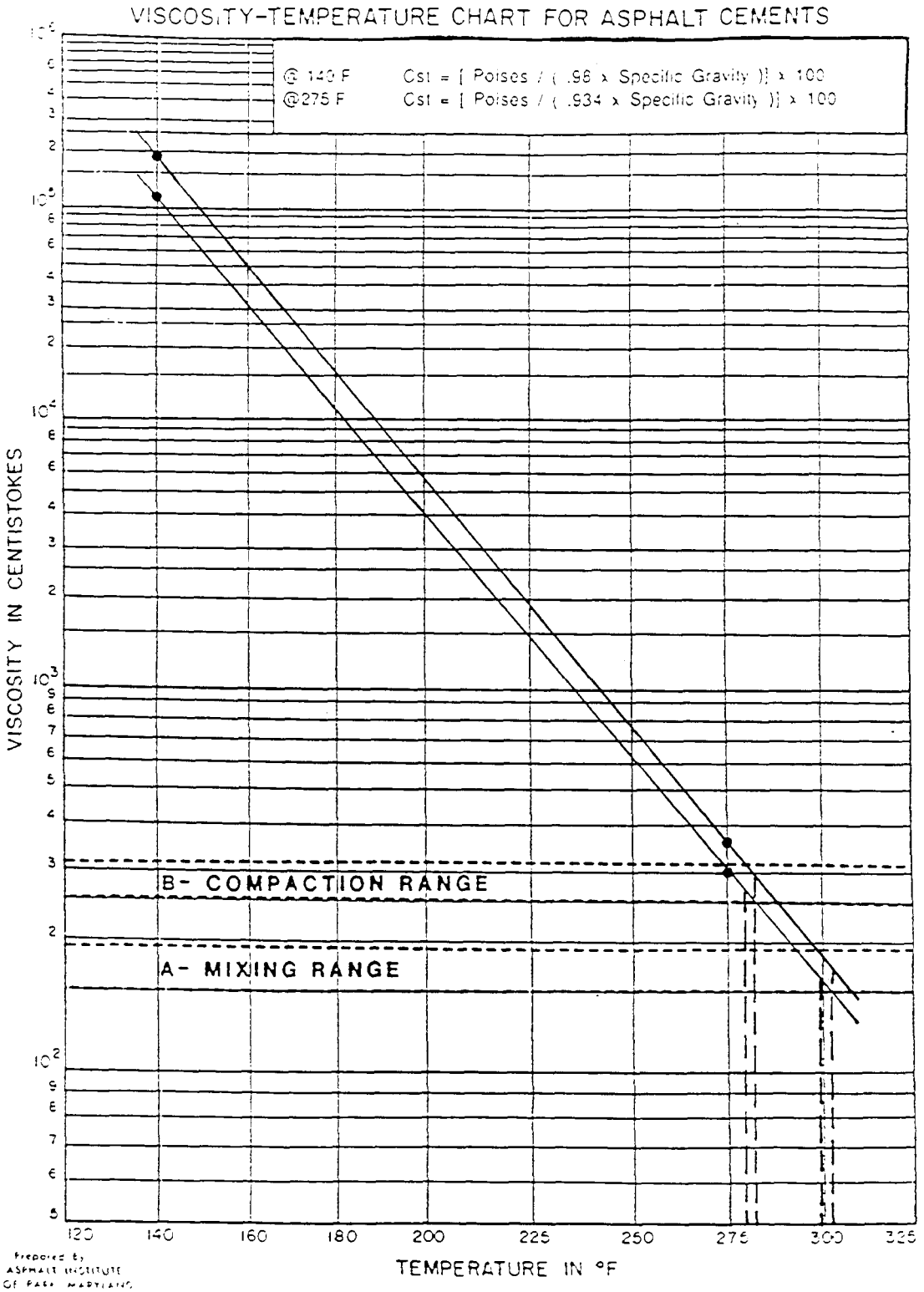

Fig. 11. Asphalt Cement Temperature – Viscosity Relationships.

279°F (AC-10) and 282°F (AC-20) were used. Details of specimen fabrication are given in Appendix C.

Bituminous base mix aggregate and mineral filler were separated into 1", 3/4", 1/2", #4, #8, #30, #200, and -#200 size fractions. Type C and IC mix aggregate and mineral filler were separated into 1", 3/4", 1/2", #4, #8, #16, #30, #50, #100, #200 and -#200 size fractions.

The Rice specific gravity specimens were made in a similar manner, with the omission of the compaction step.

MARSHALL MIX DESIGN

The stability/flow testing procedure was in accordance with AASHTO T 245-90. Prior to testing, the specimens and breaking head were heated to 140°F (60°C) in a water bath. The pucks were tested in a Pine Press Marshall device which applied the load via a motor driven mechanical jack at a deformation rate of 2 in/min (0.0847 cm/sec). The load was sensed by a 10,000 lb load cell. Flow was measured by a Schaevitz LVDT (Model GCA-121-500 S/N 4427) which has a range of ± 0.5 in.

Both signals were sent through signal conditioners; the output was recorded on a Houston Instruments 2000 XY recorder. Maximum load (stability) and flow at that load were taken from the load-deformation trace. The test arrangement is shown in Fig. 12.

MAXIMUM THEORETICAL SPECIFIC GRAVITY

The maximum theoretical specific gravity was determined for every mixture

279°F (AC-10) and 282°F (AC-20) were used. Details of specimen fabrication are given in Appendix C.

Bituminous base mix aggregate and mineral filler were separated into 1", 3/4", 1/2", #4, #8, #30, #200, and -#200 size fractions. Type C and IC mix aggregate and mineral filler were separated into 1", 3/4", 1/2", #4, #8, #16, #30, #50, #100, #200 and -#200 size fractions.

The Rice specific gravity specimens were made in a similar manner, with the omission of the compaction step.

MARSHALL MIX DESIGN

The stability/flow testing procedure was in accordance with AASHTO T 245-90. Prior to testing, the specimens and breaking head were heated to 140°F (60°C) in a water bath. The pucks were tested in a Pine Press Marshall device which applied the load via a motor driven mechanical jack at a deformation rate of 2 in/min (0.0847 cm/sec). The load was sensed by a 10,000 lb load cell. Flow was measured by a Schaevitz LVDT (Model GCA-121-500 S/N 4427) which has a range of ± 0.5 in.

Both signals were sent through signal conditioners; the output was recorded on a Houston Instruments 2000 XY recorder. Maximum load (stability) and flow at that load were taken from the load-deformation trace. The test arrangement is shown in Fig. 12.

MAXIMUM THEORETICAL SPECIFIC GRAVITY

The maximum theoretical specific gravity was determined for every mixture

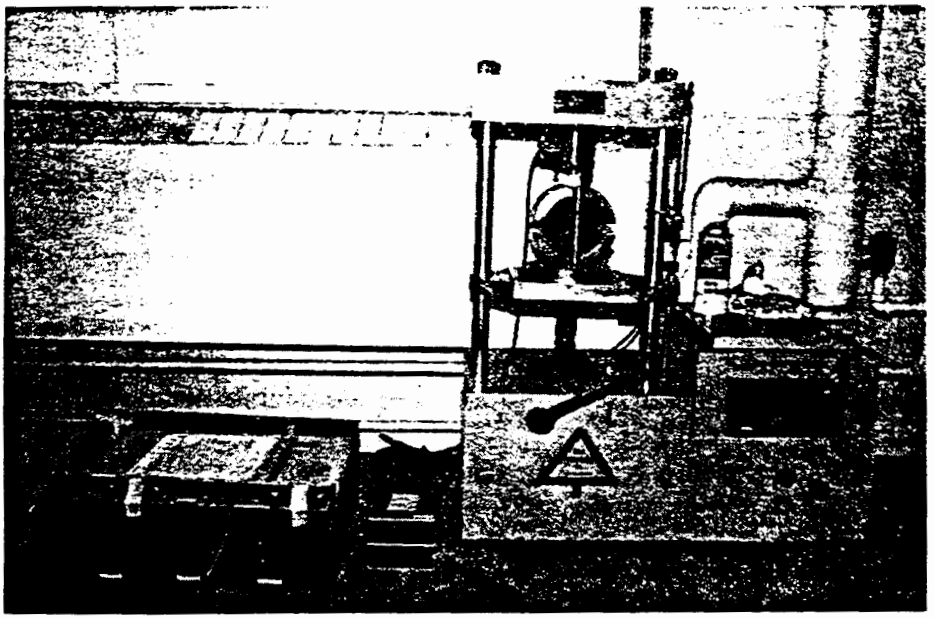

Fig. 12. Marshall Stability/Flow Test Apparatus.

Fig. 13. Rice Maximum Theoretical Specific Gravity Test Station.

to the specimen's vertical diametral plane. Lower and upper 0.5 in wide steel loading strips, which are curved at the interface to fit the radius of the specimen, distribute the compressive load to the specimen.

The application of a compressive load to the specimen induces a fairly uniform tensile stress perpendicular to the plane of the applied load and along the vertical diametral plane. This ultimately causes the specimen to fail by splitting along the vertical diameter. The tensile stresses developed within the specimen simulate the state of stress at the lower position of the asphalt layer in a pavement structure, which is generally the critical area for fracture and fatigue cracking. Procedures for the indirect tensile test have been developed and reported by Anagnos and Kennedy (48-50).

The indirect tensile strength is usually determined in order to choose the loads to be applied during the repeated load diametral resilient modulus test. A percent of the total stress at failure is normally used. In the SHRP P07 (Strategic Highway Research Program) protocol on resilient modulus testing of asphaltic mixture cores, repeated load level is tied to test temperature: 30% at 41°F (5°C), 15% at 77°F (25°C), and 5% at 104°(40°C).

The indirect tensile strength procedure involves testing a Marshall-type specimen at 77°F(25°C) in diametral indirect tension to failure. The load is applied at a rate of 2 in/min (0.0847 cm/sec). The stress at failure is calculated as follows:

$$S = \frac{2P}{\pi hD} \quad \ldots\ldots\ldots\ldots \quad (28)$$

where: S = indirect tensile strength, psi (Pa)

P = ultimate load, lbs (N)

h = specimen height, in (cm)

D = specimen diameter, in (cm).

The test apparatus is depicted in Fig. 14. It is basically a Marshall stability test press with a different breaking head. Load is sensed by a load cell; the signal is conditioned and maximum load is determined from an XY recorder plot. A more detailed description is given Appendix C.

RESILIENT MODULUS

The resilient modulus (indirect tensile) test is similar to the indirect tensile strength test except the specimen is not loaded to failure; rather, it is cyclically loaded to induce tensile stresses in the specimen.

The equipment used for testing asphalt specimens for diametral repeated load resilient modulus was developed at UMR. Several modifications over a period of time resulted in the devices pictured in Fig. 15.

The total resilient modulus was calculated as follows (as per SHRP Protocol PO7):

$$M_{Rt} = \frac{P_{cyclic} * D\left(0.080 + 0.297\mu_t + 0.0425\mu_t^2\right)}{H_t * t} \quad \ldots\ldots \quad (29)$$

where: M_{Rt} = total resilient modulus, psi

P_{cyclic} = cyclic load, lbs

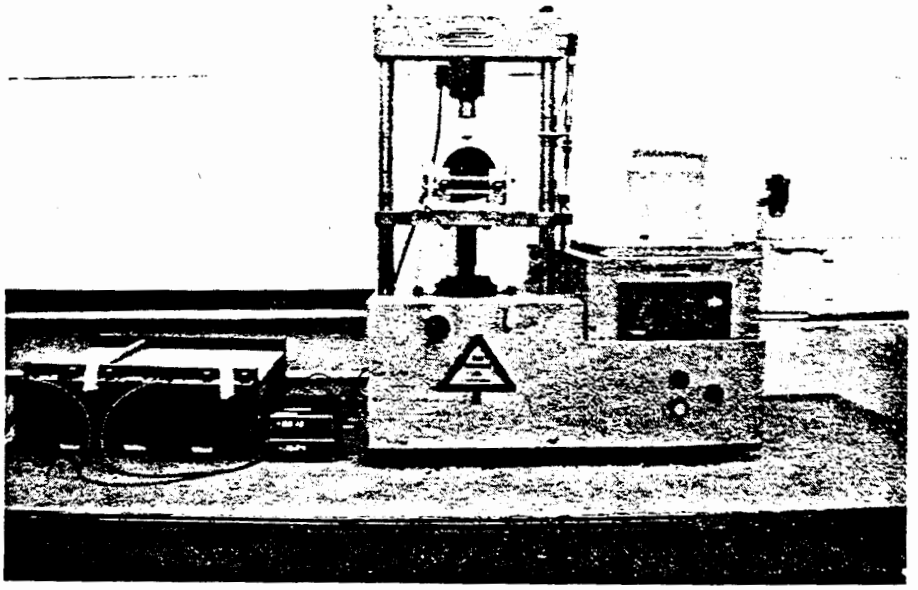

Fig. 14. Indirect Tension Test Equipment.

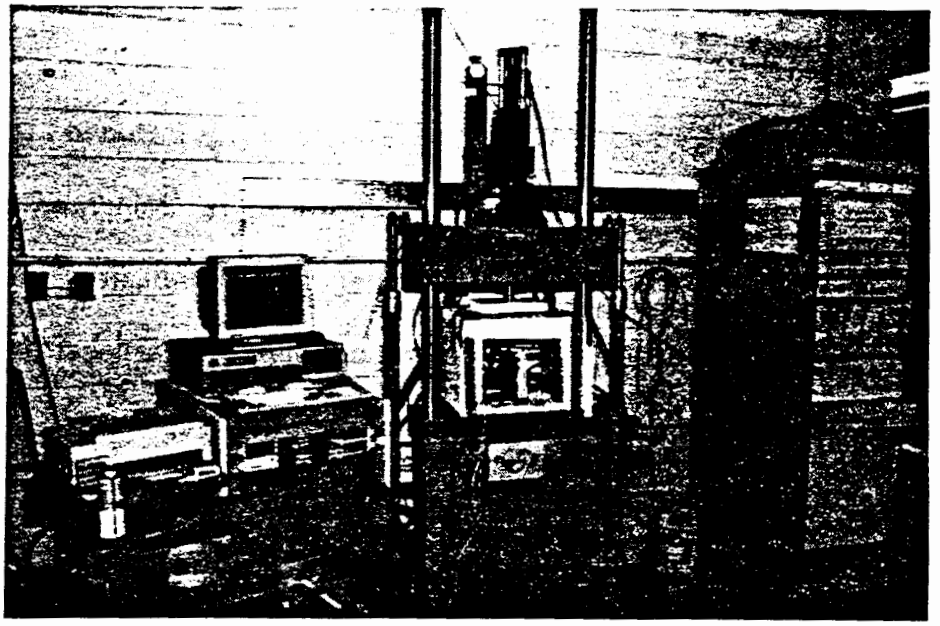

Fig. 15. Asphalt Mixture Resilient Modulus Test System.

D = specimen diameter, in

μ_t = total Poisson's ratio

$$= \frac{0.859-0.08R_t}{0.285R_t-0.04}$$

R_t = total deformation ratio = $\frac{(V_{t1}+V_{t2})}{2(H_{t1}+H_{t2})}$

H_t = H_{t1} + H_{t2} (total horizontal deformation)

H_{t1}, H_{t2} = total horizontal cyclic deformations from horizontal LVDT #1 and #2, in

t = specimen thickness, in

V_{t1}, V_{t2} = total vertical cyclic deformation values from vertical LVDT's #1 and #2.

A description of the equipment and its development is included in Appendix C. Also included is a detailed account of the test procedure. Minimum resolution of the horizontal LVDT's, vertical LVDT's, and the load cell are listed. Actual minimum deformations and loads during the testing were kept at least ten times these minimum resolutions to assure confidence in the test results.

RESULTS OF LABORATORY INVESTIGATION

ASPHALT CEMENT

The results of the asphalt cement testing are shown in Table 6. The number of test replications are shown which were necessary to stay within AASHTO

precision guidelines.

Table 6. Asphalt Cement Properties.

Parameter	AC-10		AC-20	
	Value	Reps.	Value	Reps.
penetration, 77°F (25°C), 100g, 5 sec	101	6	71	5
penetration, 37.8°F (3.2°C), 100g, 5 sec	8	3	6	3
kinematic viscosity, 275°F (135°C), Cs	301	3	361	3
absolute viscosity, 140°F (60°C), poise	1099	8	1911	4
specific gravity, 77°F (25°C)	1.007	5	1.017	5
softening point, °F (°C)	112.1 (44.5)	6	119.3 (48.5)	7

Fig. 11 depicts the asphalt cement temperature-viscosity relationship, with the mixing and compaction temperatures shown. A plot of penetration and viscosity vs. temperature is shown in Fig. 3. The penetration test at 77°F (25°C) was performed as per AASHTO T49 with 100g weight at 5 sec duration. The penetration at the lower temperature was performed under the same conditions, rather than the suggested 200g at 60 sec duration. A review of the literature (28,51) indicated that researchers favor the 100g 5 sec method when PI is being determined.

S_b values were calculated based on Eq. 14, which is based on the Van der Poel nomograph (Fig. 1). Use of Fig. 1 assumes that the asphalt is an S-type of

bitumen, as opposed to a W-type (high wax content) or B-type (high asphaltene type). de Bats and Gooswilligen (52) give criteria for qualifying the asphalts as to type. The method is given in Appendix D. From this analysis, both asphalts (AC-10 and AC-20) used in this study were classified as S-types, therefore use of Fig. 1 and Eq. 14 is appropriate. Also, Heukelom defines S-type asphalts as those that plot in an approximate straight line on the BTDC paper. Fig. 3 reveals this type of behavior for both asphalts used in this study. Fig. 3 also indicates that the T_{800} and $T_{R\&B}$ are quite close, as would be expected for S-type asphalts.

The calculation of $PI_{R\&B}$, $PI_{pen/pen}$, or PVN is required for determination of mixture stiffness. In Table 7 are aged residue estimations of penetration and $T_{R\&B}$ based on Eq. 12 and 15, respectively. In Table 8 are shown $PI_{R\&B}$, $PI_{pen/pen}$, PI_r, and PVN as calculated by Eqs. 3 and 5, Eqs. 3 and 4, Eq. 13 and Eq. 20, respectively. Use of Van der Poel's S_b nomograph (Fig. 1) indicates that the magnitude of S_b is not changed significantly by use of $PI_{R\&B}$ or $PI_{pen/pen}$ for these type S asphalts. Thus, it would seem that use of the penetration test at a second temperature (as opposed to the ring and ball softening point) is appropriate.

Table 7. Estimated Aged Penetration and $T_{R\&B}$.

Asphalt Grade	Pen_r	$T_{R\&B,r}$ °C
AC-10 @ 77°F(25°C)	66	51.2
AC-20 @ 77°F (25°C)	46	55.3

Table 8. $PI_{R\&B}$ and $PI_{pen:pen}$, PI_r, and PVN.

Asphalt Grade	$PI_{R\&B}$	$PI_{pen:pen}$	PI_r	PVN
AC-10	- 0.92	- 1.49	- 0.22	- 0.65
AC-20	- 1.88	- 1.33	- 0.15	- 0.75

Binder stiffness, S_b, was determined for loading times of 0.1 sec and 0.04 sec. These loading times correspond to the load duration time of the resilient modulus testing (0.1 sec) and to the estimated load duration time for MHTD pavements at the average vehicle speed (56.3 mph) and average asphalt pavement thickness (8.33 in) in accordance with Barksdale (53) as explained later in the "Load Duration" section. S_b is shown in Fig. 16 and Fig. 17 as a function of temperature and method of calculating PI_r or PVN and is tabulated in Table 9.

Table 9. Binder Stiffness, S_b.

Temperature	S_b (PI_r), psi				S_b(PVN), psi			
	AC-10		AC-20		AC-10		AC-20	
	0.1s	0.04s	0.1s	0.04s	0.1s	0.04s	0.1s	0.04s
40°F(4°C)	11,500	16,100	16,100	22,625	7110	10,670	14,200	21,335
68°F(20°C)	1450	2045	2480	3480	420	995	995	2276
77°F(25°C)	610	850	1160	1620	140	300	284	782
104°F(40°C)	8.8	12.3	37.8	53.1	10.7	21.3	21.3	43.5

Aged residue data were used to better reflect actual pavement conditions. PVN has been shown not to change with aging, therefore unaged penetration values

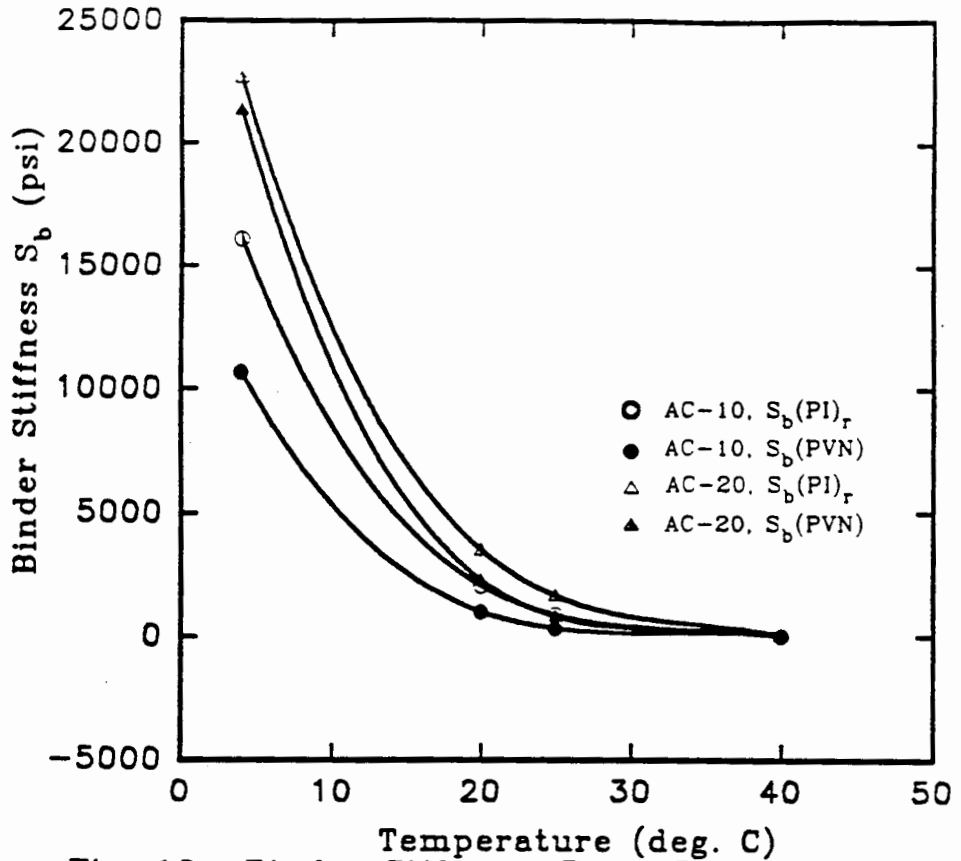

Fig. 16. Binder Stiffness From PI_r and PVN for 0.04 sec Loading Time.

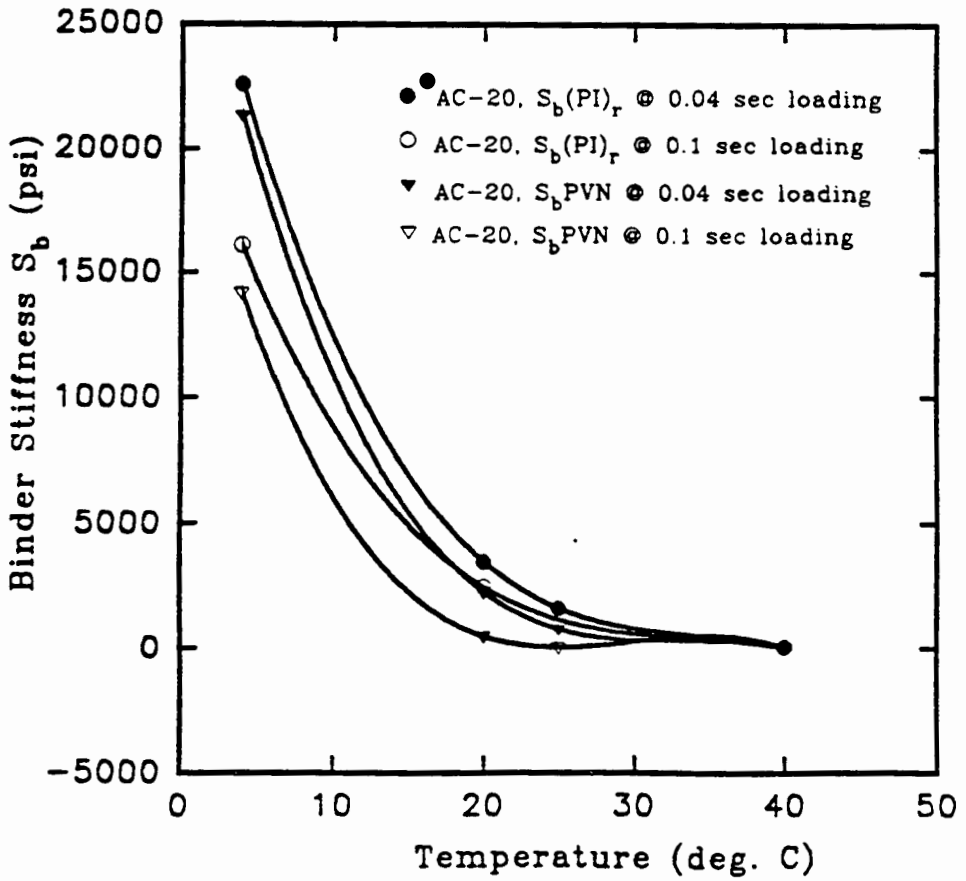

Fig. 17. Binder Stiffness From PI_r and PVN for AC-20.

were used in calculation of PVN. As can be seen, binder stiffness decreases with increasing temperature and longer load duration (or slower vehicle speed), as expected of a viscoelastic material. At most temperatures for both grades of asphalt, the PVN method exhibited lower binder stiffness than the aged residue PI method.

As discussed previously and shown in Table 4, five methods of mixture stiffness were calculated in order to determine which most accurately approximated the resilient modulus test data generated in the present study. The most accurate method would then be used in the Odemark equation to determine layer coefficients. The results are shown in Table 10.

Table 10. Results of Resilient Modulus - Mixture Stiffness Comparison.

Mixture Stiffness Method	R^2
S_m	0.914
S_{mPVN}	0.910
$S_{mrm,aged}$	0.886
$S_{m,aged}$	0.880
S_{mm}	0.849

As can be seen, all methods produced good estimations. The most accurate was the Bonnaure method utilizing the Ullidtz asphalt aging equations, and thus this method was used in the rest of the study to calculate mixture stiffness.

AGGREGATE

Gradations

General. The results of the aggregate testing are shown in Tables 11 through 19 and in Figs. 18 through 24. Table 11 shows the as-received gradations of the DR-4 through DR-11 aggregates.

Table 11. As-Received Gradations.

	Percent Passing								
Sieve size	DR4	DR5	DR6	DR7	DR8	DR9A	DR9B	MF	HL
1 in.	100	100	100	100	100	100	100	100	100
3/4 in.	100	100	100	100	100	100	100	100	100
1/2 in.	94	99	78	84	100	100	100	100	100
3/8 in.	63	71	- -	- -	100	100	100	100	100
#4	5	18	52	43	99	100	100	100	100
8	3	4	42	32	93	90	73	100	100
16	3	2	- -	- -	81	54	44	100	100
30	3	2	30	20	56	28	26	100	100
50	3	2	- -	- -	31	13	14	100	100
100	3	2	- -	- -	14	8	8	98	99
200	3	1	11	8	1	6	6	88	99
Note: MF = mineral filler; HL = Hydrated Lime									

Table 12 shows the gradations of the six final blends: two Type C's, two Type I-C's, and two bituminous bases. Fig. 18 shows the Type C MHTD master specification, and final blends (fine and coarse). Likewise, Figs. 19 and 20 depict Type I-C and bituminous base mixes, respectively. As explained previously, the

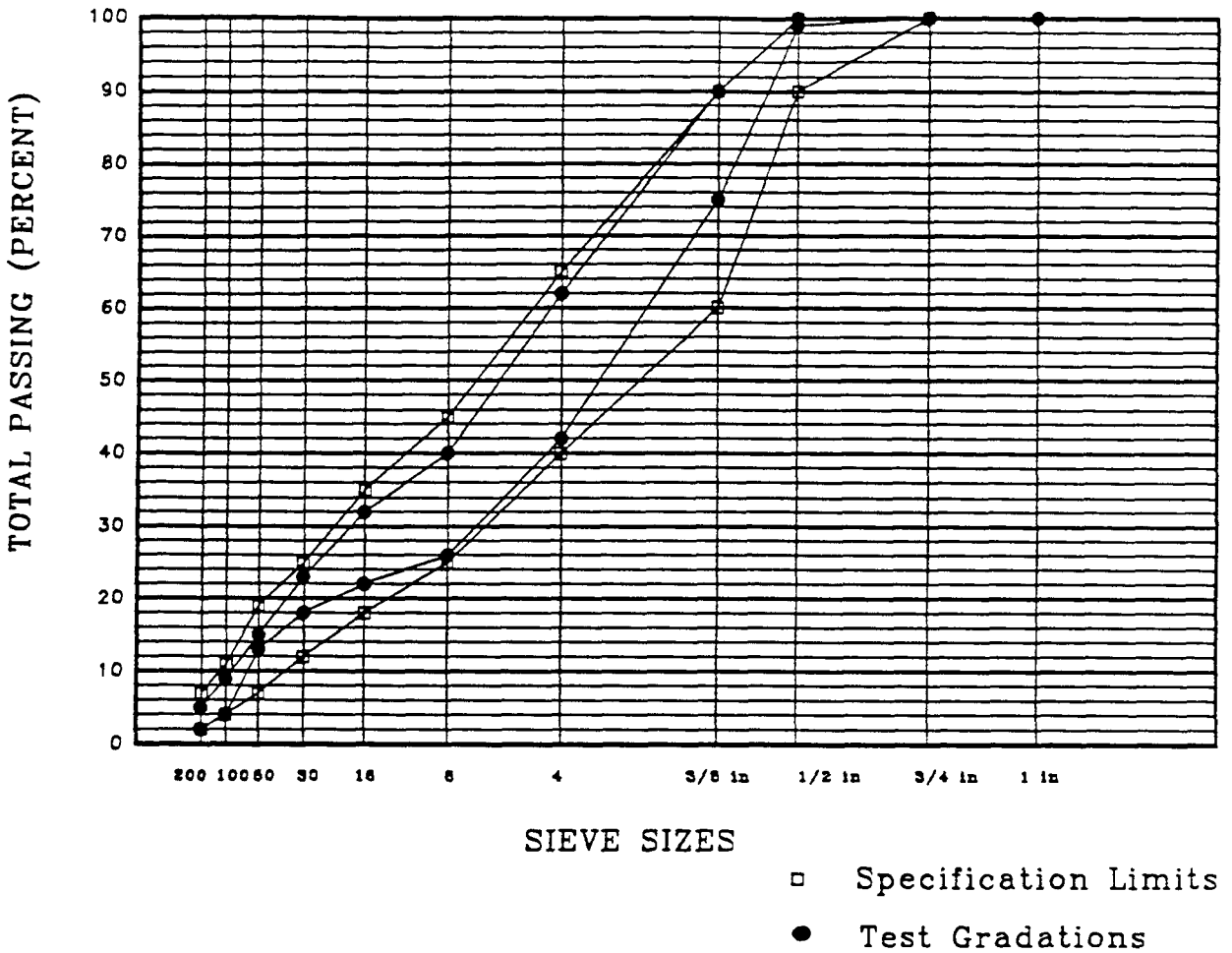

Fig. 18. Final Type C Blend Gradations.

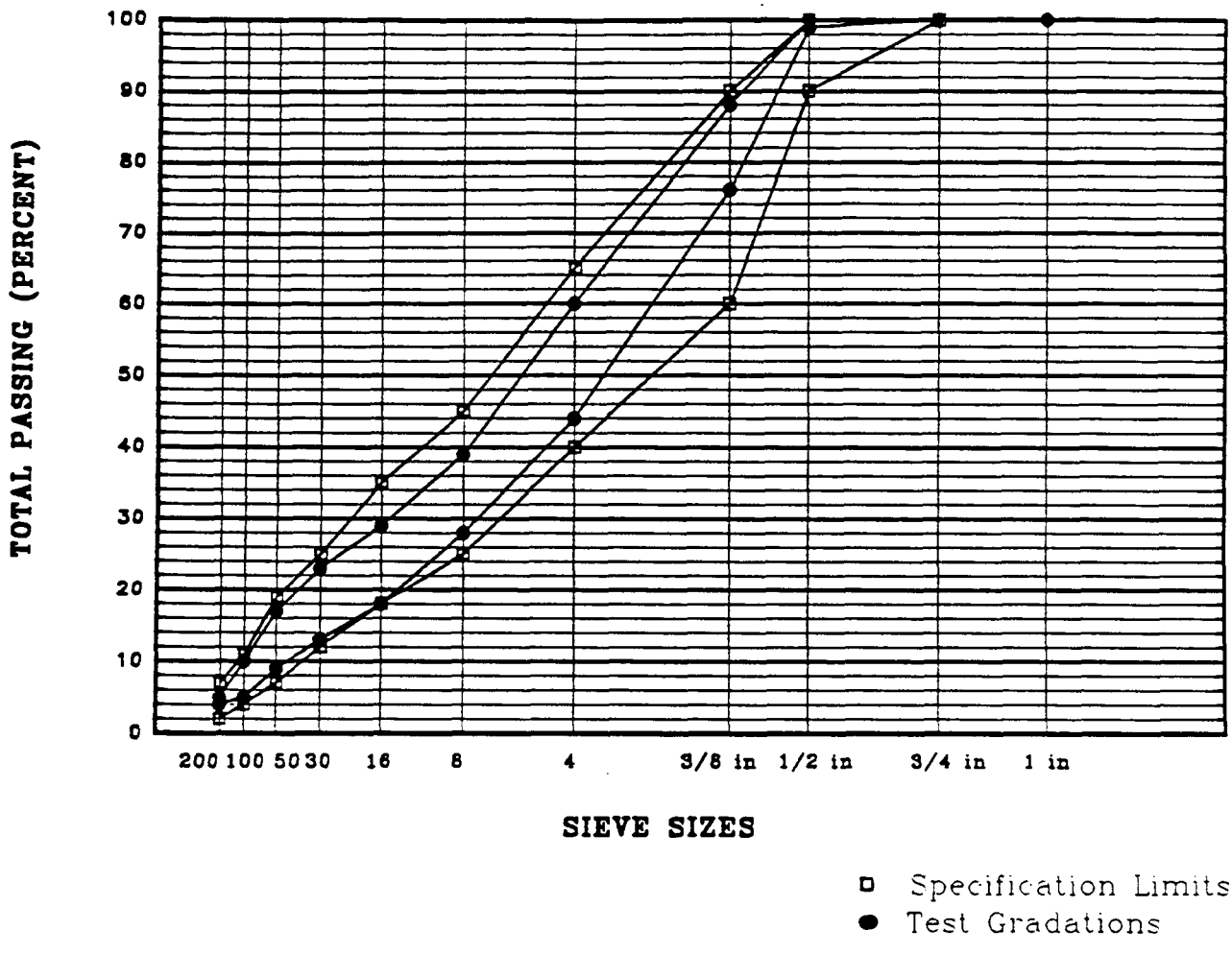

Fig. 19. Final Type IC Blend Gradations.

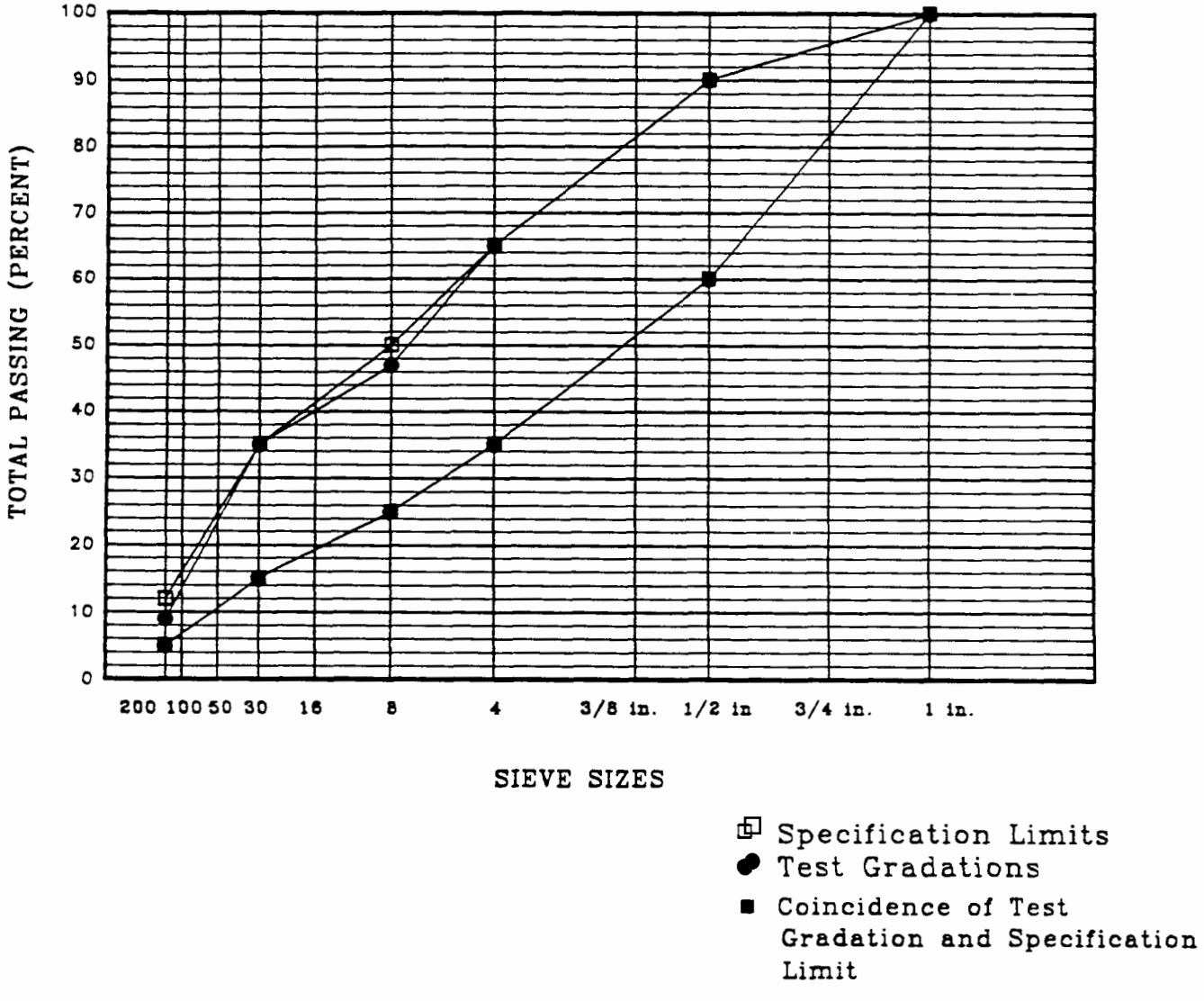

Fig. 20: Final Bituminous Base Blend Gradations.

fine and coarse blends for each of the three types of mixtures represent the finest and coarsest gradation approved by MHTD during 1990 moved to the finest or coarsest limit allowed by individual sieve tolerance. The mixtures in this study may not be totally realistic field mixes, but the wide spread in gradation was necessary to satisfy one of the major criteria for this study—the examination of the effect of gradation on resilient modulus (and hence layer coefficient).

Table 12. Gradations of Six Final Blends.

	% Passing					
	Type C		Type I-C		Bit. Base	
Sieve Size	Fine	Coarse	Fine	Coarse	Fine	Coarse
1 in.	100	100	100	100	100	100
3/4 in.	100	100	100	100	--	--
1/2 in.	100	99	100	99	90	60
3/8 in.	90	75	88	76	--	--
#4	62	42	60	44	65	35
8	40	26	39	28	47	25
16	32	22	29	18	--	--
30	23	18	23	13	35	15
50	15	13	17	9	--	--
100	9	4	10	5	--	--
200	5	2	5	4	9	5

Table 13 shows the contribution to each blend by the different sources of aggregate, on a sieve by sieve basis. The idea was to try to keep the percentage

makeup on each sieve the same for the fine and coarse gradations. Then, if during the analysis portion of the study it turned out that a particular sieve was critical to, say, resilient modulus, the fine and coarse blends could be compared.

Table 13. Contribution of Raw Materials to Each Blend.

Type C, Fine							Type C, Coarse					
Size	%Retained	%CA	%MS	%NS	%MF	%Lime	%Retained	%CA	%MS	%NS	%MF	%Lime
3/4"	0						0					
1/2"	0						1	100	0	0	0	0
3/8"	10	100	0	0	0	0	24	100	0	0	0	0
#4	28	100	0	0	0	0	33	100	0	0	0	0
8	22	0	83.3	16.7	0	0	16	0	83.3	16.7	0	0
16	8	0	21	79	0	0	4	0	21	79	0	0
30	9	0	21	79	0	0	4	0	21	79	0	0
50	8	0	21	79	0	0	5	0	21	79	0	0
100	6	0	21	79	0	0	9	0	21	79	0	0
200	4	0	10	0	90	0	2	0	10	0	90	0
-200	5	0	33	0	67	0	2	0	33	0	67	0
Type I-C, Fine							Type I-C, Coarse					
3/4	0						0					
1/2	0						1	100	0	0	0	0
3/8	12	100	0	0	0	0	23	100	0	0	0	0
#4	28	100	0	0	0	0	32	100	0	0	0	0
8	21	0	100	0	0	0	16	0	100	0	0	0
16	10	0	63	37	0	0	10	0	63	37	0	0
30	6	0	63	37	0	0	5	0	63	37	0	0
50	6	0	63	37	0	0	4	0	63	37	0	0
100	7	0	63	37	0	0	4	0	63	37	0	0
200	5	0	63	37	0	0	1	0	67	33	0	0
-200	5	0	0	0	20	80	4	0	0	0	25	75

Table 13, cont'd.

Bituminous Base, Fine							Bituminous Base, Coarse					
Size	Retained	%CA	%MS	%NS	%MF	%Lime	%Retained	%CA	%MS	%NS	%MF	%Lime
1	0	0	0	0	0	0	0	0	0	0	0	0
3/4	-	-	-	-	-	-	-	-	-	-	-	-
1/2	10	100	0	0	0	0	40	100	0	0	0	0
3/8	-	-	-	-	-	-	-	-	-	-	-	-
#4	25	100	0	0	0	0	25	100	0	0	0	0
8	18	78	0	22	0	0	10	78	0	22	0	0
16	-	-	-	-	-	-	-	-	-	-	-	-
30	12	78	0	22	0	0	10	78	0	22	0	0
50	-	-	-	-	-	-	-	-	-	-	-	-
100	-	-	-	-	-	-	-	-	-	-	-	-
200	26	78	0	22	0	0	10	78	0	22	0	0
-200	9	100	0	0	0	0	5	100	0	0	0	0

CA = coarse aggregate, DR4, DR5, DR6, DR7
NS = natural sand, DR8
MS = manufactured sand, 9A, 9B
MF = mineral filler, DR10
Lime = hydrated lime, DR11

Table 14 shows the overall contribution of each material to the final blends compared to the 1990 MHTD average mixtures. As can be seen, when viewing the percentages of combined coarse aggregate plus manufactured sand, natural sand, mineral filler, and lime, the proportions of the UMR mixtures closely followed MHTD field mixes.

Table 14. Amount of Each Material in Final Blends.

Mixture Type	Percent of Each Material in Final Blends						
	Agency	CA	MS	CA + MS	NS	MF	Lime
Type C	UMR						
	Fine	38.0	26.9	64.9	28.2	6.9	0
	Coarse	58.0	18.9	76.9	20.0	3.1	0
	MHTD	67.2	6.3	73.5	24.5	2.0	--
Type I-C	UMR						
	Fine	40.0	41.8	81.8	12.2	4.0	1.0
	Coarse	56.0	31.2	87.2	8.8	3.0	1.0
	MHTD	62.5	23.9	86.4	12.1	0.2	1.2
Bituminous Base	UMR						
	Fine	87.6	0	87.6	12.4	0	0
	Coarse	93.5	0	93.5	6.5	0	0
	MHTD	92.2	0	92.2	7.7	0.1	0

Gradation Curve Shape. An analysis was performed to determine the effect of gradation upon resilient modulus. The most promising methods were later tried in the development of the M_R multiple regression equation. To accomplish this, there was a need to characterize the gradations so that a single value of gradation "modulus" would represent the shape and position of the gradation curves. Eight different methods were tried, and are described in the following paragraphs. The results of the characterization for each gradation are shown in Table 15.

Table 15. Results of Gradation Curve Characterization.

Blend	M_R68	FM	C_U	C_z	SF	SSF	SF/SSF	Ã	Area
C-Fine	567,625	4.29	36.2	35.3	1698	242.8	6.99	4.76	7.2
C-Coarse	504,375	5.00	27.0	40.7	1803	148.7	9.07	4.02	20.3
IC-Fine	605,875	4.34	31.2	44.6	1683	257.9	6.52	4.71	7.2
IC-Coarse	508,000	5.07	18.6	27.5	1829	131.8	13.9	3.97	21.0
BB-Fine	605,125	3.93	48.4	35.5	1556	303.6	5.12	5.16	10.3
BB-Coarse	500,875	5.46	62.5	32.5	1779	165.4	10.8	3.59	16.9
R^2 *	----	0.867	0.005	0.245	0.801	0.820	0.714	0.872	0.788

*Note: R^2 indicates strength of correlation with resilient modulus at 68°F.
M_R68 = resilient modulus at 68°F

1) Fineness Modulus

Fineness modulus (FM) is defined as:

$$FM = \frac{(\Sigma \text{ cumulative \% ret'd on } 1.5'', 3/4'', 3/8'', \#4, 8, 16, 30, 50, 100 \text{ sieves})}{100} \quad (30)$$

The FM is commonly used to characterize concrete aggregate gradations. The drawback is that the effect of the minus #100 material is not accounted for, which may be a problem with asphalt mixture gradations.

2) Coefficient of Uniformity and Coefficient of Skew

The coefficient of uniformity (C_u) and the coefficient of skew (C_z) come from the geotechnical field and are used to help classify soil particle size distributions as to

"well" or "uniformly" graded:

$$C_u = \frac{D_{10}}{D_{60}} \quad \ldots\ldots\ldots\ldots \quad (31)$$

$$C_z = \frac{(D_{30})^2}{D_{10} * D_{60}} \quad \ldots\ldots\ldots\ldots \quad (32)$$

where: D_{10} = particle size corresponding to 10% passing

D_{30} = particle size corresponding to 30% passing

D_{60} = particle size corresponding to 60% passing.

3) Hudson's $\bar{A}$

Hudson's $\bar{A}$ (54) is a parameter that has been used to characterize mixtures that have appreciable fines in applications such as aggregate stockpile degradation studies (55). Hudson's $\bar{A}$ includes the effects of the minus #200 sieve material:

$$\bar{A} = \frac{(\Sigma\ \%passing\ 1.5'',\ 3/4'',\ 3/8'',\ \#4,\ 8,\ 16,\ 30,\ 50,\ 100,\ 200\ sieves)}{100} \quad \ldots \quad (33)$$

4) SF, SSF, SF/SSF

In a study concerning the effects of aggregate gradation on slump of concrete, Joel (56) developed three gradation parameters:

1) SF = Σ (cumulative percent retained * specific surface) ..... (34)

2) SSF = Σ (individual percent retained * specific surface) ..... (35)

3) SF/SSF

where: SF = surface fineness

SSF = specific surface factor

sieve series is 1 1/2", 3/4", 3/8", #4, 8, 16, 30, 50, 100, 200 for SF; for SSF the #200 sieve is omitted

specific surface = individual particle size (d) surface area divided by the corresponding volume of each particle size, assuming spherical shapes

$$= 4\pi r^2 / [(4/3)\pi r^3] = 6/d \quad \ldots\ldots\ldots\ldots \quad (36)$$

In Joel's study, the best predictor of slump was SF/SSF.

5) Position of Gradation Curve

In asphalt work, the position of the gradation curve relative to the position of the maximum density curve as plotted on the FHWA 0.45 power curve graph paper has been used to assist in predicting asphalt mixture behavior. In this study it was decided to use some measure of this relative position to help in the estimation of resilient modulus.

The method developed in this study was to determine the area between the two curves. This can be done in a variety of ways. In this study, the use of the plotting program AUTOCAD (57) was used. Use of a manual planimeter or just counting squares on graph paper could also have been done.

To find the area between the maximum density line (MDL) and the gradation curve of interest, the position of the MDL must first be determined. There are at least four methods reported in the literature that have been presented for determining the position of the MDL (58-61). The method of Goode and Lufsey (58) seems to offer the most likely way to estimate the largest maximum particle size, and hence the

truest position of the MDL, which flows from the largest particle size. In their method, a line is drawn from the origin of the 0.45 power paper up through the point on the gradation curve that represents 90% passing, then on up to the 100% passing line. If the point that is struck on the 100% passing line is to the left of the point of 100% passing of the actual gradation, the straight line is used as the MDL. If the point is to the right, another straight line is drawn between the origin and the 100% passing point of the actual gradation and this line is used as the MDL. These plots are shown in Fig. 21.

Because the positions of the MDL of each of the six experimental gradations were all different, it was decided to use a ratio of the area between the curves to the area beneath the MDL and the 0% passing line, which is a large triangle. The area calculation results are shown in Table 15. As can be seen, the C and I-C fine mixes hewed most closely to the MDL, with the bituminous base fine mix somewhat further away. The coarse mixes were, predictably, significantly further away, with the C and I-C coarse mixes exhibiting the greatest relative area under the curve.

These eight moduli were each correlated with the results of the asphalt mixture resilient modulus testing. The results are shown at the bottom of Table 15 along with the R^2 factor, which is a measure of the strength of the correlation. It appears that $\bar{A}$ correlates the best with resilient modulus. Consequently, this parameter was tried in the predictive equation for resilient modulus as discussed later in this study. Fig. 22 aids in visualizing the manner in which $\bar{A}$ changes with gradation.

Two other methods of quantifying the position of the gradation curves were

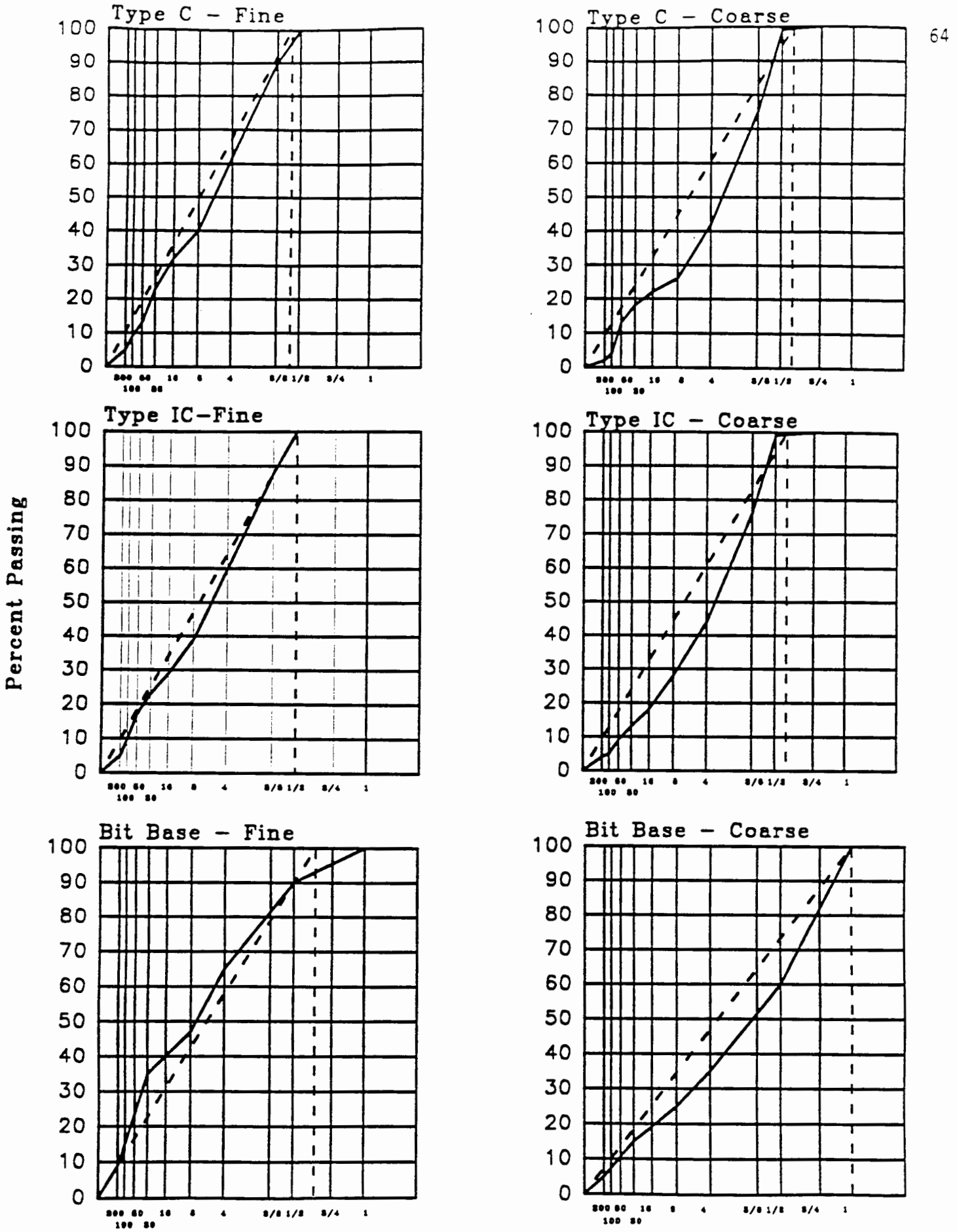

Fig. 21. Areas Under Maximum Density Lines.

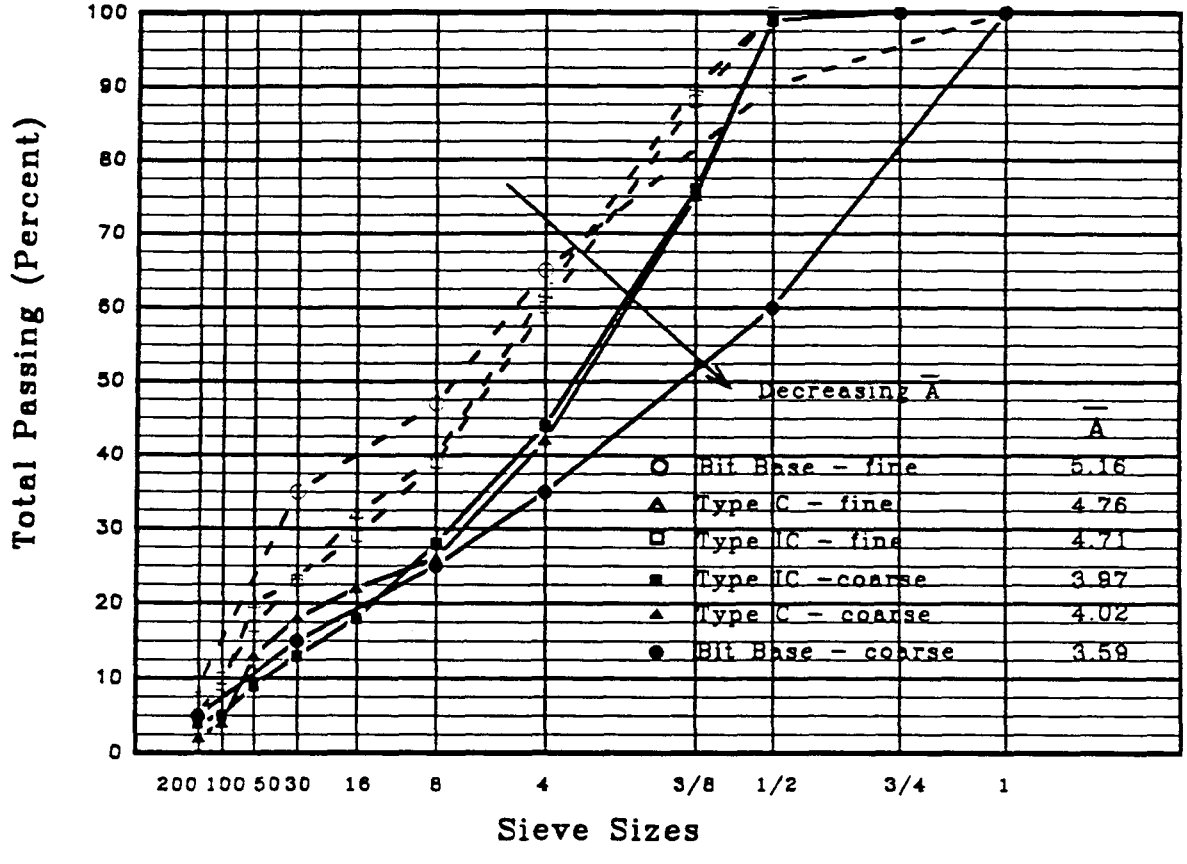

Fig. 22. Hudson's $\bar{A}$ as a Function of Gradation.

used, although the characterization could not be expressed as a single number, as could each of the eight methods just discussed. These two methods are presented below.

6) Individual Sieves, Passing or Retained

The first of these two methods was to simply use the cumulative retained percent on certain key sieves. Akhter and Witczak (34) have previously found the #4 and 3/4 in sieves to be important, and also included the percent passing the #200 sieve. The use of this approach is explained later in the section dealing with the predictive equation for asphalt material resilient modulus.

7) Slopes of Gradation Curve

The second method involved the characterization of the gradation line by breaking the line into several parts and determining the slopes of the portions. The portions were: #200 to #4 sieve, #4 to 1/2 in, and 1/2 in to 3/4 in size. The slopes were calculated as follows using the #200 to #4 portion as an example:

$$m_{4\text{-}200} = \frac{\%\ passing\ \#4\ -\ \%\ passing\ \#200}{D_4^{0.45} - D_{200}^{0.45}} \quad . \ . \ . \ . \quad (37)$$

where: D_4 = sieve opening, #4 sieve

D_{200} = sieve opening, #200 sieve.

The three slopes for each of the six test gradations are listed in Table 16. Again, the results of using this approach are outlined in the section of the report that deals with asphalt mixture resilient modulus prediction.

Table 16. Six Test Gradation Slopes.

Gradation	$m_{3/4 - 1/2}$	$m_{1/2 - 4}$	$m_{4 - 200}$
C-fine	0	145.03	143.22
C-coarse	6.85	217.56	100.50
IC-fine	0	152.67	138.19
IC-coarse	6.85	209.92	100.50
BB-fine	68.49	133.59	140.70
BB-coarse	273.97	95.42	75.38

Particle Shape and Surface Texture

These characteristics were quantified by use of ASTM D 3398 for the (+) #4 sieve material, and by NAA Method A for the (-) #8 through (+) #100 material for each blend. Both are measures of void content of bulk aggregate which is related to shape/texture. D3398 results in a "Particle Index" (IP);NAA Method A gives an "Uncompacted Voids Percent" (U). The results are shown in Table 17.

Round, smooth particles give IP's of 6 or 7, while angular, rough particles result in values of more than 15. The range of IP's of the combined aggregates in this study was 9 to 12. The Particle Index was determined for the coarse aggregate fraction of each blend and the Uncompacted Voids content was determined for the fine aggregate fraction.

Looking at Particle Index values, the DR4 aggregate averaged 12.7, indicating that it was the most angular. The other aggregates, in descending order of angularity were DR5 (10.6), DR7 (10.1), and DR6 (9.4). As it turned out, Particle Index tests were performed only on one type of aggregate per test because the (+) #4 sieve

Table 17. Particle Shape/Surface Texture Results.

Blend	Aggregate	Particle Index (IP)	Aggregates	Uncompacted Voids (%) (U)
C4F	DR4	12.4	DR4 + DR9B + DR8	40.1
C4C	DR4	12.9	DR4 + DR9B + DR8	40.0
C5F	DR5	10.8	DR5 + DR9A + DR8	39.8
C5C	DR5	10.5	DR5 + DR9A + DR8	39.5
Average		11.65		39.85
IC 4F	DR4	12.6	DR4 + DR9B + DR8	43.3
IC 4C	DR4	12.8	DR4 + DR9B + DR8	42.7
IC 5F	DR5	10.7	DR5 + DR9A + DR8	42.5
IC 5C	DR5	10.6	DR5 + DR9A + DR8	42.9
Average		11.7		42.85
BB 6F	DR6	9.1	DR6 + DR8	42.5
BB 6C	DR6	9.7	DR6 + DR8	43.0
BB 7F	DR7	10.3	DR7 + DR8	43.5
BB 7C	DR7	9.9	DR7 + DR8	43.5
Average		9.75		43.12
			DR8	38.3
			DR9A	44.1
			DR9B	44.0

DR4,5,6,7 = Coarse aggregate
DR8 = natural sand
DR9A,9B = manufactured sand

"blends" only contained coarse aggregate. So, Particle Index values were measures of individual coarse aggregate source shape/surface texture.

The NAA method was used on the fine aggregate fractions, thus the results indicate the weighted average of the combined natural sand (DR8) and manufactured sand (DR9A or DR9B). Additionally, particle shape was determined for each of the three individual sand sources. The results verify that the manufactured sands were more anglular than the natural sand (44 vs 38). The IC mixes averaged 42.85, the bituminous bases 42.5, and the C mixes 39.85. These results were not unexpected due to the smaller amounts of natural sand in the I-C and bituminous base blends compared to the C blends. The I-C average was slightly more angular than the BB average, possibly because the DR4 and DR5 aggregates were more angular than the DR6 and DR7 aggregates as indicated by the Particle Index results.

Looking at the data a little differently, the fine aggregate degrees of angularity in descending order were BB7 (43.5), IC4 (43.0), IC5 (42.7), BB6 (42.7), C4 (40.0) and the C5 (39.6).

Specific Gravity

In general, each aggregate was split into three portions (if possible): the(+) #4, (-) #4 to (+) #100, and the (-) #100. Then each portion was blended together to equate to the final gradation of interest as per the percentage contributed by the combined fraction (P_1, P_2, P_3), where:

P_1 = percent contributed by (+) #4 material

P_2 = percent contributed by (-) #4 to (+) #100 material

P_3 = percent contributed by (-) #100 material.

On the (+) #4 and the (-) #4 to #100 portions, both the bulk and apparent

specific gravities were determined, as well as their average. This average represents an estimation of effective specific gravity. Also, Rice specific gravities were performed on loose asphalt mixtures, and effective specific gravities were calculated, as shown in Table 18. For the (-) #100 material, only apparent specific gravities can be determined. The combined bulk specific gravities (G_{sb}) for each blend are also shown.

Table 18. Aggregate Blend Specific Gravities.

Blend	P_1 %	P_2 %	P_3 %	BSG_1	ASG_1	G_1	BSG_2	ASG_2	G_2	ASG_3 G_3	G_{sb}	G_{se}	D_1
C4F	38	53	9	2.606	2.711	2.659	2.622	2.678	2.650	2.736	2.626	2.661	2.661
C4C	58	38	4	2.634	2.712	2.673	2.632	2.680	2.656	2.750	2.637	2.666	2.669
C5F	38	53	9	2.580	2.693	2.636	2.617	2.666	2.642	2.750	2.614	2.642	2.649
C5C	58	38	4	2.568	2.682	2.625	2.611	2.670	2.640	2.750	2.591	2.633	2.636
IC4F	40	50	10	2.616	2.710	2.663	2.633	2.702	2.667	2.644	2.627	2.672	2.663
IC4C	56	39	5	2.629	2.718	2.673	2.638	2.712	2.675	2.619	2.632	2.669	2.671
IC5F	40	50	10	2.577	2.701	2.639	2.608	2.687	2.647	2.657	2.600	2.637	2.645
IC5C	56	39	5	2.572	2.687	2.630	2.605	2.677	2.641	2.632	2.588	2.632	2.634
BB6F	35	30	35	2.651	2.795	2.773	2.649	2.773	2.711	2.709	2.671	2.753	2.715
BB6C	65	20	15	2.667	2.790	2.729	2.661	2.766	2.714	2.750	2.678	2.726	2.729
BB7F	35	30	35	2.608	2.694	2.651	2.576	2.680	2.628	2.709	2.633	2.685	2.664
BB7C	65	20	15	2.592	2.688	2.640	2.574	2.680	2.627	2.696	2.603	2.670	2.646

Note: $BSG_{1,2}$, $ASG_{1,2}$, ASG_3 = test values of blended aggregates
G_1, G_2 = average of BSG and ASG
G_{sb} = calculated
G_{se} = from Rice test
D_1 = calculated

The calculations for effective specific gravities are shown below:

Estimation method:

$$D_1 = \frac{100}{\frac{P_1}{G_1} + \frac{P_2}{G_2} + \frac{P_3}{G_3}} \quad \ldots\ldots\ldots \quad (38)$$

where:

D_1 = effective specific gravity

$$\frac{P_1}{G_1} = \frac{\text{Percent of (+) \#4 mtr'l.}}{\text{Combined specific gravity of (+) \#4 mtr'l.}}$$

$$\frac{P_2}{G_2} = \frac{\text{Percent of (-) \#4 to (+) \#100 mtr 'l.}}{\text{Combined specific gravity of (-) \#4 to (+) \#100 mtr 'l.}}$$

$$\frac{P_3}{G_3} = \frac{\text{Percent of (-) \#100 mtr'l.}}{\text{Combined specific gravity of (-)\#100 mtr'l.}}$$

$$G_1 = \frac{BSG_1 + ASG_1 \text{ of (+) \#4 mtr'l.}}{2}$$

$$G_2 = \frac{BSG_2 + ASG_2 \text{ of (-) \#4 to (+)\#100 mtr'l.}}{2}$$

$$G_3 = ASG_3 \text{ of (-) \#100 mtr'l.}$$

$$P_1 + P_2 + P_3 = 100$$

$$G_{sb} = \frac{P_1 + P_2 + P_3}{\frac{P_1}{BSG_1} + \frac{P_2}{BSG_2} + \frac{P_3}{G_3}}$$

Rice Method:

$$G_{se} = \frac{P_{mm} - P_{b(mix)}}{\frac{P_{mm}}{G_{mm}} - \frac{P_{b(mix)}}{G_b}} \quad \ldots\ldots\ldots \quad (39)$$

where:

G_{se} = Effective specific gravity

P_{mm} = Percent of entire mix = 100

$P_{b\,(mix)}$ = Total percent asphalt by weight of mix

G_{mm} = Rice maximum theoretical density

G_b = Specific gravity of asphalt.

MAXIMUM THEORETICAL SPECIFIC GRAVITY

Maximum theoretical specific gravities were calculated in two ways. The first was based on an estimated effective specific gravity (as discussed above) and the total asphalt content by weight of mix. The second way was to calculate the maximum theoretical specific gravities based on the effective specific gravity of the aggregate which is determined by Rice specific gravity testing, as previously discussed. The calculations are as follows:

Estimation Method

$$D = \frac{100 + P_{b(agg)}}{\frac{P_1}{G_1} + \frac{P_2}{G_2} + \frac{P_3}{G_3} + \frac{P_{b(agg)}}{G_b}} \quad \ldots\ldots\ldots \quad (40)$$

where: $P_{b(agg)}$ = Total percent asphalt by wt. of aggregate.

Rice Method

$$G_{mm} = \frac{P_{mm}}{\frac{P_{s(mix)}}{G_{Se}} + \frac{P_{b(mix)}}{G_b}} \quad \ldots\ldots\ldots \quad (41)$$

where: P_s = Percent aggregate by wt. of mix.

All other variables were previously defined.

Results of the two methods of both effective specific gravity and maximum theoretical specific gravity are shown in Table 19. Comparisons of G_{se} vs D_1, and G_{mm} vs D are shown in Figs. 23 and 24, respectively. Statistical analysis indicates that the (G_{se}-D_1) and (G_{mm}-D) values for the C and IC mixes are not significantly different, but the difference between either one of them and the bituminous base is significant at the 0.05 level. It appears that for aggregates with low absorptions there is not much difference between methods of effective specific gravity and maximum theoretical specific gravity determination. However, for high absorption aggregates, the "estimated" method tends to underestimate.

VOIDS ANALYSIS

From the results of the specimen bulk specific gravities, the maximum theoretical specific gravities, and the material percentages and specific gravities, the air voids, VMA, and voids filled were calculated for the specimens made in the mix design portion of this study. Results of the voids analysis are shown in Appendix E.

Table 19. Maximum Theoretical Specific Gravities and Effective Specific Gravity by Two Methods.

Mix	G_{se}	D_1	$(G_{se}-D_1)$	G_{mm}	D	$(G_{mm}-D)$	Weighted Absorption
BBDR6F	2.753	2.715	0.038	2.584	2.551	0.033	1.82
BBDR6C	2.726	2.729	-0.003	2.560	2.582	-0.022	1.97
BBDR7F	2.685	2.664	0.021	2.508	2.491	0.017	1.35
BBDR7C	2.670	2.646	0.024	2.531	2.510	0.021	1.41
AVERAGE			0.020			0.012	1.64
CDR4F	2.661	2.661	0.000	2.467	2.467	0.000	1.09
CDR4C	2.666	2.669	-0.003	2.485	2.488	-0.003	0.93
CDR5F	2.642	2.649	-0.007	2.489	2.495	-0.006	1.04
CDR5C	2.633	2.636	-0.003	2.464	2.467	-0.003	1.34
AVERAGE			-0.003			-0.003	1.100
ICDR4F	2.672	2.663	0.009	2.515	2.507	0.008	1.12
ICDR4C	2.669	2.671	-0.002	2.477	2.479	-0.002	1.16
ICDR5F	2.637	2.645	-0.008	2.468	2.474	-0.006	1.42
ICDR5C	2.632	2.634	-0.002	2.447	2.449	-0.002	1.40
AVERAGE			-0.001			0.000	1.28

Calculations are as follows:

Estimated Method:

$$V = \frac{D-d}{D} * 100 \quad \text{(42)}$$

where: V = air voids, %

D = max. theo. sp. gravity

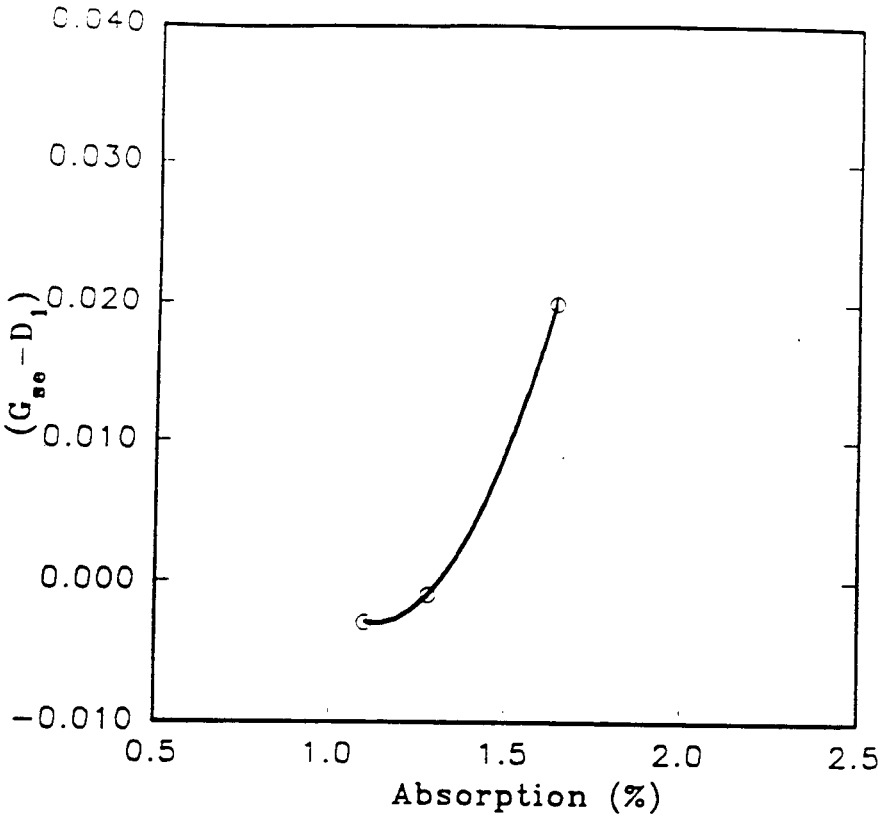

Fig 23. $(G_{SE} - D_1)$ vs. Absorption.

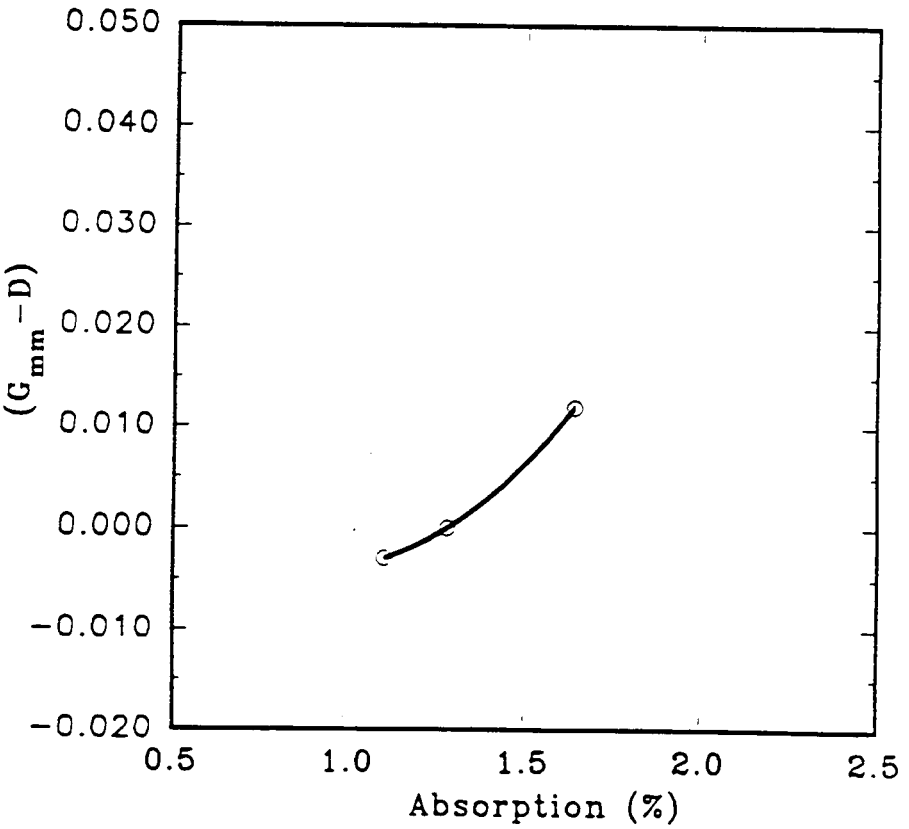

Fig. 24. $(G_{mm} - D)$ vs. Absorption.

d = compacted mixture specimen bulk sp. gravity

$$VMA = \frac{D_1 - d_1}{D_1} * 100 \quad (43)$$

d_1 = specific gravity of compacted aggregate

$$d_1 = \frac{100d}{100 + P_{b(agg)}} \quad (44)$$

$$VF = \frac{VMA - V}{VMA} * 100 \quad (45)$$

Rice Method:

$$P_a = \frac{G_{mm} - G_{mb}}{G_{mm}} * 100 \quad (46)$$

where: P_a = air voids, %

G_{mm} = max. theo. sp. gravity

G_{mb} = d

$$VMA = 100 - \frac{(G_{mb})\ (P_s)}{G_{sb}} \quad (47)$$

$$VF = \frac{VMA - P_a}{VMA} * 100 \quad (48)$$

Air voids were computed by use of: 1) the calculated effective specific gravities, and 2) the effective specific gravities derived from the Rice testing. Comparisons of these are made in Figs. 25 and 26. The use of the estimated method assumes that the effective specific gravity is midway between the bulk and apparent

d = compacted mixture specimen bulk sp. gravity

$$VMA = \frac{D_1 - d_1}{D_1} * 100 \quad (43)$$

d_1 = specific gravity of compacted aggregate

$$d_1 = \frac{100d}{100 + P_{b(agg)}} \quad (44)$$

$$VF = \frac{VMA - V}{VMA} * 100 \quad (45)$$

Rice Method:

$$P_a = \frac{G_{mm} - G_{mb}}{G_{mm}} * 100 \quad (46)$$

where: P_a = air voids, %

G_{mm} = max. theo. sp. gravity

G_{mb} = d

$$VMA = 100 - \frac{(G_{mb})\ (P_s)}{G_{sb}} \quad (47)$$

$$VF = \frac{VMA - P_a}{VMA} * 100 \quad (48)$$

Air voids were computed by use of: 1) the calculated effective specific gravities, and 2) the effective specific gravities derived from the Rice testing. Comparisons of these are made in Figs. 25 and 26. The use of the estimated method assumes that the effective specific gravity is midway between the bulk and apparent

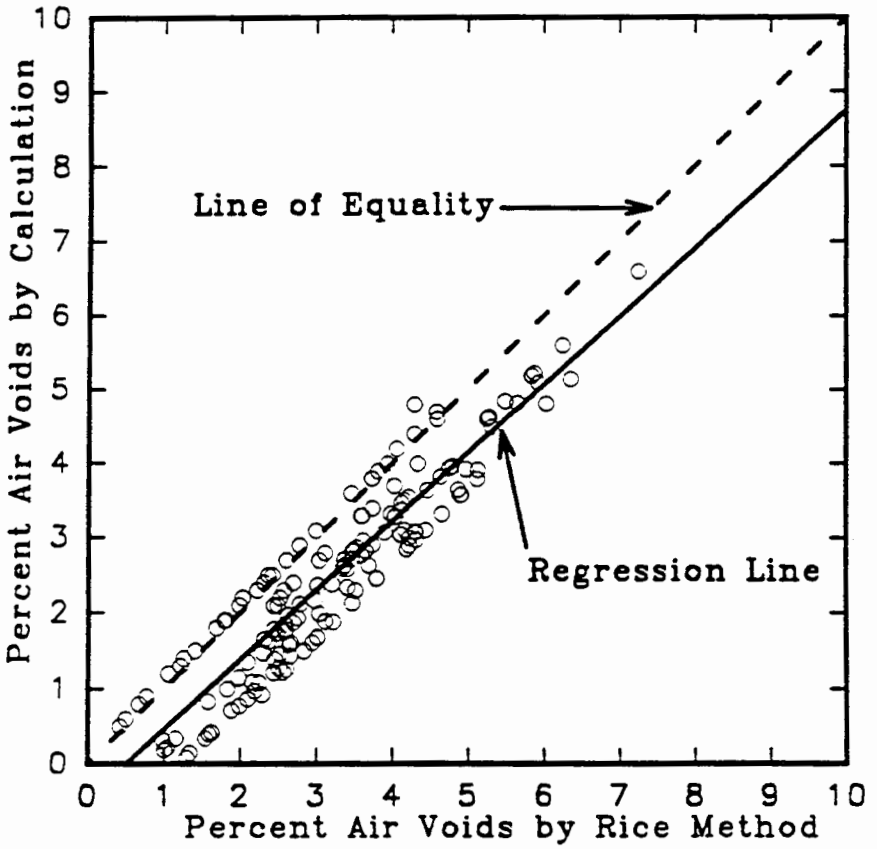

Fig. 26. Comparison of Air Voids Methods of Determination for Bituminous Base Mixtures.

specific gravities. It appears that this gave an air void value quite close to that given by the Rice method for the Type C/I-C mix aggregates. However, with the estimation method, the absorptive bituminous base coarse aggregates predict lower effective specific gravities and hence lower air voids than really exist. It seems that the more absorptive base aggregates have an effect on effective specific gravity (G_{se}). This is to be expected from the following analysis.

$$G_{se} = \frac{W_{agg}}{V_{agg} + V_{pore}} \quad \text{. . . . . (49)}$$

where: W_{agg} = dry weight of aggregate

V_{agg} = volume of water displaced by aggregate

V_{pore} = volume of aggregate pores not occupied by asphalt.

For a given aggregate particle weight, the more absorptive the aggregate is, the smaller the denominator (smaller V_{agg}), and therefore, the higher the G_{se}. The G_{se} will be closer to the apparent specific gravity which is still higher. Looking at maximum theoretical specific gravity "D":

$$D = \frac{100 + P_{b(agg)}}{\frac{P_1}{G_1} + \frac{P_2}{G_2} + \frac{P_3}{G_3} + \frac{P_{b(agg)}}{G_b}}$$

if, say, aggregate 1 is absorptive, than G_1 will really be greater than it is estimated. If a falsely low G_1 is substituted into the above equation, then D will be underestimated. The data in Table 19 bear this out. If D is too low, then from

$$V = \frac{D - d}{D} * 100$$

air voids will be underpredicted. Again, this is indicated by the data in Fig. 26.

Although the estimation method gave comparable results to the Rice method for the Types C and IC mixes, it must be remembered that this is for only two sources of aggregate. It is recommended that the Rice method be the preferred method for determination of maximum theoretical density of asphalt mixtures. In regard to Rice testing, consideration should be given to heating the mixture in an oven for several hours before testing to allow additional absorption, as per recent NCAT recommendations.

MARSHALL MIX DESIGN

Results of Marshall method unit weight, stability, flow, air voids, VMA, and voids filled are plotted and shown in Appendix F.

Optimum asphalt contents were chosen primarily on the basis of meeting the air voids content criteria of the MHTD specifications of 3 to 5%, with 4% as a target value. This was tempered by other criteria, such as voids filled, dust/asphalt content (by weight of aggregate), Marshall stability, percent asphalt, and VMA. The six mixtures and the MHTD criteria are shown in Table 20. In general, the mixes met all criteria except for dust/asphalt ratio and VMA. All four Type C mixes were on the borderline of dust/asphalt content acceptance; VMA values for both Type C and I-C were somewhat low.

Table 20. Mixture Design Parameters and MHTD Criteria.

Type C			
Parameter	MHTD Criteria	UMR Gradation	
		Fine	Coarse
natural sand, %	20-35	28.2	20.0
(-) #200, %Mineral Filler	≥ 50	67	67
air voids, %	3-5	3.0,3.0	5.0,5.0
stability, lbs (N)	≥ 750	2300,2950	2600,2000
VMA, %	≥ 15	12.0,11.2	12.0,12.5
voids filled, %	60-80	69,74	60,61
dust/asphalt, by wt. aggregate	0.6-1.2	1.3,1.2	0.5,0.5
flow, 0.01 in (mm)	------	6,6	6,6
design asphalt content, by wt. of mix	------	3.6,3.8	3.6,3.6
Type I-C			
natural sand, %	< 15	12.2	8.8
hydrated lime, %	1.0	1.0	1.0
all other (-) #200=MF	------	yes	yes
air voids, %	3-5	3.0,3.3	4.0,4.0
stability, lbs (N)	≥ 1500	3000,3500	2250,2800
VMA, %	≥ 15	11.2,11.6	12.1,12.2
voids filled, %	60-80	72.5,72	68,67.5
dust/asphalt, by wt. of aggregate	0.6-1.2	1.2,1.2	0.9,0.9
flow, 0.01 in (mm)	------	8,8	8,8
design asphalt content, by wt. of mix	------	4.0,4.0	4.0,4.1

Table 20 cont'd.

Bituminous Base			
fine aggregate, %	≤ 30	12.4	6.5
fine aggregate, % pass 3/8 in. (cm)	100	100	100
fine aggregate, % pass # 200	≤ 6	0	0
design asphalt content, %, by wt. of mix	3-6	3.9,3.9	3.5,3.5
air voids, %	------	4.0,4.0	4.0,3.8
stability, lbs (N)	------	3800,3850	3400,3500
VMA, %	------	12.1,12.4	10.1,10.0
voids filled, %	------	62,67	60,60
dust/asphalt, by wt. of aggregate	------	2.2,2.0	1.4,1.3
flow, 0.01 in (mm)	------	6,7	8,8

As mentioned previously, these mixtures may not have been approved for field use due to the low VMA, and the asphalt contents may be somewhat low (in an effort to satisfy air voids criteria). It was decided to not adjust the mixture gradations or aggregate source (particle shape) ratios because two of the major criteria of the study were to determine the effect of gradation and particle shape on resilient modulus. Also, after discussions with MHTD personnel it was felt that the voids would have been greater had the compression method of compaction been used instead of the 75 blow Marshall compaction effort. In addition, the specimens were compacted with a manual hammer. Studies at NCAT have shown that this tends to render higher densities than what is usually achieved with flat-faced mechanical hammers. MHTD compaction temperatures for the compressive strength method are approximately 35°F lower than for Marshall specimens. This may also contribute to a higher void

content. The gradations were actual approved gradations, but the MHTD mix designs associated with them reflected the standard MHTD compression method of compaction.

Note that, besides the above 24 mixtures that were prepared at the design asphalt contents, another 24 mixtures were prepared which had an asphalt content 0.5% above the design content.

INDIRECT TENSILE STRENGTH

Results

The results of the indirect tensile strength testing are shown in Table 21. The values shown are averages of two specimens per mix, in accordance with the recommendations given in NCHRP 332 (62). The mixtures reflected the following variables: 12 gradation aggregate/source combinations, two asphalt cement grades, and various asphalt contents.

The tests were performed in order to determine the seating and testing loads for the resilient moduli tests, which are based on certain percentages of indirect tensile strengths. These percentages are also shown in Table 21.

Table 21. Indirect Tensile Strength Data

Mixture	Indirect Tensile Strength	Seating Load (lbs)			Testing Load (lbs)		
		3% 41°F	1.5% 77°F	0.5% 104°F	30% 41°F	15% 77°F	5% 104°F
C4F10-3.75	98	46.5	23.3	7.8	465.0	232.5	77.5
C4F10-4.25	83	39.4	19.7	6.6	393.8	196.9	65.6
C4F20-3.75	131	62.3	31.1	10.4	622.5	311.3	103.8
C4F20-4.25	115	54.0	27.0	9.0	540.0	270.0	90.0
C4C10-3.75	82	40.1	20.1	6.7	401.3	200.6	66.9
C4C10-4.25	81	39.8	19.9	6.6	397.5	198.8	66.3
C4C20-3.75	109	53.6	26.8	8.9	536.3	268.1	89.4
C4C20-4.25	113	54.8	27.4	9.1	547.5	273.8	91.3
C5F10-4.0	98	46.9	23.4	7.8	468.8	234.4	78.1
C5F10-4.5	84	40.1	20.1	6.7	401.3	200.6	66.9
C5F20-4.0	128	60.8	30.4	10.1	607.5	303.8	101.3
C5F20-4.5	112	53.3	26.6	8.9	532.5	266.3	88.8
C5C10-3.75	92	45.0	22.5	7.5	450.0	225.0	75.0
C5C10-4.25	86	41.6	20.8	6.9	416.3	208.1	69.4
C5C20-3.75	115	56.6	28.3	9.4	566.3	283.1	94.4
C5C20-4.25	109	53.6	26.8	8.9	536.3	268.1	89.4
Average	102						
IC4F10-4.2	101	48.4	24.2	8.1	483.8	241.9	80.6
IC4F10-4.7	91	43.5	21.8	7.3	435.0	217.5	72.5
IC4F20-4.2	134	64.5	32.3	10.8	645.0	322.5	107.5
IC4F20-4.7	114	54.4	27.2	9.1	543.8	271.9	90.6
IC4F10-4.2	78	37.9	18.9	6.3	378.8	189.4	63.1
IC4F10-4.7	78	38.3	19.1	6.4	382.5	191.3	63.8
IC4C20-4.2	103	51.4	25.7	8.6	513.8	256.9	85.6
IC4C20-4.7	99	48.8	24.4	8.1	487.5	243.8	81.3
IC5F10-4.2	107	51.8	25.9	8.6	517.5	258.8	86.3

Table 21 cont'd.

IC5F10-4.7	96	46.1	23.1	7.7	461.3	230.6	76.9
IC5F20-4.2	123	60.4	30.2	10.1	603.8	301.9	100.6
IC5F20-4.7	119	57.4	28.7	9.6	573.8	286.9	95.6
IC5C10-4.3	92	45.0	22.5	7.5	450.0	225.0	75.0
IC5C10-4.8	85	41.6	20.8	6.9	416.3	208.1	69.4
IC5C20-4.3	120	58.5	29.3	9.8	585.0	292.5	97.5
IC5C20-4.8	108	52.4	26.2	8.7	524.3	262.1	87.4
Average	103						
BB6F10-4.1	123	57.8	28.9	9.6	577.5	288.8	96.3
BB6F10-4.6	116	54.4	27.2	9.1	543.8	271.9	90.6
BB6F20-4.1	143	67.9	33.9	11.3	678.8	339.4	113.1
BB6F20-4.6	138	64.5	32.3	10.8	645.0	322.5	107.5
BB6C10-3.6	112	52.5	26.3	8.8	525.0	262.5	87.5
BB6C10-4.1	94	43.9	21.9	7.3	438.8	219.4	73.1
BB6C20-3.6	127	59.6	29.8	9.9	596.3	298.1	99.4
BB6C20-4.1	126	58.9	29.4	9.8	588.8	294.4	98.1
BB7F10-4.4	113	53.3	26.6	8.9	532.5	266.3	88.8
BB7F10-4.9	88	41.6	20.8	6.9	416.3	208.1	69.4
BB7F20-4.4	143	67.5	33.8	11.3	675.0	337.5	112.5
BB7F20-4.9	116	54.8	27.4	9.1	547.5	273.8	91.3
BB7C10-3.6	99	46.9	23.4	7.8	468.8	234.4	78.1
BB7C10-4.1	87	40.9	20.4	6.8	408.8	204.4	68.1
BB7C20-3.6	129	61.1	30.6	10.2	611.3	305.6	101.9
BB7C20-4.1	118	55.9	27.9	9.3	558.8	279.4	93.1
Average	117						

The data indicate the following:

1) an increase in asphalt viscosity (one grade harder) increased tensile strength an

average of 24% in all cases,

2) a decrease in asphalt content from 0.5% above optimum down to Marshall optimum increased tensile strength by about 10% in 95% of the cases,

3) an increase in gradation fineness increased tensile strength by about 13% in 90% of the cases,

4) an increase in particle angularity and surface texture roughness decreased tensile strength by 7% in 85% of the cases,

5) an increase in VMA decreased tensile strength by 14% in 92% of the C and IC mixes, but increased tensile strength by 11% in 88% of the bituminous bases.

The data also indicate that bituminous bases had greater tensile strengths than Type IC mixes by about 14% on the average, which in turn had about equal strengths to the Type C mixes. A statistical analysis showed that the difference in mean between the bituminous base mixes and either of the C or IC mixes was significant at the 0.05 level. It appears that the greater amount of fines and the more well-graded nature of the bituminous bases contributed to the higher tensile strengths.

These results are in general agreement with trends published in the literature. Specifically, Hadley et al. (41,42) and Abkemeier (63) report increasing IDT with increasing asphalt viscosity. In regard to asphalt content, it must be remembered that optimum asphalt contents tend to be lower for IDT than for Marshall stability (64), thus it is not surprising that, for a given gradation, lowering the asphalt content resulted in higher IDT values. Hadley et al. (41) indicated that an increase in gradation fineness with an accompanying increase in asphalt content led to higher IDT. In the present study, this was true for the

bituminous base mixes, but for the C and IC mixes, the IDT increased with increasing gradation fineness with constant asphalt contents. In a review of the literature, Abkemeier (63) noted that particle shape does not seem to have a great effect upon IDT (which he verified in his study), although at least two studies (41,42) indicate an increase in IDT with increasing angularity. In the present study, the opposite was true in most cases. However, the differences in particle shape were not great. The literature (42,48,50) indicates that the relationship of change in IDT due to change in voids is not conclusive - as was shown in the present study. In general, interactions between variables makes it difficult to make sweeping statements about any specific variable effect on IDT.

Multiple Regression

Many linear multiple regression equations were developed and analyzed to estimate the indirect tensile strength from certain mixture data by use of the computer program SYSTAT (65). Multiple regression equations were fit to the indirect tensile strength data. Many combinations of variables were analyzed. The criteria for final selection included:

1. The highest adjusted squared multiple correlation (adj-R^2) that met all the below listed criteria. This statistic reflects the overall goodness of fit of the equation. It describes how well the equation would predict a population of data, not the sample data. Thus it usually is a little lower than the R^2 value which is for the sample data.
2. A low standard error of estimate compared to the mean resilient modulus ($\bar{Y}$).
3. An analysis of variance F-statistic that indicates that the relationship is significant at the 0.01 level.

4. Residuals are normally distributed.

5. Residuals have constant variance.

6. All members of the population are described in the same model.

7. No serious problems of variable collinearity.

8. No single observation influences coefficients excessively.

9. Each independent variable contributes significantly to the model.

Data to develop the equations came from Tables 6, 12, 17, and Appendix F. The equation of best fit had an R^2 value of 0.854, an adjusted R^2 = 0.846, and a standard estimate of error (SEE) of 7.151.

$$IDT = 139.064 + 21.238\eta - 7.553P_{effv} - 0.687AR_4 + 1.388U - 2.145IP \quad . \; . \; . \quad (50)$$

where: IDT = indirect tensile strength, psi(N/m^2)

P_{effv} = percent effective asphalt content by volume

η = absolute viscosity @ 70°F, poises • 10^6

AR_4 = percent accumulative retained on the #4 sieve

U = percent uncompacted voids content (a measure of particle angularity/surface texture

IP = index of particle shape

The relationship between the estimated and experimentally determined values of indirect tensile strength (IDT) is shown in Fig. 27.

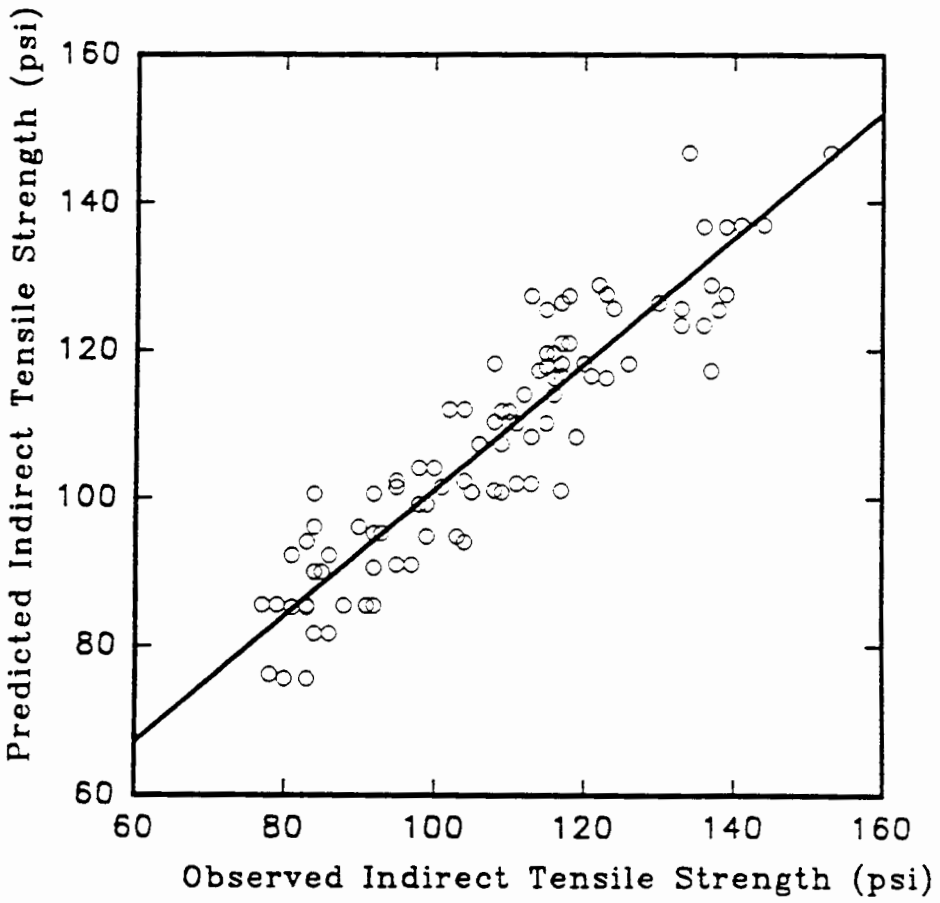

Fig. 27. Predicted vs. Observed Indirect Tensile Strength.

RESILIENT MODULUS

Test Results

Table 22 presents the results of the resilient modulus testing. The values shown are averages of four specimens per mix, in accordance with the recommendations given in NCHRP 332 (62). The tests were performed at 1 load cycle per second, with the load applied for 0.1 sec in a haversine form, followed by a 0.9 sec resting period. Both horizontal and vertical deformations were measured and Poisson's ratio calculated. The most current SHRP protocol at the time of testing (38) specified that if the calculated Poisson's ratio exceeds 0.50, a value of 0.50 should be assumed for resilient modulus calculations. This procedure was followed in this study. A previous draft of the SHRP protocol had recommended assuming values of Poisson's ratio of 0.20 at 41°F (5°C), 0.35 at 77°F (25°C) and 0.50 at 104°F (40°C). In the present study, the average Poisson's ratio at 41°F was 0.30, at 77°F it was 0.49, and at 104°F it was over 0.50 but was held at 0.50 as per the SHRP protocol. Other investigators (42,66-71) have reported values of Poisson's ratios greater that 0.5, especially at higher testing temperatures, with the majority of values between 0.1 and 0.7. All of this is not surprising considering that, as asphalt becomes warmer, it becomes less elastic in nature, thus calculations based on assumptions of elasticity become less applicable.

Table 22 . Results of Resilient Modulus Testing.

Mix	MR41F	pois41	MR77F	pois77	MR104F	pois104
BB6F10-4.1	1332205	0.30	444485	0.50	131557	0.50
BB6F10-4.6	1189461	0.37	300950	0.50	88096	0.50
BB6F20-4.1	1619316	0.36	607788	0.48	200355	0.50
BB6F20-4.6	1576178	0.49	469618	0.50	117300	0.50
BB6C10-3.6	1001320	0.36	334510	0.50	110773	0.50
BB6C10-4.1	864266	0.17	362979	0.50	118695	0.50
BB6C20-3.6	970920	0.32	360081	0.50	99405	0.50
BB6C20-4.1	1116468	0.30	460565	0.49	100156	0.50
BB7F10-4.4	1231681	0.42	390336	0.50	111549	0.50
BB7F10-4.9	1163223	0.47	290056	0.50	65117	0.49
BB7F20-4.4	1321958	0.36	466552	0.50	132760	0.50
BB7F20-4.9	1279411	0.43	412154	0.50	105368	0.50
BB7C10-3.6	806709	0.18	371155	0.49	95502	0.50
BB7C10-4.1	712903	0.24	266393	0.48	79501	0.50
BB7C20-3.6	990669	0.23	396241	0.50	138993	0.50
BB7C20-4.1	1220512	0.31	440202	0.49	115490	0.50
Bit. Base						
Average	1149825	0.33	398379	0.495	113163	0.50
Std. Dev.	253772	0.095	84759	0.007	30391	0.0025
Mix	MR41F	pois41	MR77F	pois77	MR104F	pois104
C4F10-3.75	1319480	0.34	334139	0.50	99240	0.50
C4F10-4.25	1148340	0.40	326792	0.50	100413	0.50
C4F20-3.75	1199178	0.25	464252	0.50	121361	0.50
C4F20-4.25	1519983	0.39	413749	0.50	110411	0.50
C4C10-3.75	785818	0.20	257629	0.50	81916	0.50
C4C10-4.25	874245	0.26	264348	0.50	73452	0.50
C4C20-3.75	1028246	0.17	497547	0.47	128856	0.46
C4C20-4.25	1302512	0.34	410904	0.50	70235	0.50
C5F10-4.00	1277437	0.35	358212	0.50	104171	0.50
C5F10-4.50	1191103	0.30	305779	0.50	95686	0.50
C5F20-4.00	1244735	0.29	608460	0.46	221003	0.50
C5F20-4.50	1057379	0.26	443050	0.43	201795	0.50
C5C10-3.75	1090774	0.30	378904	0.50	116155	0.50
C5C10-4.25	973954	0.33	318067	0.50	85125	0.50
C5C20-3.75	944909	0.20	443346	0.50	137806	0.50
C5C20-4.25	921963	0.20	432644	0.50	134446	0.50
Type C						
Average	1117504	0.29	391113	0.49	117629	0.50
Std. Dev.	193551	0.070	92047	0.020	42016	0.010

Mix	MR41F	pois41	MR77F	pois77	MR104F	pois104
IC4F10-4.20	1042503	0.25	356218	0.44	161044	0.50
IC4F10-4.70	1464584	0.49	303952	0.50	89102	0.50
IC4F20-4.20	1296217	0.24	481780	0.50	181547	0.50
IC4F20-4.70	1277202	0.29	564574	0.50	147858	0.50
IC4C10-4.20	847745	0.34	292395	0.50	78945	0.50
IC4C10-4.70	879666	0.21	265494	0.50	59717	0.50
IC4C20-4.20	839858	0.13	429363	0.33	98590	0.33
IC4C20-4.70	890095	0.18	372834	0.48	104021	0.48
IC5F10-4.20	1131758	0.36	359047	0.50	98266	0.50
IC5F10-4.70	1407345	0.42	389235	0.50	95642	0.50
IC5F20-4.20	1047901	0.16	637139	0.50	182961	0.50
IC5F20-4.70	1238235	0.26	510477	0.50	117678	0.50
IC5C10-4.30	819220	0.20	444177	0.50	102012	0.50
IC5C10-4.80	938142	0.33	353523	0.50	68590	0.50
IC5C20-4.30	923546	0.14	552363	0.44	133068	0.49
IC5C20-4.80	1156494	0.40	312598	0.50	56538	0.50
Type IC Average	1075032	0.28	414073	0.48	110973	0.49
Std. Dev.	212402	0.106	109000	0.045	40110	0.042
Total Avg.	1114120	0.30	401189	0.49	113922	0.50

In general, all mixtures became about an order of magnitude stiffer as temperature dropped from 104° to 41°F, as could be expected. From the temperature-modulus relationship of each mixture, the moduli at 68°F were calculated. The moduli at 68°F are necessary for entering the predictive nomographs in the 1986 AASHTO Design Guide for choosing layer coefficients. At this temperature, the I-C mixes were slightly stiffer than the bituminous base mixes and the Type C mixes were the least stiff. A regression equation was developed between resilient modulus at 77°F and indirect tension at 77°F. The R^2 coefficient was 0.536. This relationship is shown in Fig. 28.

Acceptable Range of M_R. From the Asphalt-Aggregate Mixture Analysis System (AAMAS)(37) comes Fig. 29, a chart for recommended total resilient moduli vs temperature, using indirect tensile testing conditions as was done in the present study. As can be seen, none of the UMR mixes were excessively stiff, although some

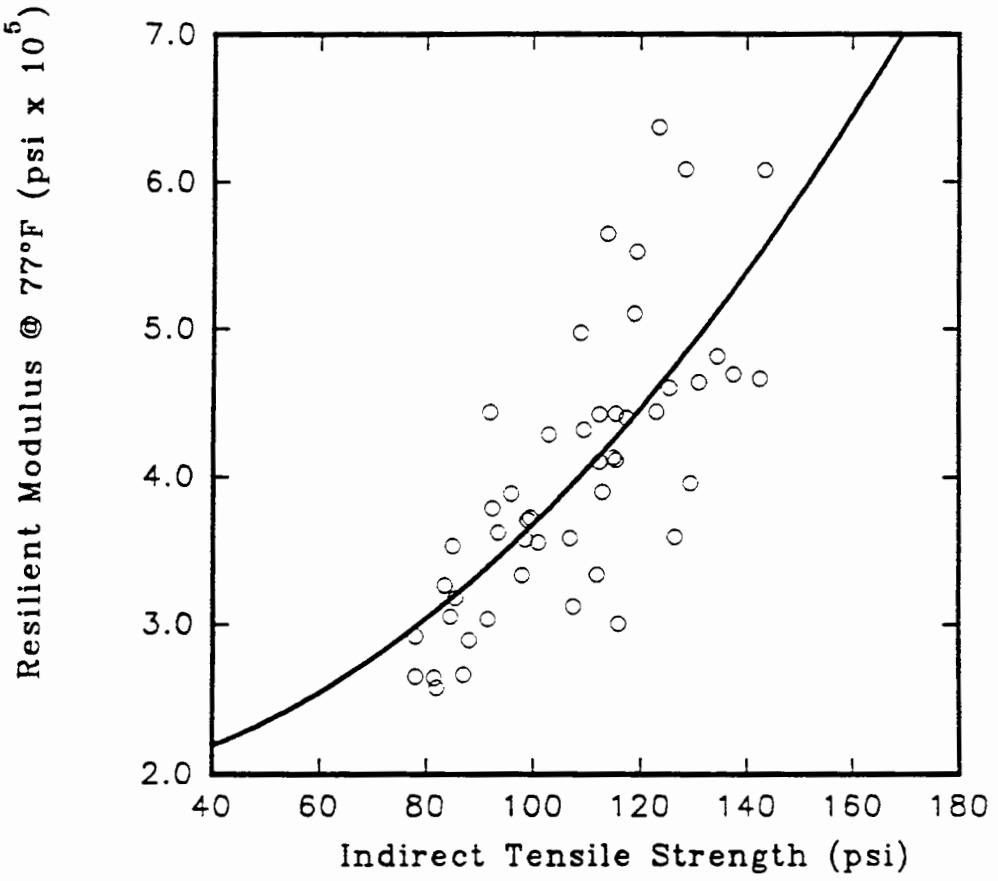

Fig. 28. Resilient Modulus at 77°F vs. Indirect Tensile Strength.

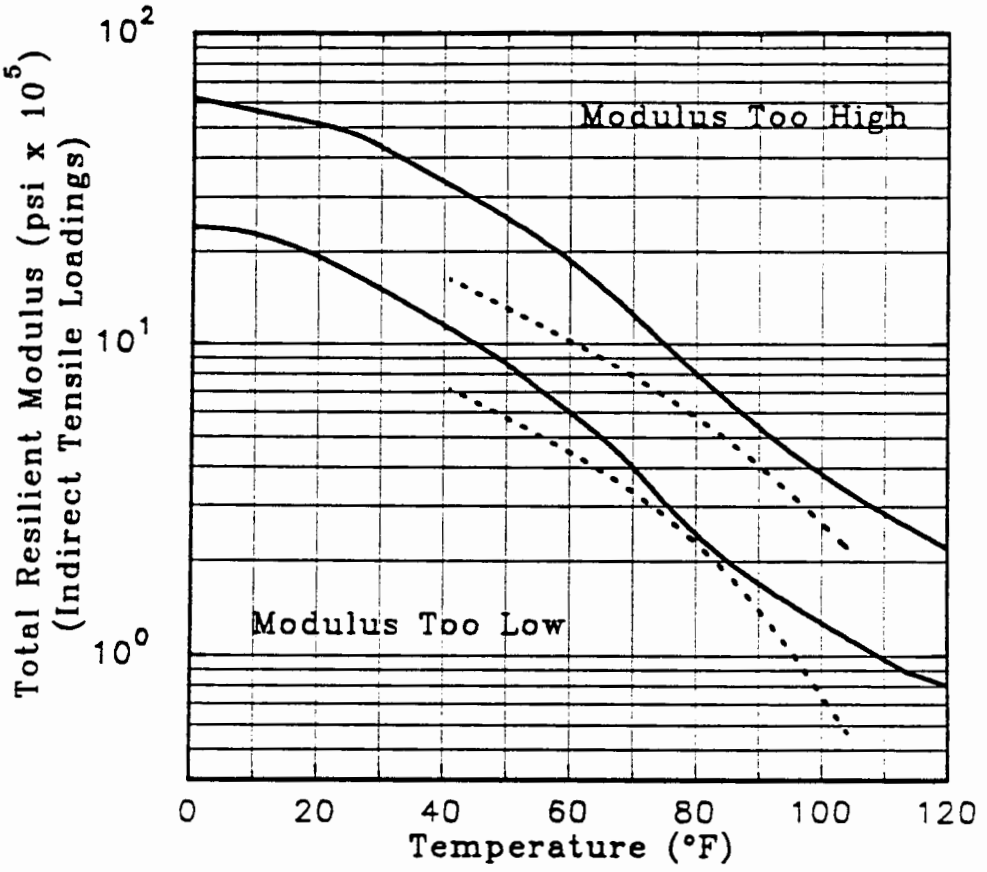

Fig. 29. UMR Mixtures on AAMAS Acceptance Chart.

of the mixes were insufficiently stiff at one or more temperatures. Analysis of the mix characteristics indicated that at 104°F, the large majority of the deficient mixes were the purposely overasphalted ones, and most were of the low-fines(coarse) gradation and contained the softer grade of asphalt (AC-10). Particle shape was not a significant factor.

AASHO Road Test asphaltic material reportedly had a modulus of 450,000 psi at 68°F. It is interesting to note where the AASHO Road Test material plots on the chart—barely stiff enough at 68°F. Yet, there is a statement in the Guide that cautions against mixes stiffer than 450,000; mixes exceeding this value are said to be prone to thermal and fatigue cracking. Perhaps one way to reconcile these two seemingly contradictory pieces of advice is to examine the types of modulus in play here. Three types of elastic modulus have been presented in the literature to any great extent over the last 20 years: dynamic modulus ($|E^*|$), resilient modulus - compression ($M_{R,comp}$), and resilient modulus - indirect tension ($M_{R,idt}$). The AASHTO Guide a_1-chart comes from NCHRP 128 (5). It is not stated upon which modulus the chart is based, but the references that are given deal with $|E^*|$. However, the 1986 Guide states that either $M_{R,comp}$ or $M_{R,idt}$ should be used to enter the chart. $|E^*|$ is not mentioned. AAMAS recommends using $M_{R,idt}$, which the industry seems to be doing. To further complicate the issue, M_R itself can be calculated in two ways: by use of total cyclic deflection in the denominator ($M_R = \sigma/\epsilon$) or instantaneous cyclic deformation (a smaller value). Which should one use? The choice may give significantly different a_1 values for the same mix.

There is very little in the literature by way of comparisons between the different moduli. First, Von Quintus et al. (72) found $M_{R,idt}$ to be significantly higher than $M_{R,comp}$ at 104 and 77°F, but equal at 40°F. The data appeared to be in terms of total M_R. Khosla and Ohmer (73) found essentially no difference between the two M_R types over a wide range of temperatures. Second, by inspection of the $M_R = \sigma/\epsilon$ relationship, instantaneous M_R would have to be larger than total M_R. Turning to M_R vs $|E^*|$, only two studies were found: Bonaquist et al. (74) indicated that $|E^*|$ was greater than total M_R. Kallas (75) found M_R to be higher than $|E^*|$ at low temperatures, lower at 104°, and the same at 68°F ($|E^*|$ was measured at 4 hz). Von Quintus et al. (72) estimated $|E^*|$ via an earlier version of the Witczak equation and found that $M_{R,idt}$ was usually higher than $|E^*|$. In the present study, total $M_{R,idt}$ is compared to Witczak's $|E^*|$ in Fig. 30. As can be seen, M_R tends to be somewhat greater than $|E^*|$.

From all this, it would seem that one should enter the AASHTO Guide a_1 - chart with $M_{R,idt}$. If one uses total $M_{R,idt}$, it should be recognized that the resulting a_1 may be somewhat high, which would explain the low position of the Road Test mix in Fig. 29. And, if one uses instantaneous $M_{R,idt}$, the resulting a_1 would be even more likely to be on the high side.

Effect of Variables. As previously mentioned, resilient modulus results for each mix were correlated with 8 different characterization methods for gradation curves, as reported in Table 15. The best correlation was with $\bar{A}$. Two other methods, which did not lend themselves to direct correlation, were evaluated in the multiple regression

There is very little in the literature by way of comparisons between the different moduli. First, Von Quintus et al. (72) found $M_{R,idt}$ to be significantly higher than $M_{R,comp}$ at 104 and 77°F, but equal at 40°F. The data appeared to be in terms of total M_R. Khosla and Ohmer (73) found essentially no difference between the two M_R types over a wide range of temperatures. Second, by inspection of the $M_R = \sigma/\epsilon$ relationship, instantaneous M_R would have to be larger than total M_R. Turning to M_R vs $|E^*|$, only two studies were found: Bonaquist et al. (74) indicated that $|E^*|$ was greater than total M_R. Kallas (75) found M_R to be higher than $|E^*|$ at low temperatures, lower at 104°, and the same at 68°F ($|E^*|$ was measured at 4 hz). Von Quintus et al. (72) estimated $|E^*|$ via an earlier version of the Witczak equation and found that $M_{R,idt}$ was usually higher than $|E^*|$. In the present study, total $M_{R,idt}$ is compared to Witczak's $|E^*|$ in Fig. 30. As can be seen, M_R tends to be somewhat greater than $|E^*|$.

From all this, it would seem that one should enter the AASHTO Guide a_1 - chart with $M_{R,idt}$. If one uses total $M_{R,idt}$, it should be recognized that the resulting a_1 may be somewhat high, which would explain the low position of the Road Test mix in Fig. 29. And, if one uses instantaneous $M_{R,idt}$, the resulting a_1 would be even more likely to be on the high side.

Effect of Variables. As previously mentioned, resilient modulus results for each mix were correlated with 8 different characterization methods for gradation curves, as reported in Table 15. The best correlation was with $\bar{A}$. Two other methods, which did not lend themselves to direct correlation, were evaluated in the multiple regression

analysis portion of the study.

Other parameters have been shown to be important to the stiffness of a given mixture (32-34). These are: temperature, asphalt viscosity at 70°F, effective asphalt content, some measure of void content, gradation, and possibly particle shape and texture.

Inspection of the data shown in Figs. 29 and 31 to 35 reveals that resilient modulus appears to increase with:

1. lower temperature,
2. greater asphalt cement viscosity,
3. more densely graded mixtures (greater % passing the #4 and #200 sieves), and
4. avoidance of over-asphalting.

Loss of modulus with increasing temperature has been well documented in the literature (37). Likewise, a loss in modulus with a decrease in asphalt viscosity is also supported by other researchers (76,77). Little has been reported in the literature about the effects of gradation specific to resilient modulus (IDT-method), or changes in asphalt content (as an independent variable). In this study, an increase in M_R was noticed for increases in $\bar{A}$, percent passing the #200 sieve, and decreases in percent accumulative retained on the #4 sieve, all of which result in a finer, more densely graded gradation.

Coarse and fine aggregate fraction particle shape, as shown in Figs. 36 and 37, did not seem to exhibit a significant trend in their effect on resilient modulus.

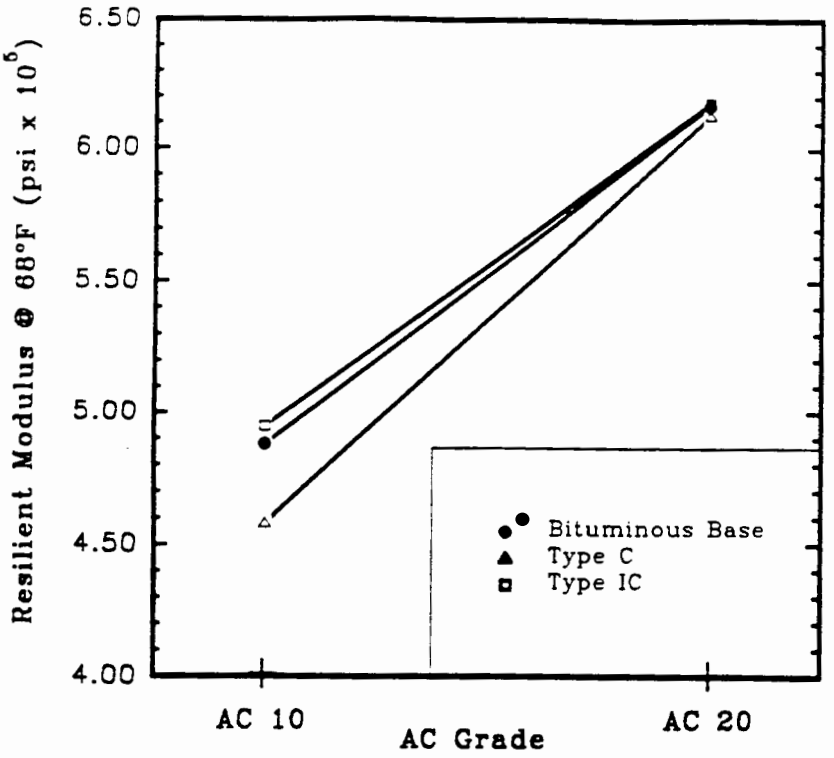

Fig. 31. Effect of Asphalt Cement Viscosity on Resilient Modulus.

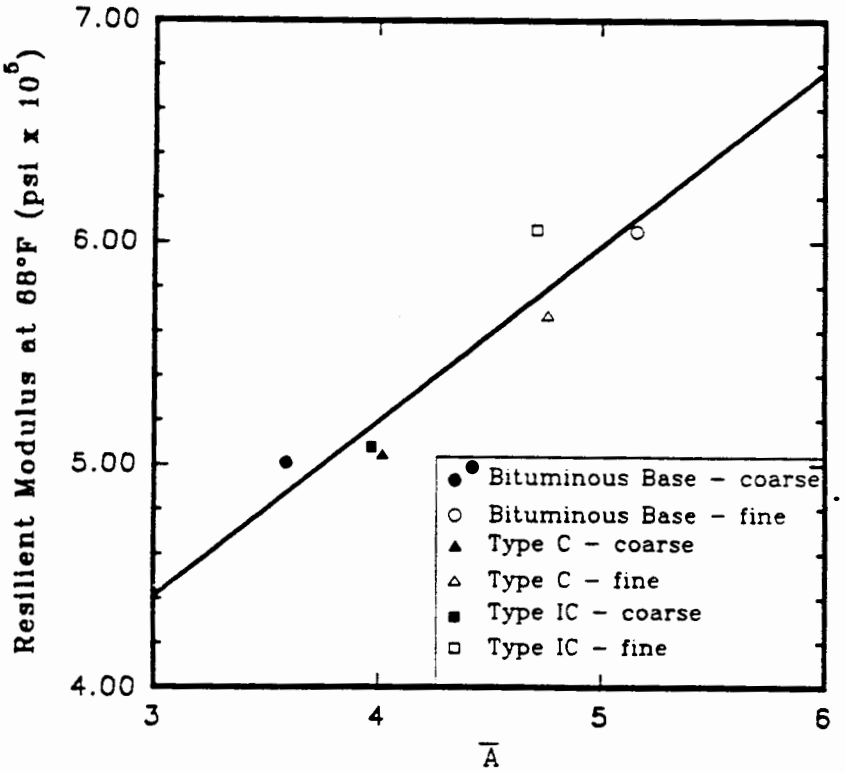

Fig. 32. Effect of Gradation on Resilient Modulus.

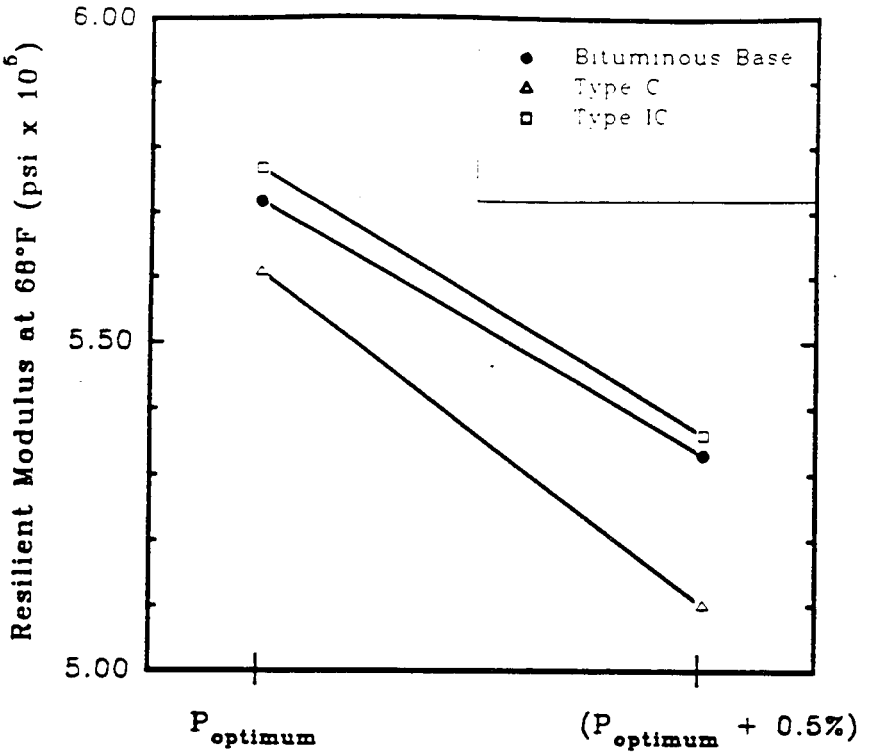

Fig. 33. Effect of Asphalt Content on Resilient Modulus.

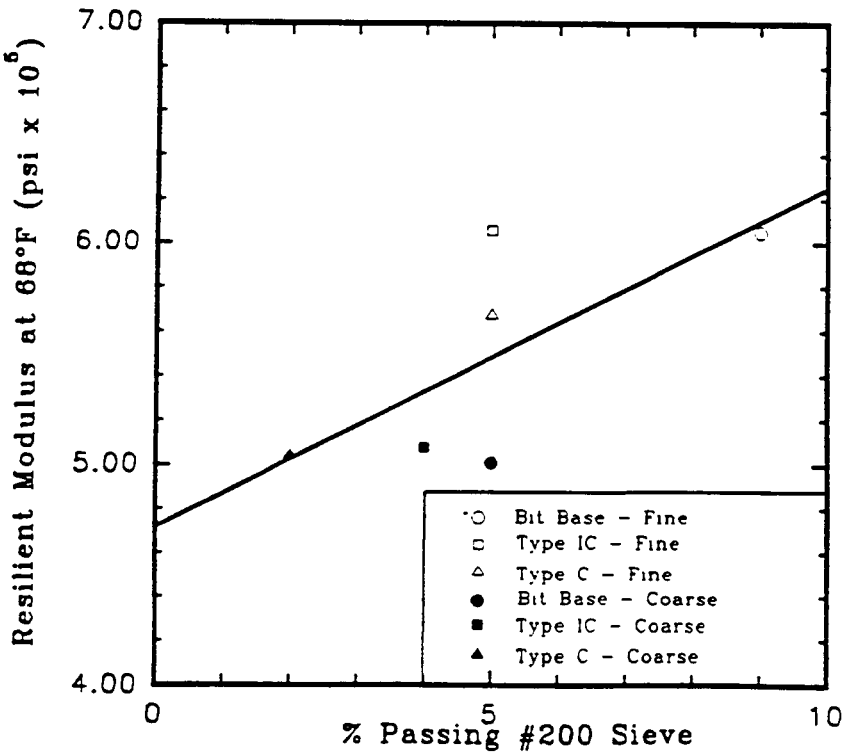

Fig. 34. Effect of % Passing the #200 Sieve on Resilient Modulus.

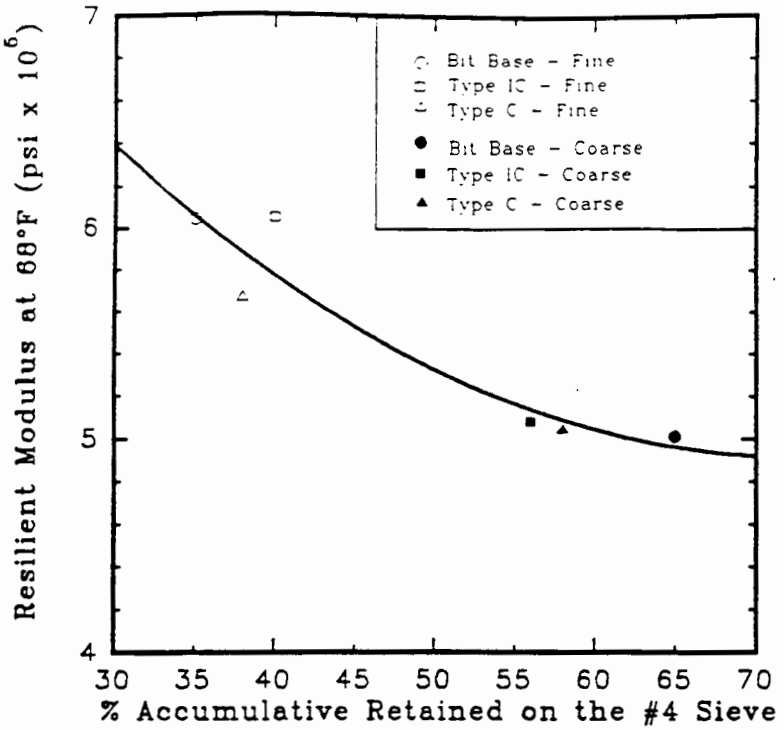

Fig. 35. Effect of Percent Accumulative Retained on the #4 Sieve on Resilient Modulus.

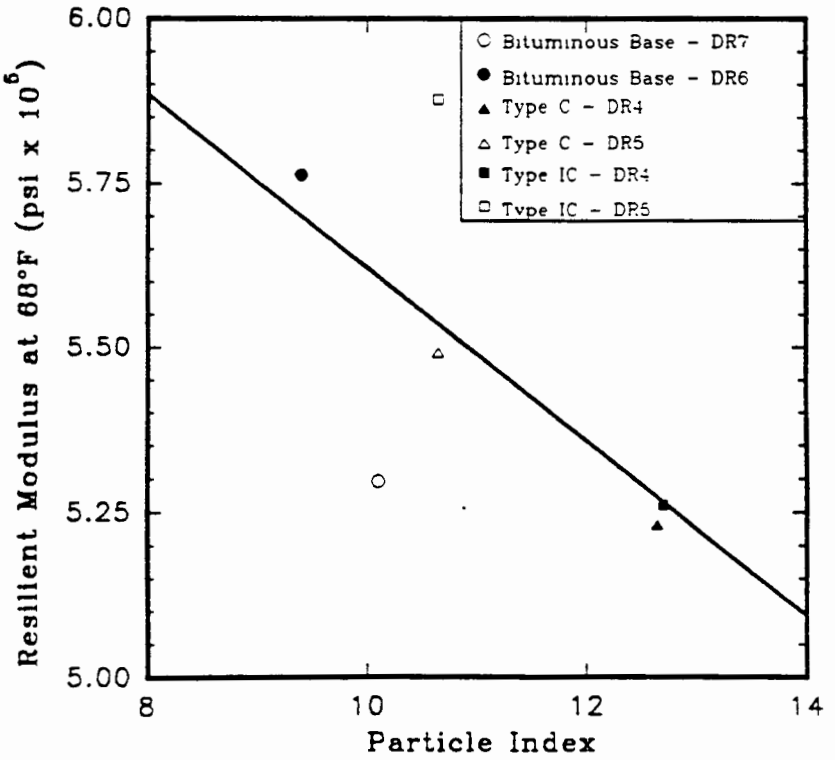

Fig. 36. Effect of Index of Particle Shape of Coarse Aggregate on Resilient Modulus.

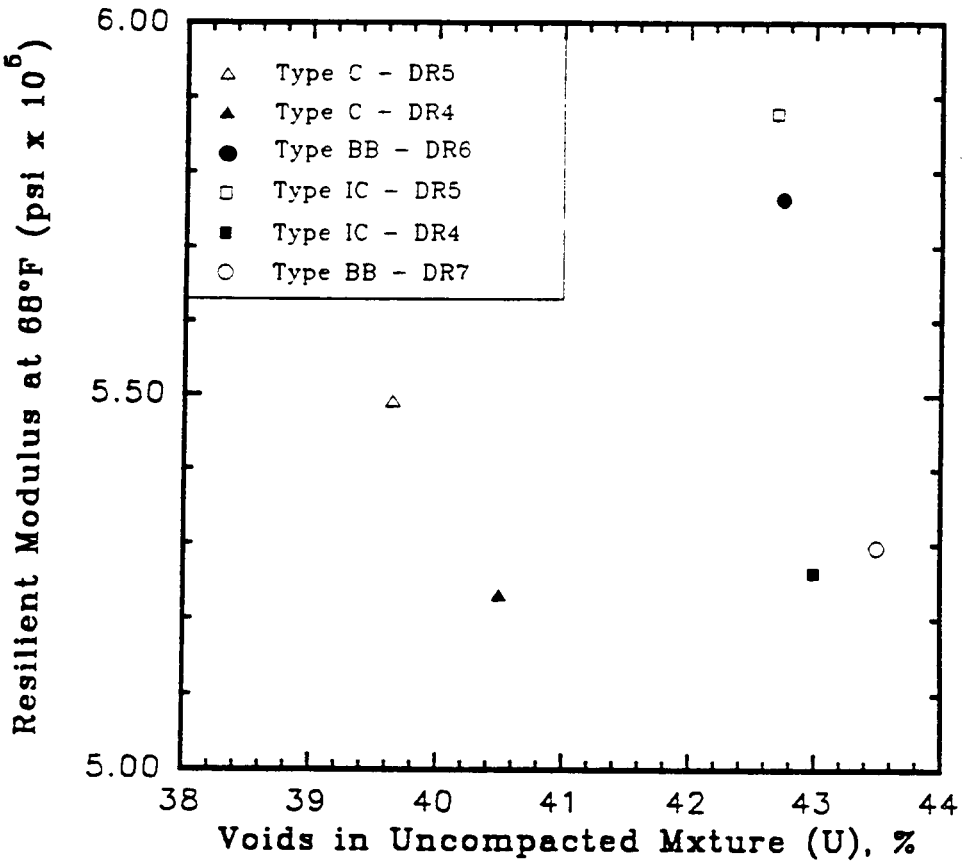

Fig. 37. Effect of Particle Shape of Fine Aggregate Fraction on Resilient Modulus.

Adedilmila and Kennedy (67) indicated that there was no significant difference in resilient moduli of gravel and crushed limestone mixes, although the gravel mixes generally had slightly higher values.

In this study, compactive effort for all specimens was held constant. Therefore, any differences in VMA and air voids were a function of differences in particle shape, gradation, and whether or not the mixture was purposely over asphalted. Changes in void content were not, then, a function of level of compaction. Being dependent variables, it was difficult to draw conclusions about their effect on M_R. For instance, air void content was lower in the overasphalted mixes, and so was M_R, but what really caused the M_R loss? As Abkemeier (63) has summarized:

> Generally, opinion and testing results have been mixed with respect to the effect of air voids on asphalt mixture properties. Most test results from the static and dynamic indirect tensile tests (31,76,78) indicate that with decreasing air void content of the asphalt mixture, tensile strength and resilient moduli will correspondingly increase.
>
> Other investigators (42,67,79) have had less conclusive results. These investigators have concluded that air voids are not directly related to fatigue life, tensile strength, and resilient moduli and that possibly an optimum air void content exists for these properties. Careful evaluation of mix factors would be required when evaluating the effect of air void content, since air voids are highly dependent upon other factors. Such factors include compactive effort, asphalt content, a change from open to dense gradation, or any combination of these.

In the present study, changes in M_R due to VMA differences caused by gradation changes were significant, both in the paired t-test and in the regression analysis.

Statistical Analysis

An analysis of the data was undertaken using the statistical software package SYSTAT. First, the means of the five independent variables were checked via Tukey's HSD test and paired t-tests to compare the means in order to determine which variables were statistically different from the others. Next, multiple regression was used to provide a model for the estimation of resilient modulus from the index data.

Tests of Significance. The first question to be answered was, for each of the five independent variables, was the difference in magnitude from high to low a significant contributor to changes in M_R? For example, for the whole data set, did switching from AC10 grade to AC20 significantly affect M_R? To test this hypothesis, the M_R data were sorted into two groups (AC10 and AC20) and the means of both groups were calculated. Then the two means were tested via Tukey's HSD to see if they were significantly different at the 0.05 level. The same sort of analysis was done on the other independent variables: two levels of asphalt content (optimum and optimum-plus-0.5%), three levels of testing temperature, six levels of gradation (Hudson's $\bar{A}$ values) or two levels of gradation (coarse and fine), and six levels of aggregate type (see Table 17). Two other variables that have been shown to be important are percent passing the #200 sieve and percent accumulative retained on the #4 sieve. These were, in effect, tested when $\bar{A}$ was tested.

The results are shown in Table 23. The analysis was broken into four parts. First, as the top portion of Table 23 indicates, results from all 48 mixtures and all three temperatures were lumped into one data set and examined. The results show

that because temperature is such a dominant variable, only temperature was significant at the 0.05 level. Of course, M_R decreased with increasing temperature.

The second portion of Table 23 shows the results when temperature was removed as a variable. The trends are the same as in the upper portion of the table, that is, greater stiffness came from mixtures that were comprised of higher viscosity asphalt, finer gradation, asphalt contents near optimum (as opposed to being overasphalted), and greater proportions of manufactured sand. Only asphalt viscosity and aggregate gradation (fine or coarse) were significant at the 0.05 level, although gradation (six levels of $\bar{A}$) was significant at the 0.089 level.

The bottom portion of Table 23 breaks the analysis down in regard to mixture type. For the bituminous base and IC mixes, viscosity and gradation (only 2 levels are possible) were significant at the 0.06 level; for the C mixes, only viscosity was significant.

Table 23. Significance of Variables to Resilient Modulus.

M_R (psi)				
CONDITION	Maximum	Minimum	Difference	Significance at 0.05 level
All 3 Temperatures, all mixtures				
Temperature, 41° and 104°	1,114,100	113,922	1,000,178	yes
Viscosity, AC 20 and AC10	587,919	498,221	89,698	no
Gradation, fine and coarse	609,651	476,489	133,162	no (yes at 0.07 level)
Gradation, fine to coarse	673,109	459,125	213,984	no
% Asphalt, opt. and (+) 0.5%	547,890	538,251	9,639	no
Agg. blend, BB6 and IC4	582,394	521,888	60,506	no
Mixture type, BB and IC	553,769	533,360	20,409	no
68°F, all mixtures				
Viscosity, AC20 and AC10	616,500	480,792	135,708	yes
Gradation, fine and coarse	592,875	504,417	88,458	yes
Gradation, fine to coarse	638,750	500,875	137,875	no (yes at 0.089 level)
% Asphalt, opt. and (+) 0.5%	570,292	527,000	43,292	no
Agg. blend, BB6 and IC4	587,750	523,000	64,750	no
Mixture type, IC and C	556,938	536,000	20,938	no
68°F, Bituminous Base				
Viscosity, AC20 and AC10	617,375	488,625	128,750	yes
Gradation, fine to coarse	605,125	500,875	104,250	yes
% Asphalt, opt. and (+) 0.5%	572,125	533,875	38,250	no
Agg. blend, BB6 and BB7	576,375	529,625	46,750	no
68°F, Type C				
Viscosity, AC20 and AC10	613,250	458,750	154,500	yes
Gradation, fine to coarse	567,625	504,375	63,250	no
% Asphalt, opt. and (+) 0.5%	561,125	510,875	50,250	no
Agg. blend, C5 and C4	549,000	523,000	26,000	no
68°F, Type IC				
Viscosity, AC20 and AC10	618,875	495,000	123,875	yes
Gradation, fine to coarse	605,875	508,000	97,875	no (yes at 0.061 level)
% Asphalt, opt. and (+) 0.5%	577,625	536,250	41,375	no
Agg. blend, IC5 and IC4	587,750	526,125	61,625	no

To examine the effect of coarse aggregate particle shape more closely, paired t-tests were performed for each mix type at each test temperature. In this way, all variables except particle shape were kept constant. For an example, refer to Table 24. Here, for C mixtures at 41°F, each pair of M_R values were for constant asphalt grade, asphalt content, temperature, and gradation (nearly). The mean of the differences was tested for significance.

Table 24. Example of Paired T-Tests: C Mixes at 41°F.

Gradation	AC	% AC	Resilient Modulus (psi)	
			DR 4	DR 5
fine	10	opt.	1,319,480	1,277,437
coarse	10	opt.	785,818	1,090,774
fine	10	(+) 0.5%	1,148,340	1,191,103
coarse	10	(+) 0.5%	874,245	973,954
fine	20	opt.	1,199,178	1,244,735
coarse	20	opt.	1,028,246	944,909
fine	20	(+) 0.5%	1,519,983	1,057,379
coarse	20	(+) 0.5%	1,302,515	921,963

The coarse aggregates that were compared were 6 vs 7, and 4 vs 5. Almost none of the nine data sets that were examined showed any significant changes in M_R due to coarse aggregate type.

A similar study was undertaken for fine aggregate. Here, IC mixes were compared to C mixes, holding all other variables constant. In essence, this was a test to see if increasing the proportion of manufactured sand at the expense of natural

sand made any difference in M_R. The results indicated that in most cases there was no significant difference.

Finally, a paired t-test was performed on VMA results. Each pair of M_R values had a common aggregate blend, asphalt viscosity, asphalt content, and testing temperature (68°F). The only variable different between the two M_R values was gradation, which caused a difference in VMA. The results indicated that VMA did differ significantly between pairs.

Multiple Regression. Multiple regression equations were fit to the resilient modulus data. Many combinations of variables were analyzed. The criteria for final selection were the same as discussed in the "Indirect Tension" section.

The following model most successfully predicted the dependent variable (resilient modulus) with an $R^2 = 0.948$, an adjusted $R^2 = 0.946$, a SEE = 0.099, and an absolute error = 18.0%. This is comparable to the results of Akhter and Witczak ($R^2 = 0.931$ and 0.934, SEE = 0.122 and 0.125). Absolute error of Akhter and Witczak's equation was not available, but an earlier model based on the same data gave an absolute error of 20.6% (33). Absolute error is calculated as:

$$Absolute\ Error = \frac{Predicted\ M_R - Measured\ M_R}{Measured\ M_R} * 100 \quad . \quad . \quad (51)$$

Data to develop the equations came from Tables 5, 10, 15 and Appendix F.

For all mixtures:

$$\log M_R = 7.137 - 0.016T - 0.005AR_4 - 0.088\eta_{70} - 0.028P_{effv} - 0.006P_{200} * \left(|P_{opteffv} - P_{effv}| \right) - 0.016Pair \quad \ldots\ldots \quad (52)$$

where:

T = mix test temperature, °F

η_{70} = asphalt absolute viscosity @70°F, poises * 10^6

P_{200} = percent material by weight passing the #200 sieve

P_{effv} = percent effective asphalt content by volume

P_{air} = percent air voids

AR_4 = percent accumulative retained on the #4 sieve

$(P_{opteffv} - P_{effv})$ = difference in effective optimum asphalt content and effective asphalt content, %.

The standardized regression coefficients indicated that the relative importance of variables were, in descending order: temperature, AR_4, viscosity, P_{eff}, P_{200} * $(P_{opteffv} - P_{effv})$, and P_{air}. Thus, by knowing relatively easily obtainable mix design data, the resilient modulus of these mix types can be approximated.

The variables included in the model are temperature, P_{200} and AR_4 (measures of gradation), viscosity of asphalt cement at 70°F, P_{air}, and effective asphalt content by volume, and the difference between the mix design effective asphalt content (optimum) and the amount actually in the mix. These were identified through use of the multiple regression analysis as being the most significant variables in their effect upon resilient modulus. Many other variables were tried, but did not contribute significantly to the model, or suffered from multicollinearity. Multicollinearity occurs

when two or more variables are highly correlated. When this happens, the regression coefficients tend to be unstable, an undesirable situation. Thus, even though several terms involving gradation description ($AR_{3/4}$, $AR_{1/2}$ or Hudson's $\bar{A}$) gave a higher adjusted R^2 to the model, they had to be excluded.

Also, it was postulated that some measure of particle angularity/surface texture would enhance the model. In fact, inclusion of U (fine aggregate particle shape index) and IP (coarse aggregate particle shape) did improve the model, but a t-statistic test indicated that they were not significant contributors. This may be because of the somewhat limited range of particle shapes involved in the study.

Some measure of void content was originally considered as potentially important. As it turned out, air voids had a slight edge over VMA.

Other variables that were tried unsuccessfully were percent absorbed asphalt content, voids filled, dust ratio, aggregate gradation curve slopes ($M_{4\text{-}200}$, $M_{1/2\text{-}4}$, $M_{3/4\text{-}1/2}$), percent retained on each sieve, and SF/SSF. Both Hudson's $\bar{A}$ and the gradation curve slopes enhanced equation accuracy, but using individual sieves proved to be somewhat better.

In regard to each variable's regression coefficients, it should be pointed out that the relative importance of prediction cannot be gaged from the magnitude of the coefficient because this is influenced by the scale of the variable. Also, the direction of the association between the dependent variable (resilient modulus) and any independent variables cannot be ascertained by the sign of the coefficient. And it must be emphasized that regression equations are only valid for the ranges of data

studied. Extrapolation should be done with caution, especially in the lower temperature range where errors (scatter of data) is much higher. This is typical for any kind of modulus testing. And, if one is tempted to play "what if" by substitution of hypothetical mixture data into the equation, it must be remembered that certain variables tend to be dependent upon each other in the real world (e.g., - #200 sieve material and #4 material), so any substitution of values must be done in a realistic manner.

It can be seen that Eq. 52 is similar to Akhter and Witczak's Eq. 26 which contains the variables temperature, η_{70}, P_{200}, P_{effv}, P_{air}, AR_4, and $(P_{effv} - P_{opt\ effv})$ as well as $AR_{3/4}$, f, and P_{absw}. In the present study, $AR_{3/4}$ was excluded because of multicollinearity problems, testing frequency (f) was not a variable in this study, and P_{absw} was shown to be an insignificant contributor. Many interactions, such as $(A*\eta_{70})$, proved to be collinear with other parameters.

The relationship between estimated and experimental values of resilient modulus is shown in Fig. 38. The high R^2 value demonstrates a strong correlation.

Applications

Because layer coefficients are directly affected by resilient modulus, the practical impact of the above trends is that higher layer coefficients can be obtained by:

1. using a harder grade of asphalt (higher η_{70}),
2. using a more well-graded gradation (higher $\bar{A}$, adjusting P_{200} and AR_4), and
3. avoiding overasphalting (optimum P_{effv}).

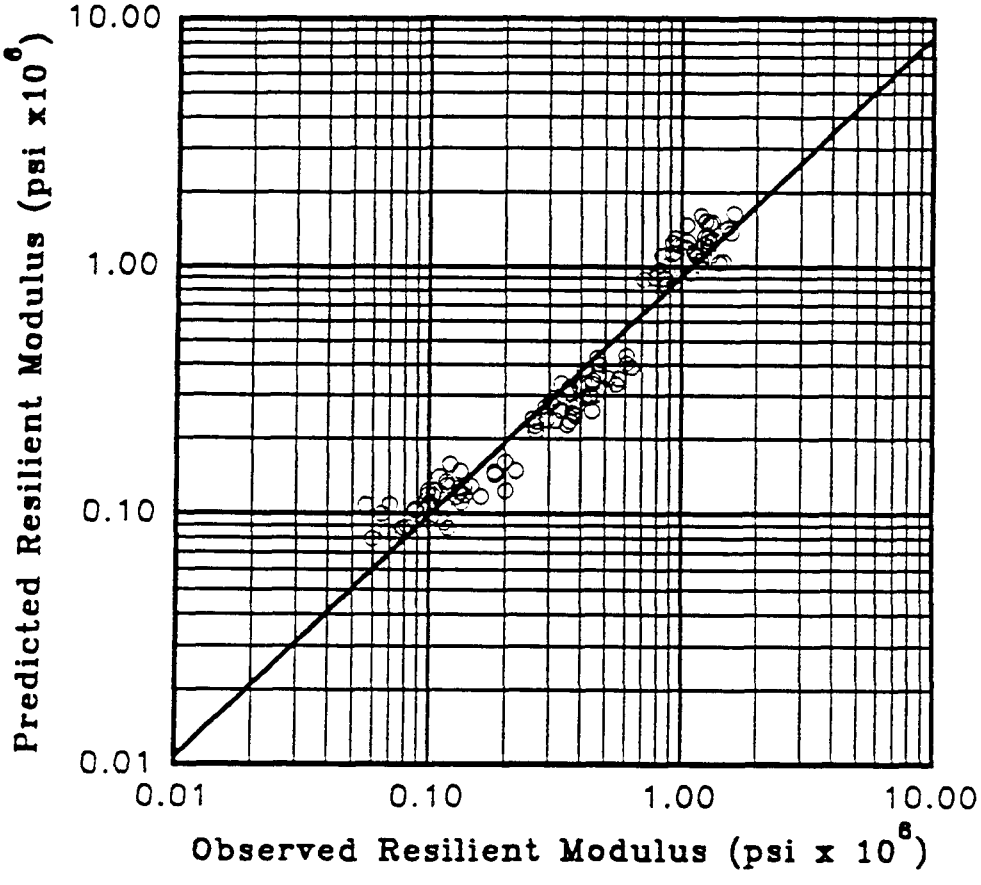

Fig. 38. Estimated vs. Experimental Resilient Moduli for UMR – Study Data.

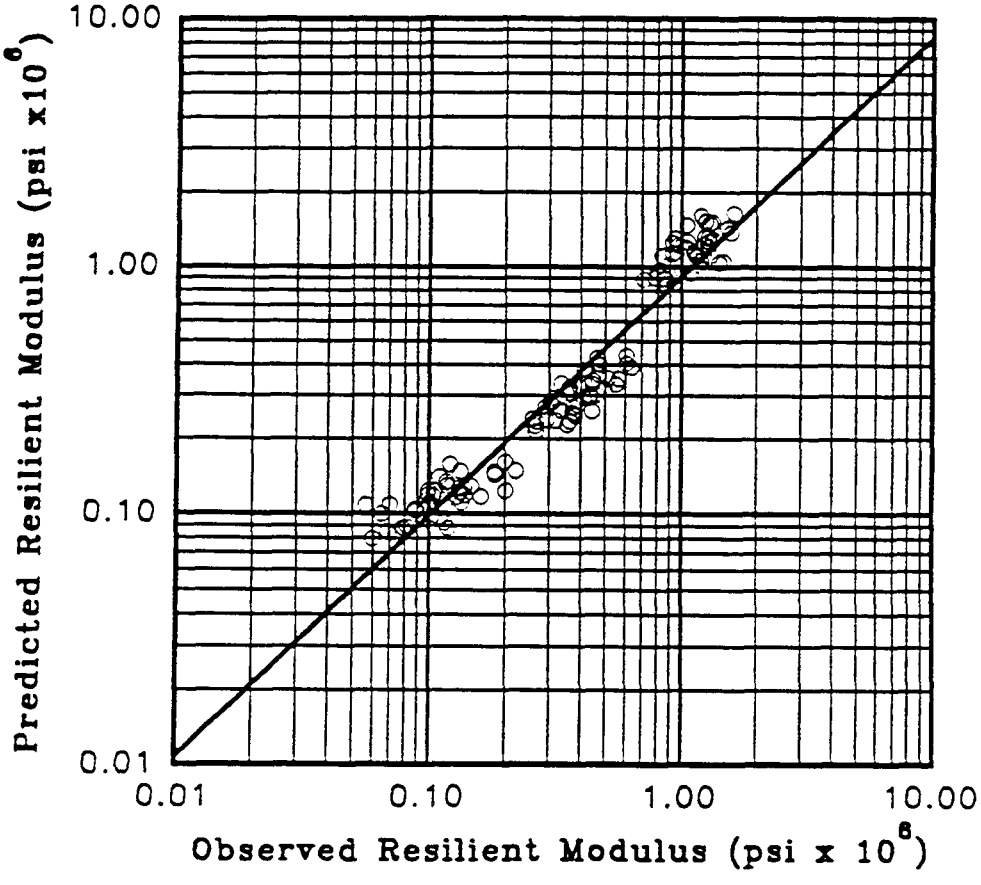

Fig. 38. Estimated vs. Experimental Resilient Moduli for UMR – Study Data.

M_R = resilient modulus, psi

T = mixture temperature, °F

P_{air} = percent air voids

η_{70} = asphalt absolute viscosity at 70°F, poise * 10^6

P_{200} = percent passing to #200 sieve

$AR_{3/4}$ = accumulative percent retained on the 3/4 in sieve

P_{effv} = percent effective asphalt content by volume

The standardized regression coefficients indicated that the relative importance of variables were, in descending order: temperature, P_{air}, viscosity, P_{200}, $AR_{3/4}$, and P_{effv}. Again, the model was based on the highest adjusted R^2 compatible with the model criteria previously discussed. The model resulted in R^2 = 0.846, adjusted R^2 = 0.842, SEE = 0.164, and an absolute error of 32.9%. The model is less accurate than the model developed from laboratory data developed in the present study, which had an absolute error = 18.0%. This is not surprising, because the general data base reflected five different testing programs which included different operators, equipment, and, most likely, test methodology. And, to put things in perspective, it should be remembered that the Shell method for S_m determination is based on Van der Poel's work, which was claimed to have an accuracy within a factor of ±2; it would appear that the model in Eq. 53 is considerably more accurate than this.

The method of cross-validation was used to determine the variables which were significant. The whole data set was split into two parts in a random fashion. A regression model was developed for the first portion as per the above criteria. Once

the variables were chosen, the second data set was applied to the model. The SEE of each set were compared, and were shown to be close. Finally, the data sets were recombined. A final model was calculated, using the same variables as were previously determined for the first half of the data set.

The ranges of variables that the industry-wide portion of the data represented are shown in Table 25. The industry-wide portion of the data set is included in Appendix G.

Table 25. Ranges of Variables in Industry-Wide Data Base.

Variable	Range
Temperature, °F	24 - 104
Viscosity at 70°F, poise x 10^6	0.17 - 9.5
Asphalt effective volume, %	4.1 - 14.5
Accumulative retained on 3/4 in. sieve, %	0 - 0
Accumulative retained on 1/2 in. sieve, %	1 - 29
Accumulative retained on #4 sieve, %	37 - 60
Passing #200 sieve, %	4.0 - 8.3
Air voids, %	0.2 - 15.4
Resilient modulus, psi x 10^6	0.032 - 4.3

Range of loading time was very small (0.1 to 0.15 sec) with most of the data at 0.1 sec. Because the industry is standardizing at 0.1 sec., it was decided to remove loading time as a variable. Thus, the data set was limited to a loading time of 0.1 sec. The fact that the equation does not reflect loading time or frequency

effects is, although unavoidable, unfortunate because the repeated modulus of asphalt mixtures is to a certain degree a function of loading time. However, the standard time of 0.1 sec is conservative because this is 3 to 10 times longer than dwell times under actual traffic conditions, and thus should render a lower modulus.

Not all data were present in the desired form, and had to be converted from the existing form. Witczak (32) faced the same dilemma when he developed his model, so he created several equations to supply the missing data. Where necessary, equations developed by Witczak were utilized:

$$\eta_{70,poise \times 10^6} = 29,508.2\ (penetration_{77^\circ F})^{-2.1939} \quad . \ . \ . \quad (54)$$

$$P_{effv} = \frac{P_b}{0.483} \quad . \ . \ . \ . \ . \ . \ . \ . \ . \ . \quad (55)$$

where:

P_{effv} = percent effective asphalt content, by volume

P_b = percent total asphalt content, by weight of mix

A plot was made of estimated resilient moduli vs experimentally-determined moduli for the general model and is shown in Fig. 39.

Even though the general model is less accurate than the UMR model, the data on which Eq. 53 is based contains variables that exhibit a wider range of values. Thus, it would seem that the general equation would be more generally applicable. Thus, this is the model that is recommended for further use.

Data from 236 MHTD mixtures approved in 1990 were substituted into Eq. 53 to estimate resilient modulus. The results are shown in Table 26.

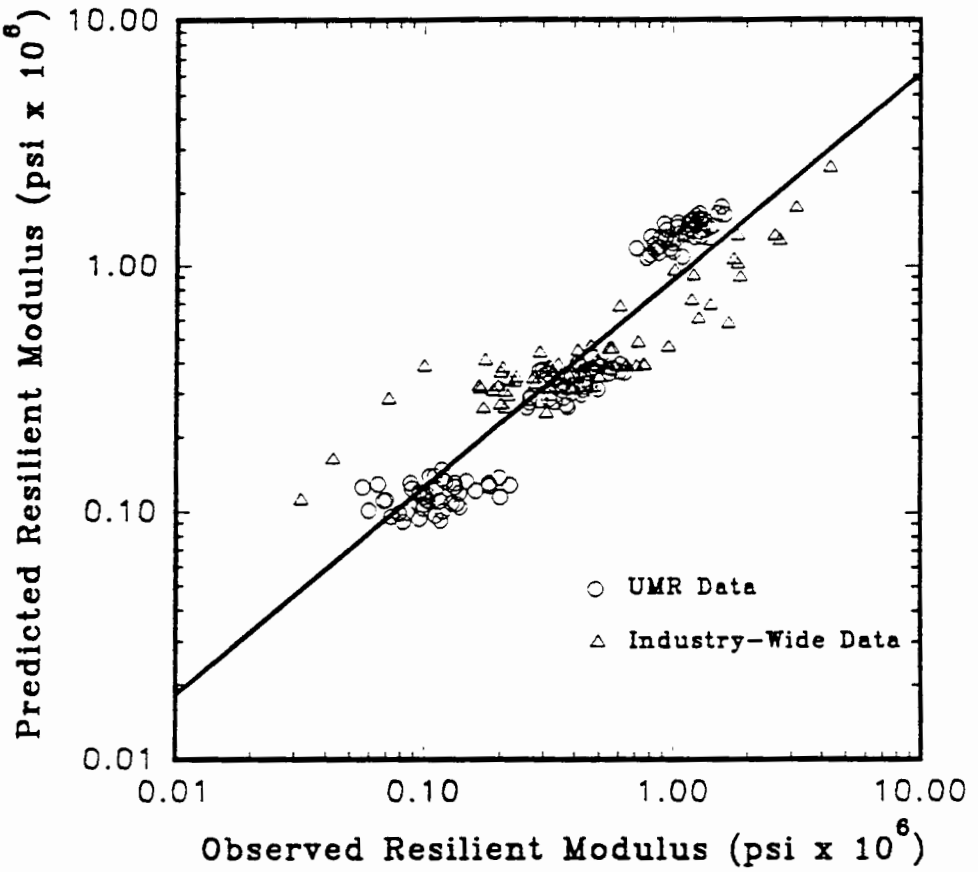

Fig. 39. Relationship of Estimated vs. Experimentally Derived Resilient Modulus Data from General Data Base.

Table 26. Resilient Modulus of MHTD Approved 1990 Mixes.

MHTD Mix			
	Min.	Max.	Mean
Type C	360,415	439,198	403,819
Type I-C	370,998	425,394	404,973
Bit. Base	377,642	581,453	460,000

In regard to each variable's regression coefficients, it should be pointed out that the relative importance of prediction cannot be gaged from the magnitude of the coefficient, because this is influenced by the scale of the variable. Also, the direction of the association between the dependent variable (resilient modulus) and any independent variables cannot necessarily be ascertained by the sign of the coefficient. And it must be emphasized that regression equations are only valid for the ranges of data studied. Extrapolation should be done with caution, especially in the lower temperature range where errors (scatter of data) are much higher. This is typical for any kind of asphalt modulus testing. And, if one is tempted to play "what if" by substitution of hypothetical mixture data into the equation, it must be remembered that certain variables tend to be dependent upon each other in the real world (e.g., #200 sieve material and VMA), so any substitution of values must be done in a realistic manner.

PAVEMENT TEMPERATURE

The modulus of an asphalt mixture is significantly affected by temperature. Values of temperature are necessary for the estimation of dynamic modulus (Akhter

and Witczak), mixture stiffness (Shell), and resilient modulus (as developed in the present study). Because layer coefficients are applied to field conditions, it becomes necessary to determine or estimate pavement field temperatures.

In this study, representative temperatures of the asphalt layers were estimated by use of Witczak's method (24) as previously discussed. Use of Witczak's equation (Eq. 16) requires input of mean air temperature and one representative depth in a given layer.

Climatological data from 104 reporting stations in Missouri were analyzed in order to calculate a mean monthly air temperature of 55.06 °F. This data is tabulated in the companion study of this report (2).

Pavement temperature is also a function of its thickness. Pavement thickness data supplied by the MHTD were analyzed for mean thicknesses of asphalt surface, binder, and base layers. Because surface and binder layers were considered as one layer at the AASHO Road Test in computation of layer coefficients, the MHTD surface and binder layers also were combined for temperature analysis. The Missouri data indicated that for full-depth and asphalt-over-unbound base structures, the mean surface-plus-binder thickness was 3.26 in and the mean bituminous base thickness was 5.07 in. Typically, the temperature at a depth of one third the layer thickness is taken as representative of the mean temperature of the entire layer. This can be shown to be close to the mean pavement temperature by use of the mean value theorem (25). Use of these points in the mean pavement structure in Eq. 16 yielded representative MHTD pavement temperatures of 65.2 °F (18.4 °C) and 63.4 °F (17.4

°C) for the surface-plus-binder and bituminous base layers, respectively.

In a similar manner, from AASHO Road Test data, pavement temperatures were predicted for the surface/binder layer and the bituminous base as shown in Table 27.

There is some question about the average pavement temperature at the Road Test. In NCHRP 128 it is stated that this temperature was 67.5°F and in the 1986 AASHTO Design Guide, the flexible pavement modulus-layer coefficient nomograph is standardized at 68°F. It is stated in the Road Test Special Report 5 that pavement temperatures were recorded. Corree and White (12) state that in a search of the special reports and computer data from the Road test, no such information could be found. Personal communication with White revealed that some records have been lost in a fire. A search by the authors has also been fruitless. NCHRP 128 states that the standardized modulus of the surface layer was 450,000 psi. In NCHRP 291, data from Road Test asphalt mixture modulus testing are presented. An analysis of these data indicates that the average pavement temperature at the Road Test would have been 63°F in order to give a dynamic modulus of 450,000 psi. In the classic study of asphalt pavement temperatures at College Park, Maryland, Kallas (81) found that the average pavement temperature at all depths was about 63 to 64°F for an average air temperature of 54°F, which is about a 10°F difference. In a study of actual pavement temperatures in a similar climate, Croney (82) found that average pavement temperatures were about 7°F above the average air temperature of 49°F. According to data in Appendix C of Special Report 5, the average air temperature during the Road Test was about 50°F. Using this temperature, the Witczak equation (Eq. 16)

predicts a pavement temperature of 58 to 59°F, which is about 8 to 9°F above the average air temperature. Thus, it would seem reasonable that average pavement temperatures would be 7 to 10°F above average air temperatures, or about 57 to 60°, at the Road Test. This is significantly lower than the 68°F stated in NCHRP 128, and is close to the 58.1 and 59.1°F predicted by the Witczak equation. It also then seems reasonable to use the Witzcak equation to predict Missouri pavement temperatures. However, the analysis of pavement moduli hinges on the predicted temperatures of both MHTD and Road Test pavements. The use of the AASHTO layer coefficient chart, which calls for moduli input at 68°F, is thus brought into question. Use of this information will be discussed in the layer coefficient portion of the study.

LOAD DURATION AND FREQUENCY

Duration of load pulse (or frequency of application) has been shown to have an effect upon modulus or stiffness of asphalt mixtures (15,31). Either pulse duration or frequency is used as an input into the Shell method of stiffness estimation, and frequency is used as an input in Akhter and Witczak's dynamic modulus estimation.

At any given point in an asphalt layer, both pulse duration and frequency are dependent upon vehicle speed and depth of interest. From data supplied by the Planning Division of MHTD, the mean vehicle speed of all highways in the Missouri state system is 56.3 mph. Barksdale (53) has developed a relationship between vehicle speed, depth, and pulse duration, as shown in Fig. 40. Using the mid-depth of both the mean surface and bituminous layers (as determined above), and a vehicle speed of 56.3 mph, load pulse durations of 0.020 and 0.032 sec were determined for

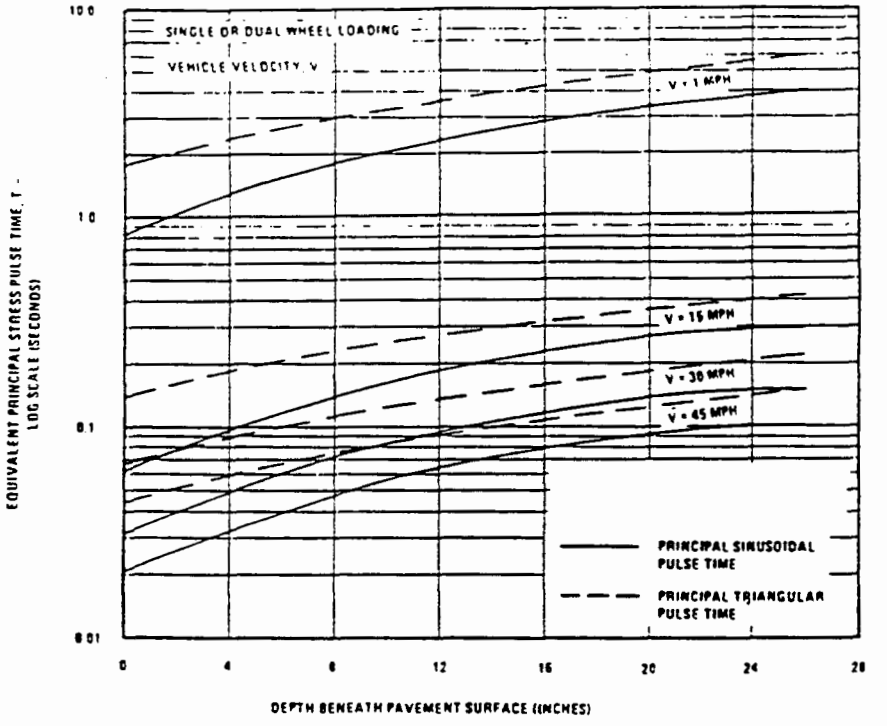

Fig. 40. Barksdale's Load Duration Chart.

the surface and base layers, respectively.

To convert load pulse duration (t) to load frequency (f), the relationship from Van der Poel (15) was used:

$$f = \frac{1}{2\pi t} \quad \text{(56)}$$

Thus, at the midpoints of the surface and base layers, the mean load frequency for MHTD pavements is taken as 8 and 5 cycles per second, respectively.

In a similar manner, from AASHO Road Test data, times of loading and frequencies were predicted for the surface/binder layer and bituminous base. The results of this analysis are shown in Table 27.

Table 27. Pavement Temperatures, Load Durations, and Frequencies.

Layer	Veh. Speed mph	D in	t sec	f cps	T_p °F (°C)
MHTD					
surface/binder	56.3	3.26	0.020	8	65.2(18.4)
base	56.3	5.07	0.032	5	63.4(17.4)
AASHO					
surface/binder	35	4.0	0.035	4.5	58.5(14.7)
base	35	8.83	0.068	2.3	57.1(14.0)
D = layer thickness					

These values were substituted into Eqs. 6,26,52, and 53 to estimate mixture stiffness and dynamic modulus, respectively. The results are discussed in the following sections.

ESTIMATION OF MIXTURE STIFFNESS

UMR MIXTURE STIFFNESS (S_m)

Mix stiffness via the Shell method for all 48 mixes used in this study were estimated by use of Eq. 6. For each mixture, values of asphalt content, aggregate content, asphalt cement penetration, time of loading (0.1 sec) and test temperature (41,77,104 °F) were substituted into Eqs. 3,4,13,15, and 16 in order to utilize Eq.6.

The resulting values of S_m were correlated with resilient modulus test data. The results are shown in Fig. 41.

Finally, using AASHO Road Test mixture data, S_m values for the surface/binder and bituminous base layers were calculated and are shown in Table 28, using Road Test temperature and loading time data.

Table 28. Estimation of AASHO Road Test Mixture Stiffness Under Road Test Conditions.

Layer	Pen	V_b %	V_a %	t sec	T °C	S_m psi
surface	91	12.67	83.74	0.032	15.0	687,320
binder	91	10.64	84.56	0.038	14.5	778,168
surface/binder	-	-	-	-	-	740,194
base	91	11.36	82.40	0.068	14.0	565,276
Note: AASHO Road Test average surface = 1.67 in, binder = 2.32 in						

Note that the Shell method considers six variables: three that address the viscoelastic properties of aged asphalt cement, and three that address the effects of mix properties. The gradation and particle shape/texture of the aggregate are ignored. Mixture stiffness increases with:

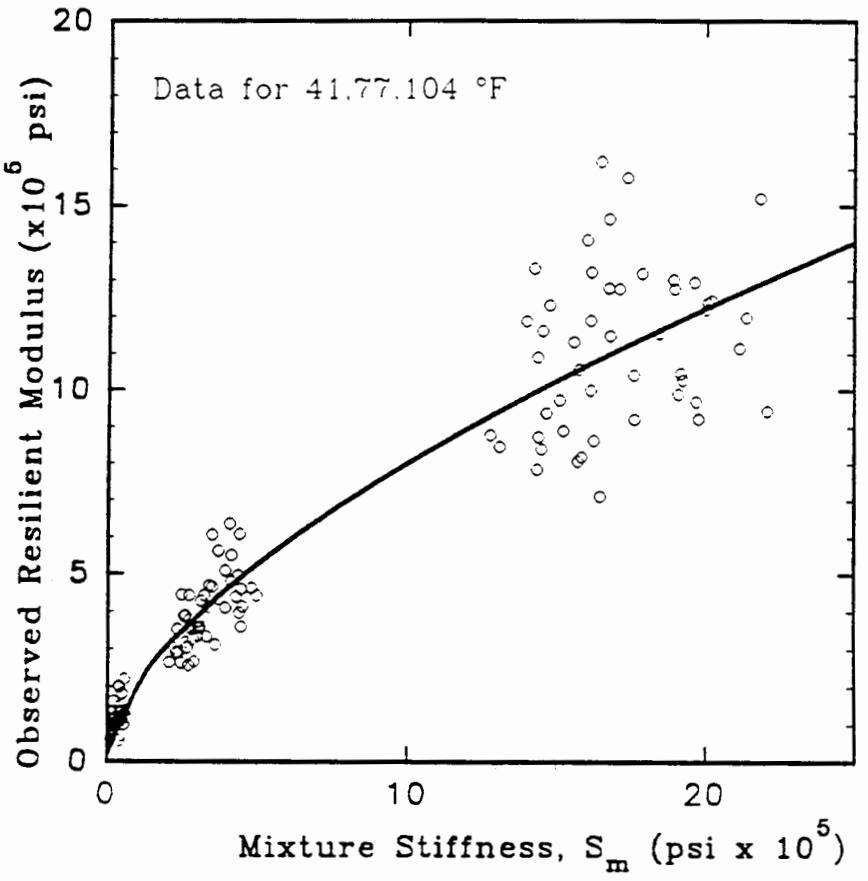

Fig. 41. Observed Resilient Modulus vs. Shell Mixture Stiffness for UMR Data.

- lower temperature
- lower penetration asphalt
- shorter load duration
- lower asphalt content
- higher aggregate content
- lower air void content

The resilient modulus testing program indicated that, on the average, the I-C mixes were slightly stiffer than the bituminous base mixes, and both were stiffer than the Type C mixes, which was the result of gradation and sand shape/texture differences. Because these variables are not considered in the Shell method, and because temperature, time, and asphalt grade were held constant, the relative rankings by the Shell method were the result of only relative material proportion differences. Because of the slightly higher aggregate and lower asphalt proportions, the predicted Shell stiffness of the C mixes averaged higher than the bituminous base mixes, followed by the I-C mixes. Table 29 shows the UMR, MHTD, and AASHO S_m data calculated at 68 °F and 0.1 sec load time for comparison.

- lower temperature
- lower penetration asphalt
- shorter load duration
- lower asphalt content
- higher aggregate content
- lower air void content

The resilient modulus testing program indicated that, on the average, the I-C mixes were slightly stiffer than the bituminous base mixes, and both were stiffer than the Type C mixes, which was the result of gradation and sand shape/texture differences. Because these variables are not considered in the Shell method, and because temperature, time, and asphalt grade were held constant, the relative rankings by the Shell method were the result of only relative material proportion differences. Because of the slightly higher aggregate and lower asphalt proportions, the predicted Shell stiffness of the C mixes averaged higher than the bituminous base mixes, followed by the I-C mixes. Table 29 shows the UMR, MHTD, and AASHO S_m data calculated at 68 °F and 0.1 sec load time for comparison.

viscosity at 70 °F, test temperature (41, 77, 104 °F), load frequency (1.6 H_z), effective asphalt content by volume, mix design optimum effective asphalt content by volume, accumulative percent aggregate retained on the #4 sieve, percent passing the #200 sieve, and percent absorbed asphalt by weight of mix were substituted into the equation.

The resulting values of dynamic modulus were correlated with resilient modulus test data, as previously shown in Fig. 30.

In a similar manner, using AASHO Road Test data, dynamic modulus values for the surface/binder and bituminous base layers were calculated by use of Eq. 26 and are shown in Table 30.

Table 30. Estimation of AASHO Road Test Dynamic Modulus Under Road Test Conditions.

Layer	P_{air} (%)	$AR_{3/4}$ (%)	n_{70} (poise x 10^6)	P_{eff} (%)	P_{abs} (%)	AR_4 (%)	P_{200} (%)	f (H_z)	T (°F)	E (psi)
surface	3.6	0	1.49	10.83	0.8	37	5.9	5	59.1	663,218
binder	4.8	4	1.49	7.81	1.2	64	4.3	4.2	58.1	681,678
base	6.2	4	1.49	10.77	1.2	28	5.6	2.3	57.1	627,656

Note: P_{air} = after traffic
$n_{70} = 29{,}508.2\ (pen_{77})^{-2.1939}$
$P_{eff} = P_b/0.483$
$P_{abs} = (P_b/0.434) - (P/0.483)$

It was reported in NCHRP 291 that the Asphalt Institute performed dynamic modulus tests on actual Road Test materials. An analysis of the data was performed and dynamic moduli were determined for both the surface and binder mixtures, which

viscosity at 70 °F, test temperature (41, 77, 104 °F), load frequency (1.6 H_z), effective asphalt content by volume, mix design optimum effective asphalt content by volume, accumulative percent aggregate retained on the #4 sieve, percent passing the #200 sieve, and percent absorbed asphalt by weight of mix were substituted into the equation.

The resulting values of dynamic modulus were correlated with resilient modulus test data, as previously shown in Fig. 30.

In a similar manner, using AASHO Road Test data, dynamic modulus values for the surface/binder and bituminous base layers were calculated by use of Eq. 26 and are shown in Table 30.

Table 30. Estimation of AASHO Road Test Dynamic Modulus Under Road Test Conditions.

Layer	P_{air} (%)	$AR_{3/4}$ (%)	n_{70} (poise x 10^6)	P_{eff} (%)	P_{abs} (%)	AR_4 (%)	P_{200} (%)	f (H_z)	T (°F)	E (psi)
surface	3.6	0	1.49	10.83	0.8	37	5.9	5	59.1	663,218
binder	4.8	4	1.49	7.81	1.2	64	4.3	4.2	58.1	681,678
base	6.2	4	1.49	10.77	1.2	28	5.6	2.3	57.1	627,656

Note: P_{air} = after traffic
$n_{70} = 29{,}508.2\ (pen_{77})^{-2.1939}$
$P_{eff} = P_b/0.483$
$P_{abs} = (P_b/0.434) - (P/0.483)$

It was reported in NCHRP 291 that the Asphalt Institute performed dynamic modulus tests on actual Road Test materials. An analysis of the data was performed and dynamic moduli were determined for both the surface and binder mixtures, which

A comparison is made between AASHO, UMR, and MHTD mixes in Table 31, at the same conditions of temperature and frequency.

Table 31. Comparison of Dynamic Modulus for AASHO, UMR and MHTD Mixtures.

Layer	Dynamic Modulus (|E*|)		
	AASHO	UMR	MHTD
Surface	366,703	-	-
Type C	-	352,059	320,640
Type I-C	-	361,790	314,556
Binder	377,704	-	-
Bituminous Base	381,097	570,158	484,789
Note: 68°F (20°C), 1.6 hz frequency			

The UMR bituminous base mixes are rated stiffer than the I-C (and C) mixes due to greater (+) 3/4 in sieve and minus #200 sieve size materials. The effect of gradation is still only partially accounted for if one considers the displacement of the gradation curve from the 0.45 power maximum density curve as an important criteria. And, again, the superior sand particle shape of IC aggregate is ignored.

The MHTD 1990 mixes were ranked from high to low: bituminous base, Type C, and then Type IC. Bituminous bases were predicted stiffer because of lower air contents, greater amount of (+) 3/4 in material, lower effective asphalt contents, and greater amount of minus #200 sieve material. Type C mixes were rated stiffer than I-C because of somewhat lower air void contents.

In comparing UMR mixes to MHTD mixes, UMR mixes were stiffer for all three mixture types due to lower asphalt contents, lower air void contents, and, in the case

of the bituminous base mixes, somewhat higher (+) 3/4 in material contents.

Looking at the AASHO Road Test mixes, in descending order of stiffness, the rankings were bituminous base, binder, and then surface, although the spread of values is not great. The difference in predicted values is primarily due to gradational differences.

The AASHO surface and binder moduli are predicted to be greater than the UMR (and MHTD) mixes primarily due to higher percent retained on the #4 sieve and lower (-) #200 sieve material (and greater air void content in the case of MHTD data). However, the AASHO bituminous base was less stiff than both the UMR and MHTD averages because of a greater percent (+) 3/4 in. material, lower air voids, greater (-) #200 sieve material, and lower effective asphalt contents. These relationships of UMR and MHTD to AASHO modulus values become important when estimating layer coefficients, as will be shown later.

MHTD MIXTURE DYNAMIC MODULUS (|E*|)

In a similar manner to UMR mixture dynamic modulus, data from MHTD mix designs approved in 1990 were used for estimation of each design's dynamic modulus by use of Eq. 26. Frequency and pavement temperature were taken as 4.5 hz and 17.4°C for surface mixtures Type C and I-C, and 2.34 hz and 18.4°C for bituminous base mixtures, respectively. The mean dynamic modulus values for Type C,IC, and bituminous base mixtures were 518,864; 509,020; and 600,821 psi, respectively.

DETERMINATION OF LAYER COEFFICIENTS

Five different methods were used for determination of layer coefficients. These

are presented below.

AASHTO NOMOGRAPHS

Use of the layer coefficient nomographs (Figs. 42 and 43) available in the 1986 AASHTO Guide require that asphalt resilient modulus values be at a temperature of 68°F. It is assumed that the Road Test conditions of loading time or frequency are also in effect. The modulus values at 68°F for the 48 mixtures used in this study were estimated from the temperature-modulus relationship developed for each mixture. An example is shown in Fig. 44. From inspection of the AASHTO nomographs, equations were developed to represent the curves for a_1 (asphalt mixture surface layer) and a_2 (bituminous base):

$$a_1 = 0.391071 \log E - 1.77224 \quad (57)$$

$$a_2 = 0.324553 \log E - 1.49975 \quad (58)$$

Each UMR resilient modulus at 68°F and at the test loading time of 0.1 sec for the Types C, I-C, and bituminous base were substituted into Eqs. 57 and 58 to obtain layer coefficients. The results are shown in Table 32 in the column marked "AASHTO Chart-UMR".

Secondly, the UMR-study mix data (48 mixes) were used in Eq. 53 (the General Model) to estimate M_R (68°F and 0.1 sec). Then, these M_R values were used in the AASHTO nomograph to obtain layer coefficients. The results are also shown in Table 32.

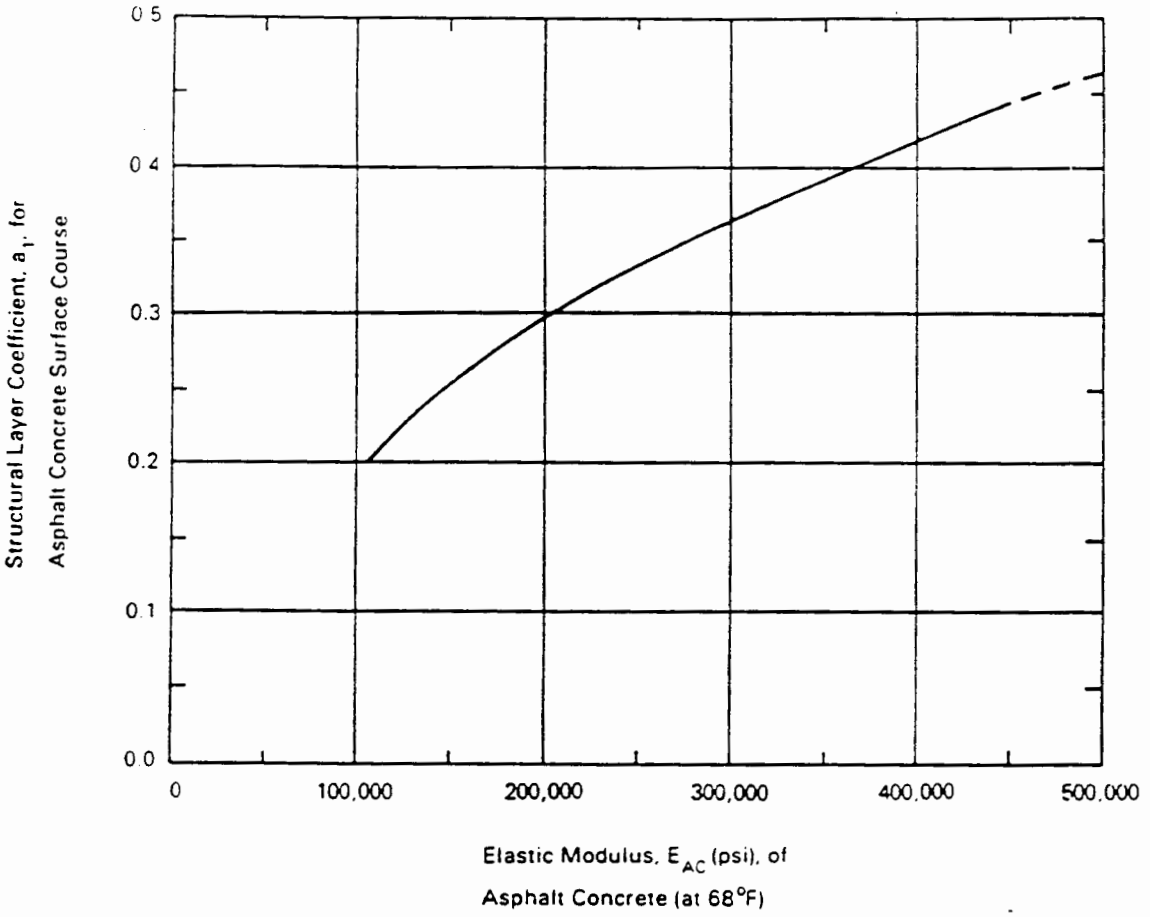

Fig. 42. AASHTO a_1 Layer Coefficient Nomograph.

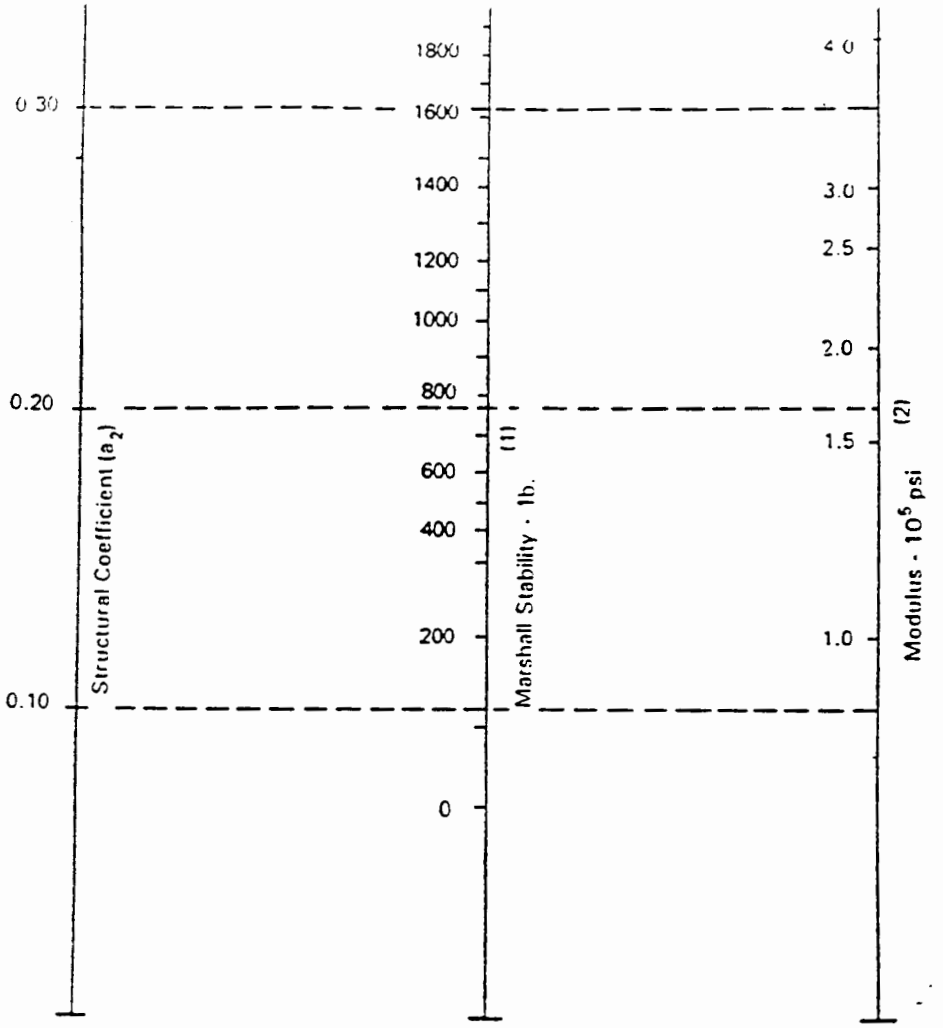

(1) Scale derived by correlation obtained from Illinois.

(2) Scale derived on NCHRP project (3).

Fig. 43. AASHTO a_2 Layer Coefficient Nomograph.

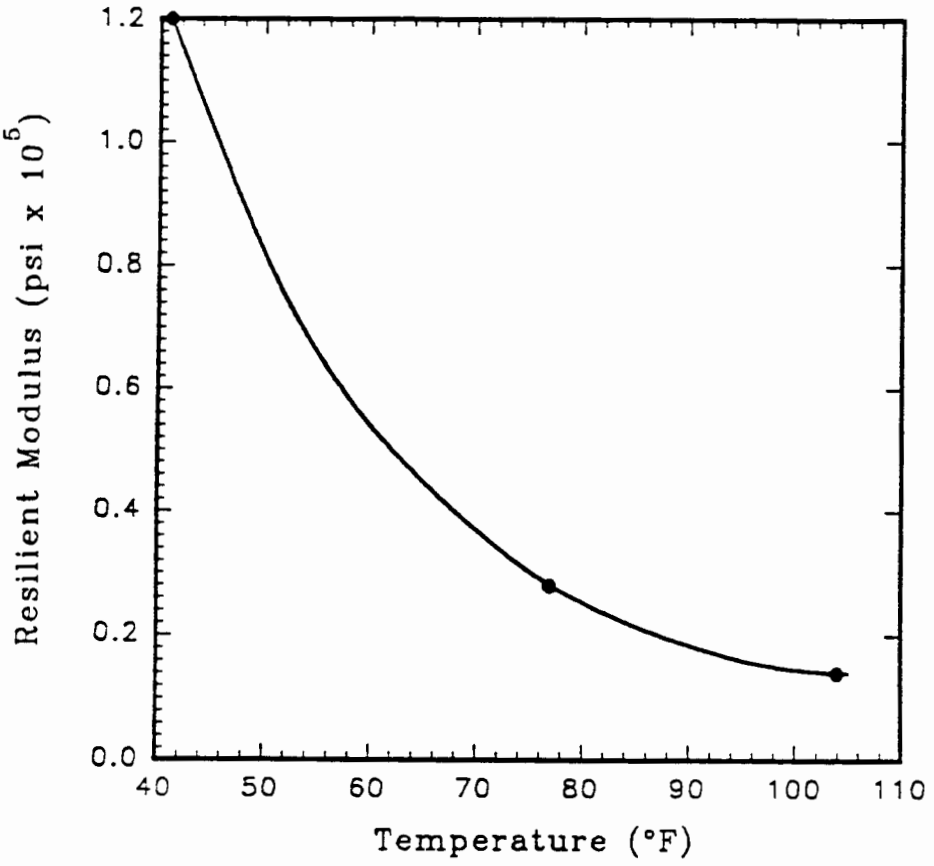

Fig. 44. Typical Temperature – Resilient Modulus Relationship.

EQUIVALENT STIFFNESS

Layer coefficients were also calculated by use of the Odemark equation for equivalent stiffness:

$$a = a_{AASHO}\left[\frac{stiffness}{stiffness,AASHO}\right]^{1/3}$$

where layer stiffness in this study was represented by mixture stiffness (S_m), dynamic modulus ($|E^*|$), and estimated resilient modulus (M_R) as follows.

Mixture Stiffness

Mixture stiffness (S_m) values were determined as previously discussed for UMR laboratory data and AASHO Road Test materials. Each mixture set of values were substituted into Eq. 6. The temperature and loading time of Missouri conditions were used for the UMR study dataset in the numerator, and AASHO Road Test conditions were used for the AASHO Road Test mixes in the denominator:

$$a_{1,2} = a_{AASHO\ 1,2}\left[\frac{S_m}{S_m,AASHO}\right]^{1/3}$$

The results are shown in Table 32.

Dynamic Modulus

In a manner similar to mixture stiffness, dynamic modulus values were substituted into Eq. 6:

$$a_{1,2} = a_{AASHO\ 1,2}\left[\frac{|E^*|}{|E^*|_{AASHO}}\right]^{1/3}$$

The results are shown in Table 32.

Resilient Modulus

Again, in a manner similar to the above, estimations of M_R for UMR study data (Missouri road conditions) and AASHO Road Test mixes (Road Test conditions) were substituted into Eq. 6:

$$a_{1,2} = a_{AASHO\ 1,2}\left[\frac{M_{Rest}}{M_{R,AASHO}}\right]^{1/3}$$

The results are shown in Table 32.

Table 32. Layer Coefficients for Bituminous Mixtures.

Mix Types	AASHO	AASHTO Chart		$a(E/E/)^n$	$a(S_m/S_m)^n$	$a(\hat{M}_R/\hat{M}_R)^n$
		UMR[1]	UMRest[2]	UMR[3]	UMR[4]	UMR[5]
C	0.44	0.471	0.450	0.321	0.476	0.406
I-C	0.44	0.465	0.443	0.324	0.464	0.412
Bit.Base	0.34	0.362	0.345	0.378	0.393	0.335

Notes:
1. M_R laboratory data; 68°F; 0.1 sec duration
2. M_R estimated from industry-wide regression equation; 68°F; AASHO Road Test field conditions
3. E estimated from Witczak equation;Missouri field conditions for UMR data; AASHO Road Test field conditions for AASHO data
4. S_m estimated from Shell equations; Missouri field conditions for UMR data; AASHO Road Test field conditions for AASHO data
5. $\hat{M}_R$ estimated from industry-wide regression equation; Missouri field conditions for UMR data; AASHO Road Test field conditions for AASHO data.

METHOD OF CHOICE

Based on a review of the literature, all of the above methods appeared to give reasonable results with the possible exception of the Odemark method using $|E^*|$.

Resilient Modulus

Again, in a manner similar to the above, estimations of M_R for UMR study data (Missouri road conditions) and AASHO Road Test mixes (Road Test conditions) were substituted into Eq. 6:

$$a_{1,2} = a_{AASHO\ 1,2}\left[\frac{M_{Rest}}{M_{R,AASHO}}\right]^{1/3}$$

The results are shown in Table 32.

Table 32. Layer Coefficients for Bituminous Mixtures.

Mix Types	AASHO	AASHTO Chart		$a(E/E/)^n$	$a(S_m/S_m)^n$	$a(\hat{M}_R/\hat{M}_R)^n$
		UMR[1]	UMRest[2]	UMR[3]	UMR[4]	UMR[5]
C	0.44	0.471	0.450	0.321	0.476	0.406
I-C	0.44	0.465	0.443	0.324	0.464	0.412
Bit.Base	0.34	0.362	0.345	0.378	0.393	0.335

Notes:
1. M_R laboratory data; 68°F; 0.1 sec duration
2. M_R estimated from industry-wide regression equation; 68°F; AASHO Road Test field conditions
3. E estimated from Witczak equation;Missouri field conditions for UMR data; AASHO Road Test field conditions for AASHO data
4. S_m estimated from Shell equations; Missouri field conditions for UMR data; AASHO Road Test field conditions for AASHO data
5. $\hat{M}_R$ estimated from industry-wide regression equation; Missouri field conditions for UMR data; AASHO Road Test field conditions for AASHO data.

METHOD OF CHOICE

Based on a review of the literature, all of the above methods appeared to give reasonable results with the possible exception of the Odemark method using $|E^*|$.

Table 34. Layer Coefficients for 1990 MHTD Mixes.

Mixture Type	Layer Coefficient
Type C	0.42
Type I-C	0.42
Bituminous Base	0.34

Option Two

The above option is recommended in the 1986 AASHTO Guide, which relies on determination of a specific modulus at 68°F. This ignores the fact that pavement temperatures in Missouri are different than those in Ottowa, Illinois. An alternative solution would be to determine layer coefficients as a function of pavement temperature. Use of Eq. 16 will allow this concept to be utilized.

The method is easily implemented. The steps are shown in Table 35. The necessary information includes: asphalt layer thickness, average annual air temperature (See Fig. 45) and mix design data or M_R data at three temperatures. As indicated in Fig. 45, mean annual air temperatures range from 50 to 60°F in Missouri. By use of Witczak's pavement temperature equation, this means that across the state, for a pavement of 1.75 in of Type C or IC over an 8 in bituminous base, the mean pavement temperatures would be 59.8 to 72.2 and 58.9 to 70.8°F for the surface and base courses, respectively. The 1990 MHTD mix designs were substituted into the equations in Table 35 and the results are shown Fig. 46. Note that the 1990 mixes straddle the lower boundary of acceptance in accordance with AAMAS criteria. As an example, the layer coefficients corresponding to these moduli were calculated

Table 35. Layer Coefficient Determination.

Step No.	Action
1	Obtain mean annual air temperature ($\overline{T}_A$) from Fig. 45
2	Calculate mean annual pavement temperature: $\overline{T}_p = 6.0 - \frac{34}{[(D/3)+4]} + \overline{T}_A \left[1 + \frac{1}{[(D/3)+4]}\right]$
3	Calculate mean annual resilient modulus (M_R): $M_R = 10^{\wedge}[6.871 - 0.017\overline{T}_p - 0.024P_{air} + 0.043\eta_{70} + 0.018P_{200} - 0.004AR_{3/4} - 0.011P_{effv}]$ Where: $\eta_{70} = 29{,}508.2\ (\text{penetration}_{77°F})^{-2.1939}$ $P_{effv} = P_b/0.483$ P_b = total asphalt content by weight of mix P_{effv} can also be calculated more accurately by weight-volume calculations.
4	Calculate layer coefficient: $a_1 = 0.44 \left[\frac{M_R}{656{,}772}\right]^{0.333}$ $a_2 = 0.34 \left[\frac{M_R}{604{,}962}\right]^{0.333}$

Note: 1. M_R of AASHO Road Test surface/binder = 656,772 psi at Witczak-estimated pavement temperature, weighted for thicknesses of surface and binder.

2. M_R of AASHO Road Test base = 604,962 psi at estimated base temperature.

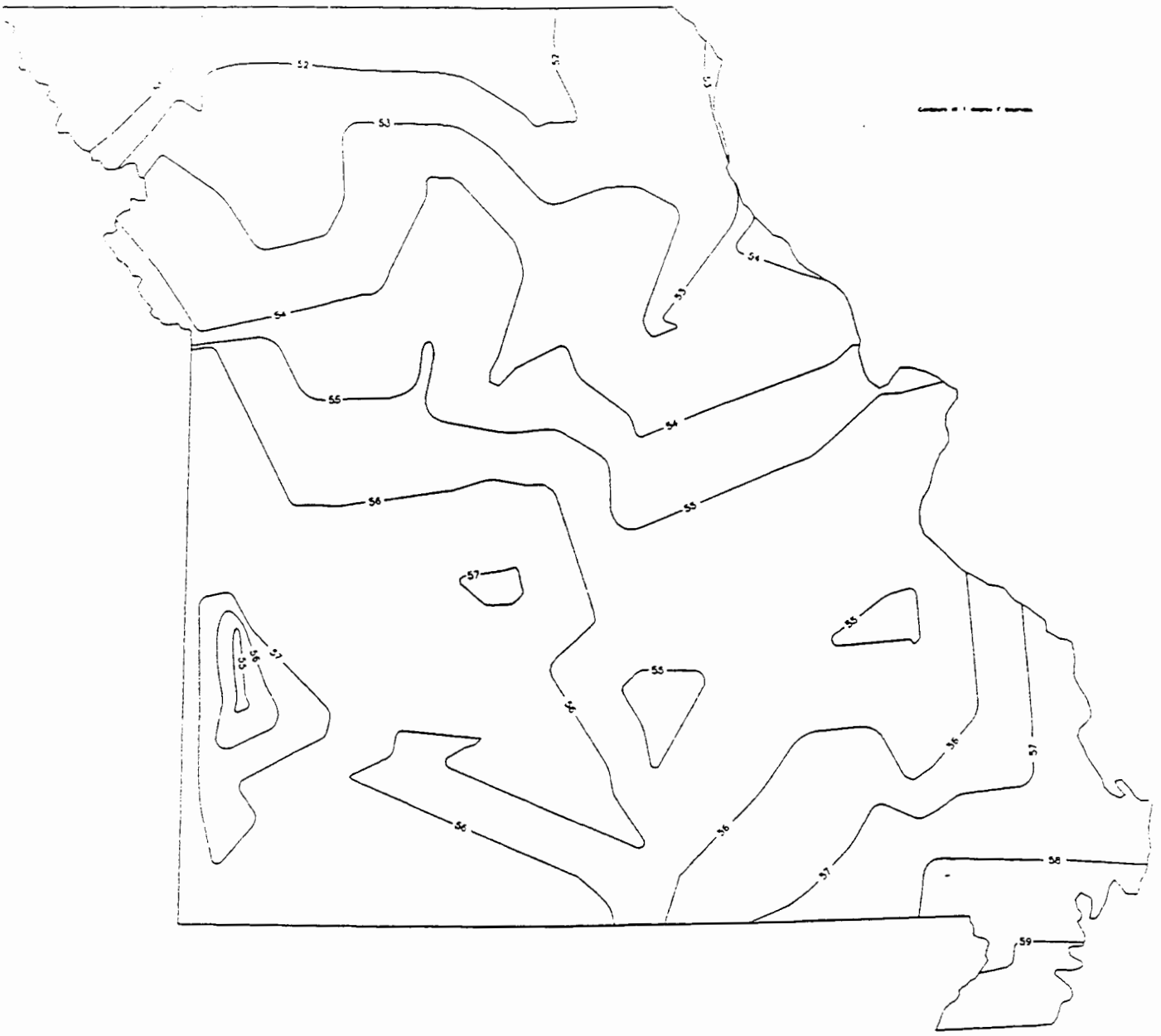

Fig. 45. Temperature Contour Map of Missouri.

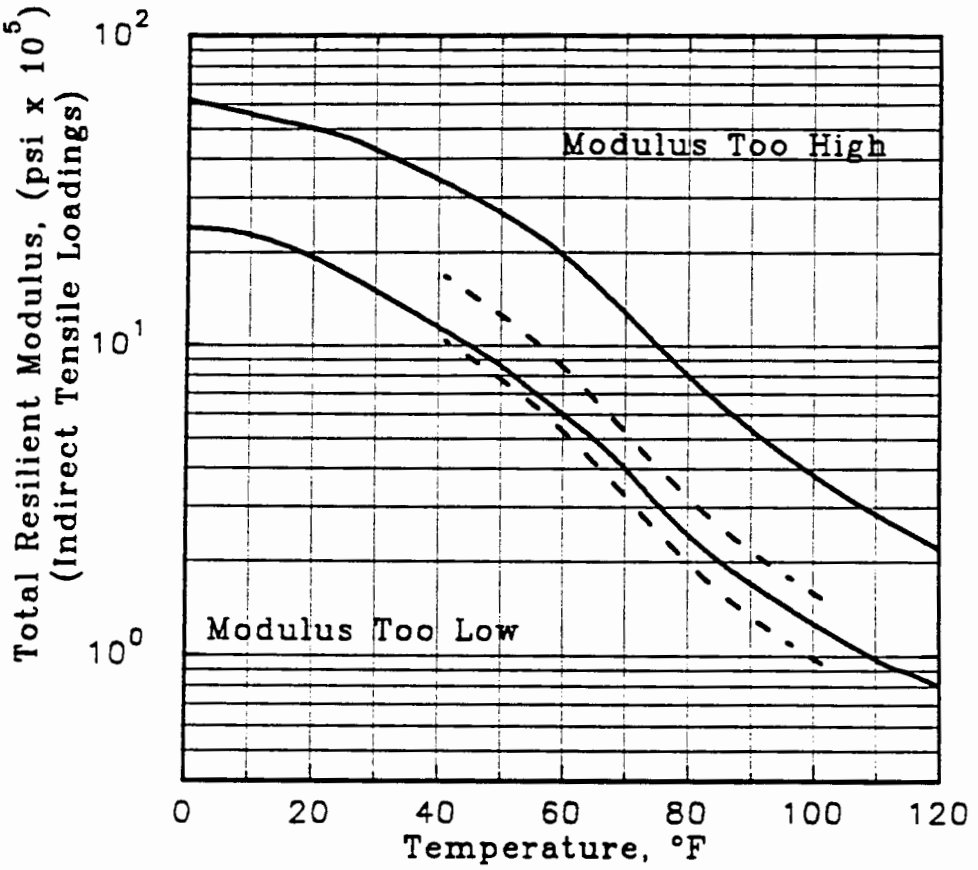

Fig. 46. MHTD 1990 Mixtures on AAMAS Acceptance Chart.

via Table 35 and are presented in Table 36.

Table 36. 1990 MHTD Mix Designs Resilient Moduli in Three Parts of Missouri.

Mix Type	$\overline{T}_A$ (°F)	$\overline{T}_p$ (°F)	Layer Coefficients			
			Min[1]	Avg[2]	Max[3]	AASHO
C	50	59.8	0.40	0.42	0.43	0.44
	55.1	65.2	0.37	0.39	0.40	
	60	72.2	0.34	0.35	0.36	
IC	50	59.8	0.40	0.42	0.42	0.44
	55.1	65.2	0.38	0.39	0.40	
	60	72.2	0.34	0.36	0.36	
BB	50	58.9	0.33	0.35	0.38	0.34
	55.1	63.4	0.31	0.33	0.36	
	60	70.8	0.28	0.30	0.32	

Note: 1 = least stiff 1990 mix design
2 = average of all 1990 mix design
3 = most stiff 1990 mix design

Option Two gives somewhat lower coefficients than option One for the surface mixes, but about the same for the bituminous base mixes. The reason for this is found by looking at the M_R predictive equation. First, the average air temperature in Missouri is about 5°F warmer than that which was recorded at Ottowa during the Road Test. This accounts for a great deal of the loss in M_R when comparing MHTD to Road Test material. Now, keeping temperature constant for both kinds of materials, for average conditions of temperature and mix design, the Type C and IC mixes had the following differences in mix variables.

C and IC vs AASHO. Looking at Table 37, MHTD mix designs on the average have higher air voids, lower P_{200}, and higher asphalt contents, all of which diminish M_R according to the M_R predictive equation. Asphalt viscosity and $AR_{3/4}$ are about the same. Thus, one would expect the AASHO M_R to be higher, even at the same temperature.

Table 37. Comparison of AASHO and MHTD Mix Designs.

Material	P_{air}	η_{70}	P_{200}	$AR_{3/4}$	P_{effv}
AASHO*	4.3	1.49	5.0	2.3	9.1
MHTD-C	5.3	1.49	3.5	0	10.0
MHTD-IC	6.0	1.51	4.3	0	9.6
AASHO Base	6.2	1.49	5.6	4.0	10.8
MHTD-BB	4.8	1.51	7.7	10.6	9.1
*weighted average of surface plus binder courses					

Bituminous Base vs AASHO. MHTD mix designs averaged lower air voids, higher P_{200}, and lower effective asphalt contents, all of which would increase the predicted moduli. MHTD did have more $AR_{3/4}$ than AASHO, but care must be taken when interpreting the effect of changing variable magnitudes that are interactive with other variables, such as different sieve sizes.

Thus, keeping in mind differences in mix design and temperature between MHTD pavements and Road Test pavements, one might expect MHTD C and IC layer coefficients to be somewhat lower, but bituminous bases about the same as AASHO pavement layers.

SENSITIVITY ANALYSIS

A sensitivity analysis was performed by looking at the effect on required pavement thickness by 1) mixture variables, and 2) layer coefficients.

MIXTURE VARIABLE EFFECT ON THICKNESS

As shown in Table 23, only asphalt viscosity and extremes in gradation were significant in their effect on M_R. An analysis was performed to ascertain the effect on layer thickness of varying asphalt viscosity grade or aggregate gradation. Thickness of the surface layer was varied at 1.25 in and 4 in for both Type C and IC mixes. For the bituminous base mixes, thickness was examined at 4, 8, and 14 in. Three levels of viscosity or gradation change were looked at: most significant change in the UMR data set, least significant change in the UMR data set, and average change for all mixes of a certain type. For instance, for the Type C mixtures, the largest change in M_R as a result of a change in gradation occured in the C5F20-4.0 mixture as gradation changed from the fine side (M_R = 762,000 psi) to the coarse side (M_R = 562,000). The least change occured where the C4C20-4.25 mix changed from the fine side to the coarse side (essentially no change in measured M_R). The "average" condition was simply a comparison of the average of the M_R values for all the Type C fine gradation mixtures to the average of the M_R values for all the coarse gradations at 68°F (as shown in Table 23). Gradation or viscosity was changed from high to low with a resulting change in M_R. Then the resulting change in layer coefficients (a_1 or a_2) were calculated from the AASHTO nomographs. Finally, the required change in thickness was computed as needed to maintain the initial structural

number rendered by the initial assumption of layer thickness. The results are shown in Table 38. All data are based on 68°F. For example, what is the average change in required surface layer thickness for an initial thickness of 1.25 in using a Type C mix when gradation is changed from the fine side to the coarse side? Looking at row 3 in Table 38, the M_R for the fine side Type C is 567,625 psi. Moving to the coarse side results in a reduction to 504,375 psi. Using the AASHTO nomograph, the corresponding loss in a_1 is 0.02. The structural number (SN) provided by the fine side mix is $SN = a_1D_1$ or $SN = 0.48 * 1.25 = 0.60$. When the layer coefficient is reduced from 0.48 to 0.46, the new required thickness $D_2 = SN/a_1 = 0.60/0.46 = 1.30$, or, an additional requirement of 0.05 in. This is not significant in a practical sense.

From Table 38, it appears that wide swings in gradation are not significant for thin (1.25 in) layers, and are marginally significant for 4 in layers. For thicker layers, as encountered with bituminous bases, the effect becomes more important. At an initial 8 in required thickness, changes varied from 0.02 to about 1.5 in. At 14 in, the variation was from 0.04 to 2.66 in (on the average, the required extra thicknesses were 0.61 and 1.06 in for the 8 and 14 in initial thicknesses, respectively).

Changes in viscosity grade rendered the following results. For the C and IC mixes, thin surface layer (1.25 in) thickness changes varied from 0.03 to 0.31 (0.15 average) in, while 4 in layer thickness changes were 0.11 to 1.00 (0.48 average) in. For the bituminous bases, the variance for a 4 in layer ranged from 0.08 to 0.94 (0.38 average) in. An 8 in layer could see a variance from 0.16 to 1.88 (0.76 average) in,

Table 38. Thickness Sensitivity to Changes in Gradation and Viscosity.

GRADATION CHANGE										
D11 in.	CASE	MR1 psi	MR2 psi	MRdiff psi	a,11	a,12	a1 diff	SN	D12 in.	D1diff in.
TYPE C										
1.25	WORST	762000	562000	200000	0.53	0.48	0.05	0.66	1.39	0.14
4.00		762000	562000	200000	0.53	0.48	0.05	2.11	4.43	0.43
1.25	AVG	567625	504375	63250	0.48	0.46	0.02	0.60	1.30	0.05
4.00		567625	504375	63250	0.48	0.46	0.02	1.91	4.18	0.18
1.25	LEAST	no	change	0						0
4.00		no	change	0						0
TYPE IC										
1.25	WORST	725000	500000	225000	0.52	0.46	0.06	0.65	1.42	0.17
4.00		725000	500000	225000	0.52	0.46	0.06	2.08	4.55	0.55
1.25	AVG	605875	508000	97875	0.49	0.46	0.03	0.61	1.33	0.08
4.00		605875	508000	97875	0.49	0.46	0.03	1.95	4.26	0.26
1.25	LEAST	no	change	0						0
4.00		no	change	0						0
BITUMINOUS BASE										
D21 in.	CASE	MR1 psi	MR2 psi	MRdiff psi	a21	a22	a2 diff	SN	D22 in.	D2diff in.
4	WORST	790000	494000	296000	0.41	0.35	0.07	1.66	4.76	0.76
8		790000	494000	296000	0.41	0.35	0.07	3.31	9.52	1.52
14		790000	494000	296000	0.41	0.35	0.07	5.80	16.66	2.66
4	AVG	605125	500875	104250	0.38	0.35	0.03	1.51	4.30	0.30
8		605125	500875	104250	0.38	0.35	0.03	3.01	8.61	0.61
14		605125	500875	104250	0.38	0.35	0.03	5.27	15.07	1.07
4	LEAST	606000	601000	5000	0.38	0.38	0.00	1.51	4.01	0.01
8		606000	601000	5000	0.38	0.38	0.00	3.02	8.02	0.02
14		606000	601000	5000	0.38	0.38	0.00	5.28	14.04	0.04

VISCOSITY CHANGE										
D11 in.	CASE	MR1 psi	MR2 psi	MRdiff psi	a11	a12	a1 diff	SN	D12 in.	D1diff in.
TYPE C										
1.25	WORST	626000	364000	262000	0.38	0.31	0.08	0.48	1.56	0.31
4.00		626000	364000	262000	0.38	0.31	0.08	1.53	5.00	1.00
1.25	AVG	613250	458750	154500	0.38	0.34	0.04	0.47	1.40	0.15
4.00		613250	458750	154500	0.38	0.34	0.04	1.51	4.48	0.48
1.25	LEAST	562000	525000	37000	0.37	0.36	0.01	0.46	1.28	0.03
4.00		562000	525000	37000	0.37	0.36	0.01	1.47	4.11	0.11
TYPE IC										
1.25	WORST	725000	480000	245000	0.40	0.34	0.06	0.50	1.46	0.21
4.00		725000	480000	245000	0.40	0.34	0.06	1.61	4.68	0.68
1.25	AVG	613250	458750	154500	0.38	0.34	0.04	0.47	1.40	0.15
4.00		613250	458750	154500	0.38	0.34	0.04	1.51	4.48	0.48
1.25	LEAST	533000	475000	58000	0.36	0.34	0.02	0.45	1.31	0.06
4.00		533000	475000	58000	0.36	0.34	0.02	1.44	4.19	0.19
BITUMINOUS BASE										
D21 in.	CASE	MR1 psi	MR2 psi	MRdiff psi	a21	a22	a2 diff	SN	D22 in.	D2diff in.
4	WORST	601000	362000	239000	0.38	0.30	0.07	1.50	4.94	0.94
8		601000	362000	239000	0.38	0.30	0.07	3.01	9.88	1.88
14		601000	362000	239000	0.38	0.30	0.07	5.26	17.29	3.29
4	AVG	617375	488625	128750	0.38	0.35	0.03	1.52	4.38	0.38
8		617375	488625	128750	0.38	0.35	0.03	3.04	8.76	0.76
14		617375	488625	128750	0.38	0.35	0.03	5.31	15.33	1.33
4	LEAST	494000	470000	24000	0.35	0.34	0.01	1.39	4.08	0.08
8		494000	470000	24000	0.35	0.34	0.01	2.79	8.16	0.16
14		494000	470000	24000	0.35	0.34	0.01	4.87	14.29	0.29

while a thick 14 in layer's required change might be from 0.29 to 3.29 (1.33 average) in. So, for thicker pavements, using a harder grade of asphalt could lead to significant changes in design thickness.

LAYER COEFFICIENT EFFECT ON THICKNESS

As previously discussed, layer coefficients calculated in accordance with Option

Two can vary as a result of changes in temperature and mix design. The following is an analysis of the effect of these two variables on required layer thickness.

Three typical pavement sections were examined, and the change in required D_2 (bituminous base thickness) was calculated. The three sections all contained a 1.25 in surface layer D_1, with D_2 varying as 4, 8, and 14 in. Using the AASHO Road Test layer coefficients (a_1 = 0.44, a_2 = 0.34), structural numbers (SN) were calculated for these pavements. Then, using a constant D_1 = 1.25 in, D_2's were calculated based on worst, average, and best temperature conditions and mix quality in Missouri. From Table 35, layer coefficients for these conditions for the surface and base layers were obtained. Finally, the D_2's required to maintain the computed SN's were calculated. The results are shown in Table 39. As an example, using the AASHO layer coefficients of a_1 = 0.44 and a_2 = 0.34, for a 1.25 in over 8 in bituminous base structure, the provided SN = 3.27. Now, for average conditions in Missouri (temperature and 1990 mix quality), using a 1.25 in surface layer, the required D_2 = 8.43 in, or a required increase of 0.43 in. From examination of the table, several things are apparent. First, <u>average</u> temperature and mix quality conditions lead to rather small changes in required base thickness. <u>Worst case</u> scenerios of lower quality mix used in the warmest part of the state lead to significant increases in required base thickness. On the other hand, use of higher quality mixes in cooler parts of the state lead to reductions in required thickness.

Table 39. Thickness Sensitivity to Ranges of Layer Coefficients.

AASHO			MHTD			
D_1 (in) $a_1 = 0.44$	D_2 (in) $a_2 = 0.34$	SN provided	D_1 (in)	D_2(in)		
				Worst	Average	Best
				$a_1 = 0.34$ $a_2 = 0.28$	$a_1 = 0.39$ $a_2 = 0.33$	$a_1 = 0.43$ $a_2 = 0.38$
1.25	4	1.91	1.25	5.30	4.31	3.61
1.25	8	3.27	1.25	10.16	8.43	7.19
1.25	14	5.31	1.25	17.45	14.61	12.56

SUMMARY

The purpose of this investigation was to determine layer coefficients for several MHTD specified pavement materials. The coefficients are necessary as input to the AASHTO pavement design method. Volume I of this study involves asphaltic materials, and is reported herein. Volume II deals with unbound aggregate base and soil-cement base materials, and is reported elsewhere.

Besides determining layer coefficients, the study also entailed the determination of the effect on layer coefficient by changes in asphalt cement grade, aggregate gradation, testing temperature, aggregate source, and asphalt content within the limits of MHTD specifications. This resulted in 48 mix designs.

1. All materials were sampled and delivered to UMR by MHTD personal. Choice of material sources was made by MHTD. The types of pavement materials were Type C, Type I-C, and bituminous base. The specific materials making up

these types were two grades of asphalt cement, two surface mix sources of coarse aggregate, two base mix sources of coarse aggregate, one source of natural sand, two sources of manufactured sand, one source of mineral filler, and one source of hydrated lime.

2. Routine index and specification tests were performed. For the asphalt cement, the tests were: penetration at 38° and 77°F, kinematic viscosity, absolute viscosity, specific gravity, and softening point. The aggregates were tested for gradation, specific gravity, and particle shape/texture. Equipment was fabricated for the particle shape/texture tests.

3. The aggregates were separated on each sieve size and stored.

4. The optimum asphalt content of each of the 12 gradation/aggregate source combinations was determined by use of the Marshall mix design method (75 blow, manual flat-faced hammer). The same optimum asphalt content was used for both the AC10 and AC20 grades because mixing and compaction temperatures were adjusted to give equal mixing and compaction viscosities for both grades. This resulted in 24 mixes. Finally, 24 additional mixes were used which had 0.5% asphalt added above optimum. Thus, the total number of mixtures was 48. Approximately 200 specimens were made.

5. Maximum theoretical specific gravities were determined in two ways: 1) Rice method, and 2) calculation from material proportions and specific gravities. 96 specimens were tested.

6. A voids analysis was conducted to determine the effect of estimation of

maximum theoretical specific gravity.

7. Ten methods of characterizing gradation curve shape and position were used. Two of these were unique to this study. The first involved the area between the gradation curve and the maximum density line as plotted on FHWA 0.45 power paper. The second method involved determination of slopes of three portions of each gradation curve.

8. Each mix was tested for indirect tensile strength. A regression model was fit to the data. 96 tests were performed.

9. Each mix was tested for total resilient modulus (indirect tension) at three temperatures: 41°, 77°, 104°F. Necessary software and equipment were programmed and developed to perform the tests, and to acquire, store, and analyze the data. A total of 192 specimens were tested at three temperatures for a total of 576 tests.

10. The results of the M_R testing were analyzed statistically to determine the variables that were significant to changes in M_R. The variables that were examined were asphalt viscosity, asphalt content, testing temperature, changes in gradation, and particle shape/texture.

11. A regression model was fit to the M_R data.

12. Resilient modulus data from other studies found in the literature were merged with the UMR data. A general regression model was fit to the overall data base.

13. Air temperature data from 104 weather stations in Missouri were analyzed to

produce an air temperature contour map of Missouri.

14. Pavement thickness data for MHTD flexible pavements were analyzed for mean pavement thickness.

15. Information from steps 13 and 14 was necessary to calculate pavement temperatures for Missouri.

16. Steps 13 and 14 were repeated to obtain pavement temperatures at the AASHO Road Test.

17. Mean vehicle speed data was supplied by MHTD. This was converted to load dwell times and frequency for MHTD pavements. The same was done for AASHO Road Test pavements.

18. UMR, AASHO Road Test, and MHTD 1990 mix data were used to estimate resilient modulus, mixture stiffness (Shell method), and dynamic modulus at both laboratory conditions and field conditions of pavement temperature and loading rate. This was in order to see which modulus would be most useful for layer coefficient determination.

19. Five different methods of calculating mixture stiffness (S_m) were compared; each varied in the manner of handling asphalt aging or source.

20. Layer coefficients a_1 (for Types C and IC mixes) and a_2 (for bituminous base mixes) were determined in several ways:

    a. M_R was estimated via the general regression model equation developed in step 12. Then, these M_R values were used in the AASHTO nomographs to obtain a_1 or a_2.

    b. Use of the Odemark equation was made in three ways:

$$a_{UMR} = a_{AASHO}\left[\frac{M_{R,UMR}}{M_{R,AASHO}}\right]^{1/3}$$

$$a_{UMR} = a_{AASHO}\left[\frac{|E^*|_{UMR}}{|E^*|_{AASHO}}\right]^{1/3}$$

$$a_{UMR} = a_{AASHO}\left[\frac{S_{m,UMR}}{S_{m,AASHO}}\right]^{1/3}$$

The above numerators were calculated at Missouri pavement temperatures (high, average, and low areas of the state) and the denominators were calculated at the mean pavement temperature at the Road Test.

21. Two options were presented for the calculation of layer coefficients. Option One resulted in a fixed layer coefficient per material. For 1990 mixes, Type C a_1 = 0.42, Type IC a_1 = 0.42, and bituminous base a_2 = 0.34. Option Two is a method for pavement designers to calculate layer coefficients for a specific mix and location in the state.

22. A sensitivity analysis was performed which examined the effect of specific important mix characteristics (viscosity and gradation), pavement temperature, and overall mixture quality.

CONCLUSIONS

1. Ten methods were used to characterize gradation curve shape and position; two of these were developed during the course of the study. The method of determining the area between the 0.45 power maximum density line (MDL) and

the gradation line had only a fair (R^2 = 0.79) correlation with resilient modulus, M_R. This was because the area was not sensitive to relatively small differences in position of the curve relative to the MDL. The second unique method involved calculation of the slope of three different parts of the gradation curve. This method was shown to be of assistance in creating a more accurate M_R regression model. However it was not quite as helpful as Hudson's $\bar{A}$, which is much easier to calculate. But, Hudson's $\bar{A}$ was not quite as helpful as merely including certain critical sieve sizes directly in the regression equation.

2. The voids analysis indicated that the method of assuming that the effective specific gravities of low absorption aggregates is midway between the bulk and the apparent specific gravities correlates very well with results from Rice method testing. However, for absorptive aggregates (eg., the bituminous base materials in this study), the estimation method underpredicts air voids by about 1%.

3. Of the five different methods for computation of mixture stiffness (S_m), the method of Bonnaure, which uses the Ullidtz asphalt aging approximations, was found to be the most accurate for the purposes of this study.

4. The regression model for indirect tensile strength was relatively strong (adj-R^2 = 0.840) and was as follows:

$$IDT = 134.064 + 21.238\eta_{70} - 7.553\ p_{effv} - 0.687\ AR_4 + 1.388U - 2.145\ IP$$

where:

the gradation line had only a fair (R^2 = 0.79) correlation with resilient modulus, M_R. This was because the area was not sensitive to relatively small differences in position of the curve relative to the MDL. The second unique method involved calculation of the slope of three different parts of the gradation curve. This method was shown to be of assistance in creating a more accurate M_R regression model. However it was not quite as helpful as Hudson's $\bar{A}$, which is much easier to calculate. But, Hudson's $\bar{A}$ was not quite as helpful as merely including certain critical sieve sizes directly in the regression equation.

2. The voids analysis indicated that the method of assuming that the effective specific gravities of low absorption aggregates is midway between the bulk and the apparent specific gravities correlates very well with results from Rice method testing. However, for absorptive aggregates (eg., the bituminous base materials in this study), the estimation method underpredicts air voids by about 1%.

3. Of the five different methods for computation of mixture stiffness (S_m), the method of Bonnaure, which uses the Ullidtz asphalt aging approximations, was found to be the most accurate for the purposes of this study.

4. The regression model for indirect tensile strength was relatively strong (adj-R^2 = 0.840) and was as follows:

$$IDT = 134.064 + 21.238\eta_{70} - 7.553\ p_{effv} - 0.687\ AR_4 + 1.388U - 2.145\ IP$$

where:

effective asphalt content and actual effective asphalt content, by volume.

7. A statistical analysis of the data indicated that temperature was by far the most important variable that affects M_R, followed by asphalt viscosity and whether the gradation was very fine or very coarse. Overasphalting by 0.5% tended to lower M_R, but was not statistically significant. Increases in (-) #200 material and decreases in (+) #4 material tended to increase M_R. Particle shape of coarse or fine aggregate did not seem to affect M_R in a consistent manner. It should be noted that both coarse aggregates were crushed limestones, and that all mixes contained varying amounts of manufactured sand, so large ranges in particle shape were not present. All other things held constant, decreasing air voids tended to increase M_R.

8. Because layer coefficients are directly affected by resilient modulus, the practical impact of the trends is that higher layer coefficients can be obtained by:

   1. using a harder grade of asphalt (higher η_{70}),
   2. using a more well-graded gradation (higher $\bar{A}$, adjusting P_{200} and AR_4),
   3. avoiding overasphalting (optimum P_{effv}), and
   4. increasing density (lower air voids).

   Of course, caution should be exercised when considering these options. Excessively hard asphalts, highly angular aggregates, and low air void values can lead to such problems as thermal cracking, lack of workability, poor

effective asphalt content and actual effective asphalt content, by volume.

7. A statistical analysis of the data indicated that temperature was by far the most important variable that affects M_R, followed by asphalt viscosity and whether the gradation was very fine or very coarse. Overasphalting by 0.5% tended to lower M_R, but was not statistically significant. Increases in (-) #200 material and decreases in (+) #4 material tended to increase M_R. Particle shape of coarse or fine aggregate did not seem to affect M_R in a consistent manner. It should be noted that both coarse aggregates were crushed limestones, and that all mixes contained varying amounts of manufactured sand, so large ranges in particle shape were not present. All other things held constant, decreasing air voids tended to increase M_R.

8. Because layer coefficients are directly affected by resilient modulus, the practical impact of the trends is that higher layer coefficients can be obtained by:

   1. using a harder grade of asphalt (higher η_{70}),
   2. using a more well-graded gradation (higher $\bar{A}$, adjusting P_{200} and AR_4),
   3. avoiding overasphalting (optimum P_{effv}), and
   4. increasing density (lower air voids).

   Of course, caution should be exercised when considering these options. Excessively hard asphalts, highly angular aggregates, and low air void values can lead to such problems as thermal cracking, lack of workability, poor

which relates the MHTD M_R to the AASHO Road Test M_R.

RECOMMENDATIONS

For Missouri pavement designers, two options are presented. Option One is the simplest: if M_R test data are available for a given mix (say, for three temperatures), the M_R value at 68° should be ascertained; then the AASHTO nomographs (Figs. 42 and 43) should be entered with the M_{R68} value and the a_1 or a_2 value determined. If M_R test data are not available, the specific mix data should be substituted into Eq. 53, repeated here, and the above procedure followed to obtain a_1 or a_2 values.

$$M_R = 10^{(6.871-0.017\bar{T}_p-0.024P_{air}+0.043\eta_{70}+0.018P_{200}-0.004AR_{3/4}-0.011P_{effv})}$$

Alternatively, if a designer wishes to obtain a layer coefficient value more in keeping with the design location and pavement thickness, the procedure in Table 35 should be followed.

It is highly recommended that the MHTD pursue M_R testing of various mixtures in present use in order to update or replace the above equation by use of a more representative data set of the materials. A greater degree of accuracy will also probably be achieved. Then, both Options One and Two will render more representative layer coefficient values for MHTD designers.

It should be remembered that this study is in the mold of the traditional method of determination of layer coefficients, that is, by a comparison of some sort of strength or stiffness of MHTD materials to Road Test materials. Tendencies for asphaltic material problems with thermal cracking and rutting, for instance, are not directly addressed. To address a wider range of material issues, creep testing and

gyratory shear testing may be in order. These kinds of tests were beyond the scope of this project. Also, this project was conceived in 1989 and the bulk of the testing was performed in 1991, before the SHRP project results became generally known. In the future, it may be that some of the recommendations coming out of the SHRP program can be used to update the quest for layer coefficient determination.

ACKNOWLEDGEMENT

The authors wish to thank the MHTD for its sponsorship and support of this research project. They also thank the UMR Department of Civil Engineering for its support. Special thanks go to Mr. J.D. Stevenson and Mr. Kevin Hubbard for their assistance in the computer analysis portion of the study.

REFERENCES

1. AASHTO 1986 Guide for Design of Pavement Structures, AASHTO, Washington, D.C., 1986.

2. Richardson, D.N., W.J. Morrison, and P.A. Kremer, "Determination of AASHTO Drainage Coefficients, Missouri Cooperative Highway Res. Program Final Report, Study 90-4, Univ. of Missouri-Rolla, Rolla, Missouri, 1994.

3. Gomez, M. and M.R. Thompson,"Structural Coefficients and Thickness Equivalency Ratios, "Trans. Engrg. Series No. 38," Illinois Cooperative Highway and Transportation Series No. 202, University of Illinois, 1983, 48 p.

4. Transportation Engineering Handbook, Ch. 50, Pavement, U.S. Forest Service, 1974, p. 51.1-54.4-16.

5. Van Til, C.J., B.F. McCullough, B.A. Vallerga, and R.G. Hicks, "Evaluation of AASHO Interim Guides for Design of Pavement Structures," NCHRP 128, Hwy. Res. Bd., 1972, 111 p.

6. Wang, M.C., T.D. Larson, and W.P. Kilareski, "Structural Coefficients of Bituminous Concrete and Aggregate Cement Base Materials by the Limiting Criteria Approach," Report No. FHWA-PA-RD-75-2-4, Pennsylvania State University, University Park, PA, 1977, 52 p.

7. Sowers, G.F., "Georgia Satellite Flexible Pavement Evaluation and Its Application to Design," Hwy. Res. Rec. 71, 1965, pp. 151-171.

8. Walters, R. "Implementation of the New AASHTO Design Practice," 31st Annual UMR Asphalt Conference, University of Missouri-Rolla, Rolla, Missouri, 1988.

9. Rada, G. and M.W. Witczak, "Material Layer Coefficients of Unbound Granular Materials from Resilient Modulus, "Trans. Res. Rec. 852, Trans. Res. Bd., 1982, pp. 15-21.

10. Jorenby, B.N. and R.G. Hicks, "Base Course Contamination Limits, Trans. Res. Rec. 1095, Trans. Res. Bd., 1986, pp. 86-101.

11. The AASHO Road Test - Report 5 - Pavement Research, Spec. Report 61E, Highway Res. Bd., 1962, 352 p.

12. Corree, B.J.D. and T.D. White, "The Synthesis of Mixture Strength Parameters Applied to the Determination of AASHTO Layer Coefficient Distributions," Proc. of Assn. of Asphalt Paving Tech., Vol. 58, 1989, pp.

109-141.

13. Richardson, D.N. and P.A. Kremer, "Determination of AASHTO Layer Coefficients, Vol. II: Unbound Granular Bases and Cement Treated Bases," Missouri Cooperative Highway Res. Program Final Report, Study 90-5, University of Missouri-Rolla, Rolla, Missouri, 1994.

14. Odemark, N. "Undersokning av Elasticitetsegenskaperna hos Olika Jordarter Samt Teori for Berakning av Belagninger Enligt Elasticitetsteorien," Statens Uaginstitut, Meddelande, 77, 1949.

15. Van der Poel, C. "A General System Describing the Viscoelastic Properties of Bitumens and Its Relation to Routine Test Data," Shell Bitumen Reprint No. 9.

16. Pfeiffer, J.P. and P.M. Van Doormaal, "The Rheological Properties of Asphaltic Bitumen," J. Inst. of Petroleum Tech., Vol. 22, 1936, pp. 414.

17. Heukelom, W., "An Improved Method of Characterizing Asphaltic Bitumens with the Aid of Their Mechanical Properties," Proc. Assn. of Asphalt Paving Tech. Vol. 42, 1973, pp.67-98.

18. Heukelom, W. and A. I. G. Klomp, "Road Design and Dynamic Loading," Proc. of Assn. Asphalt Paving Tech., Vol. 33, 1964, pp. 92-123.

19. Van Draat, F. and P. Sommer, "Ein Geratzar Bestimmung der Dynamischen Elastizitats Modulu von Asphalt," Strasse und Autobohn, Vol. 35, 1965.

20. McLeod, N.W., "Asphalt Cements: Pen-Vis Number and Its Application to Moduli of Stiffness," J. of Testing and Eval., Vol. 4, No. 4, 1976, pp. 275 -

282.

21. Bonnaure, F., G. Gest, A. Gravois and P. Uge, "A New Method of Predicting the Stiffness of Asphalt Paving Mixtures," Proc. of Assn. of Asphalt Paving Tech., Vol. 46, 1977, pp. 64 -104.

22. Claessen, A.I.M., J.M. Edwards, P. Sommer, and P. Uge, "Asphalt Pavement Design: The Shell Method," Proc. 4th Int'l. Conf. on Structural Design of Asphalt Pavements, Univ. of Michigan, Ann Arbor, 1977.

23. Ullidtz, P., "A Fundamental Method for Prediction of Roughness, Rutting, and Cracking of Pavements," Proc. of Assn. of Asphalt Paving Tech., Vol. 48, 1979, pp. 557-586.

24. Witczak, M.W., "Design of Full Depth Asphalt Airfield Pavements, " Proc. Third Int'l. Conf. on the Structural Design of Asphalt Pavements, Vol. 1, 1972, London, England, pp. 550-567.

25. Harr, M.E., Reliability-Based Design in Civil Engineering, McGraw-Hill Book Co., 1987.

26. Lefebvre, J.A., "A Modified Penetration Index for Canadian Asphalts," Proc. of Assn. of Asphalt Paving Tech., Vol. 39, 1970, pp. 443.

27. Kandhal, P.S., and W.C. Koehler, "Effect of Rheological Properties of Asphalts on Pavement Cracking, Proc. of Assn. of Asphalt Paving Tech., pp. 99-117.

28. Bell, C. A., "Use of the Shell Bitumen Test Data Chart in Evaluation of Asphalt Data," Proc. of Assn. of Asphalt Paving Tech., Vol. 52, pp., pp.1 -

31 (1983).

29. Button, J.W., J.A. Epps, D.N. Little, and B.M. Galloway, "Asphalt Temperature Susceptibility and Its Effect on Pavements," Trans. Res. Rec. 843, Trans. Res. Bd., pp. 118-126.

30. Puzinauskas, V.P. "Properties of Asphalt Cements," Proc. of Assn. of Asphalt Paving Tech., Vol. 48, 1979, pp. 646-710.

31. Shook, J. F. and B.F. Kallas, "Factors Influencing Dynamic Modulus of Asphalt Concrete," Proc. of Assn. of Asphalt Paving Tech., Vol. 38, 1969, pp.140 - 178.

32. Witczak, M.W., Development of Regression Model for Asphalt Concrete Modulus for Use in MS-1 Study, Asphalt Institute, 1978, 39 p.

33. Miller, J.S., J. Uzan, and M.W. Witczak, "Modification of the Asphalt Institute Bituminous Mix Modulus Predictive Equation," Trans. Res. Rec. 911 Trans. Res. Bd., 1983, pp. 27-36.

34. Akhter, G.F. and M.W. Witczak, "Sensitivity of Flexible Pavement Performance to Bituminous Mix Properties," Trans. Res. Rec. 1034, Trans. Res. Bd., 1985, pp. 70 - 79.

35. "Standard Test Method for Resilient Modulus of Subgrade Soils," AASHTO T-274 (1986), Standard Specifications for Transportation Materials and Methods of Sampling and Testing, 14th ed, Part III, Methods of Sampling and Testing, AASHTO, Washington, D.C., 1986, pp. 1198-1218.

36. "Standard Test Method for Indirect Tension Test for Resilient Modulus of

Bituminous Mixtures," ASTM D4123-82, Annual Book of ASTM Standards, Vol. 04.03, ASTM, Philadelphia, PA, 1992, pp. 507-509.

37. Von Quintus, H.L., J.A. Scherocman, C.S. Hughs, and T.W. Kennedy, "Asphalt-Aggregate Mixture Analysis System," NCHRP Rpt. 338, Trans. Res. Bd., Washington, D.C., 1991, 183 p.

38. Resilient Modulus for Asphalt Concrete, SHRP Protocol P07, Strategic Hwy. Res. Pgm., Nat'l. Res. Council, Washington, D.C., 1992, pp. PB07B-PB07B-17.

39. Standard Specifications for Transportation Materials and Methods of Sampling and Testing, 15th Ed., Part II, Tests, AASHTO, Washington, D.C., 1990.

40. Kalcheff, I.V., and D.G. Tunnicliff, "Effects of Crushed Stone Aggregate Size and Shape on Properties of Asphalt Concrete," Proc. of Assn. of Asphalt Paving Tech., Vol. 51, 1982, pp. 453 -483.

41. Hadley, W.O., W. R. Hudson, and T. W. Kennedy, "An Evaluation of Factors Affecting the Tensile Properties of Asphalt-Treated Materials," Res. Report 98-2, Center for Hwy. Res., Univ. of Texas at Austin, 1969.

42. Hadley, W. O., W.R. Hudson, and T. W. Kennedy, "Evaluation and Prediction of the Tensile Properties of Asphalt-Treated Materials," Res. Report 98-9, Center for Hwy. Res., Univ. of Texas at Austin, 1971.

43. Meier, W.R., and E.J. Elnicky, "Laboratory Evaluation of Shape and Surface Texture of Fine Aggregate for Asphalt Concrete," Trans. Res. Rec. 1250,

Trans. Res. Bd., 1989, pp. 25-34.

44. Mogawer, W.S. and K.D. Stuart, "Evaluation of Test Methods Used to Quantify Sand Shape and Texture," TRB 71st Annual Meeting, Trans. Res. Bd., Washington, D.C., 1992, 23 p.

45. Kandhal, P.S., J. B. Motter, and M.A. Khatri, "Evaluation of Particle Shape and Texture: Manufactured vs. Natural Sands, "NCAT Rpt. No. 91-3, NCAT, Auburn, Ala., 1991, 23 p.

46. "Test Method for Index of Aggregate Particle Shape and Texture," ASTM D3398-87, Annual Book of ASTM Standards, Vol. 05.03 ASTM, Philadelphia, PA, 1992, pp. 393-396.

47. "Standard Test Method for Particle Shape, Texture, and Uncompacted Void Content of Fine Aggregate," Draft, National Aggregate Assn., Silver Spring, MD, 1991, 12p.

48. Anagnos, J. N. and T. W. Kennedy, "Practical Method of Conducting the Indirect Tensile Test," Res. Report 98 -10, Center for Hwy. Res., Univ. of Texas at Austin, 1972.

49. Kennedy, T.W., and J.N. Anagnos, "Procedures for the Static and Repeated-Load Indirect Tensile Test," Res. Report 183-14, Center for Trans. Res., Univ. of Texas at Austin, 1983, 44 p.

50. "Test Procedures for Characterizing Dynamic Stress-Strain Properties of Pavement Materials: Indirect Tensile Test," Special Report 162, Washington, D.C., 1975, pp. 32-39.

51. May, R.W., and M.W. Witczak, "An Automated Asphalt Concrete Mix Analysis System," Proc. of Assn. of Asphalt Paving Tech., Vol. 61, 1992, pp. 154-187.

52. de Bats, F. Th., and G. van Gooswilligen, "Practical Rheological Characterization of Paving Grade Bitumens," Fourth Eurobitume Symp., Madrid, pp. 1-8 (1989).

53. Barksdale, R.D., "Compressive Stress Pulse Times in Flexible Pavements for Use in Dynamic Testing," Hwy. Res. Rec. 345, Hwy. Res. Bd., 1971, pp.32 - 44.

54. Hudson, S. B., and H. F. Waller, "Evaluation of Construction Control Procedures - Aggregate Variations and Effects," NCHRP Rpt. No. 69, Hwy. Res. Bd., Washington, D.C., 1969, 58 p.

55. Miller-Warden Assoc., "Effects of Different Methods of Stockpiling and Handling Aggregates," NCHRP Rpt. No. 46, Hwy. Res. Bd., Washington,D.C., 1967, 102 p.

56. Joel, R.N., "A Method for Controlling Concrete Workability Using Aggregate Gradation Control," M.S. Thesis, Univ. of Missouri-Rolla, Rolla, Missouri, 1990, 318 p.

57. AUTOCAD, Autodesk, Inc., Sausalito, CA, 94965.

58. Goode, J.F., and L.A. Lufsey, "A New Graphical Chart for Evaluating Aggregate Gradations," Proc. of Assn. of Asphalt Paving Tech., Vol. 31, 1962, pp. 176-207.

59. Mix Design Methods for Asphalt Concrete, MS-2, Asphalt Institute, Lexington, KY, 1984, 102 p.

60. Kandhal, P.S., "Maximum Density Line: Which One Should Be Used?" Asphalt Technology News, Fall 1989, p. 6.

61. "Responses to 'Maximum Density Line: Which One Should be Used?", Asphalt Technology News, Vol. 2, No.1, 1990, pp. 2-3.

62. Anderson, D.A., D.R. Luhr, and C.E. Antle, "Framework for Development of Performance - Related Specifications for Hot-Mix Asphaltic Concrete," NCHRP Rpt. No. 332, Trans. Res. Bd., Washington, D.C., 1990, 118 p.

63. Abkemeier, T.J., "Indirect Tensile Test Correlative Study," M.S. Thesis, Univ. of Missouri-Rolla, Rolla, Missouri, 1992, 132 p.

64. Adedimila, A.S., "A Comparison of the Marshall and the Indirect Tensile Tests in Relation to Asphalt Mixture Design," Proc. Inst. of Civil Engineers, Part 2, 81, 1986, pp. 461 - 469.

65. SYSTAT, 1990, Systat, Inc., Evanston, Ill.

66. Monismith, C.L. and K.E. Secor, "Viscoelastic Behavior of Asphalt Concrete Pavements," Proc. Int'l. Conf. of Structural Design of Asphalt Pavements, University of Michigan, Ann Arbor, 1962, pp. 476-498.

67. Adedimila, A.S. and T.W. Kennedy, "Fatigue and Resilient Characteristics of Asphalt Mixtures by Repeated-Load Indirect Tensile Test," Res. Report 183-5, Center for Hwy. Res. Univ. of Texas at Austin, 1975.

68. Gonzalez, G., T. W. Kennedy, and J.N. Anagonos, "Evaluation of the

Resilient Elastic Characteristics of Asphalt Mixtures Using the Indirect Tensile Test," Res. Report 183-6, Center for Hwy. Res., Univ. of Texas at Austin, 1975.

69. Adedimila, A. S. and T.W. Kennedy, "Effects of Repeated Tensile Stresses on the Resilient Properties of Asphalt Mixtures," Trans. Res. Rec. 616, Trans. Res. Bd., Washington, D.C., 1976.

70. Kennedy, T.W., "Characterization of Asphalt Pavement Materials Using the Indirect Tensile Test,"Proc. of Assn. of Asphalt Paving Tech., Vol. 46, 1977, pp. 132-150.

71. Machemehl, R. B. and T. W. Kennedy, "Asphalt Mixtures: Comparative Analysis of Characterization for Design," Trans. Res. Rec. 821, Trans. Res. Bd., Washington, D.C. 1981, pp. 22-29.

72. Von Quintus, H.L., J.B. Rauhut, and T.W. Kennedy, "Comparisons of Asphalt Concrete Stiffness as Measured by Various Testing Techniques," Proc. of Assn. of Asphalt Paving Tech., Vol. 51, 1982, pp. 35-52.

73. Khosla, N.P., and M.S. Omer, "Characterization of Asphaltc Mixtures for Prediction of Pavement Performance," Trans. Res. Rec. 1034, Trans. Res. Bd., pp. 47-55.

74. Bonaquist, R., D.A. Anderson, and E. Fernando, "Relationship Between Moduli Measured in the Laboratory by Different Procedures and Field Deflection Measurements," Proc. of Assn. of Asphalt Paving Tech., Vol. 55, 1986, pp. 419-452.

75. Kallas, B.F., "Elastic and Fatigue Behavior of Emulsified Asphalt Paving Mixtures," Res. Rpt. No. 79-1, 1979, 57 p.

76. Baladi, G.Y., "Integrated Material And Structural Method for Flexible Pavements," Report No. FHWA-RD-88-109, Fed. Hwy. Admin., Vol. 1., 1988, 313 p.

77. Maupin, G.W., "Results of Indirect Tensile Tests Related to Asphalt Fatigue," Hwy. Res. Rec. 404, Hwy. Res. Bd., Washington, D.C., 1972, pp. 1-7.

78. Stroup-Gardiner, M. and J. Epps. "Four Variables that Affect the Performance of Lime in Asphalt-Aggregate Mixtures, " Trans. Res. Rec. 1115, Trans. Res. Bd., Washington, D.C., 1987, pp. 12-22.

79. Moore, R.K. and T.W. Kennedy, "Tensile Behavior of Asphalt-Treated Materials Under Repetitive Loading," Proc. Third Int'l. Conf. of Structural Design of Asphalt Pavements, London, England, Vol. 1, 1972.

80. Schmidt, R.J. and P.E. Graf, "The Effects of Water on the Resilient Modulus of Asphalt-Treated Mixes," Proc. of Assn. of Asphalt Paving Tech., Vol. 41, 1972, pp. 118-162.

81. Kallas, B.F., "Asphalt Pavement Temperatures," Hwy. Res. Rec. 150, Hwy. Res. Bd., 1966, pp. 1-11.

82. Croney, D.C. and P. Croney, The Design and Performance of Road Pavements, McGraw Hill Book Co., 1991, London.

83. Fairhurst, G.E., Y.R. Kim, and N.P. Khosla, "Resilient Modulus Testing of Asphalt Specimens in Accordance with ASTM D 4123-82," MTS, 7 p.

75. Kallas, B.F., "Elastic and Fatigue Behavior of Emulsified Asphalt Paving Mixtures," Res. Rpt. No. 79-1, 1979, 57 p.

76. Baladi, G.Y., "Integrated Material And Structural Method for Flexible Pavements," Report No. FHWA-RD-88-109, Fed. Hwy. Admin., Vol. 1., 1988, 313 p.

77. Maupin, G.W., "Results of Indirect Tensile Tests Related to Asphalt Fatigue," Hwy. Res. Rec. 404, Hwy. Res. Bd., Washington, D.C., 1972, pp. 1-7.

78. Stroup-Gardiner, M. and J. Epps. "Four Variables that Affect the Performance of Lime in Asphalt-Aggregate Mixtures, " Trans. Res. Rec. 1115, Trans. Res. Bd., Washington, D.C., 1987, pp. 12-22.

79. Moore, R.K. and T.W. Kennedy, "Tensile Behavior of Asphalt-Treated Materials Under Repetitive Loading," Proc. Third Int'l. Conf. of Structural Design of Asphalt Pavements, London, England, Vol. 1, 1972.

80. Schmidt, R.J. and P.E. Graf, "The Effects of Water on the Resilient Modulus of Asphalt-Treated Mixes," Proc. of Assn. of Asphalt Paving Tech., Vol. 41, 1972, pp. 118-162.

81. Kallas, B.F., "Asphalt Pavement Temperatures," Hwy. Res. Rec. 150, Hwy. Res. Bd., 1966, pp. 1-11.

82. Croney, D.C. and P. Croney, The Design and Performance of Road Pavements, McGraw Hill Book Co., 1991, London.

83. Fairhurst, G.E., Y.R. Kim, and N.P. Khosla, "Resilient Modulus Testing of Asphalt Specimens in Accordance with ASTM D 4123-82," MTS, 7 p.

APPENDIX A

FINE AGGREGATE

PARTICLE SHAPE DETERMINATION

$$V = \frac{W}{0.998}$$

where:

V = volume of cylinder, cm^3

W = net mass of water, g

PROCEDURE

1. Determine the bulk specific gravity of each material that is to be blended into the combined gradation (e.g., the natural sand, the manufactured sand, etc.). Each material should be a blend of sizes as per the as-delivered gradation.
2. Calculate the average specific gravity of the blend of the different types of sand:

$$G = \frac{P_1 + P_2}{\frac{P_1}{G_1} + \frac{P_2}{G_2}}$$

where:

G = average bulk specific gravity of the combined types of sand.

$G_{1,2}$ = bulk sp. grav. of each type of sand.

$P_{1,2}$ = percent of each type of sand in the asphalt mixture gradation for the (+)#100 to (-)#16 size. For example, for a total sand content of 300g between the (+) #100 and (+) #16 sizes, if 200g is supplied from sand #1, then P_1 = 66.7%.

3. Each type of sand is washed over a No. 100 sieve in accordance with the

methods in ASTM C 117 and then dried and sieved into separate size fractions using ASTM C 136 procedures.

4. Weigh out and combine the following quantities of dry sand from each of the sizes. These quantities are combined from the different types of sands in proportion to their representation in the asphalt mixture for the specific sieve size (see Data Sheet Calculation):

Individual Size Fraction	Combined Mass, g
No. 8 to No. 16	44
No. 16 to No. 30	57
No. 30 to No. 50	72
No. 50 to No. 100	17
	190

5. Set the funnel stand in the pan. Place the funnel on the funnel stand.
6. Mix the test sample until it is homogenous. Using a finger to block the opening of the funnel, pour the test sample into the funnel. Level the material in the funnel with the spatula. Center the measure under the funnel, remove the finger, and allow the sample to fall freely into the measure.
7. After the funnel empties, remove excess heaped sand from the measure by a single pass of the spatula with the blade vertical using the straight part of its edge in light contact with the top of the measure. Until this operation is

complete, exercise care to avoid vibration or disturbance that could cause compaction of the fine aggregate in the measure (Note 3). Brush adhering grains from the outside of the measure and determine the mass of the measure and contents to the nearest 0.1 g. Retain all sand grains.

Note 3 -- After strikeoff, the measure may be tapped lightly to compact the sample to make it easier to transfer the measure to scale or balance without spilling any of the sample.

8. Collect the sample from the retaining pan and measure, recombine, and repeat the procedure again. The results of two runs are averaged. See Calculation section below.

9. Calculate the uncompacted voids to the nearest 0.1 percent for each determination as follows:

$$U = \frac{V - (M/G)}{V} \times 100$$

V = volume of measure, cm^3

M = net mass of fine aggregate in measure (gross mass minus the mass of the empty measure)

G = bulk dry specific gravity of the combined fine aggregate, step 2

U = uncompacted voids, percent, in the material

Note 4 -- For most aggregate sources the fine aggregate specific gravity does not vary much from sample to sample or from size to size finer than the 2.36-mm (No. 8) sieve. Therefore, unless the specific gravity of individual sizes is appreciably

different, it is intended that the value used in this calculation may be from a routine specific gravity test of an as-received grading of the fine aggregate. If significant variation between different samples is expected, the specific gravity should be determined on material from the same field sample from which the uncompacted void content sample was derived, Normally the as-received grading can be tested for specific gravity, particularly if the 2.36-mm (No. 8) to 150-um (No. 100) size fraction represents more than 50 percent of the as-received grading. However, it may be necessary to test the graded 2.36-um (No. 8) to 150-mm (No. 100) sizes for specific gravity for use with the graded void sample, Method A or the individual size fractions for use with the individual size method, Method B, (not included here). A difference in specific gravity of the 0.05 will change the calculated void content about one percent.

DATA SHEET

Sample _____ Date Tested____ Technician _____

Total percent of each sand per asphalt mixture puck:

Sieve	Sand #1 Wt. Ret. g	Sand #2 Wt. Ret. g	Total Wt. Ret. g	Fraction of Total, Sand #1, (F_1)	Fraction of Total, Sand #2 (F_2)
#16					
30					
50					
100					
Total:	A =	B =	C =		

$$P_1 = \frac{A}{C} = \frac{\textit{Total wt. Ret., sand \#1 (A)}}{\textit{Total Wt. Ret., both sands (C)}} * 100$$

$$P_2 = \frac{B}{C} = \frac{\textit{Total wt. Ret., sand \#2 (B)}}{\textit{Total Wt. Ret., both sands (C)}} * 100$$

$$F_{1,16} = \frac{\textit{wt. Ret. on \#16, sand 1}}{\textit{Wt. Ret. on \#16, both}}$$

$$F_{2,16} = \frac{\textit{wt. Ret. on \#16, sand 2}}{\textit{Wt. Ret. on \#16, both}}$$

$$F_{1,30} = \frac{\textit{Wt. Ret. on \#30, sand 1}}{\textit{Wt. Ret. on \#30, both}}$$

$$F_{2,30} = \frac{\textit{Wt. Ret. on \#30, sand 2}}{\textit{Wt. Ret. on \#30, both}}$$

$F_{1,50} = \frac{Wt.\ Ret.\ on\ \#50,\ sand\ 1}{Wt.\ Ret.\ on\ \#50,\ both}$	
$F_{2,50} = \frac{Wt.\ Ret.\ on\ \#50,\ sand\ 2}{Wt.\ Ret.\ on\ \#50,\ both}$	
$F_{1,100} = \frac{Wt.\ Ret.\ on\ \#100\ ,\ sand\ 1}{Wt.\ Ret.\ on\ \#100,\ both}$	
$F_{2,100} = \frac{Wt.\ Ret.\ on\ \#100,\ sand\ 2}{Wt.\ Ret.\ on\ \#100,\ both}$	

DATA SHEET
PARTICLE SHAPE AND TEXTURE OF FINE AGGREGATE

Sample _____
Date Tested _____
Technician _____

Specific Gravity		
	$G_{1,2}$	$P_{1,2}$
Sand #1		
Sand #2		
$G = (P_1 + P_2) / \left[\frac{P_1}{G1} + \frac{P_2}{G_2}\right]$		
		$\Sigma = 100$

STANDARD GRADATION

Size Fraction		
#16 to #8	Mass sand #1 = F_1 * 44 _____ g	
	Mass sand #2 = F_2 * 44 _____ g	
#30 to #16	Mass sand #1 = F_1 * 57 _____ g	
	Mass sand #2 = F_2 * 57 _____ g	
#50 to #30	Mass sand #1 = F_1 * 72 _____ g	
	Mass sand #2 = F_2 * 72 _____ g	
#100 to #50	Mass sand #1 = F_1 * 17 _____ g	
	Mass sand #2 = F_2 * 17 _____ g	
	TOTAL 190 g	

UNCOMPACTED VOIDS		
	Trial 1	Trial 2
Weight sand + measure, g		
Weight measure, g		
Weight sand (M), g		
Combined specific gravity (G)		
Uncompacted voids (U), % U = [V-(M/G)/V] * 100		
Average Uncompacted Voids		

APPENDIX B

COARSE AGGREGATE

PARTICLE SHAPE DETERMINATION

APPENDIX B

COARSE AGGREGATE

PARTICLE SHAPE DETERMINATION

INDEX OF AGGREGATE PARTICLE SHAPE AND TEXTURE
ASTM D 3398-87

APPLICATION

For asphalt mixture aggregate from (+) #4 sieve to the (-) 1 in sieve size fractions.

EQUIPMENT

1. 6 in dia. Mold - inside height 7.00 ± 0.01 in for testing the following fractions:

   (+) 3/4" to (-) 1 in
   (+) 1/2" to (-) 3/4 in

2. 4 in dia. Mold - inside height 4.6 ± 0.01 in for testing the following fractions:

   (+) 3/8" to (-) 1/2 in
   (+) #4 to (-) 3/8 in

3. 24 in Tamping Rod - for use with 6 in mold

4. 16 in Tamping Rod - for use with 4 in mold

CALIBRATION OF MOLD

1. Fill the mold with water at room temperature and cover with a piece of plate glass in such a way as to eliminate bubbles and excess water.

2. Determine the mass of water in the mold to an accuracy of 4 g or less.

3. Measure the temperature of the water and determine the volume of the mold by multiplying the mass of the water by the corresponding specific volume of water given in Table B-1 for the temperature involved.

PROCEDURE

1. Test each of the above-listed fractions if present in the gradation in amounts of 10% or more.

2. Obtain a sample of each fraction to be tested as per:

   6 in mold 13 lbs
   4 in mold 4 lbs

3. Wash the sample of aggregate by decanting the wash water through a sieve at least one size smaller than that being used. Continue the washing and decanting operation until the wash water is clear. Then flush the residue on the sieve back into the aggregate sample. Dry the sample to constant weight at a temperature of 230 $\pm$ 9°F (110 $\pm$ 5°C).

4. Determine the bulk-dry specific gravity of each size fraction.

5. Place the cylindrical mold on a uniform, solid foundation. Gently place the aggregate, from the lowest height possible, into the mold until it is approximately one-third full. Level the surface with the fingers, and compact the layer using 10 drops of the tamping rod evenly distributed over the surface. Apply each drop by holding the rod vertically with its rounded end 2 in (50 mm) above the surface of the aggregate (controlled by the slot-and-pin arrangement) and releasing it so that it falls freely. Place a second layer in the mold using the same procedure, filling the mold approximately two-thirds full. As before, level the surface and apply the same compactive effort, 10 drops of the rod. After the final layer has been compacted, add individual pieces of aggregate to make the surface of the aggregate mass even with the rim of the mold, with no projections above the rim. Determine the mass of the aggregate in the mold to an accuracy of at least 4 g.

6. Repeat the filling of the mold using the same specimen and compaction. Make a second determination of the mass of the aggregate in the mold as described above. Use the average mass of the two runs in calculating the percentage of voids at 10 drops for each size.

7. For the higher degree of compaction, follow the steps outlined in #5 and #6, except use 50 drops of the tamping rod in compacting each layer. Again average the masses from the two runs for use in computing the percentage of voids at 50 drops for each size fraction.

8. Calculate the percentage of voids in each size fraction of the aggregate at 10 drops per layer and at 50 drops per layer, respectively, by the following relationships:

$$V_{10} = [1-(M_{10}/SV)] \times 100$$
$$V_{50} = [1-(M_{50}/SV)] \times 100$$

where:

V_{10} = voids in aggregate compacted at 10 drops per layer, %,
V_{50} = voids in aggregate compacted at 50 drops per layer, %,
M_{10} = average mass of the aggregate in the mold compacted at 10 drops per layer, g
M_{50} = average mass of the aggregate in the mold compacted at 50 drops per layer, g

S = bulk-dry specific gravity of the aggregate size fraction
V = volume of the cylindrical mold, mL

9. Determine the particle index (I_a) for each size fraction tested as follows:

$$I_a = 1.25\ V_{10} - 0.25\ V_{50} - 32.0$$

10. Calculate the weighted particle index of an aggregate containing several sizes by averaging the particle index data for each size fraction, weighted on the basis of the percentage of the fractions in the grading of the sample:

$$I_T = (P_1 * I_{a1}) + (P_2 * I_{a2}) + (P_3 * I_{a3}) + \ldots + (P_n * I_{an})$$

where $P_1 \ldots P_n$ = percent of the fraction in the sample (not the entire asphalt mixture gradation)
$I_{a1} \ldots I_{an}$ = particle index of each fraction

For sizes represented by less than 10% in the grading, for which no particle index data were obtained, use the average particle index of the next coarser and finer sizes for which data are available or the particle index for the next coarser or finer size if a value is available only in one direction.

Table B-1 Specific Volume of Water at Different Temperatures

Temperature, °F(°C)	Specific Volume, mL/g
54 (12)	1.0005
57 (14)	1.0007
61 (16)	1.0010
64 (18)	1.0014
68 (20)	1.0018
72 (22)	1.0022
75 (24)	1.0027
79 (26)	1.0032
82 (28)	1.0038
86 (30)	1.0044
90 (32)	1.0050

DATA SHEET
Index of Particle Shape and Texture (D3398)

Sample _____ Technician _____ Date _____

Percent of each fraction in each puck:			
Sieve	Wt. Ret. g	% Ret. (P1,2,3)	Spec. Grav. S
1/2" to 3/4"			
3/8" to 1/2"			
#4 to 3/8"			
Total		100	

$$P_{1,2,3} = \frac{wt.\ ret.\ on\ a\ given\ sieve}{wt.\ ret.,\ total} \times 100$$

PARTICLE INDEX			
Fraction	10 Drops	Trial 1	Trial 2
1/2" to 3/4"	Mass of aggregate + mold, g		
	Mass of mold, g		
	Mass of aggregate, g		
	Average of 2 trials (M_{10})g		
	50 Drops	Trial 1	Trial 2
	Mass of aggregate + mold, g		
	Moss of mold, g		
	Mass of aggregate, g		
	Average of 2 trials (M_{50}), g		
	Volume of 6 in cylinder mold (V), ml		
	Bulk specific gravity (S)		
	Mass of aggregate (M_{10}), g		
	Mass of aggregate (M_{50}), g		
	V_{10} = [1 - (M_{10}/SV)] * 100, %		
	V_{50} = [1 - (M_{50}/SV)] * 100, %		
	I_{a1} = 1.25 V_{10} - 0.25 V_{50} - 32.0		

PARTICLE INDEX			
Fraction	10 Drops	Trial 1	Trial 2
3/8" to 1/2"	Mass of aggregate + mold, g		
	Mass of mold, g		
	Mass of aggregate, g		
	Average of 2 trials (M_{10})g		
	50 Drops	Trial 1	Trial 2
	Mass of aggregate + mold, g		
	Moss of mold, g		
	Mass of aggregate, g		
	Average of 2 trials (M_{50}), g		
	Volume of 6 in cylinder mold (V), ml		
	Bulk specific gravity (S)		
	Mass of aggregate (M_{10}), g		
	Mass of aggregate (M_{50}), g		
	V_{10} = [1 - (M_{10}/SV)] * 100, %		
	V_{50} = [1 - (M_{50}/SV)] * 100, %		
	I_{a2} = 1.25 V_{10} - 0.25 V_{50} - 32.0		

PARTICLE INDEX			
Fraction	10 Drops	Trial 1	Trial 2
#4 to 3/8"	Mass of aggregate + mold, g		
	Mass of mold, g		
	Mass of aggregate, g		
	Average of 2 trials (M_{10})g		
	50 Drops	Trial 1	Trial 2
	Mass of aggregate + mold, g		
	Moss of mold, g		
	Mass of aggregate, g		
	Average of 2 trials (M_{50}), g		
	Volume of 6 in cylinder mold (V), ml		
	Bulk specific gravity (S)		
	Mass of aggregate (M_{10}), g		
	Mass of aggregate (M_{50}), g		
	$V_{10} = [1 - (M_{10}/SV)] * 100$, %		
	$V_{50} = [1 - (M_{50}/SV)] * 100$, %		
	$I_{a3} = 1.25\ V_{10} - 0.25\ V_{50} - 32.0$		
PARTICLE INDEX FOR ALL FRACTIONS:			
$I_T = (P_1 * I_{a1}) + (P_2 * I_{a2}) + (P_3 * I_{a3})$			

DETERMINATION OF INDIRECT TENSILE STRENGTH AND RESILIENT MODULUS FOR BITUMINOUS MIXTURES

SHRP Designation: P07

ASTM Designation: D-4123

1. INTRODUCTION

1.1 Three levels of temperature (41 ± 2 °F, 77 ± 2 °F and 104 ± 2 °F) were tested using repetitive compressive haversine load pulses of 1 Hz frequency with a 0.1 second load duration and a 0.9 second rest period. The thickness of the specimens tested varied between 2.4 in and 2.7 in. Prior to performing the resilient modulus test, the indirect tensile strength was determined at 77 ± 2 °F for each combination of mix type (bituminous base, Type C and Type IC), gradation (fine and coarse), asphalt cement grade (AC-10 and AC-20), asphalt cement content (optimum and 0.5% above optimum) and aggregate (DR-6 and DR-7 for bituminous base mixes, DR-4 and DR-5 for Type C and IC mixes). Duplicate specimens were prepared for the 48 mixes. In all, 96 indirect tensile strength specimens were prepared. The specimens were aged for one week before testing. The value of tensile strength determined by this procedure was used to estimate the indirect tensile stress and corresponding compressive load to be repetitively applied to similar test specimens during subsequent resilient modulus testing. For resilient modulus testing, four specimens were made for each mix. In all, 192 specimens were tested. The specimens were aged for one week before testing.

1.2 Typically, the specimens were built on a Tuesday and then testing would begin for those specimens on the following Tuesday at 41 °F, continue at 77 °F on Wednesday, and finish at 104 °F on Thursday. The testing was done from lower to higher temperature levels to reduce permanent damage to the specimen. The specimens were brought to the test temperature 24 hours before testing began.

1.3 Once the test was completed, plots were made of load, horizontal deformation and vertical deformation with time. The measured total recoverable horizontal and vertical deformations were used to calculate values of resilient Poisson's ratio. The resilient modulus values were then calculated using cyclic loads and the calculated Poisson's ratio.

2. PREPARATION OF TEST SPECIMENS

2.1 Both the indirect tensile strength and the resilient modulus specimens are made using the same procedure as that described in the Marshall Mix Design portion of this report. In addition, all other specimen properties except flow and stability are determined as described in the Marshall Mix Design section.

2.2 Specimens are marked and measured as follows after determination of the specimen SSD BSG:

2.2.1 For indirect tensile strength specimens use a paint marker and a straight edge to draw a thin line along the diameter of the specimen face with the smoothest texture. Use a 4 in filter paper with notches on opposite sides of its diameter to mark the two points needed to draw the line. Avoid drawing the line along a diameter that has voids on the sides of the specimen.

2.2.2 For resilient modulus specimens, mark a diametrical axis on the test specimen as specified in 2.2.1. Add an arrow tip to one end of the line. Using the paint marker and a straight edge, draw a thin horizontal line at the mid-thickness of the specimen on both sides of the diametrical axis line.

2.2.3 Measure the thickness and the diameter of indirect tensile strength and resilient modulus test specimens to the nearest 0.01 in using dial calipers. Determine the thickness by averaging a single center measurement with three equally spaced measurements located 0.5 in from the test specimen edge. Determine the diameter by averaging the diameter of the specimen at midheight along (1) the

diametrical axis drawn in 2.2.1 and 2.2.2 above and the axis perpendicular to the axis measured in (1) above.

3. STATIC INDIRECT TENSILE STRENGTH TESTS

3.1 Adjust the thermostat in the testing room to 77 °F.

3.2 Place the specimens to be tested in watertight buckets and then put the buckets in a constant temperature water bath at 77 ± 2 °F for 24 hours.

3.3 Prepare the xy plotter, LVDT signal conditioner, and the strain gage signal conditioner as specified in the Marshall Mix Design procedure, section 5.8.3.

3.4 Place the test specimen in the test press loading apparatus and position it so that the mid thickness of the test specimen is located in the line of action of the load cell. Use the diametrical marking to ensure that the specimen is aligned from top to bottom—the diametrical marking should be centered on the top and bottom loading strips.

3.5 Turn on the test press, check the zero point on the xy plotter, make sure the plotter pen is touching the paper, and depress the UP button on the test press to apply a compressive load to the specimen by maintaining a constant rate of movement of the test press platen of 2 in/min. The platen will continue to move until the maximum load is reached and the load decreases as indicated by the strain gage indicator. The upper limit switch on the test press forces the platen to stop moving. The upper and lower limit switches on the test press can be adjusted using the button underneath the test press. Record the maximum load reading from the strain gage conditioner on the chart paper. Note: if the beam holding the plotter pen binds during the test, quickly turn off the power to the plotter and straighten the beam so it can move freely, then turn on the plotter.

3.6 Depress the DOWN button on the test press to lower the platen. The lower limit switch on the test press will stop the platen. Remove the breaking head

from the platen, sweep any loose asphalt off of the platen, and save the test specimen by placing it in a plastic bag or some other suitable container. Write the specimen ID on the bag. Remove the recording chart from the xy plotter and fill in the chart data block. Clean the breaking head loading strips and lubricate the guide rods with silicone spray and a towel.

3.7 Make a sketch of the specimen failure on the data sheet and calculate the indirect tensile strength as follows:

$$S_t = \frac{2P_o}{\pi h D}$$

where:

S_t is the indirect tensile strength in lbs

P_o is the maximum load sustained by the specimen in lbs

h is the specimen thickness in inches

D is the specimen diameter in inches

3.8 Prepare a table of average indirect tensile strength values for each mix along with tensile stress levels of 30, 15, and 5 percent of the tensile strength to be used in conducting the resilient modulus determinations at the test temperatures of 41, 77, and 104°F, respectively. Include specimen contact loads shown in Table 21 of 3, 1.5, and 0.5 percent of the tensile strength to be used during resilient modulus determinations at 41, 77, and 104 °F respectively. Contact loads and cyclic test loads will be discussed below.

4. RESILIENT MODULUS TESTING

The system includes an MTS 810 closed loop electrohydraulic load system equipped with a 3.3K actuator, an environmental chamber, a temperature bath, a specimen yoke, a yoke stand, and a data acquisition and load signal generation computer/software system. The specimens were seated on the lower concave loading

strip which was affixed to the loading frame. Both upper and lower loading strips had a radius of curvature of 2in (5.1cm) and a width of 0.5in (1.3cm).

The specimen yoke was a small frame that held two horizontal LVDT'S which were diametrally opposite. Originally, the LVDT's were fixed to a base. However, specimens tended to rock under load; this could be discerned by both visual observation and by examining the readout from each horizontal channel. Ideally, both LVDT's should be compressed upon loading; however, sometimes one of the readouts indicated that one LVDT was extending. It was thought that possibly one of the tips of the LVDT could be slipping down into a surface void. So, the tips were replaced with disk-type tips that threaded onto the LVDT cores. The idea was that the 1/4 in (0.64cm) diameter disks would bridge across surface voids. Next, the method of transferring the load was changed. Originally, the upper load strip was not fixed; a ball bearing was used to transfer the load from the load cell, which was fixed to the MTS load ram, to the top of the upper load strip. This configuration was basically the state of the art several years ago. Additionally, vertical deformation was measured with an LVDT internal to the MTS system; the LVDT had a full range of 6in (2.4cm). Data indicated that the specimen was unstable, and that the vertical LVDT was not sensitive enough, even though the controls of the MTS were set to utilize 10 percent of the full range (0.6in = 0.2cm) for greater accuracy.

The second generation device consisted of mounting a more sensitive vertical LVDT to the yoke base, and fixing the upper loading strip to the load cell in order to prevent it from rotating. The vertical measurements appeared to be more sensible, but there still seemed to be specimen movement, even under higher baseline static loads. The yoke base still had to be centered manually to align the upper and lower load strips.

In an effort to assure better vertical alignment of the upper and lower load

strips, a new base was purchased which was manufactured for the purpose of performing repeated load and static load indirect tension tests. This device featured an upper platen which slid vertically by way of two guide posts, thus aligning the upper and lower load strips. The horizontal LVDT's were fixed to the base as well as the vertical LVTD. However, some rocking was still evident, possibly due to slight looseness in the guide bearings and to the difficulty of aligning the upper platen with the load cell/ram.

A fourth generation set-up involved a different horizontal LVDT yoke. In this case, a light gauge steel frame holding the two LVDTs was mounted directly onto the specimen, reminiscent of the original Schmidt device (80) and the newer MTS resilient modulus system (83). This allows the LVDTs to follow the specimen should rocking occur. This, coupled with the higher static background loads recommended by the latest draft of the SHRP protocol, and coupled with the use of guide rods, seems to have eliminated or reduced experimental problems to acceptable levels. Also, as per the SHRP protocol, two vertical LVDT's were mounted to monitor the movement of the upper platen, rather than the ram movement. This virtually eliminates machine deflection from the vertical deformation measurement, and allows for a more accurate calculation of Poisson's ratio, which is necessary for a truer calculation of resilient modulus. The final setup is shown in Fig. D1. An auxiliary device was necessary in order to mount the yoke accurately and consistently on the sample, as shown in Fig. D2.

The environmental chamber had to be capable of maintaining temperatures of 41°, 77°, and 104°F (4, 25, and 40°C) plus or minus 2°F(1°C). A 1.5 in (3.8cm) thick styrofoam box was built to surround the yoke. Also surrounding the yoke on three sides were 0.25in (0.64cm) copper coils through which was circulated a mixture of ethylene glycol and water. The solution was circulated through a

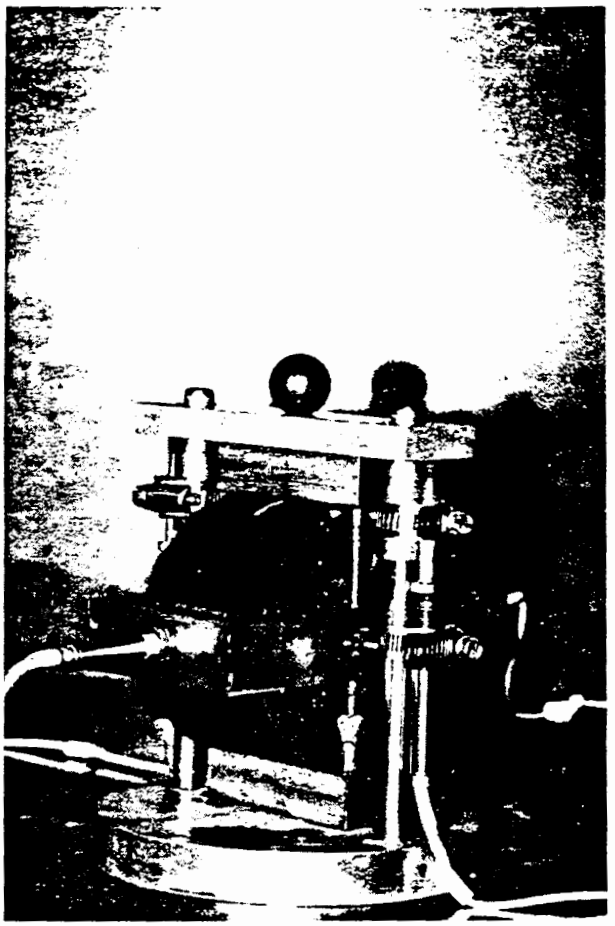

Fig. D1. Final Resilient Modulus Device.

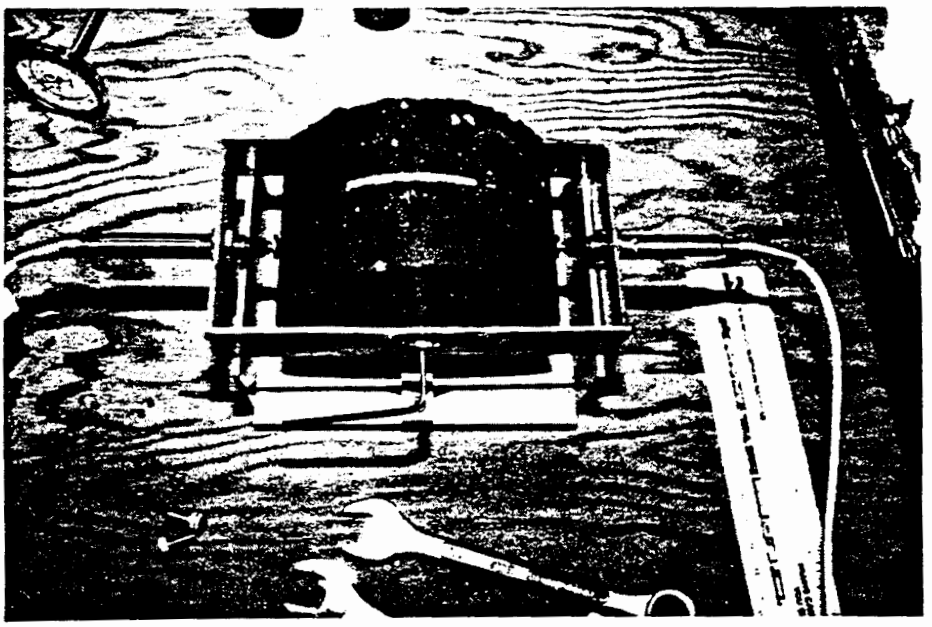

Fig. D2. Resilient Modulus Yoke Mounting Template.

heating/refrigeration unit. A small fan was mounted inside the environmental chamber to distribute the air. A dial gage thermometer was mounted through the box to monitor air temperature. The chamber was found to be able to maintain the temperature within the ASTM 4123 specified 2°F (1°C). The environmental chamber is shown in Fig. D3. Prior to testing, specimens were stored in an environment controlled at the test temperature: refrigerator at 41°F (4°C), at room ambient conditions at 77°F (25°C), or in an oven at 104°F (40°C).

The data acquisition/load signal generation system consisted of the following components: an IBM-compatible 386 personal computer with 8 kilobyte memory, 80 megabyte hard disk, Data Translation DT 2801A 12 bit analog/digital board, printer, color monitor, one strain gage conditioner, four LVDT conditioners, ASYST software, a 2500 lb. Strain-sert load cell, two Schaevitz LBB-375-TA-100 LVDTs with a range of $\pm$0.100in (0.25cm) of travel (horizontal deformation), and two Schaevitz PCA-220-100 LVDTs with a range of $\pm$0.100 in (0.25cm) of travel (vertical deformation).

The minimum value measurable with the system setup is calculated as follows. The input voltage range of the horizontal LVDT's was -10 to +10 V. The precision of the input signal measured by the 12 bit A/D board is $20V/2^{12}$ which is 0.00488 V. When 0.1 in full scale displacement LVDT's were used, the horizontal transducers were ranged 10% of full scale which calibrates the output to a finer scale travel and allows higher resolution measurements. The vertical transducers were ranged 33% of full scale. The minimum value of horizontal displacement measured was then (0.01 in/10V)*(0.00488V) which is 0.00000488 in. The vertical LVDT's could be read to $(20/2^{12})*(0.033/10) = 0.000016$ in. The load cell could be read to (2500 lb/10V)•(0.00488) = 1.22 lbs.

4.1 Specimen preparation. Place the specimens in the appropriate controlled temperature environment needed to bring them to the specified test temperature at

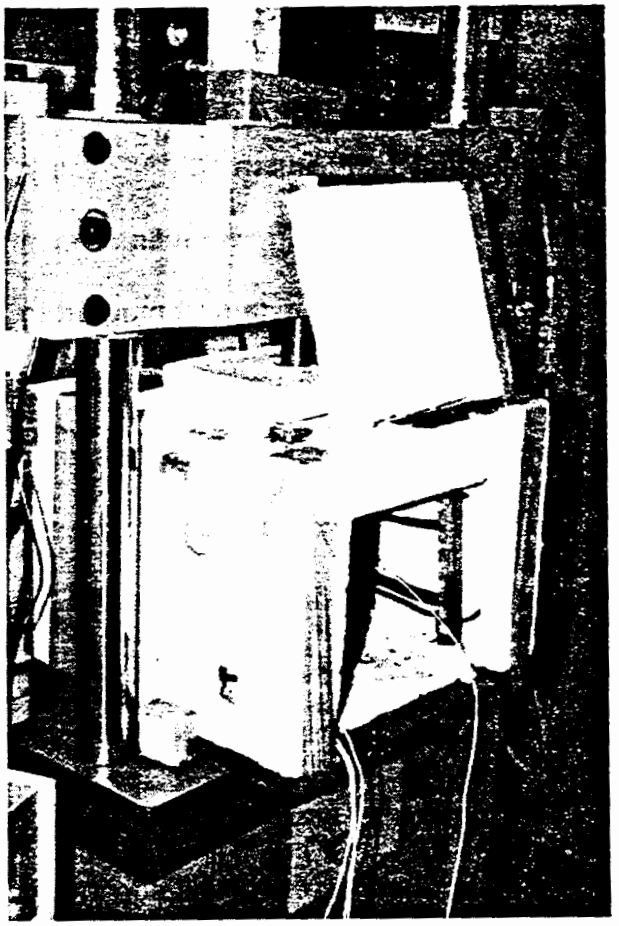

Fig. D3. Resilient Modulus Environmental Chamber.

least 24 hours prior to testing. A water bath is used to cool the specimens to 41 °F. The specimens are placed in 2 gal polyethylene buckets before being put in the water bath. Each bucket can hold 6 specimens. Use the hole in top of each bucket to check the specimen temperature with a dial gage thermometer. Allow the specimens to sit in the ambient air to come to 77 °(the ambient conditions can be controlled by opening the door of the testing room or by turning the room air conditioner on and off), and use an oven to bring the specimens to 104 °F. Keep a dial gage or mercury-in-glass thermometer with the specimens in the oven at all times.

4.2 Temperature cabinet. A constant temperature circulator is used to maintain the testing temperatures of 41 °F and 104 °F during resilient modulus tests. A 50-50 mixture of antifreeze and water is used as the circulating liquid. Check the level of coolant in the circulator reservoir before turning the circulator on. The coolant level should be above the coils in the reservoir at all times. Set the thermoregulator to -13 °C to bring the chamber to 41 °F and 45 °C to bring the chamber to 104 °F (read to the top of the thermoregulator indicator). Check the temperature of the cabinet using a dial gage thermometer and the thermometer access port on the top left of the cabinet. Both the circulator heating and cooling switches should be "on" to reach 41 °F and the "heating only" switch should be "on" to reach 104 °F. Move the control valve lever forward on the right side of the circulator to circulate coolant through the temperature cabinet coils. At the 77 °F test temperature, maintain 77 °F as specified in 4.1. Place the loading head with the vertical LVDTs and the horizontal frame with the horizontal LVDTs in the temperature cabinet 24 hours prior to testing.

4.3 Equipment calibration. Before each test, make sure that all LVDTs and the load cell are securely mounted for testing and that there are no loose connections with their respective signal conditioner and the computer.

4.3.1 Calibrate the LVDTs before any testing begins, and monitor their calibration after every 48 resilient modulus tests using the micrometer calibration block. Monitor the calibration of the LVDTs at each test temperature since there is a slight variation of LVDT response with temperature. Prior to each specimen test, make sure that the shaft of each LVDT is not sticking by depressing and releasing the LVDT tip. Apply silicone spray or WD-40 on a regular basis to the LVDT shafts. Also check the LVDT tips for tightness.

4.3.2 Calibrate two load cells before performing resilient modulus tests. One load cell is used as the MTS load cell during testing and the other is used to check the calibration of the testing load cell every 48 resilient modulus tests at 77 °F only.

4.4 Prepare testing log. For each combination of mix, gradation, asphalt cement type, asphalt cement percentage and aggregate, a testing log is prepared before testing. The log uses the maximum suggested seating load ($P_{contact}$) and the recommended maximum load for testing and preconditioning (P_{max}) as specified in 3.8, along with load cell calibration data to determine the necessary cyclic load (P_{cyclic}), MTS set point and haversine load pulse for testing the 4 specimens represented by each log at 41, 77, and 104 °F.

4.4.1 The cyclic load can be determined using:

$$P_{cyclic} = P_{max} - P_{contact}$$

Note: round P_{max} and $P_{contact}$ down to the nearest 10 lbs and 1 lb respectively before calculating P_{cyclic} to avoid overloading the specimen. Round P_{cyclic} to the nearest 1 lb.

4.4.2 The log also has space for recording the cumulative vertical deformation and the number of preconditioning and load cycles used for each

specimen test. The cumulative deformation is measured using the dial gage magnetically mounted to the hydraulic actuator shaft. Subtract the dial gage reading in 4.7 from the reading in 4.8 to get the cumulative vertical deformation. If total cumulative vertical deformations greater than 0.025 inch for 41 °F or 0.050 in for 77° and 104 °F occur, reduce the applied load to the minimum value possible and still retain an adequate deformation for measurement purposes.

4.5 Mounting specimen in MTS load frame.

4.5.1 Take the loading head assembly from the temperature cabinet. Place the lucite specimen on the lower section loading strip. Place the upper section of the loading head on top of the specimen by sliding it over the guide rods. Rotate the lucite specimen so that its diametrical marking is coincident with the upper and lower loading strips. Place a weight on top of the upper section and make sure that the tips of the vertical LVDTs are touching the heads of the bolts clamped to the upper section. Use the hose clamps to adjust the position of the LVDTs until their respective LVDT conditioner reads about +0.4500 for the front LVDT and -0.4500 for the rear LVDT. Make sure that the engraved 14's on the upper and lower section of the loading head are on the same side. After the vertical LVDTs are adjusted, remove the lucite specimen and return the loading head assembly to the temperature cabinet.

4.5.2 Get a specimen for testing from the appropriate controlled temperature environment (make sure that the specimen and the MTS temperature cabinet are within the specified temperature limits for testing).

4.5.3 Take the horizontal LVDT frame from the temperature cabinet and place it on top of the alignment loading strip. Place the specimen in the horizontal LVDT frame so that the diametrical axis of the specimen is perpendicular to the plane of the LVDTs. The arrow of the diametrical axis should be pointing down. Use the

thin piece of rubber to protect the unmarked face of the specimen from the pointed piece of metal in the frame.

4.5.3.1 Use an allen head screw to secure the specimen in the frame. The screw should make contact at the center point of the specimen along the marked diametrical axis. Do not allow the screw to penetrate more than 1/16 in into the face of the specimen. The pointed tip screw works well on specimens with smooth faces, and the flat tip screw works well on specimens with rough faces. It is helpful to hold the specimen and the frame with one hand while turning the screw with the other hand. Make sure that there is no gap between the frame and the alignment loading strip sides.

4.5.3.2 Use a 1/2 in wrench to adjust the horizontal LVDTs so that their respective LVDT conditioner is reading about +0.2500. Make sure that the LVDT tips are not touching any voids on the sides of the specimen.

4.5.4 Place the horizontal LVDT frame and specimen on the bottom section of the loading head inside the temperature cabinet. Move the frame and specimen by grabbing hold of the top of the specimen. Rotate the specimen sideways to clear the loading head guide posts when placing it in the cabinet. Place the upper section of the loading head making sure that the engraved 14's line up as specified in 4.5.1. Place the steel contact ball in the center of the loading head upper section. Keep the LVDT wires along the edges of the cabinet .

4.5.5 Position the specimen so that the diametrical axis marking is coincident with the upper and lower loading strips, and the mid-thickness marks on the specimen are located in the line of action of the actuator shaft. Use the peep hole on the left side of the cabinet to center the specimen on the upper and lower loading strips. Use the ruler to ensure that the horizontal LVDTs are at the same height above the base of the loading head.

4.5.6 Remove the dial gage from the hydraulic shaft. Use the setpoint knob (turn the knob clockwise for loading) on the MTS 442 controller panel to bring down the load frame loading ram. Overshoot the setpoint specified in 4.5.2 to get the ram moving, but be careful not to get the ram moving too fast, otherwise the specimen may be damaged if too large a load is applied. When the load cell on the end of the loading ram is near the steel ball on top of the loading head, adjust the setpoint to the exact value specified in 4.4.1. The steel ball should seat uniformly in both the loading head and the depression in the center of the load cell. Return the peep hole cover and the front cover of the cabinet to bring the cabinet back to the test temperature. No more than five minutes should elapse between removal of the specimen from its controlled temperature environment and application of the contact load on the specimen in the loading frame. Return the dial gage to its position on the hydraulic shaft.

4.6 Configuring data acquisition and control software. Turn on the computer, monitor and printer and wait for the DOS prompt **C:>**.

4.6.1 Enter haversine load pulse.

4.6.2 Enter preconditioning cycles.

4.7 Specimen preconditioning. Make a note of the hydraulic shaft dial gage reading. Precondition the specimen along the diametrical axis prior to testing by applying the repeated haversine-shaped load pulse of 0.1 sec with a 0.9 sec rest period for the specified number of cycles in 4.6.2. After each sequence of preconditioning cycles, view the channel plots by using the **Enter** key to go to the next plot. While inspecting the vertical and horizontal response curves, calculate the vertical and horizontal deformation ratios to ensure that the ratios are less than or equal to 1.5. Calculate the ratios as $R_v = V_{max}/V_{min}$ and $R_h = H_{max}/H_{min}$ where R_v is the vertical ratio and R_h the horizontal ratio. V_{max} is the maximum total

deformation of the two vertical LVDT curves and Vmin is the minimum total deformation of the two curves. Likewise Hmax is the maximum total deformation of the two horizontal LVDT curves and Hmin is the minimum deformation of the two curves. The deformations are measured by taking the difference in height of the peak and baseline of the largest peak on each plot. When inspecting the plots, check that successive deformation readings agree within 10 percent and that a line drawn through the peaks on each plot would be sloping upward for all plots or sloping downward for all plots. Preconditioning can be stopped when the minimum number of cycles specified in 4.4.2 and the criteria outlined above are met. If the criteria above are not met, make adjustments to the seating of the specimen in the loading head without removing the contact load. In no case should the maximum number of preconditioning cycles be exceeded. If the criteria above cannot be met within the maximum number of preconditioning cycles, remove the contact load from the specimen, enter **bye** to get back to the DOS prompt on the computer and repeat steps 4.5.5 through 4.7 above.

4.8 Specimen testing. After preconditioning the test specimen, load the resilient modulus testing program. "Resmod.run" will apply 37 load pulses to the specimen as explained in 4.7. The last 7 load pulses and the resultant measured deformations can be viewed in the channel plots after the 37 load cycles have completed. To determine when loading is completed, use a stopwatch to time the 37 load cycles (each cycle is 1 second). The criteria in 4.7 are used to accept or reject the test except that the range in deformation values of five successive horizontal deformation values must be less than 10% of the average of the five deformation values. If the criteria are not met, remove the contact load from the specimen, enter **bye** to get back to the DOS prompt on the computer and repeat steps 4.5.5 through 4.7 above. Make a note of the hydraulic shaft dial gage reading and record the

cumulative vertical deformation as specified in 4.4.2.

4.9 Print channel plots.

APPENDIX D

DETERMINATION OF ASPHALT TYPE

APPENDIX D

DETERMINATION OF ASPHALT TYPE

APPENDIX D: DETERMINATION OF ASPHALT TYPE

To determine the type (S,B,or W) of asphalt, the Heukelom Bitumen Test Data Chart (BTDC) is used (Fig. 3). The vertical axis is actually in consistency units "C". At viscosity = 1 poise, c = 0, and where penetration = 1, c = 1000. In the viscosity range, c is:

$$C = \frac{1310 \log viscosity(poise)}{4.35 + \log viscosity(poise)} \quad . \ . \ . \ . \ . \quad (84)$$

The criteria for classification as an S-type asphalt are two-fold:

$$1) \quad \Delta T = |T_{13,000\,p} - T_{R\&B}| \leq 8^{\circ}\,C \quad . \ . \ . \ . \ . \ . \quad (85)$$

$$2) \quad \Delta BTS = |BTS_{visc} - BTS_{pen/R\&B}| \leq 1.8 \quad . \ . \ . \ . \quad (86)$$

where BTS (Bitumen Temperature Susceptibility) is a measure of the temperature sensitivity of the asphalt and is calculated in the temperature range of penetration applicability as:

$BTS_{pen/R\&B} = PI_{pen/R\&B}$

and is calculated in the temperature range of viscosity applicability as:

$$BTS_{visc} = \frac{30}{0.4\,(C_1 - C_2)\,(T_2 - T_1)^{-1} + 1} - 10 \quad . \ . \ . \ . \ . \quad (87)$$

$$T_{13,000p} = T_1 + (T_2 - T_1)\left(\frac{C_{13,000} - C_1}{C_2 - C_1}\right) \quad . \ . \ . \ . \ . \quad (88)$$

$$C_{13,000} = \frac{1310 \log 13,000}{4.35 + \log 13,000} \quad . \ . \ . \ . \ . \ . \ . \quad (89)$$
$$= 636.73$$

where:

T_1 = 60°C (test temperature for absolute viscosity)

T_2 = 135°C (test temperature for kinematic viscosity)

To convert kinematic to absolute viscosity n:

$$n, poise = \frac{(kinematic\ visc., cs)(sp.\ grav,\ 25°)(0.934)}{100} \quad (90)$$

Table D-1 shows the results of the analysis.

As can be seen, both criteria are met in regard to classification as "S" type asphalts. Additionally, Heukelom defines "S" -type asphalts as those that plot in approximately a straight line on the BTDC paper. Both asphalts used in this study exhibit this type of plot.

Table D-1. Bitumen Type Classification.

Asphalt	T(°C)		Kin. Visc	Abs. Visc (p)		Sp. Grav.	$T_{R\&B}$	$PI_{pen/R\&B}$	ΔT	$\lvert\Delta BTS\rvert$
	1	2	(C_s)	1	2	(25°C)	(°C)		(o C)	
AC-10	60	135	301	1099	2.83	1.007	44.5	-0.92	2.1	0.24
AC-20	60	135	361	1911	3.43	1.017	48.5	-1.88	1.6	1.14

APPENDIX E

SPECIFIC GRAVITY AND VOIDS DATA

APPENDIX E

SPECIFIC GRAVITY AND VOIDS DATA

Puck I.D.	%Air Voids (Calc.)	%Air Voids (Rice)	VMA (Calc.)	VMA (Rice)	VFAC (Calc.)	VFAC (Rice)
BB-6C-10-3.6-1	3.7	4.0	11.9	9.8	71.9	59.0
BB-6C-10-3.6-2	2.8	3.1	11.1	9.0	78.1	65.3
BB-6C-10-4.1-1	2.4	2.7	11.8	9.7	83.0	72.2
BB-6C-10-4.1-2	2.3	2.6	11.7	9.6	83.9	73.1
BB-6C-20-3.6-1	4.2	4.1	12.3	10.2	68.9	60.1
BB-6C-20-3.6-2	3.1	3.0	11.3	9.2	75.7	67.4
BB-6C-20-4.1-1	2.5	2.4	11.8	9.7	82.1	75.6
BB-6C-20-4.1-2	2.2	2.0	11.5	9.4	84.5	78.4
BB-6F-10-4.1-1	2.9	4.2	12.5	11.1	77.2	62.2
BB-6F-10-4.1-2	3.1	4.4	12.7	11.3	75.6	60.7
BB-6F-10-4.6-1	1.7	3.0	12.5	11.1	86.6	72.8
BB-6F-10-4.6-2	2.9	4.2	13.6	12.2	78.7	65.3
BB-6F-20-4.1-1	3.9	5.1	13.4	12.0	70.8	57.1
BB-6F-20-4.1-2	3.7	4.9	13.2	11.7	72.2	58.4
BB-6F-20-4.6-1	2.3	3.5	13.0	11.5	82.3	69.5
BB-6F-20-4.6-2	1.9	3.1	12.6	11.2	85.0	72.1
BB-7C-10-3.6-1	2.6	3.7	11.0	9.6	76.2	61.6
BB-7C-10-3.6-2	2.3	3.4	10.8	9.3	78.3	63.5
BB-7C-10-4.1-1	1.1	2.2	10.7	9.3	89.8	76.7
BB-7C-10-4.1-2	1.4	2.5	11.0	9.5	87.4	74.3
BB-7C-20-3.6-1	2.4	3.2	10.7	9.3	77.9	65.5
BB-7C-20-3.6-2	1.7	2.6	10.2	8.7	82.8	70.3
BB-7C-20-4.1-1	2.2	3.0	11.6	10.2	81.4	70.6
BB-7C-20-4.1-2	1.0	1.8	10.5	9.1	90.6	79.9
BB-7F-10-4.4-1	2.6	3.3	12.8	11.7	79.7	71.5
BB-7F-10-4.4-2	2.6	3.4	12.8	11.7	79.5	71.3
BB-7F-10-4.9-1	0.8	1.6	12.2	11.2	93.2	85.8
BB-7F-10-4.9-2	1.3	2.1	12.7	11.6	89.4	82.0
BB-7F-20-4.4-1	1.6	2.3	11.8	10.8	86.1	78.5
BB-7F-20-4.4-2	2.1	2.8	12.2	11.2	82.7	75.2
BB-7F-20-4.9-1	0.3	1.0	11.7	10.6	97.3	90.7
BB-7F-20-4.9-2	1.8	2.4	13.0	11.9	86.2	79.5
BB2.5C-DR7-1	5.1	5.9	10.9	9.4	53.2	37.3
BB2.5C-DR7-2	4.8	5.6	10.6	9.2	54.7	38.5
BB3.0C-DR6-1	4.6	4.6	11.8	9.7	69.8	60.9
BB3.0C-DR6-2	4.8	4.5	11.9	9.9	69.0	60.0
BB3.0C-DR7-1	4.0	4.8	10.9	9.5	63.7	49.4
BB3.0C-DR7-2	4.5	5.3	11.4	10.0	60.6	46.7
BB3.5C-DR6-1	4.7	4.6	12.5	10.5	65.3	56.1
BB3.5C-DR6-3	3.9	3.8	11.8	9.7	69.8	60.8
BB3.5C-DR7-1	2.8	3.6	10.9	9.4	74.6	61.9
BB3.5C-DR7-2	2.9	3.7	11.0	9.6	73.6	60.9
BB3.5F-DR6-1	5.1	6.4	13.2	11.8	61.2	46.2
BB3.5F-DR6-2	4.8	6.0	12.9	11.5	62.8	47.6
BB3.5F-DR7-1	5.6	6.2	13.5	12.5	58.6	50.0
BB3.5F-DR7-2	6.6	7.2	14.4	13.4	54.3	46.0
BB4.0C-DR7-1	2.6	3.4	11.8	10.3	78.0	67.0
BB4.0C-DR7-2	2.8	3.6	12.0	10.6	76.4	65.5
BB4.0F-DR6-1	3.1	4.3	12.4	11.0	75.2	60.7
BB4.0F-DR6-2	3.0	4.2	12.4	10.9	75.7	61.2
BB4.0F-DR7-1	4.8	5.5	13.9	12.8	65.1	57.2
BB4.0F-DR7-2	4.6	5.3	13.7	12.6	66.2	58.2
BB4.5C-DR6-4	1.8	1.7	12.0	10.0	88.0	83.0
BB4.5C-DR6-5	1.5	1.4	11.8	9.7	90.2	85.5
BB4.5C-DR6-6	1.3	1.2	11.6	9.5	91.7	87.3

Puck I.D.	%Air Voids (Calc.)	%Air Voids (Rice)	VMA (Calc.)	VMA (Rice)	VFAC (Calc.)	VFAC (Rice)
BB4.5C-DR7-1	1.2	2.0	11.5	10.1	90.0	80.4
BB4.5C-DR7-2	1.5	2.3	11.8	10.4	87.5	77.9
BB4.5F-DR6-1	3.1	4.3	13.5	12.0	77.1	64.3
BB4.5F-DR6-2	1.3	2.5	11.9	10.4	89.3	75.9
BB4.5F-DR7-1	2.9	3.5	13.1	12.1	78.1	70.8
BB4.5F-DR7-2	3.3	4.0	13.5	12.5	75.4	68.1
BB4C-DR6-1	3.6	3.5	12.6	10.5	74.4	67.1
BB4C-DR6-2	2.9	2.8	11.9	9.9	78.8	71.8
BB4C-DR6-3	2.7	2.6	11.8	9.7	80.0	73.2
BB5.0C-DR7-1	0.2	1.0	11.7	10.3	98.2	89.9
BB5.0C-DR7-2	0.2	1.0	11.7	10.2	98.4	90.2
BB5.0F-DR7-1	3.5	4.2	14.7	13.7	76.1	69.6
BB5.0F-DR7-2	2.8	3.5	14.1	13.1	79.9	73.4
BB5.5C-DR6-10	0.6	0.5	13.0	11.0	98.1	95.5
BB5.5C-DR6-11	1.4	1.3	13.7	11.7	92.6	89.2
BB5.5C-DR6-12	0.5	0.4	13.0	10.9	98.7	96.1
BB5.5C-DR7-1	0.3	1.2	12.8	11.4	97.3	89.9
BB5.5F-DR6-4	0.8	2.0	13.5	12.0	94.3	83.5
BB5.5F-DR6-5	0.4	1.6	13.2	11.7	96.9	86.1
BB5.5F-DR6-6	1.0	2.2	13.7	12.2	92.9	82.1
BB5.5F-DR7-1	2.4	3.0	14.7	13.6	83.9	77.9
BB5.5F-DR7-2	2.0	2.6	14.3	13.3	86.2	80.3
BB5C-DR6-7	1.2	1.1	12.5	10.4	93.6	89.9
BB5C-DR6-8	0.9	0.8	12.2	10.2	95.8	92.4
BB5C-DR6-9	0.8	0.7	12.2	10.1	96.6	93.4
BB5F-DR6-1	1.2	2.4	12.8	11.4	90.6	78.6
BB5F-DR6-2	0.9	2.1	12.5	11.1	93.1	81.1
BB5F-DR6-3	1.4	2.7	13.0	11.6	89.0	77.1
BB6.5F-DR6-10	0.1	1.3	14.9	13.5	99.0	90.1
BB6.5F-DR6-12	0.4	1.6	15.1	13.7	97.4	88.4
BB6C-DR6-14	1.9	1.8	15.2	13.2	89.7	86.3
BB6C-DR6-15	2.3	2.2	15.5	13.5	87.3	83.6
BB6C10-3.6-1	4.0	4.3	12.2	10.1	70.1	57.1
BB6C10-3.6-2	3.3	3.6	11.5	9.4	74.8	61.9
BB6C10-3.6-3	3.3	3.6	11.5	9.4	74.7	61.8
BB6C10-3.6-4	3.4	3.7	11.6	9.6	73.8	60.8
BB6C10-4.1-1	2.7	3.0	12.1	10.0	80.6	69.6
BB6C10-4.1-2	2.1	2.4	11.5	9.5	84.9	74.2
BB6C10-4.1-3	2.2	2.5	11.6	9.5	84.3	73.5
BB6C10-4.1-4	2.1	2.5	11.6	9.5	84.5	73.8
BB6C20-3.6-1	4.4	4.3	12.5	10.4	67.5	58.7
BB6C20-3.6-2	3.8	3.7	11.9	9.9	70.9	62.3
BB6C20-3.6-3	4.0	3.9	12.1	10.1	69.6	60.9
BB6C20-3.6-4	3.8	3.7	12.0	9.9	70.8	62.2
BB6C20-4.1-1	2.1	2.0	11.4	9.4	84.8	78.8
BB6C20-4.1-2	2.4	2.3	11.7	9.7	82.4	76.0
BB6C20-4.1-3	1.9	1.8	11.3	9.2	86.4	80.5
BB6C20-4.1-4	2.5	2.4	11.8	9.8	81.7	75.2
BB6F-DR6-7	0.1	1.3	13.9	12.5	99.4	89.6
BB6F-DR6-8	0.4	1.6	14.2	12.7	97.0	87.3
BB6F-DR6-9	0.3	1.5	14.1	12.7	97.6	87.8
BB6F10-4.1-1	3.0	4.3	12.6	11.2	76.4	61.5
BB6F10-4.1-2	3.3	4.7	12.9	11.5	74.3	59.5
BB6F10-4.1-3	2.5	3.8	12.2	10.7	79.8	64.5
BB6F10-4.1-4	2.1	3.5	11.9	10.4	82.1	66.6
BB6F10-4.6-1	1.2	2.6	12.1	10.7	89.9	76.0

Puck I.D.	%Air Voids (Calc.)	%Air Voids (Rice)	VMA (Calc.)	VMA (Rice)	VFAC (Calc.)	VFAC (Rice)
BB6F10-4.6-2	1.7	3.0	12.5	11.1	86.6	72.8
BB6F10-4.6-3	1.5	2.8	12.4	10.9	87.9	74.0
BB6F10-4.6-4	1.6	2.9	12.5	11.0	87.1	73.3
BB6F20-4.1-1	3.6	4.9	13.2	11.7	72.8	58.2
BB6F20-4.1-2	3.1	4.4	12.7	11.3	75.6	60.7
BB6F20-4.1-3	3.6	4.9	13.2	11.7	72.9	58.2
BB6F20-4.1-4	3.8	5.1	13.4	11.9	71.6	57.1
BB6F20-4.6-1	1.3	2.6	12.1	10.7	89.7	75.6
BB6F20-4.6-2	2.5	3.8	13.2	11.8	81.4	67.8
BB6F20-4.6-3	1.9	3.2	12.7	11.3	85.2	71.3
BB6F20-4.6-4	0.9	2.3	11.9	10.4	92.2	78.0
BB7C10-3.6-1	3.1	4.2	11.5	10.0	72.9	58.5
BB7C10-3.6-2	3.9	5.0	12.2	10.8	67.9	54.0
BB7C10-3.6-3	3.1	4.1	11.4	10.0	73.3	58.9
BB7C10-3.6-4	3.1	4.1	11.4	10.0	73.3	58.9
BB7C10-4.1-1	1.5	2.5	11.0	9.6	86.8	73.7
BB7C10-4.1-2	2.0	3.0	11.5	10.1	82.8	69.8
BB7C10-4.1-3	1.6	2.6	11.1	9.7	85.8	72.8
BB7C10-4.1-4	1.6	2.7	11.2	9.7	85.7	72.6
BB7C20-3.6-1	3.8	4.6	12.1	10.6	68.3	56.4
BB7C20-3.6-2	3.6	4.5	11.9	10.5	69.4	57.4
BB7C20-3.6-3	3.1	3.9	11.4	9.9	73.0	60.7
BB7C20-3.6-4	3.9	4.8	12.2	10.7	67.6	55.7
BB7C20-4.1-1	2.8	3.6	12.2	10.8	76.8	66.1
BB7C20-4.1-2	1.9	2.7	11.3	9.9	83.5	72.7
BB7C20-4.1-3	1.8	2.6	11.2	9.8	84.2	73.5
BB7C20-4.1-4	1.9	2.8	11.4	10.0	83.0	72.3
BB7F-DR6-13	0.7	1.9	16.3	15.0	95.7	87.4
BB7F-DR6-14	1.1	2.2	16.7	15.3	93.5	85.3
BB7F10-4.4-1	3.3	4.0	12.7	11.7	74.2	65.6
BB7F10-4.4-2	3.3	4.0	12.8	11.7	74.2	65.5
BB7F10-4.4-3	2.7	3.5	12.2	11.2	77.8	69.1
BB7F10-4.4-4	3.4	4.1	12.8	11.8	73.7	65.1
BB7F10-4.9-1	1.8	2.6	12.5	11.5	85.2	77.4
BB7F10-4.9-2	2.6	3.4	13.2	12.2	80.1	72.3
BB7F10-4.9-3	1.7	2.5	12.4	11.3	86.1	78.2
BB7F10-4.9-4	1.6	2.4	12.3	11.3	86.8	78.9
BB7F20-4.4-1	5.2	5.8	14.4	13.4	63.9	56.3
BB7F20-4.4-2	5.2	5.9	14.4	13.4	63.8	56.2
BB7F20-4.4-3	3.6	4.2	12.9	11.9	72.5	64.5
BB7F20-4.4-4	4.6	5.3	13.9	12.8	66.8	59.0
BB7F20-4.9-1	3.0	3.6	13.4	12.4	77.9	70.7
BB7F20-4.9-2	2.8	3.5	13.3	12.3	78.6	71.5
BB7F20-4.9-3	2.7	3.4	13.2	12.1	79.4	72.3
BB7F20-4.9-4	3.5	4.1	13.9	12.8	74.9	67.8
C-4C-10-3.75-1	6.0	5.9	14.5	13.5	58.6	56.1
C-4C-10-3.75-2	5.8	5.7	14.4	13.3	59.3	56.9
C-4C-10-4.25-1	4.6	4.5	14.2	13.2	67.9	66.1
C-4C-10-4.25-2	4.7	4.6	14.3	13.3	67.3	65.5
C-4C-20-3.75-1	6.2	6.1	14.6	13.6	57.6	55.1
C-4C-20-3.75-2	6.0	5.9	14.5	13.4	58.2	55.8
C-4C-20-4.25-1	4.1	4.0	13.7	12.6	70.3	68.8
C-4C-20-4.25-2	4.1	4.0	13.7	12.7	70.3	68.7
C-4F-10-3.75-1	3.1	3.3	11.8	10.6	73.9	68.9
C-4F-10-3.75-2	3.2	3.4	11.9	10.8	73.0	68.0
C-4F-10-4.25-1	2.1	2.3	11.9	10.8	82.7	78.8

Puck I.D.	%Air Voids (Calc.)	%Air Voids (Rice)	VMA (Calc.)	VMA (Rice)	VFAC (Calc.)	VFAC (Rice)
C-4F-10-4.25-2	2.0	2.2	11.9	10.7	83.2	79.3
C-4F-20-3.75-1	2.6	2.7	11.3	10.2	76.7	73.9
C-4F-20-3.75-2	2.5	2.5	11.2	10.0	78.1	75.4
C-4F-20-4.25-1	1.5	1.6	11.4	10.2	86.4	84.8
C-4F-20-4.25-2	1.5	1.5	11.4	10.2	86.6	85.0
C-5C-10-3.75-1	4.7	4.7	13.2	11.7	64.4	60.2
C-5C-10-3.75-2	5.0	4.9	13.5	12.0	63.1	58.8
C-5C-10-4.25-1	3.9	3.9	13.5	12.1	71.0	67.8
C-5C-10-4.25-2	3.8	3.8	13.4	12.0	71.6	68.4
C-5C-20-3.75-1	5.5	5.4	13.8	12.4	60.5	56.5
C-5C-20-3.75-2	5.5	5.4	13.9	12.4	60.4	56.3
C-5C-20-4.25-1	4.2	4.1	13.7	12.2	69.3	66.2
C-5C-20-4.25-2	4.2	4.1	13.7	12.2	69.4	66.4
C-5F-10-4.0-1	2.6	2.4	11.9	10.7	78.2	77.3
C-5F-10-4.0-2	3.2	3.1	12.4	11.3	74.0	72.7
C-5F-10-4.5-1	1.8	1.7	12.2	11.1	85.0	84.8
C-5F-10-4.5-2	2.0	1.8	12.3	11.2	84.2	83.9
C-5F-20-4.0-1	3.1	2.8	12.2	11.0	74.8	74.4
C-5F-20-4.0-2	2.9	2.7	12.1	10.9	75.8	75.5
C-5F-20-4.5-1	2.0	1.7	12.2	11.1	84.0	84.6
C-5F-20-4.5-2	2.2	2.0	12.5	11.3	82.2	82.6
C2.5F-DR5-1	9.0	8.8	14.6	13.4	38.2	34.7
C2.5F-DR5-2	8.2	8.0	13.8	12.7	40.6	37.1
C3.0F-DR4-1	5.2	5.2	12.1	10.9	57.1	52.4
C3.0F-DR4-2	5.5	5.5	12.3	11.2	55.8	51.1
C3.0F-DR5-1	7.0	6.8	13.8	12.6	48.9	46.2
C3.5F-DR4-1	4.2	4.2	12.2	11.1	65.7	61.9
C3.5F-DR4-2	3.8	3.8	11.9	10.7	67.9	64.3
C3.5F-DR5-1	3.7	3.4	11.7	10.6	68.6	67.4
C3.5F-DR5-2	4.9	4.7	12.8	11.7	61.9	60.2
C3.6C-DR5-1	5.9	5.8	13.9	12.4	57.7	53.4
C3.6C-DR5-2	5.5	5.4	13.6	12.1	59.5	55.3
C4.0C-DR5-1	3.1	3.0	12.2	10.6	74.9	72.1
C4.0C-DR5-2	4.6	4.5	13.6	12.1	66.1	62.7
C4.0F-DR4-1	2.6	2.6	11.8	10.6	78.0	75.5
C4.0F-DR4-1	2.8	2.8	12.0	10.8	76.6	73.9
C4.0F-DR4-2	2.3	2.3	11.5	10.3	80.4	78.1
C4.0F-DR5-1	2.8	2.5	11.9	10.8	76.9	76.7
C4.0F-DR5-2	3.9	3.6	12.9	11.8	70.1	69.2
C4.5C-DR5-1	2.0	1.9	12.2	10.7	83.6	82.1
C4.5C-DR5-2	2.4	2.4	12.6	11.1	80.6	78.8
C4.5F-DR4-1	1.8	1.8	12.2	11.0	85.0	83.4
C4.5F-DR4-2	1.6	1.6	12.0	10.8	86.4	84.8
C4.5F-DR4-3	1.5	1.5	11.8	10.7	87.7	86.2
C4.5F-DR5-1	2.3	2.1	12.6	11.4	81.5	81.8
C4.5F-DR5-2	2.3	2.1	12.6	11.4	81.4	81.6
C4C10-3.75-1	5.1	5.0	13.6	12.6	63.0	60.6
C4C10-3.75-2	5.2	5.1	13.8	12.8	62.1	59.7
C4C10-3.75-3	5.2	5.1	13.8	12.8	62.1	59.7
C4C10-3.75-4	5.3	5.3	13.9	12.9	61.5	59.1
C4C10-4.25-1	3.8	3.7	13.5	12.5	72.0	70.4
C4C10-4.25-2	3.9	3.8	13.6	12.6	71.4	69.8
C4C10-4.25-3	3.8	3.7	13.5	12.5	72.1	70.5
C4C10-4.25-4	3.8	3.7	13.6	12.5	71.8	70.2
C4C20-3.75-1	4.1	3.9	12.7	11.6	67.7	66.5
C4C20-3.75-2	4.6	4.4	13.2	12.1	65.0	63.6

Puck I.D.	%Air Voids (Calc.)	%Air Voids (Rice)	VMA (Calc.)	VMA (Rice)	VFAC (Calc.)	VFAC (Rice)
C4C20-3.75-3	4.2	4.0	12.8	11.7	67.1	65.9
C4C20-3.75-4	4.5	4.3	13.0	12.0	65.7	64.4
C4C20-4.25-1	3.3	3.1	13.0	11.9	74.9	74.4
C4C20-4.25-2	3.3	3.1	13.0	12.0	74.5	74.0
C4C20-4.25-3	3.4	3.2	13.1	12.0	74.3	73.7
C4C20-4.25-4	3.2	3.0	12.9	11.9	75.1	74.6
C4F10-3.75-1	2.6	2.8	11.4	10.2	77.2	72.4
C4F10-3.75-2	2.5	2.7	11.3	10.1	77.8	73.0
C4F10-3.75-3	2.6	2.9	11.4	10.2	76.8	72.0
C4F10-3.75-4	2.1	2.4	11.0	9.8	80.5	75.9
C4F10-4.25-1	1.8	2.0	11.7	10.5	84.7	80.9
C4F10-4.25-2	1.7	1.9	11.6	10.4	85.6	81.9
C4F10-4.25-3	1.8	2.0	11.7	10.5	84.8	81.0
C4F10-4.25-4	1.8	2.0	11.7	10.5	84.7	80.9
C4F20-3.75-1	3.1	3.2	11.8	10.6	73.6	69.8
C4F20-3.75-2	3.1	3.2	11.7	10.6	73.8	69.9
C4F20-3.75-3	2.7	2.8	11.4	10.2	76.3	72.6
C4F20-3.75-4	2.6	2.7	11.3	10.1	76.8	73.1
C4F20-4.25-1	1.5	1.6	11.4	10.2	86.4	83.9
C4F20-4.25-2	1.6	1.7	11.4	10.3	86.1	83.5
C4F20-4.25-3	1.1	1.2	11.0	9.8	90.1	87.9
C4F20-4.25-4	1.3	1.4	11.2	10.0	88.3	85.9
C5.0C-DR5-1	1.6	1.6	12.9	11.4	87.3	86.4
C5.0C-DR5-2	1.7	1.6	13.0	11.5	86.7	85.7
C5.0F-DR4-4	0.9	0.9	12.4	11.2	92.6	91.7
C5.0F-DR4-5	0.7	0.7	12.2	11.0	94.1	93.4
C5.0F-DR4-6	1.0	1.0	12.5	11.3	91.8	90.9
C5.0F-DR5-1	1.7	1.5	13.1	11.9	86.6	87.4
C5.1F-DR4-1	1.4	1.4	13.0	11.8	89.4	88.3
C5.1F-DR4-2	1.2	1.2	12.8	11.6	91.0	90.0
C5.5C-DR5-1	1.5	1.4	13.8	12.3	88.9	88.3
C5.5F-DR4-7	0.4	0.4	12.9	11.7	97.2	96.8
C5.5F-DR4-8	0.6	0.6	13.1	12.0	95.2	94.7
C5.5F-DR4-9	0.6	0.6	13.1	12.0	95.2	94.6
C5.5F-DR5-1	1.2	0.9	13.5	12.4	91.5	92.7
C5C10-3.75-1	5.2	5.2	13.7	12.2	61.9	57.6
C5C10-3.75-2	4.7	4.7	13.2	11.7	64.4	60.2
C5C10-3.75-3	5.5	5.5	14.0	12.5	60.4	56.0
C5C10-3.75-4	5.6	5.6	14.1	12.6	60.0	55.6
C5C10-4.25-1	3.4	3.3	13.0	11.5	74.1	71.1
C5C10-4.25-2	3.1	3.1	12.8	11.3	75.6	72.8
C5C10-4.25-3	3.7	3.7	13.4	11.9	72.2	69.0
C5C10-4.25-4	3.2	3.1	12.9	11.4	75.3	72.4
C5C20-3.75-1	2.6	2.5	11.2	9.7	76.8	74.6
C5C20-3.75-2	2.9	2.7	11.5	9.9	75.0	72.6
C5C20-3.75-3	3.1	3.0	11.7	10.2	73.4	70.9
C5C20-3.75-4	2.9	2.7	11.5	10.0	75.0	72.6
C5C20-4.25-1	3.9	3.8	13.5	12.0	70.8	68.4
C5C20-4.25-2	4.5	4.3	14.0	12.5	67.9	65.2
C5C20-4.25-3	4.2	4.1	13.7	12.2	69.2	66.6
C5C20-4.25-4	4.0	3.9	13.5	12.0	70.4	67.9
C5F10-4.00-1	2.9	2.7	12.1	11.0	76.2	75.1
C5F10-4.00-2	2.9	2.7	12.1	11.0	76.2	75.1
C5F10-4.00-3	2.8	2.7	12.1	10.9	76.6	75.5
C5F10-4.00-4	2.8	2.7	12.1	10.9	76.7	75.6
C5F10-4.50-1	2.3	2.1	12.6	11.4	82.1	81.7

Puck I.D.	%Air Voids (Calc.)	%Air Voids (Rice)	VMA (Calc.)	VMA (Rice)	VFAC (Calc.)	VFAC (Rice)
C5F10-4.50-2	2.0	1.9	12.4	11.2	83.8	83.5
C5F10-4.50-3	2.1	2.0	12.5	11.3	83.0	82.6
C5F10-4.50-4	2.1	1.9	12.5	11.3	83.2	82.9
C5F20-4.00-1	3.4	3.2	12.6	11.4	72.6	71.9
C5F20-4.00-2	3.3	3.0	12.4	11.3	73.5	72.9
C5F20-4.00-3	3.6	3.3	12.7	11.5	71.8	71.1
C5F20-4.00-4	3.4	3.1	12.5	11.3	72.9	72.3
C5F20-4.50-1	5.1	4.8	15.0	13.9	66.3	65.3
C5F20-4.50-2	4.9	4.7	14.9	13.8	67.0	66.0
C5F20-4.50-3	5.1	4.9	15.1	13.9	66.0	65.0
C5F20-4.50-4	5.0	4.7	14.9	13.8	66.7	65.7
C6.0F-DR4-10	0.4	0.4	13.9	12.7	97.3	96.9
C6.0F-DR4-11	0.4	0.4	13.9	12.8	97.2	96.8
C6.0F-DR4-12	0.4	0.4	13.9	12.8	97.0	96.6
C6.5F-DR4-14	0.6	0.6	15.1	13.9	95.9	95.5
C6.5F-DR4-15	1.4	1.4	15.7	14.6	91.1	90.4
CC3.5DR4-1	5.4	5.3	13.4	12.4	59.3	56.8
CC3.5DR4-2	6.0	5.8	13.9	12.8	57.1	54.4
CC3.5DR4-3	6.3	6.2	14.2	13.2	55.5	52.8
CC3DR4-1	7.5	7.4	14.3	13.3	47.2	43.9
CC3DR4-2	6.0	5.9	12.8	11.8	53.5	50.3
CC3DR4-3	7.8	7.7	14.6	13.5	46.2	42.9
CC4.7DR4-1	3.3	3.2	13.9	12.9	76.2	75.1
CC4.7DR4-2	3.0	2.9	13.6	12.6	78.1	77.1
CC4.7DR4-3	3.0	2.9	13.6	12.6	78.1	77.2
CC4DR4-1	6.1	6.0	15.0	14.0	59.5	57.3
CC4DR4-2	4.0	3.9	13.1	12.1	69.5	67.8
CC4DR4-3	4.6	4.4	13.6	12.6	66.6	64.7
CC5.1DR4-1	1.9	1.8	13.5	12.5	85.8	85.5
CC5.1DR4-2	2.1	2.0	13.6	12.6	84.7	84.3
CC5.1DR4-3	1.7	1.6	13.3	12.3	87.0	86.8
CC5.8DR4-1	1.2	1.1	14.3	13.2	91.5	91.7
CC5.8DR4-2	1.0	0.9	14.0	13.0	93.2	93.5
IC-4C-10-4.2-1	4.4	4.5	14.0	12.7	68.6	64.9
IC-4C-10-4.2-2	4.8	4.8	14.3	13.0	66.6	62.8
IC-4C-10-4.7-1	3.4	3.4	14.1	12.8	76.1	73.1
IC-4C-10-4.7-2	3.9	3.9	14.5	13.2	73.4	70.3
IC-4C-20-4.2-1	5.8	5.7	15.1	13.9	61.8	59.0
IC-4C-20-4.2-2	5.9	5.8	15.3	14.0	61.2	58.3
IC-4C-20-4.7-1	4.1	4.1	14.7	13.4	71.8	69.7
IC-4C-20-4.7-2	4.6	4.5	15.1	13.8	69.4	67.2
IC-4F-10-4.2-1	3.1	3.3	12.8	11.6	75.5	71.8
IC-4F-10-4.2-2	3.4	3.5	13.0	11.9	74.0	70.3
IC-4F-10-4.7-1	1.7	1.9	12.6	11.4	86.1	83.5
IC-4F-10-4.7-2	1.4	1.6	12.3	11.1	88.3	85.8
IC-4F-20-4.2-1	3.3	3.6	12.9	11.7	74.5	69.4
IC-4F-20-4.2-2	3.1	3.4	12.7	11.5	75.3	70.3
IC-4F-20-4.7-1	2.1	2.4	12.8	11.6	83.6	79.4
IC-4F-20-4.7-2	2.0	2.3	12.7	11.5	84.5	80.4
IC-5C-10-4.8-1	2.9	3.0	13.7	12.2	79.0	75.8
IC-5C-20-4.8-1	3.1	3.0	13.8	12.3	77.5	75.2
IC-5F-10-4.2-1	3.1	3.0	12.7	11.2	75.8	73.4
IC-5F-10-4.2-2	3.2	3.1	12.8	11.3	75.1	72.6
IC-5F-10-4.7-1	2.0	1.9	12.7	11.2	84.7	83.4
IC-5F-10-4.7-2	2.2	2.1	12.9	11.4	83.1	81.7
IC-5F-20-4.2-1	4.1	3.8	13.5	12.0	69.8	68.3

Puck I.D.	%Air Voids (Calc.)	%Air Voids (Rice)	VMA (Calc.)	VMA (Rice)	VFAC (Calc.)	VFAC (Rice)
IC-5F-20-4.2-2	4.4	4.1	13.8	12.3	68.2	66.6
IC-5F-20-4.7-1	2.4	2.2	13.1	11.6	81.3	81.2
IC-5F-20-4.7-2	2.0	1.7	12.7	11.2	84.2	84.5
IC3.2F-DR4-1	5.9	6.2	13.2	12.0	55.2	48.4
IC3.2F-DR4-2	6.6	6.9	13.8	12.6	52.2	45.5
IC3.5C-DR4-1	5.8	5.7	13.7	12.4	57.8	54.0
IC3.5C-DR4-2	7.1	7.0	14.9	13.6	52.5	48.7
IC3.5C-DR5-1	6.1	6.0	13.9	12.3	56.3	51.4
IC3.5C-DR5-2	6.6	6.6	14.4	12.9	53.9	49.0
IC3.5F-DR5-1	4.8	4.6	12.8	11.3	62.2	59.6
IC3.5F-DR5-2	5.7	5.4	13.5	12.1	58.1	55.2
IC3.6F-DR4-1	4.6	4.9	12.8	11.6	64.3	58.1
IC3.6F-DR4-2	4.5	4.8	12.8	11.6	64.4	58.3
IC4.0C-DR4-1	4.1	4.0	13.2	11.9	69.1	66.5
IC4.0C-DR4-2	4.9	4.8	14.0	12.7	64.7	61.8
IC4.0C-DR5-1	4.9	4.8	13.8	12.3	64.6	60.7
IC4.0C-DR5-2	5.2	5.2	14.1	12.6	62.9	59.0
IC4.0F-DR4-1	3.3	3.6	12.5	11.3	73.3	67.9
IC4.0F-DR4-2	3.3	3.6	12.5	11.3	73.3	68.0
IC4.0F-DR5-1	3.6	3.4	12.7	11.2	71.4	70.0
IC4.0F-DR5-2	4.5	4.2	13.5	12.0	66.6	64.7
IC4.5C-DR4-1	3.0	2.9	13.3	12.0	77.2	75.4
IC4.5C-DR4-2	4.7	4.6	14.8	13.5	68.1	65.7
IC4.5C-DR5-1	3.6	3.5	13.6	12.1	73.8	71.0
IC4.5C-DR5-2	3.5	3.4	13.5	12.0	74.4	71.7
IC4.5F-DR4-1	2.0	2.3	12.4	11.2	83.6	79.2
IC4.5F-DR4-2	2.0	2.3	12.4	11.2	83.5	79.1
IC4.5F-DR5-1	2.8	2.6	13.0	11.5	78.2	77.7
IC4.5F-DR5-2	3.8	3.5	13.9	12.4	72.7	71.6
IC4C10-4.2-1	5.4	5.4	14.9	13.6	63.8	59.9
IC4C10-4.2-2	5.0	5.1	14.5	13.2	65.6	61.8
IC4C10-4.2-3	4.7	4.8	14.3	13.0	67.0	63.2
IC4C10-4.2-4	4.9	5.0	14.5	13.2	65.9	62.1
IC4C10-4.7-1	4.3	4.4	14.9	13.6	71.2	68.1
IC4C10-4.7-2	3.6	3.7	14.3	13.0	74.7	71.7
IC4C10-4.7-3	4.3	4.4	15.0	13.7	70.9	67.7
IC4C10-4.7-4	3.4	3.5	14.1	12.8	75.9	73.0
IC4C20-4.2-1	9.5	9.4	18.5	17.3	48.6	45.4
IC4C20-4.2-2	4.4	4.4	13.9	12.6	68.1	65.6
IC4C20-4.2-3	5.5	5.5	14.9	13.6	62.9	60.0
IC4C20-4.2-4	6.3	6.2	15.6	14.3	59.7	56.8
IC4C20-4.7-1	4.6	4.6	15.1	13.8	69.3	67.1
IC4C20-4.7-2	4.3	4.2	14.8	13.6	70.9	68.7
IC4C20-4.7-3	4.4	4.3	14.9	13.6	70.6	68.4
IC4C20-4.7-4	5.3	5.2	15.7	14.4	66.5	64.1
IC4F10-4.2-1	1.6	1.7	11.4	10.2	86.0	83.0
IC4F10-4.2-2	1.5	1.7	11.4	10.1	86.6	83.7
IC4F10-4.2-3	1.6	1.7	11.4	10.2	86.3	83.3
IC4F10-4.2-4	1.7	1.9	11.6	10.3	85.0	81.9
IC4F10-4.7-1	0.7	0.9	11.7	10.5	93.6	91.6
IC4F10-4.7-2	0.8	0.9	11.7	10.5	93.4	91.3
IC4F10-4.7-3	0.8	0.9	11.8	10.6	93.2	91.1
IC4F10-4.7-4	0.7	0.8	11.7	10.5	94.0	92.0
IC4F20-4.2-1	3.1	3.4	12.7	11.5	75.4	70.4
IC4F20-4.2-2	2.6	2.9	12.3	11.1	78.7	73.8
IC4F20-4.2-3	2.3	2.6	12.0	10.8	80.6	75.7

Puck I.D.	%Air Voids (Calc.)	%Air Voids (Rice)	VMA (Calc.)	VMA (Rice)	VFAC (Calc.)	VFAC (Rice)
IC4F20-4.2-4	2.4	2.6	12.0	10.8	80.4	75.5
IC4F20-4.7-1	1.9	2.2	12.7	11.5	84.9	80.8
IC4F20-4.7-2	1.8	2.1	12.6	11.4	85.5	81.5
IC4F20-4.7-3	1.5	1.8	12.3	11.1	88.0	84.1
IC4F20-4.7-4	1.8	2.1	12.6	11.4	85.7	81.6
IC5.0C-DR4-1	2.4	2.3	13.7	12.4	82.5	81.4
IC5.0C-DR4-2	3.1	3.0	14.3	13.0	78.6	77.1
IC5.0C-DR5-1	2.3	2.2	13.5	11.9	83.1	81.5
IC5.0C-DR5-2	2.1	2.0	13.3	11.7	84.5	83.0
IC5.0F-DR4-1	1.0	1.3	12.5	11.3	91.9	88.5
IC5.0F-DR4-2	1.0	1.3	12.5	11.2	92.1	88.7
IC5.0F-DR5-1	2.0	1.8	13.3	11.8	84.7	85.0
IC5.0F-DR5-2	2.1	1.8	13.4	11.9	84.2	84.5
IC5.5C-DR5-1	2.9	2.8	15.0	13.5	80.7	79.0
IC5.5C-DR5-2	1.2	1.2	13.6	12.0	90.9	90.3
IC5.5F-DR4-1	0.7	1.0	13.2	12.0	94.7	91.8
IC5.5F-DR4-2	0.8	1.1	13.3	12.1	94.0	91.1
IC5.5F-DR5-1	1.1	0.9	13.5	12.0	91.7	92.9
IC5.5F-DR5-2	1.0	0.7	13.4	11.9	92.5	93.9
IC5C10-4.3-1	3.1	3.2	12.9	11.4	75.7	71.8
IC5C10-4.3-2	2.8	2.9	12.7	11.1	77.6	73.9
IC5C10-4.3-3	2.8	2.9	12.6	11.1	77.7	74.0
IC5C10-4.3-4	2.9	2.9	12.7	11.1	77.3	73.6
IC5C10-4.8-1	2.1	2.2	13.1	11.5	83.6	80.8
IC5C10-4.8-2	2.0	2.0	12.9	11.3	84.8	82.2
IC5C10-4.8-3	2.2	2.3	13.1	11.5	83.3	80.5
IC5C10-4.8-4	2.1	2.2	13.1	11.5	83.6	80.8
IC5C20-4.3-1	3.2	3.1	12.9	11.4	75.1	72.3
IC5C20-4.3-2	3.7	3.7	13.4	11.8	72.1	69.1
IC5C20-4.3-3	2.7	2.6	12.5	10.9	78.3	75.8
IC5C20-4.3-4	2.5	2.5	12.3	10.7	79.4	77.0
IC5C20-4.8-1	2.7	2.6	13.4	11.9	80.2	78.2
IC5C20-4.8-2	1.8	1.8	12.7	11.1	85.6	84.2
IC5C20-4.8-3	2.6	2.5	13.4	11.8	80.5	78.5
IC5C20-4.8-4	2.2	2.2	13.1	11.5	82.8	81.1
IC5F10-4.2-1	3.5	3.4	13.1	11.6	73.4	70.7
IC5F10-4.2-2	3.3	3.2	12.9	11.4	74.7	72.1
IC5F10-4.2-3	3.3	3.3	13.0	11.5	74.1	71.5
IC5F10-4.2-4	3.1	3.0	12.7	11.2	75.9	73.5
IC5F10-4.7-1	1.6	1.5	12.4	10.9	86.9	85.9
IC5F10-4.7-2	1.4	1.4	12.3	10.8	88.2	87.4
IC5F10-4.7-3	1.5	1.4	12.4	10.8	87.6	86.7
IC5F10-4.7-4	1.8	1.7	12.6	11.1	85.6	84.4
IC5F20-4.2-1	4.0	3.7	13.4	12.0	70.3	68.9
IC5F20-4.2-2	4.2	3.9	13.6	12.1	69.2	67.7
IC5F20-4.2-3	3.4	3.2	12.9	11.4	73.5	72.4
IC5F20-4.2-4	2.6	2.4	12.2	10.7	78.4	77.9
IC5F20-4.7-1	1.9	1.7	12.6	11.1	84.7	85.1
IC5F20-4.7-2	1.8	1.5	12.5	11.0	85.9	86.4
IC5F20-4.7-3	1.8	1.5	12.5	11.0	85.8	86.4
IC5F20-4.7-4	1.7	1.5	12.4	10.9	86.1	86.6
IC6.0F-DR5-1	1.1	0.8	14.4	13.0	92.5	93.7
IC6.0F-DR5-2	1.0	0.8	14.4	12.9	92.8	94.0

APPENDIX F

RESULTS OF MARSHALL MIX DESIGNS

APPENDIX F

RESULTS OF MARSHALL MIX DESIGNS

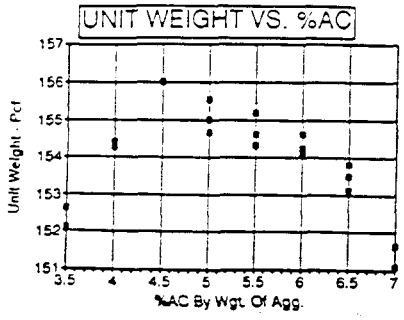
UNIT WEIGHT VS. %AC
Unit Weight - Pcf
157
156
155
154
153
152
151
3.5 4 4.5 5 5.5 6 6.5 7
%AC By Wgt. Of Agg.

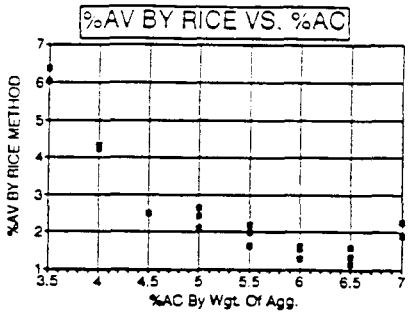
%AV BY RICE VS. %AC
%AV BY RICE METHOD
7
6
5
4
3
2
1
3.5 4 4.5 5 5.5 6 6.5 7
%AC By Wgt. Of Agg.

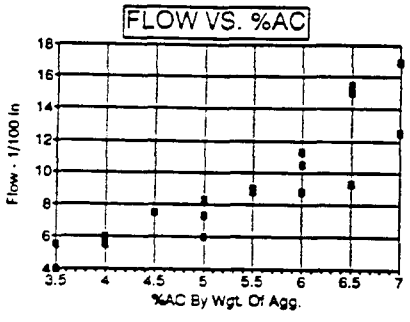
FLOW VS. %AC
Flow - 1/100 in
18
16
14
12
10
8
6
4
3.5 4 4.5 5 5.5 6 6.5 7
%AC By Wgt. Of Agg.

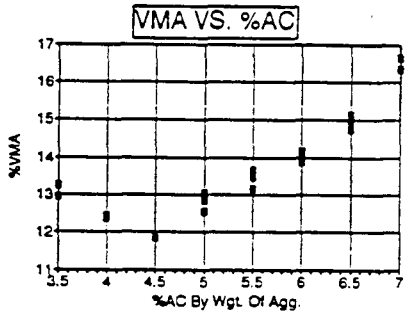
VMA VS. %AC
%VMA
17
16
15
14
13
12
11
3.5 4 4.5 5 5.5 6 6.5 7
%AC By Wgt. Of Agg.

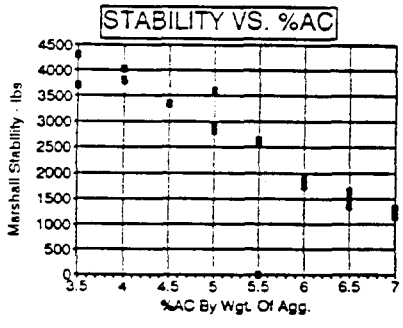
STABILITY VS. %AC
Marshall Stability - lbs
4500
4000
3500
3000
2500
2000
1500
1000
500
0
3.5 4 4.5 5 5.5 6 6.5 7
%AC By Wgt. Of Agg.

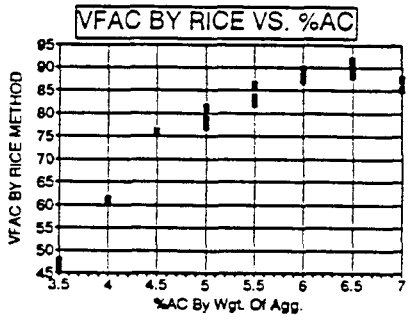
VFAC BY RICE VS. %AC
VFAC BY RICE METHOD
95
90
85
80
75
70
65
60
55
50
45
3.5 4 4.5 5 5.5 6 6.5 7
%AC By Wgt. Of Agg.

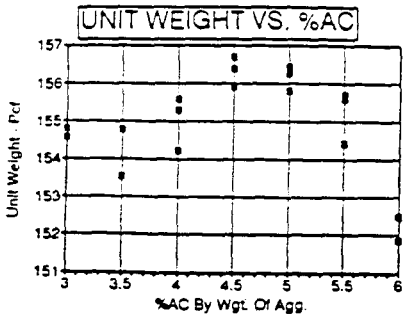
UNIT WEIGHT VS. %AC
Unit Weight - Pcf
157
156
155
154
153
152
151
3
3.5
4
4.5
5
5.5
6
%AC By Wgt. Of Agg.

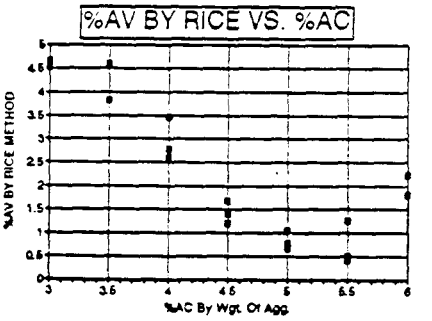
%AV BY RICE VS. %AC
%AV BY RICE METHOD
%AC By Wgt. Of Agg.

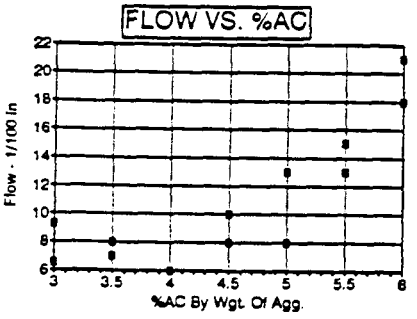
FLOW VS. %AC
Flow - 1/100 in
22
20
18
16
14
12
10
8
6
3
3.5
4
4.5
5
5.5
6
%AC By Wgt. Of Agg.

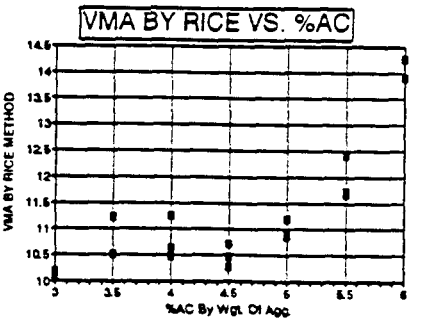
VMA BY RICE VS. %AC
VMA BY RICE METHOD
%AC By Wgt. Of Agg.

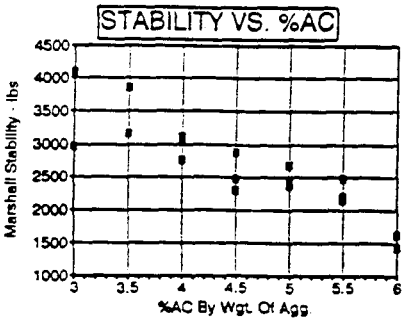
STABILITY VS. %AC
Marshall Stability - lbs
4500
4000
3500
3000
2500
2000
1500
1000
3
3.5
4
4.5
5
5.5
6
%AC By Wgt. Of Agg.

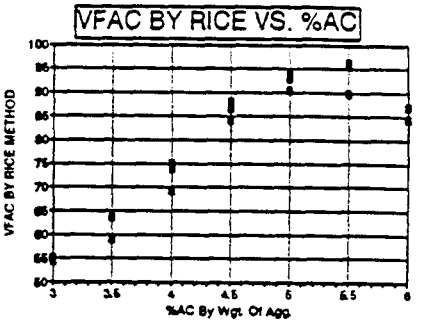
VFAC BY RICE VS. %AC
VFAC BY RICE METHOD
%AC By Wgt. Of Agg.

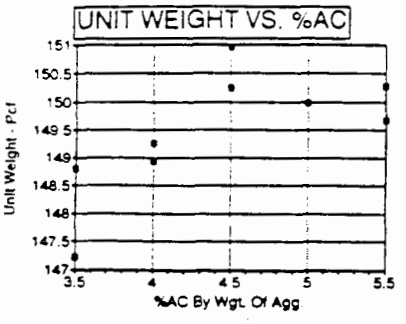
UNIT WEIGHT VS. %AC
Unit Weight - Pcf
151
150.5
150
149.5
149
148.5
148
147.5
147
3.5
4
4.5
5
5.5
%AC By Wgt. Of Agg

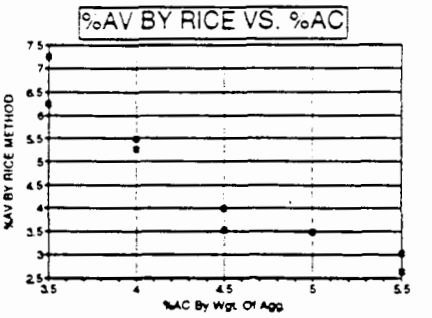
%AV BY RICE VS. %AC
%AV BY RICE METHOD
7.5
7
6.5
6
5.5
5
4.5
4
3.5
3
2.5
3.5
4
4.5
5
5.5
%AC By Wgt. Of Agg

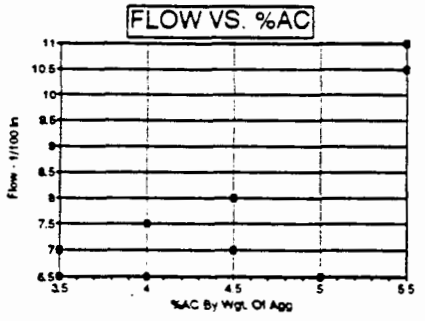
FLOW VS. %AC
Flow - 1/100 In
11
10.5
10
9.5
9
8.5
8
7.5
7
6.5
3.5
4
4.5
5
5.5
%AC By Wgt. Of Agg

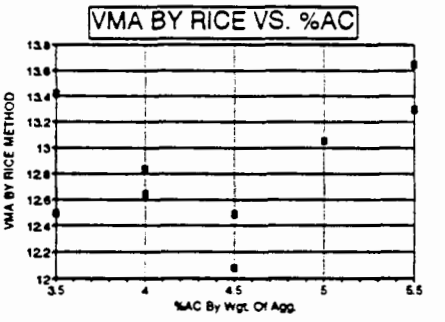
VMA BY RICE VS. %AC
VMA BY RICE METHOD
13.8
13.6
13.4
13.2
13
12.8
12.6
12.4
12.2
12
3.5
4
4.5
5
5.5
%AC By Wgt. Of Agg

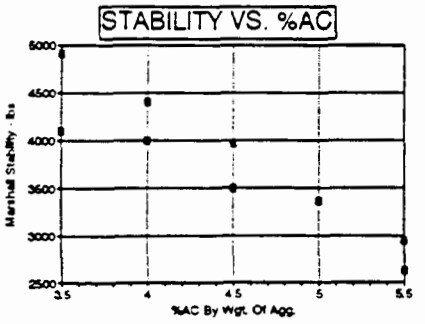
STABILITY VS. %AC
Marshall Stability - lbs
5000
4500
4000
3500
3000
2500
3.5
4
4.5
5
5.5
%AC By Wgt. Of Agg

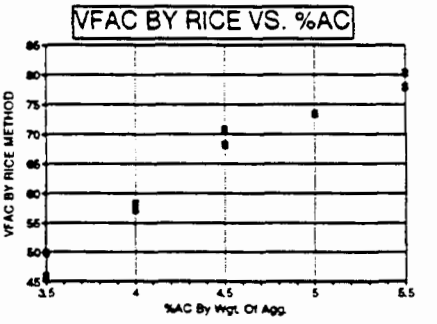
VFAC BY RICE VS. %AC
VFAC BY RICE METHOD
85
80
75
70
65
60
55
50
45
3.5
4
4.5
5
5.5
%AC By Wgt. Of Agg

UNIT WEIGHT VS. %AC

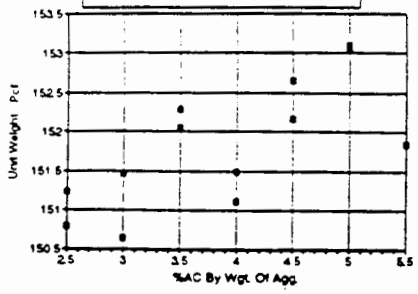

%AV BY RICE VS. %AC

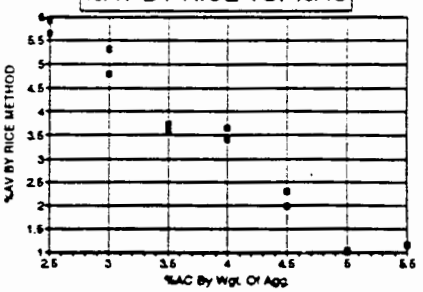

FLOW VS. %AC

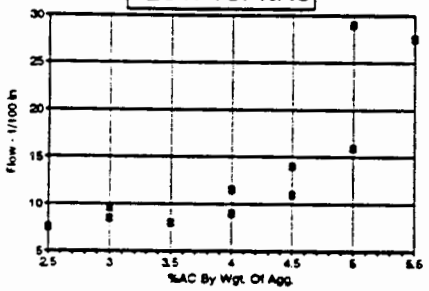

VMA BY RICE VS. %AC

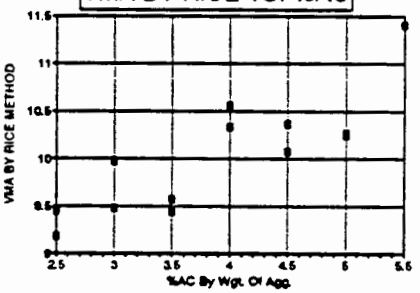

STABILITY VS. %AC

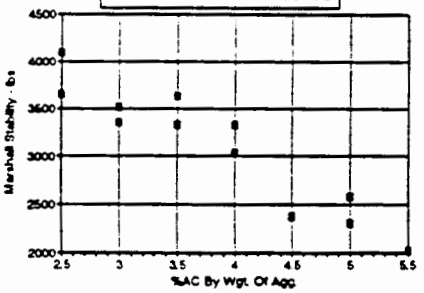

VFAC BY RICE VS. %AC

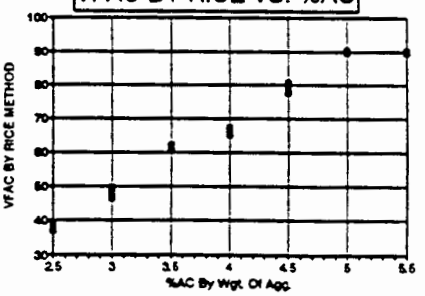

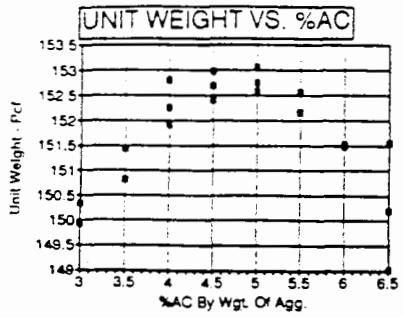
UNIT WEIGHT VS. %AC
Unit Weight - Pcf
153.5
153
152.5
152
151.5
151
150.5
150
149.5
149
3 3.5 4 4.5 5 5.5 6 6.5
%AC By Wgt. Of Agg.

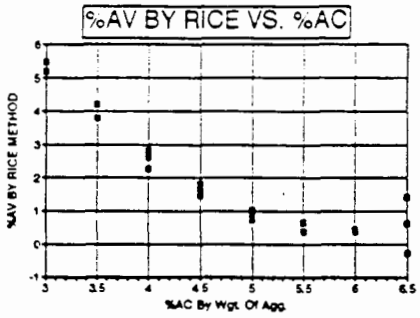
%AV BY RICE VS. %AC
%AV BY RICE METHOD
6
5
4
3
2
1
0
-1
3 3.5 4 4.5 5 5.5 6 6.5
%AC By Wgt. Of Agg.

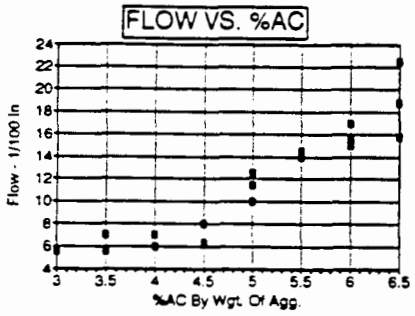
FLOW VS. %AC
Flow - 1/100 In
24
22
20
18
16
14
12
10
8
6
4
3 3.5 4 4.5 5 5.5 6 6.5
%AC By Wgt. Of Agg.

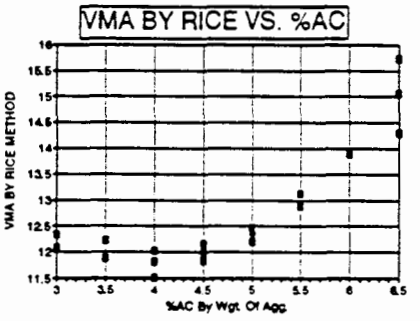
VMA BY RICE VS. %AC
VMA BY RICE METHOD
16
15.5
15
14.5
14
13.5
13
12.5
12
11.5
3 3.5 4 4.5 5 5.5 6 6.5
%AC By Wgt. Of Agg.

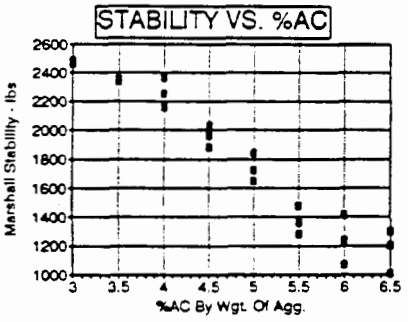
STABILITY VS. %AC
Marshall Stability - lbs
2600
2400
2200
2000
1800
1600
1400
1200
1000
3 3.5 4 4.5 5 5.5 6 6.5
%AC By Wgt. Of Agg.

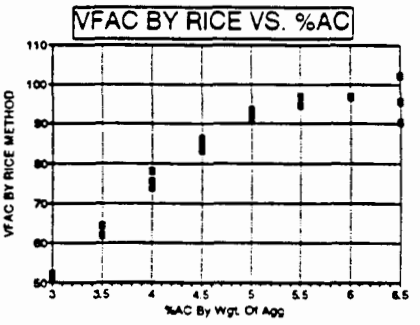
VFAC BY RICE VS. %AC
VFAC BY RICE METHOD
110
100
90
80
70
60
50
3 3.5 4 4.5 5 5.5 6 6.5
%AC By Wgt. Of Agg.

Test Property Curves for CDR4C Mix

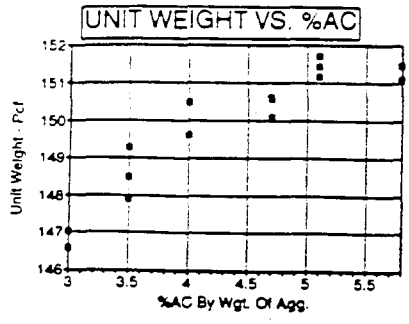

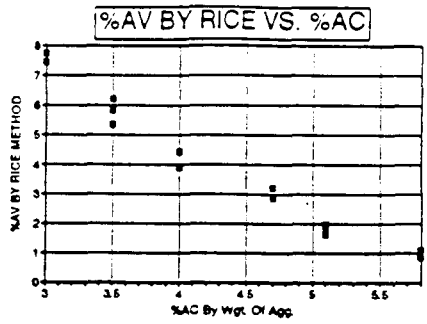

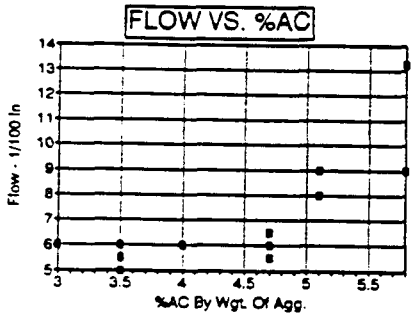

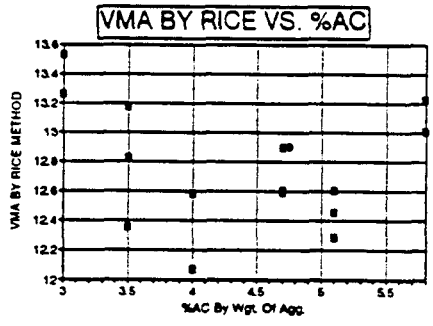

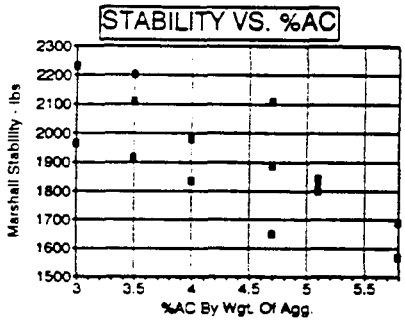

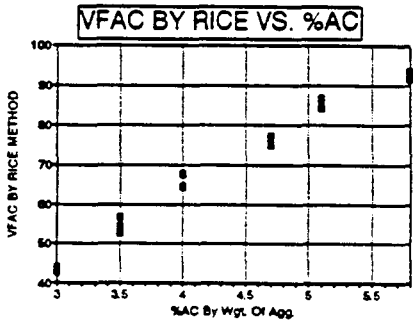

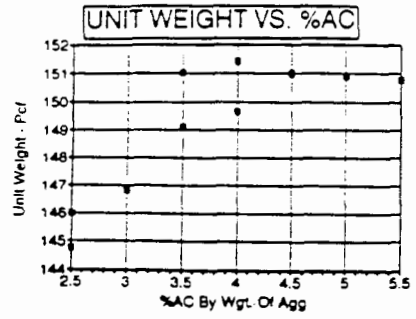
UNIT WEIGHT VS. %AC
Unit Weight - Pcf
152
151
150
149
148
147
146
145
144
2.5 3 3.5 4 4.5 5 5.5
%AC By Wgt. Of Agg.

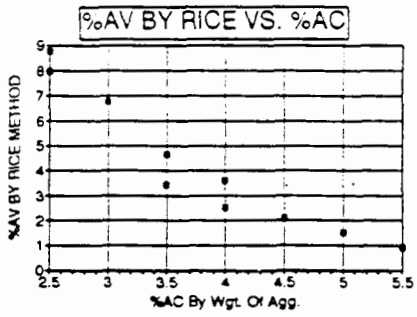
%AV BY RICE VS. %AC
%AV BY RICE METHOD
9
8
7
6
5
4
3
2
1
0
2.5 3 3.5 4 4.5 5 5.5
%AC By Wgt. Of Agg.

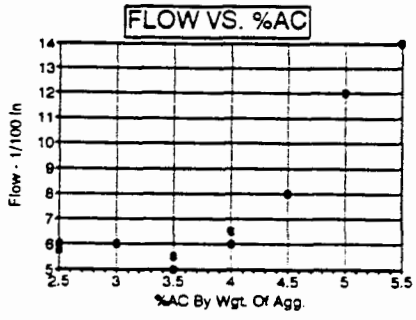
FLOW VS. %AC
Flow - 1/100 In
14
13
12
11
10
9
8
7
6
5
2.5 3 3.5 4 4.5 5 5.5
%AC By Wgt. Of Agg.

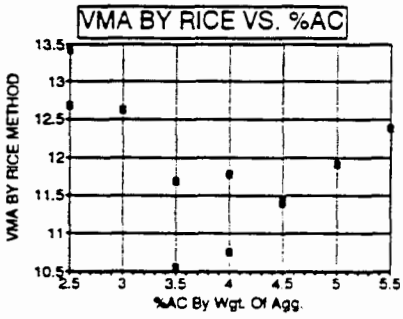
VMA BY RICE VS. %AC
VMA BY RICE METHOD
13.5
13
12.5
12
11.5
11
10.5
2.5 3 3.5 4 4.5 5 5.5
%AC By Wgt. Of Agg.

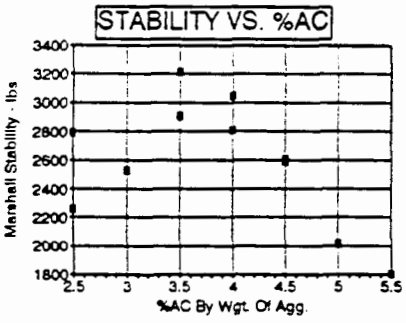
STABILITY VS. %AC
Marshall Stability - lbs
3400
3200
3000
2800
2600
2400
2200
2000
1800
2.5 3 3.5 4 4.5 5 5.5
%AC By Wgt. Of Agg.

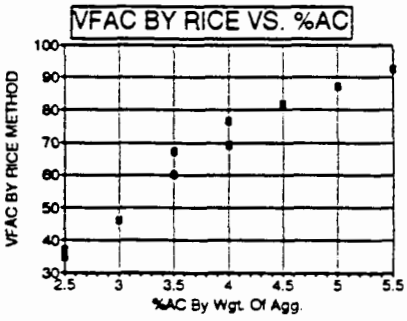
VFAC BY RICE VS. %AC
VFAC BY RICE METHOD
100
90
80
70
60
50
40
30
2.5 3 3.5 4 4.5 5 5.5
%AC By Wgt. Of Agg.

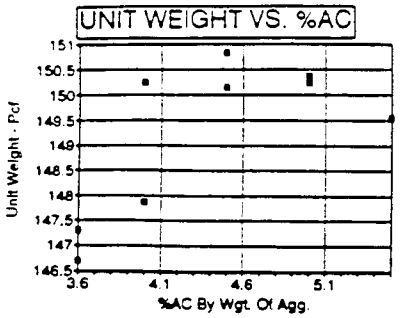
UNIT WEIGHT VS. %AC
Unit Weight - Pcf
151
150.5
150
149.5
149
148.5
148
147.5
147
146.5
3.6
4.1
4.6
5.1
%AC By Wgt. Of Agg.

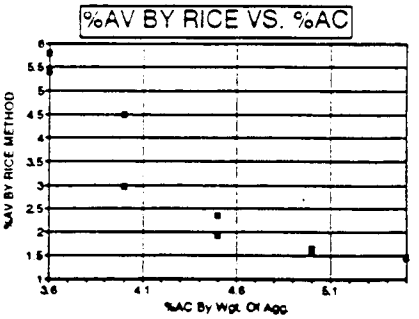
%AV BY RICE VS. %AC
%AV BY RICE METHOD
%AC By Wgt. Of Agg.

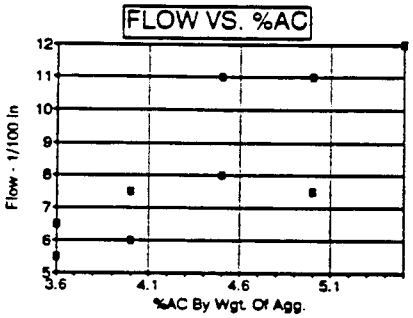
FLOW VS. %AC
Flow - 1/100 in
12
11
10
9
8
7
6
5
3.6
4.1
4.6
5.1
%AC By Wgt. Of Agg.

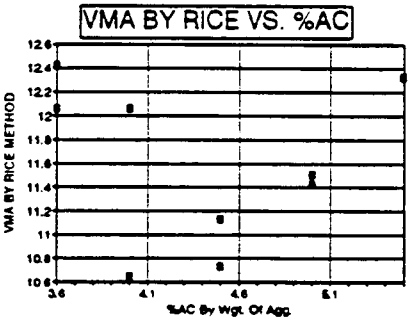
VMA BY RICE VS. %AC
VMA BY RICE METHOD
%AC By Wgt. Of Agg.

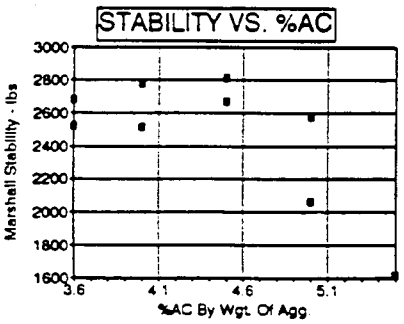
STABILITY VS. %AC
Marshall Stability - lbs
3000
2800
2600
2400
2200
2000
1800
1600
3.6
4.1
4.6
5.1
%AC By Wgt. Of Agg.

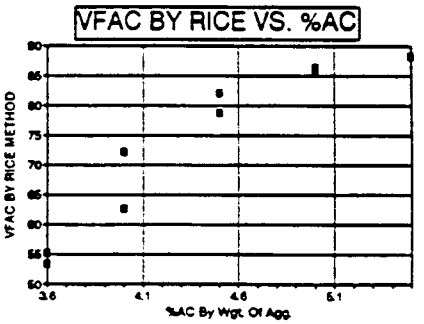
VFAC BY RICE VS. %AC
VFAC BY RICE METHOD
%AC By Wgt. Of Agg.

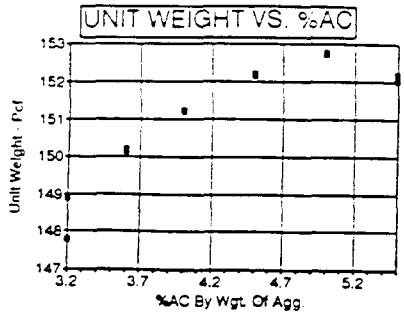
UNIT WEIGHT VS. %AC
Unit Weight - Pcf
153
152
151
150
149
148
147
3.2
3.7
4.2
4.7
5.2
%AC By Wgt. Of Agg.

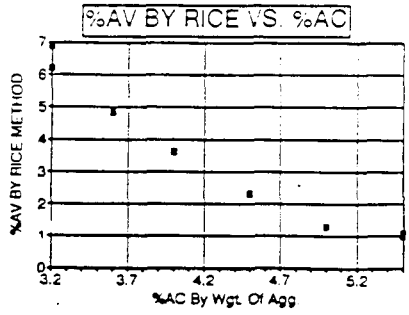
%AV BY RICE VS. %AC
%AV BY RICE METHOD
7
6
5
4
3
2
1
0
3.2
3.7
4.2
4.7
5.2
%AC By Wgt. Of Agg.

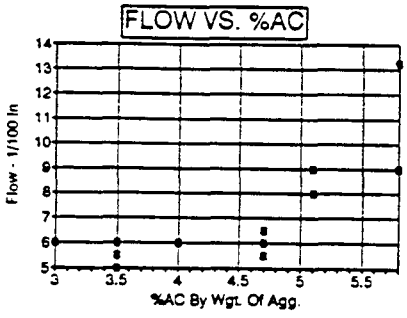
FLOW VS. %AC
Flow - 1/100 In
14
13
12
11
10
9
8
7
6
5
3
3.5
4
4.5
5
5.5
%AC By Wgt. Of Agg.

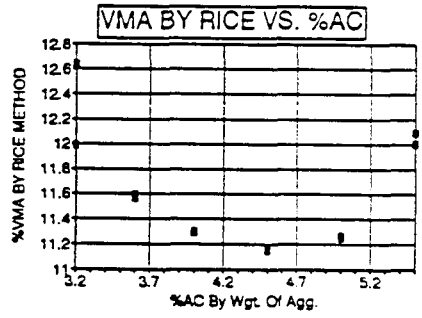
VMA BY RICE VS. %AC
%VMA BY RICE METHOD
12.8
12.6
12.4
12.2
12
11.8
11.6
11.4
11.2
11
3.2
3.7
4.2
4.7
5.2
%AC By Wgt. Of Agg.

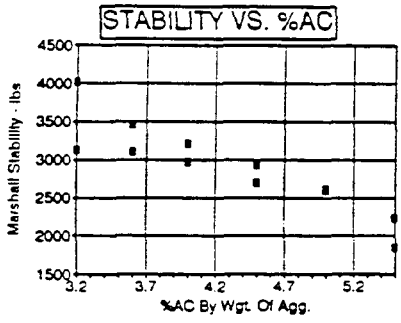
STABILITY VS. %AC
Marshall Stability - lbs
4500
4000
3500
3000
2500
2000
1500
3.2
3.7
4.2
4.7
5.2
%AC By Wgt. Of Agg.

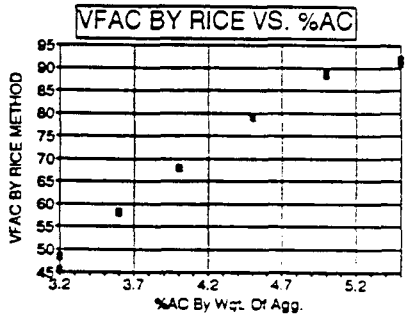
VFAC BY RICE VS. %AC
VFAC BY RICE METHOD
95
90
85
80
75
70
65
60
55
50
45
3.2
3.7
4.2
4.7
5.2
%AC By Wgt. Of Agg.

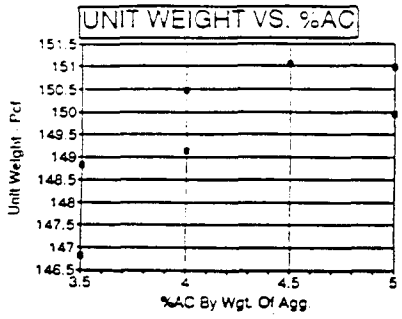
UNIT WEIGHT VS. %AC
Unit Weight - Pcf
151.5
151
150.5
150
149.5
149
148.5
148
147.5
147
146.5
3.5
4
4.5
5
%AC By Wgt. Of Agg.

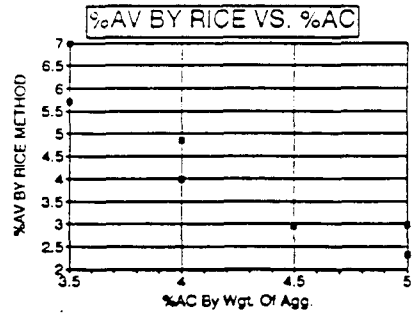
%AV BY RICE VS. %AC
%AV BY RICE METHOD
7
6.5
6
5.5
5
4.5
4
3.5
3
2.5
2
3.5
4
4.5
5
%AC By Wgt. Of Agg.

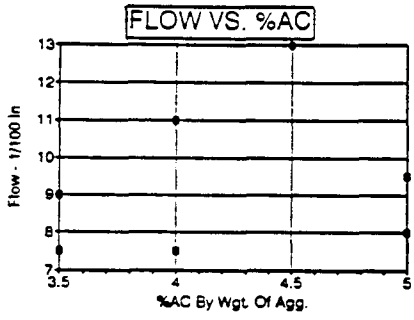
FLOW VS. %AC
Flow - 1/100 In
13
12
11
10
9
8
7
3.5
4
4.5
5
%AC By Wgt. Of Agg.

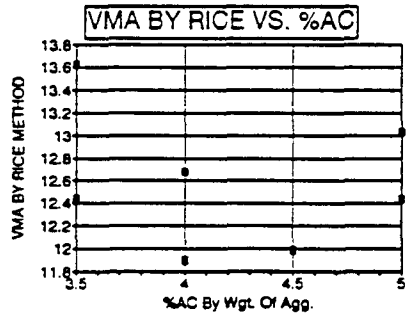
VMA BY RICE VS. %AC
VMA BY RICE METHOD
13.8
13.6
13.4
13.2
13
12.8
12.6
12.4
12.2
12
11.8
3.5
4
4.5
5
%AC By Wgt. Of Agg.

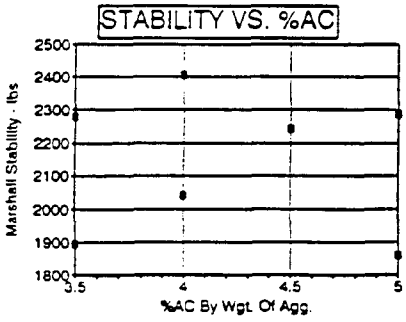
STABILITY VS. %AC
Marshall Stability - lbs
2500
2400
2300
2200
2100
2000
1900
1800
3.5
4
4.5
5
%AC By Wgt. Of Agg.

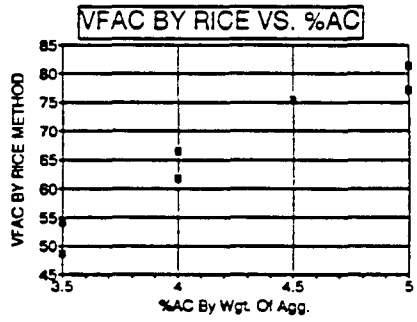
VFAC BY RICE VS. %AC
VFAC BY RICE METHOD
85
80
75
70
65
60
55
50
45
3.5
4
4.5
5
%AC By Wgt. Of Agg.

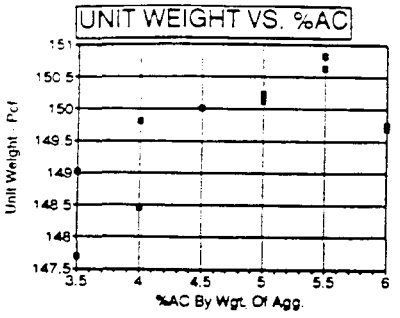
UNIT WEIGHT VS. %AC
Unit Weight - Pcf
151
150.5
150
149.5
149
148.5
148
147.5
3.5
4
4.5
5
5.5
6
%AC By Wgt. Of Agg.

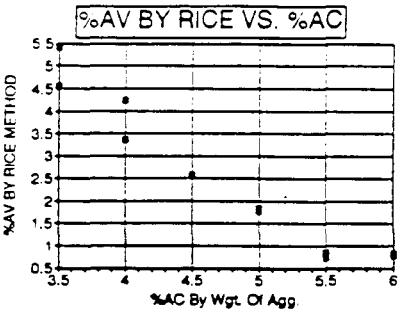
%AV BY RICE VS. %AC
%AV BY RICE METHOD
5.5
5
4.5
4
3.5
3
2.5
2
1.5
1
0.5
3.5
4
4.5
5
5.5
6
%AC By Wgt. Of Agg.

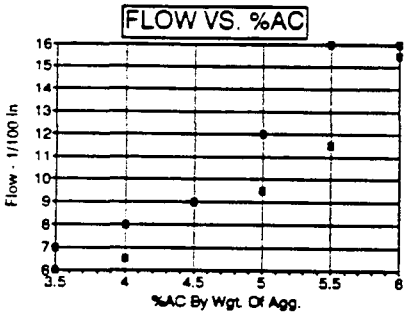
FLOW VS. %AC
Flow - 1/100 In
16
15
14
13
12
11
10
9
8
7
6
3.5
4
4.5
5
5.5
6
%AC By Wgt. Of Agg.

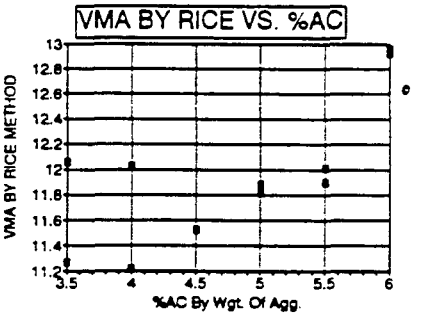
VMA BY RICE VS. %AC
VMA BY RICE METHOD
13
12.8
12.6
12.4
12.2
12
11.8
11.6
11.4
11.2
3.5
4
4.5
5
5.5
6
%AC By Wgt. Of Agg.

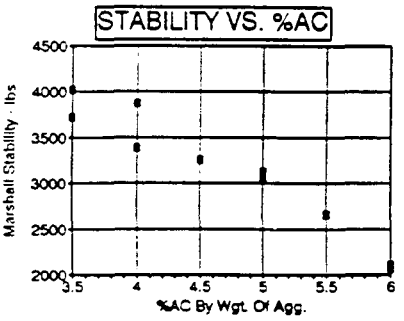
STABILITY VS. %AC
Marshall Stability - lbs
4500
4000
3500
3000
2500
2000
3.5
4
4.5
5
5.5
6
%AC By Wgt. Of Agg.

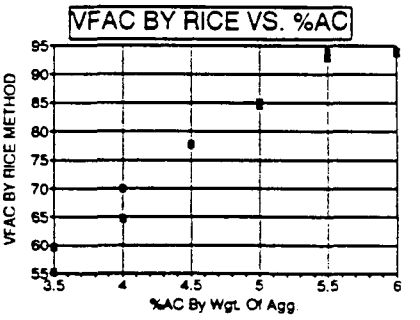
VFAC BY RICE VS. %AC
VFAC BY RICE METHOD
95
90
85
80
75
70
65
60
55
3.5
4
4.5
5
5.5
6
%AC By Wgt. Of Agg.

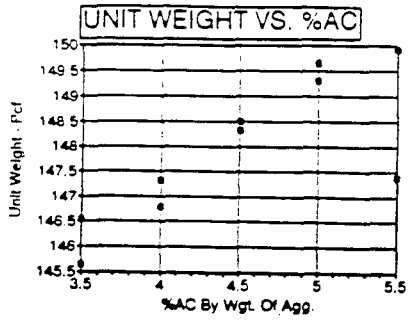
UNIT WEIGHT VS. %AC
Unit Weight - Pcf
150
149.5
149
148.5
148
147.5
147
146.5
146
145.5
3.5
4
4.5
5
5.5
%AC By Wgt. Of Agg.

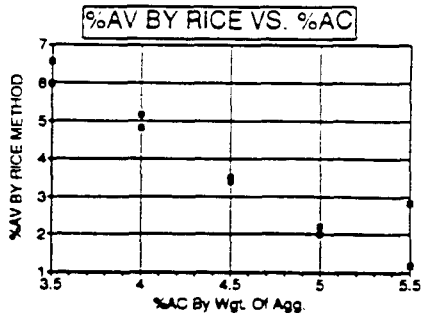
%AV BY RICE VS. %AC
%AV BY RICE METHOD
7
6
5
4
3
2
1
3.5
4
4.5
5
5.5
%AC By Wgt. Of Agg.

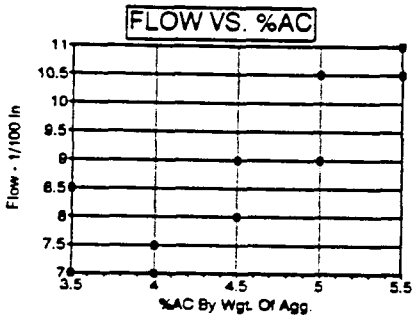
FLOW VS. %AC
Flow - 1/100 In
11
10.5
10
9.5
9
8.5
8
7.5
7
3.5
4
4.5
5
5.5
%AC By Wgt. Of Agg.

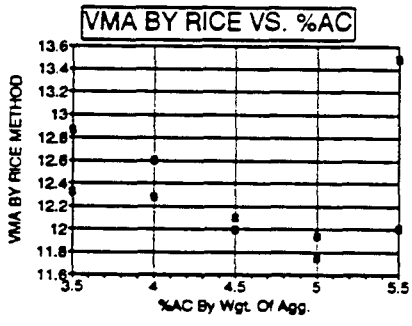
VMA BY RICE VS. %AC
VMA BY RICE METHOD
13.6
13.4
13.2
13
12.8
12.6
12.4
12.2
12
11.8
11.6
3.5
4
4.5
5
5.5
%AC By Wgt. Of Agg.

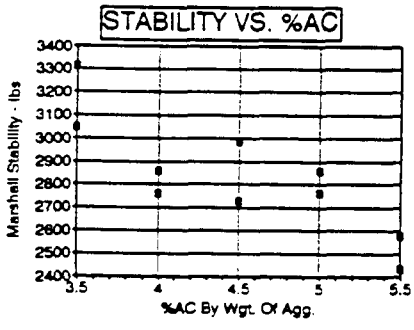
STABILITY VS. %AC
Marshall Stability - lbs
3400
3300
3200
3100
3000
2900
2800
2700
2600
2500
2400
3.5
4
4.5
5
5.5
%AC By Wgt. Of Agg.

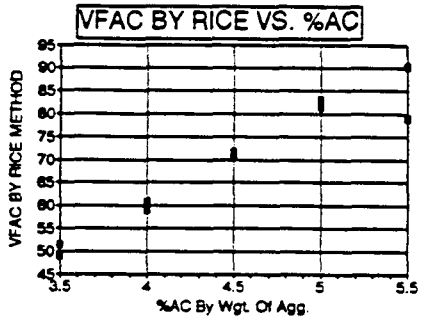
VFAC BY RICE VS. %AC
VFAC BY RICE METHOD
95
90
85
80
75
70
65
60
55
50
45
3.5
4
4.5
5
5.5
%AC By Wgt. Of Agg.

Test Property Curves for ICDR5C Mix

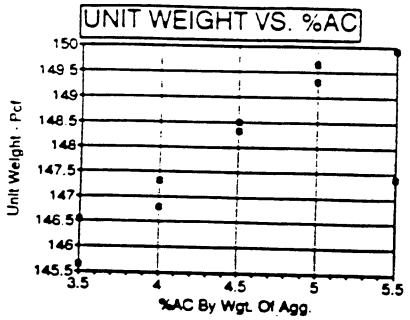

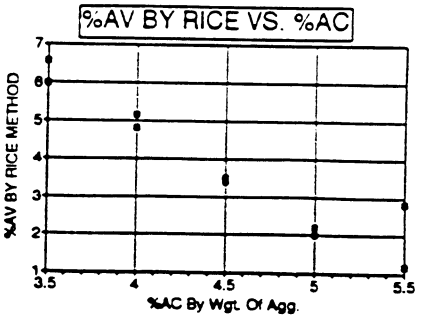

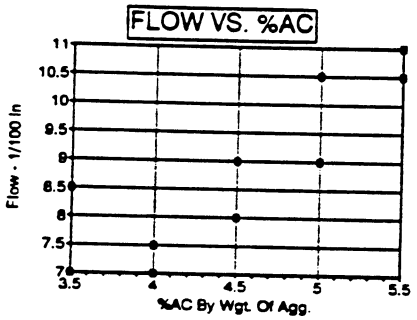

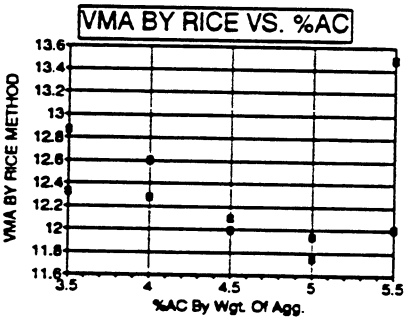

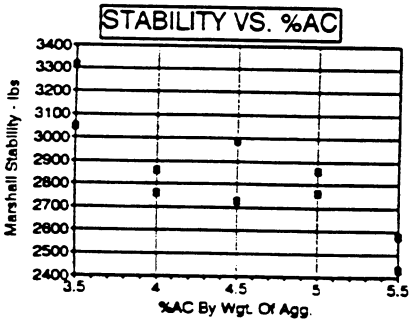

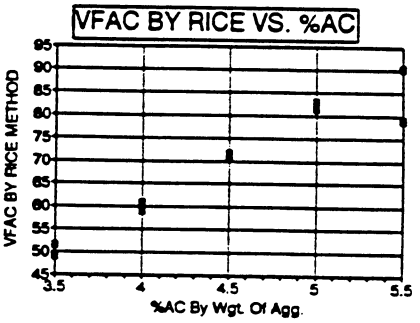

Authors	Agg.Type	MR (psi)	Pair (%)	n70*	Pen@77°F	t (sec)
Boudreau	CB	1.840E+06	4	1.771	84	0.1
Boudreau	CB	4.090E+05	4	1.771	84	0.1
Boudreau		1.406E+06	4	1.771	84	0.1
Boudreau		4.090E+05	4	1.771	84	0.1
Boudreau		1.017E+06	10	1.771	84	0.1
Boudreau		2.110E+05	10	1.771	84	0.1
Boudreau		1.211E+06	10	1.771	84	0.1
Boudreau		3.100E+05	10	1.771	84	0.1
Boudreau		2.595E+06	4	1.771	84	0.1
Boudreau		1.882E+06	4	1.771	84	0.1
Boudreau		1.271E+06	4	1.771	84	0.1
Boudreau		4.960E+05	4	1.771	84	0.1
Boudreau		2.717E+06	4	1.771	84	0.1
Boudreau		2.213E+06	4	1.771	84	0.1
Boudreau		1.686E+06	4	1.771	84	0.1
Boudreau		7.710E+05	4	1.771	84	0.1
Boudreau		1.768E+06	8	1.771	84	0.1
Boudreau		1.189E+06	8	1.771	84	0.1
Boudreau		7.250E+05	8	1.771	84	0.1
Boudreau		2.800E+05	8	1.771	84	0.1
Boudreau		1.831E+06	8	1.771	84	0.1
Boudreau		1.421E+06	8	1.771	84	0.1
Boudreau		9.600E+05	8	1.771	84	0.1
Boudreau		3.220E+05	8	1.771	84	0.1
Schmidt & Graf	G	3.650E+05	8.1	1.818	83	0.1
Schmidt & Graf	G	3.290E+05	6.3	1.818	83	0.1
Schmidt & Graf	G	3.500E+05	8.2	1.818	83	0.1
Schmidt & Graf	G	3.230E+05	10.4	1.818	83	0.1
Schmidt & Graf	G	2.030E+05	6.5	1.818	83	0.1
Schmidt & Graf	G	2.340E+05	7.3	1.818	83	0.1
Schmidt & Graf	G	2.170E+05	7.7	1.818	83	0.1
Schmidt & Graf	G	3.210E+05	5.5	1.818	83	0.1
Schmidt & Graf	G	1.000E+05	1.6	1.818	83	0.1
Schmidt & Graf	G	2.070E+05	3.8	1.818	83	0.1
Schmidt & Graf	G	2.170E+05	10.4	1.818	83	0.1
Schmidt & Graf	G	2.020E+05	13.8	1.818	83	0.1
Schmidt & Graf	G	1.730E+05	15.4	1.818	83	0.1
Schmidt & Graf	G	4.080E+05	2.1	1.818	83	0.1
Schmidt & Graf	G	1.760E+05	0.2	1.818	83	0.1
Schmidt & Graf	G	4.230E+05	6.1	1.818	83	0.1
Schmidt & Graf	G	1.890E+05	10.2	1.818	83	0.1

* 10^6poise

Authors	Agg.Type	MR (psi)	Pair (%)	n70*	Pen@77°F	t (sec)
Schmidt & Graf	G	6.120E+05	9.1	9.535	39	0.1
Schmidt & Graf	G	4.150E+05	8.6	5.072	52	0.1
Schmidt & Graf	G	3.000E+05	8.6	1.818	83	0.1
Schmidt & Graf	G	2.100E+05	7.9	0.795	121	0.1
Schmidt & Graf	G	7.200E+04	8	0.171	244	0.1
Schmidt & Graf	Ca	5.050E+05	4.6	1.818	83	0.1
Schmidt & Graf	Si	1.660E+05	8.8	1.818	83	0.1
Schmidt & Graf	Ca	5.700E+05	2.4	1.818	83	0.1
Schmidt & Graf	G	3.290E+05	6.3	1.818	83	0.1
Schmidt & Graf	Si	1.664E+05	8.8	1.818	83	0.1
Schmidt & Graf	Ca	5.540E+05	2.4	1.818	83	0.1
Schmidt & Graf	LS	2.920E+05	3.1	1.818	83	0.1
Schmidt & Graf	Gran	2.750E+05	7.4	1.818	83	0.1
Str-Gar&Epps	G	8.208E+06	2	4.669	54	0.1
Str-Gar&Epps	G	4.354E+06	2	4.669	54	0.1
Str-Gar&Epps	G	4.670E+05	2	4.669	54	0.1
Str-Gar&Epps	G	4.300E+04	2	4.669	54	0.1
Str-Gar&Epps	G	2.310E+05	8	4.669	54	0.1
Str-Gar&Epps	G	5.600E+06	7	4.669	54	0.1
Str-Gar&Epps	G	3.173E+06	7	4.669	54	0.1
Str-Gar&Epps	G	1.980E+05	7	4.669	54	0.1
Str-Gar&Epps	G	3.200E+04	7	4.669	54	0.1
Baladi	LS	7.600E+05	3.01	1.321	96	0.1
Baladi	LS	6.501E+05	3.09	1.321	96	0.1
Baladi	LS	5.463E+05	2.99	1.321	96	0.1
Baladi	LS	7.132E+05	3.35	1.321	96	0.1
Baladi	LS	6.480E+05	3.37	1.321	96	0.1
Baladi	LS	5.890E+05	3.29	1.321	96	0.1
Baladi	LS	5.056E+05	5.15	1.321	96	0.1
Baladi	LS	5.008E+05	5.1	1.321	96	0.1
Baladi	LS	3.825E+05	5.2	1.321	96	0.1
Baladi	LS	4.690E+05	6.85	1.321	96	0.1
Baladi	LS	4.810E+05	6.8	1.321	96	0.1
Baladi	LS	3.200E+05	6.89	1.321	96	0.1
Baladi	LS	4.688E+05	3.11	1.321	96	0.1
Baladi	LS	4.400E+05	3.06	1.321	96	0.1
Baladi	LS	3.460E+05	3	1.321	96	0.1
Baladi	LS	4.864E+05	3.48	1.321	96	0.1
Baladi	LS	4.442E+05	3.46	1.321	96	0.1
Baladi	LS	3.134E+05	3.45	1.321	96	0.1
Baladi	LS	5.526E+05	3.85	1.321	96	0.1
Baladi	LS	4.523E+05	4.8	1.321	96	0.1
Baladi	LS	3.818E+05	4.8	1.321	96	0.1
Baladi	LS	3.974E+05	7.15	1.321	96	0.1
Baladi	LS	3.919E+05	7.18	1.321	96	0.1
Baladi	LS	1.684E+05	7.12	1.321	96	0.1

* 10^6poise

Authors	Agg.Type	Peff(%)	Pabs(%)	Pb(%)	P200(%)	AR4(%)
Boudreau	CB	12.4224	1.4025	6	5	44
Boudreau	CB	12.4224	1.4025	6	5	44
Boudreau		13.8716	1.5662	6.7	4.8	43
Boudreau		13.8716	1.5662	6.7	4.8	43
Boudreau		12.4224	1.4025	6	5	44
Boudreau		12.4224	1.4025	6	5	44
Boudreau		13.8716	1.5662	6.7	4.8	43
Boudreau		13.8716	1.5662	6.7	4.8	43
Boudreau		12.4224	1.4025	6	5	44
Boudreau		12.4224	1.4025	6	5	44
Boudreau		12.4224	1.4025	6	5	44
Boudreau		12.4224	1.4025	6	5	44
Boudreau		13.8716	1.5662	6.7	4.8	43
Boudreau		13.8716	1.5662	6.7	4.8	43
Boudreau		13.8716	1.5662	6.7	4.8	43
Boudreau		13.8716	1.5662	6.7	4.8	43
Boudreau		12.4224	1.4025	6	5	44
Boudreau		12.4224	1.4025	6	5	44
Boudreau		12.4224	1.4025	6	5	44
Boudreau		12.4224	1.4025	6	5	44
Boudreau		13.8716	1.5662	6.7	4.8	43
Boudreau		13.8716	1.5662	6.7	4.8	43
Boudreau		13.8716	1.5662	6.7	4.8	43
Boudreau		13.8716	1.5662	6.7	4.8	43
Schmidt & Graf	G	10.3520	1.1688	5	7	37
Schmidt & Graf	G	10.3520	1.1688	5	7	37
Schmidt & Graf	G	10.3520	1.1688	5	7	37
Schmidt & Graf	G	10.3520	1.1688	5	7	37
Schmidt & Graf	G	10.3520	1.1688	5	7	37
Schmidt & Graf	G	10.3520	1.1688	5	7	37
Schmidt & Graf	G	10.3520	1.1688	5	7	37
Schmidt & Graf	G	10.3520	1.1688	5	7	37
Schmidt & Graf	G	18.6335	2.1038	9	7	37
Schmidt & Graf	G	14.4928	1.6363	7	7	37
Schmidt & Graf	G	10.3520	1.1688	5	7	37
Schmidt & Graf	G	6.2112	0.7013	3	7	37
Schmidt & Graf	G	4.1408	0.4675	2	7	37
Schmidt & Graf	G	10.3520	1.1688	5	4	60
Schmidt & Graf	G	14.4928	1.6363	7	4	60
Schmidt & Graf	G	6.2112	0.7013	3	4	60
Schmidt & Graf	G	4.1408	0.4675	2	4	60

Authors	Agg.Type	Peff(%)	Pabs(%)	Pb(%)	P200(%)	AR4(%)
Schmidt & Graf	G	10.3520	1.1688	5	7	37
Schmidt & Graf	G	10.3520	1.1688	5	7	37
Schmidt & Graf	G	10.3520	1.1688	5	7	37
Schmidt & Graf	G	10.3520	1.1688	5	7	37
Schmidt & Graf	G	10.3520	1.1688	5	7	37
Schmidt & Graf	Ca	10.3520	1.1688	5	7	37
Schmidt & Graf	Si	10.3520	1.1688	5	7	37
Schmidt & Graf	Ca	10.3520	1.1688	5	7	37
Schmidt & Graf	G	10.3520	1.1688	5	7	37
Schmidt & Graf	Si	10.3520	1.1688	5	7	37
Schmidt & Graf	Ca	10.3520	1.1688	5	7	37
Schmidt & Graf	LS	10.3520	1.1688	5	7	37
Schmidt & Graf	Gran	10.3520	1.1688	5	7	37
Str-Gar&Epps	G	13.4576	1.5194	6.5	5.8	47.8
Str-Gar&Epps	G	13.4576	1.5194	6.5	5.8	47.8
Str-Gar&Epps	G	13.4576	1.5194	6.5	5.8	47.8
Str-Gar&Epps	G	13.4576	1.5194	6.5	5.8	47.8
Str-Gar&Epps	G	13.4576	1.5194	6.5	5.8	47.8
Str-Gar&Epps	G	14.4928	1.6363	7	4.1	47.9
Str-Gar&Epps	G	14.4928	1.6363	7	4.1	47.9
Str-Gar&Epps	G	14.4928	1.6363	7	4.1	47.9
Str-Gar&Epps	G	14.4928	1.6363	7	4.1	47.9
Baladi	LS	8.9234	1.0075	4.31	8.3	50.2
Baladi	LS	8.9234	1.0075	4.31	8.3	50.2
Baladi	LS	8.9234	1.0075	4.31	8.3	50.2
Baladi	LS	8.9234	1.0075	4.31	8.3	50.2
Baladi	LS	8.9234	1.0075	4.31	8.3	50.2
Baladi	LS	8.9234	1.0075	4.31	8.3	50.2
Baladi	LS	8.9234	1.0075	4.31	8.3	50.2
Baladi	LS	8.9234	1.0075	4.31	8.3	50.2
Baladi	LS	8.9234	1.0075	4.31	8.3	50.2
Baladi	LS	8.9234	1.0075	4.31	8.3	50.2
Baladi	LS	8.9234	1.0075	4.31	8.3	50.2
Baladi	LS	8.9234	1.0075	4.31	8.3	50.2
Baladi	LS	8.9234	1.0075	4.31	8.3	50.2
Baladi	LS	8.9234	1.0075	4.31	8.3	50.2
Baladi	LS	8.9234	1.0075	4.31	8.3	50.2
Baladi	LS	8.9234	1.0075	4.31	8.3	50.2
Baladi	LS	8.9234	1.0075	4.31	8.3	50.2
Baladi	LS	8.9234	1.0075	4.31	8.3	50.2
Baladi	LS	8.9234	1.0075	4.31	8.3	50.2
Baladi	LS	8.9234	1.0075	4.31	8.3	50.2
Baladi	LS	8.9234	1.0075	4.31	8.3	50.2
Baladi	LS	8.9234	1.0075	4.31	8.3	50.2
Baladi	LS	8.9234	1.0075	4.31	8.3	50.2
Baladi	LS	8.9234	1.0075	4.31	8.3	50.2
Baladi	LS	8.9234	1.0075	4.31	8.3	50.2

Authors	Agg.Type	AR3/4(%)	AR1/2(%)	T(°F)
Boudreau	CB	0	2	40
Boudreau	CB	0	2	73
Boudreau		0	1	40
Boudreau		0	1	73
Boudreau		0	2	40
Boudreau		0	2	73
Boudreau		0	1	40
Boudreau		0	1	73
Boudreau		0	2	40
Boudreau		0	2	50
Boudreau		0	2	60
Boudreau		0	2	70
Boudreau		0	1	40
Boudreau		0	1	50
Boudreau		0	1	60
Boudreau		0	1	70
Boudreau		0	2	40
Boudreau		0	2	50
Boudreau		0	2	60
Boudreau		0	2	70
Boudreau		0	1	40
Boudreau		0	1	50
Boudreau		0	1	60
Boudreau		0	1	70
Schmidt & Graf	G	0	9	73
Schmidt & Graf	G	0	9	73
Schmidt & Graf	G	0	9	73
Schmidt & Graf	G	0	9	73
Schmidt & Graf	G	0	9	73

Authors	Agg.Type	AR3/4(%)	AR1/2(%)	T(°F)
Schmidt & Graf	G	0	9	73
Schmidt & Graf	G	0	9	73
Schmidt & Graf	G	0	9	73
Schmidt & Graf	G	0	9	73
Schmidt & Graf	G	0	9	73
Schmidt & Graf	G	0	9	73
Schmidt & Graf	G	0	9	73
Schmidt & Graf	G	0	9	73
Schmidt & Graf	G	0	29	73
Schmidt & Graf	G	0	29	73
Schmidt & Graf	G	0	29	73
Schmidt & Graf	G	0	29	73
Schmidt & Graf	G	0	9	73
Schmidt & Graf	G	0	9	73
Schmidt & Graf	G	0	9	73
Schmidt & Graf	G	0	9	73
Schmidt & Graf	G	0	9	73
Schmidt & Graf	Ca	0	9	73
Schmidt & Graf	Si	0	9	73
Schmidt & Graf	Ca	0	9	73
Schmidt & Graf	G	0	9	73
Schmidt & Graf	Si	0	9	73
Schmidt & Graf	Ca	0	9	73
Schmidt & Graf	LS	0	9	73
Schmidt & Graf	Gran	0	9	73
Str-Gar&Epps	G	0	5.3	-20
Str-Gar&Epps	G	0	5.3	34
Str-Gar&Epps	G	0	5.3	77
Str-Gar&Epps	G	0	5.3	104
Str-Gar&Epps	G	0	5.3	77
Str-Gar&Epps	G	0	5.1	-20
Str-Gar&Epps	G	0	5.1	34
Str-Gar&Epps	G	0	5.1	77
Str-Gar&Epps	G	0	5.1	104
Baladi	LS	0	18	77
Baladi	LS	0	18	77
Baladi	LS	0	18	77
Baladi	LS	0	18	77
Baladi	LS	0	18	77
Baladi	LS	0	18	77
Baladi	LS	0	18	77
Baladi	LS	0	18	77
Baladi	LS	0	18	77
Baladi	LS	0	18	77
Baladi	LS	0	18	77
Baladi	LS	0	18	77
Baladi	LS	0	18	77
Baladi	LS	0	18	77
Baladi	LS	0	18	77
Baladi	LS	0	18	77
Baladi	LS	0	18	77
Baladi	LS	0	18	77
Baladi	LS	0	18	77
Baladi	LS	0	18	77
Baladi	LS	0	18	77
Baladi	LS	0	18	77
Baladi	LS	0	18	77
Baladi	LS	0	18	77

CLS = Crushed Limestone; CB = Crushed Basalt; G = Gravel
Ca = Calcite Si = Silica Gran = Granite
LS = Limestone